UNIVERSITÀ VITA-SALUTE SAN RAFFAELE

CORSO DI DOTTORATO DI RICERCA IN NEUROSCIENZE COGNITIVE

NEUROBIOLOGICAL UNDERPINNINGS OF COGNITIVE DISTORTION IN MOOD DISORDERS

DoS: Dott.ssa Sara Poletti

Tesi di DOTTORATO di RICERCA di Federica Colombo

Matr. 019544

Ciclo di dottorato XXXVII

SSS MED/25

Anno Accademico 2023/2024

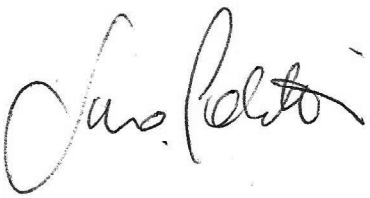

CONSULTAZIONE TESI DI DOTTORATO DI RICERCA

Il/la sottoscritto/*I*	Federica Colombo
Matricola / *registration number*	019544
nata/ *born at*	Carate Brianza (MI)
il/*on*	29/06/1996

autore della tesi di Dottorato di ricerca dal titolo / *author of the PhD Thesis titled*

NEUROBIOLOGICAL UNDERPINNINGS OF COGNITIVE DISTORTION IN MOOD DISORDERS

☑ AUTORIZZA la Consultazione della tesi / AUTHORIZES *the public release of the thesis*

☐ NON AUTORIZZA la Consultazione della tesi per …… mesi /DOES NOT AUTHORIZE *the public release of the thesis for …… months*

a partire dalla data di conseguimento del titolo e precisamente */ from the PhD thesis date, specifically*

Dal / *from* ……/……/…… Al / *to* ……/……/……

Poiché */ because*:

□ l'intera ricerca o parti di essa sono potenzialmente soggette a brevettabilità/ *The whole project or part of it might be subject to patentability;*

□ ci sono parti di tesi che sono già state sottoposte a un editore o sono in attesa di pubblicazione/ *Parts of the thesis have been or are being submitted to a publisher or are in press;*

□ la tesi è finanziata da enti esterni che vantano dei diritti su di esse e sulla loro pubblicazione/ *the thesis project is financed by external bodies that have rights over it and on its publication.*

E' fatto divieto di riprodurre, in tutto o in parte, quanto in essa contenuto / *Copyright the contents of the thesis in whole or in part is forbidden*

Data /Date 28/10/2024 Firma /Signature Federica Colombo

DECLARATION

This thesis has been:

- composed by myself and has not been used in any previous application for a degree. Throughout the text I use both 'I' and 'We' interchangeably.
- has been written according to the editing guidelines approved by the University.

Permission to use images and other material covered by copyright has been sought and obtained.

All the results presented here were obtained by myself, except for:

1) *Luminex quantification was performed by Dott.ssa Cristina M. Lorenzi and Dott.ssa Sara Spadini, from the Psychiatry and Clinical Psychobiology research group, Division of Neuroscience, San Raffaele Scientific Institute, Milan, Italy.*

2) *Flow cytometry experiments were performed by Dott.ssa Veronica Aggio from the Psychiatry and Clinical Psychobiology research group, Division of Neuroscience, San Raffaele Scientific Institute, Milan, Italy, and Dott.ssa Lorena Fabbella from the Clinical Immunology research group, Division of Neuroscience, San Raffaele Scientific Institute, Milan, Italy.*

All sources of information are acknowledged by means of reference.

ACKNOWLEDGEMENTS

This thesis has been produced with the financial support of the University Vita-Salute San Raffaele (Milan, Italy), which offered me a doctoral scholarship, and with the support of Unit of Psychiatry and Clinical Psychobiology, Division of Neuroscience, IRCSS San Raffaele Scientific Institute (Milan, Italy), which provided me all the necessary means required for this project. Moreover, we collaborated with C.E.R.M.A.C. (Centro Eccellenza Risonanza Magnetica ad Alto Campo, Scientific Institute Ospedale San Raffaele, Milan) for MRI acquisitions and the Unit of Neuroimmunology (Division of Neuroscience) for the cytofluorimetry experiments.

ABSTRACT

One of the main features of depression is negatively distorted cognition, which contributes to severe clinical outcomes by sustaining negative affect. However, the clinical manifestation of depression is highly heterogeneous, reflecting complex interactions between neuro-biological and environmental factors in modelling disease trajectories. Characterizing this heterogeneity based on multimodal data could help identify how such mechanisms map onto different phenotypic manifestations and discover high-impact biomarkers. By leveraging a novel unsupervised machine learning pipeline, in this work 344 depressed patients (135 Major Depressive Disorder, 209 Bipolar Disorder) were stratified based on a wide set of neuro-biological data, including grey matter volumes, cortical thickness, white matter diffusivity indexes, resting-state functional connectivity (FC) and spontaneous neural activity, as well as peripheral immune-inflammatory markers and immune cells count. Together with stratification models based on single modalities, a multimodal neuroimaging approach was also implemented. For each model, the discovered clusters were then profiled for adverse childhood experiences (ACEs) and cognitive distortions. The results showed that both neuroimaging and immune-inflammatory data retain information to stratify depressed patients into 2 clusters, with accuracies in clusters' differentiation ranging from 40% to 85%. Clusters derived from immune-based profiles exhibited significant differences in cognitive distortions, with patients characterized by a more neurotoxic profile showing a worse negative thinking style. Unique multivariate neurobiological-ACEs relationships were observed between the FC-based and immune-based clusters, suggesting that depression subtypes derived from these measures are differentially affected by childhood trauma. Mediation analyses showed that individual multivariate FC scores mediate the relationship between childhood trauma and the tendency to overgeneralize only in a depression subtype characterized by global functional hypo-connectivity. Functional alterations involved in these effects pinpoint to brain regions particularly sensible to maturational neural changes supporting the development of socioemotional and cognitive functions. These results provided evidence of clinically meaningful "biotypes" of depressed patients based on neuroimaging and immune-inflammatory data, underlining the feasibility of computational psychiatry tools to uncover data-driven patterns in the realm of precision psychiatry.

TABLE OF CONTENTS

TABLE OF CONTENTS 1
ACRONYMS AND ABBREVIATIONS 4
LIST OF FIGURES AND TABLES 9
Figures 9
Tables 10
Appendix 10
1. INTRODUCTION 12
1.1 Mood Disorders 12
1.1.1 Major Depressive Disorder 12
1.1.2 Bipolar Disorders 13
1.2 Sources of heterogeneity in Mood Disorders 15
1.2.1 Genetics and epigenetic factors 15
1.2.2 Structural neuroimaging correlates 17
1.2.3 Functional neuroimaging correlates 23
1.2.4 Inflammatory markers 25
1.2.5 Environmental factors 29
1.2.6 Clinical features: cognitive distortions in Mood Disorders 32
1.3 Computational approaches for neuro-biological phenotyping in Mood Disorders 35
1.3.1 Applications of unsupervised learning methods in psychiatry 38
2. AIM OF THE WORK 45
3. RESULTS 46
3.1 Descriptive statistics 46
3.2 Unsupervised data-driven stratification 47
3.2.1 Performances of the stability-based relative clustering stratification models 47
3.2.2 Biological and clinical characterization of the FC-based stratification model 48
3.2.3 Biological and clinical characterization of the GM-based stratification model 49
3.2.4 Biological and clinical characterization of the CT-based stratification model 51

3.2.5 Biological and clinical characterization of the DTI-based stratification models 52

3.2.6 Biological and clinical characterization of the multimodal neuroimaging stratification model 57

3.2.7 Biological and clinical characterization of the FACS-based stratification model 59

3.2.8 Biological and clinical characterization of the stratification model based on immune-inflammatory profiles 61

3.3 Differential multivariate neuro-biological-ACEs associations among clusters 63

3.3.1 Grouped PLSC results for the FC-based stratification model 64

3.3.2 Grouped PLSC results for the stratification model based on immune-inflammatory profiles 65

3.4 General linear models and mediation analyses 66

3.4.1 Effect of FC strength on cognitive distortions in the FC-derived clusters 66

3.4.2 Effect of inflammation on cognitive distortions in clusters derived from immune-inflammatory profiles 67

4. DISCUSSION 68

4.1 Neuroimaging data provide information for stable data-driven stratifications of Mood Disorders 68

4.2 Immune-inflammatory markers provide information for stable and clinically meaningful data-driven stratifications of Mood Disorders 73

4.3 Brain functional and immune-based clusters show specific multivariate associations with childhood trauma and cognitive distortions 76

4.4 Strengths and limitations 79

4.5 Conclusions 82

5. MATERIALS AND METHODS 83

5.1 Participants 83

5.2 Assessment of childhood trauma and cognitive distortions 83

5.3 MRI data acquisition and preprocessing 84

5.3.1 Data acquisition 84

5.3.2 Grey matter processing and features extraction 86

5.3.3 DTI processing and features extraction 86

5.3.4 rs-fMRI processing and features extraction 87

5.3.5 ComBat harmonization 88

5.4 Immune-inflammatory markers 89

5.4.1 Luminex quantification 89
5.4.2 Immune-inflammatory profiles calculation 90
5.5 Immunophenotyping 91
5.5.1 PBMCs isolation 91
5.5.2 Flow-cytometry Multiparametric Analysis 91
5.5.3 Gating strategies 93
5.6 Statistical analysis 100
5.6.1 Unsupervised machine learning analyses 100
5.6.2. Clinical and neurobiological characterization of the clusters 105
REFERENCES 107
APPENDIX 140

ACRONYMS AND ABBREVIATIONS

ACC: anterior cingulate cortex

Acc: accuracy

ACE: Adverse Childhood Experience

aCompCor: anatomical component correction

ACR: anterior corona radiata

AD: axial diffusivity

ADHD: attention-deficit/hyperactivity disorder

ALIC: anterior limb of internal capsule

ASD: autism spectrum disorder

basic FGF: basic fibroblast growth factor

BCC: body of corpus callosum

BD: bipolar disorders

BD-I: type I bipolar disorder

BD-II: type II bipolar disorder

BDNF: brain-derived neurotrophic factors

BMI: body mass index

BSR: bootstrap ratio

CAT12: Computational Anatomy Toolbox

CC: corpus callosum

C-C: C-C motif chemokine ligand

CCA: canonical correlation analysis

CGC: cingulate gyrus

CGH: perihippocampal cingulum tract

CI: confidence intervals

CIRS: compensatory immunoregulatory system

CM: central memory

CNV: copy number variation

CQ: Cognition Questionnaire

CR: corona radiata

CRP: C-reactive protein

CSF: cerebrospinal fluid

CST: cortico-spinal tract

CT: cortical thickness

CTQ: Childhood Trauma Questionnaire

C-X-C: C-X-C motif chemokine ligand

DB: Davies-Bouldin score

DMN: default mode network

DSM: Diagnostic and Statistical Manual of Mental Disorders

DTI: Diffusion Tensor Imaging

EC: external capsule

ECT: Electro-Convulsive Treatment

EM: effector memory

EN: elasticnet

ENIGMA: Enhancing Neuro Imaging Genetics through Meta-Analysis

FA: fractional anisotropy

FACS: fluorescence-activated cell sorting

fALFF: fractional amplitude of low-frequency fluctuations

FBS: Fetal Bovie Serum

FC: functional connectivity

FDR: false discovery rate

FMO: Fluorescence Minus One

fMRI: functional magnetic resonance imaging

FPN: fronto-parietal network

FSC-A: Forward scatter

FSL: FMRIB Software Library

FWHM: full width at half maximum

FX: fornix

FXST: fornix – stria terminalis

GCC: genu of corpus callosum

G-CSF: granulocyte colony stimulating factor

GLM: general linear model

GM: grey matter

GM-CSF: granulocyte macrophage colony stimulating factor

GPC: Psychiatric Genomic Consortium

Grz: granzyme

GWAS: genome-wide association studies

HALFFpipe: Harmonized AnaLysis of Functional MRI pipeline

HDL: High-Density Lipoprotein

HDRS-21: Hamilton depression rating scale – 21 items

HGF: hepatocyte growth factor

HiTOP: Hierarchical Taxonomy of Psychopathology

HPA: hypothalamic-pituitary-adrenal axis

IC: internal capsule

ICD: International Classification of Diseases

IFG: inferior frontal gyrus

IFOF: inferior fronto-occipital fasciculus

IL: interleukin

IL-1Ra: interleukin-1 receptor antagonist

INF: interferon

IPL: inferior parietal lobule

IRS: immune-inflammatory response system

LIF: leukaemia inhibitory factor

LV: latent variable

MAIT: Mucosal Associated Invariant T-cells

M-CSF: macrophage colony stimulating factor

MD: mean diffusivity

MDD: Major Depressive Disorder

MFC: medial frontal cortex

MFG: middle frontal gyrus

MFI: median fluorescence intensities

MIF: migration inhibitory factor

ML: machine learning

MNI: Montreal Neurological Institute

MOG: middle occipital gyrus

MRI: magnetic resonance imaging

MTG: medial temporal gyrus

NGF: nerve growth factor

NK: natural killer

NODDI: neurite orientation and density imaging

OFC: orbitofrontal cortices

PBMC: peripheral blood mononuclear cells

PCC: posterior cingulate cortex

PCR: posterior corona radiata

PDGF-BB: platelet-derived growth factor-BB

Perf: perforin

PFC: prefrontal cortices

PLIC: posterior limb of internal capsule

PLS: partial least squared

PLSC: partial least squared correlation

PMA: phorbol 12-myristate 13-acetate

PTR: posterior thalamic radiation

RD: radial diffusivity

RDoC: Research Domain Criteria

ReHo: regional homogeneity

RLIC: retrolenticular limb of internal capsule

ROI: regions of interest

RPMI: Roswell Park Memorial Institute

rs-fMRI: resting state functional magnetic resonance imaging

SCC: splenium of corpus callosum

SCF: stem cell factor

SCID-5: Structured Clinical Interview for the Diagnosis of Axis I Disorders

SCR: superior corona radiata

SFG: superior frontal gyrus

SFO: superior fronto-occipital fasciculus

Sil: Silhouette score

SLF: superior longitudinal fasciculus

SN: salience network

Sneg: negative functional connectivity strength

SNP: single nucleotide polymorphism

SPM: statistical parametric mapping

Spos: positive functional connectivity strength

SS: sagittal stratum

SSC-A: Side scatter

STG: superior temporal gyrus

SVM: support vector machine

SZ: schizophrenia

TBSS: Tract Based Spatial Statistics

TEMRA: T cells re-expressing CD45RA

Th: T helper cells

TIV: total intracranial volume

TMS: Transcranial Magnetic Stimulation

TNF: tumour necrosis factor

TRAIL: TNF-related apoptosis-inducing ligand

TTG: transverse temporal gyrus

UNC: uncinate fasciculus

VEGF: vascular endothelial growth factor

WHO: World Health Organization

WM: white matter

YLDs: years lived with disability

LIST OF FIGURES AND TABLES

Figures

Figure 1. Cortical alterations in MDD patients compared to healthy controls 19
Figure 2. Cortical alterations in BD patients compared to healthy controls 21
Figure 3. Immune-related neurobiological mechanisms involved in Mood Disorders. 29
Figure 4. Schematic representation of Beck's cognitive model of depression. 33
Figure 5. Approaches for disentangling heterogeneity in psychiatry 39
Figure 6. Cohen's d values describing the magnitude of differences in positive and negative strength values between the FC-based clusters. 49
Figure 7. Cohen's d values describing the magnitude of differences in regional grey matter volumes between clusters 51
Figure 8. Cohen's d values describing the magnitude of differences in cortical thickness between clusters 52
Figure 9. Cohen's d values describing the magnitude of differences in DTI diffusivity values between clusters. 57
Figure 10. Cohen's d values describing the magnitude of differences in neuroimaging features between the multimodal-derived clusters 59
Figure 11. Cohen's d values describing the magnitude of differences in immune cell counts between clusters 61
Figure 12. Cohen's d values describing the magnitude of differences in immune-inflammatory profiles between clusters. 63
Figure 13. Differences in multivariate brain-ACEs relationships between the FC-based clusters 65
Figure 14. Differences in multivariate biological-trauma relationships between the immune-based clusters 66
Figure 15. Mediation effect of FC LV scores in the relationship between CTQ LV scores and CQ generalization across time in Cluster 2 67
Figure 16. Gating strategy for Lymphocytes and Mait cells. 95
Figure 17. Gating strategy for Cytotoxic T-lymphocytes, NK, and T γδ panel 96
Figure 18. Gating strategy for T-lymphocytes and NK cells cytokines panel 97
Figure 19. Gating strategy for T regulatory lymphocytes panel 98
Figure 20. **Graphic representation of the analysis pipeline** 100

Tables

Table 1. Descriptive statistics of the whole sample 46
Table 2. Clustering models' performance 47
Table 3. Clinical and demographic comparisons for the FC-based clusters 48
Table 4. Clinical and demographic comparisons for clusters derived from extracted GM volumes 50
Table 5. Clinical and demographic comparisons for clusters derived from cortical thickness 51
Table 6. Clinical and demographic comparisons for the AD-based clusters 53
Table 7. Clinical and demographic comparisons for the FA-based clusters 54
Table 8. Clinical and demographic comparisons for the MD-based clusters 55
Table 9. Clinical and demographic comparisons for the RD-based clusters 56
Table 10. Clinical and demographic comparisons for the multimodal-derived clusters 58
Table 11. Clinical and demographic comparisons for the FACS-derived clusters 60
Table 12. Clinical and demographic comparisons for the clusters derived from immune-inflammatory profiles. 62
Table 13. Definition of immune-inflammatory profiles. 90
Table 14. Immune cells populations for each panel used for ML analyses 99

Appendix

Appendix 1. List of the selected ROIs for fMRI features 140
Appendix 2. ML algorithms used in single-feature stratification models 144
Appendix 3. Normalized stability plots for each clustering model 148
Appendix 4. Differences in positive and negative strength values for each region between the FC-based clusters 148
Appendix 5. Differences in grey matter volumes for each region between the GM-based clusters. 158
Appendix 6 Differences in cortical thickness for each region between the CT-based clusters. 161
Appendix 7. Differences in axial diffusivity values for each tract between the AD-based clusters 163
Appendix 8. Differences in fractional anisotropy values for each tract between the FA-based clusters 164

Appendix 9. Differences in mean diffusivity values for each tract between the MD-based clusters..... 165
Appendix 10. Differences in radial diffusivity values for each tract between the RD-based clusters..... 167
Appendix 11. Differences in neuroimaging features between the multimodal-based clusters 168
Appendix 12. Differences in immune cells count between the FACS-based clusters..... 186
Appendix 13. Differences in immune-inflammatory Z-scores between the clusters derived from immune-inflammatory profiles...... 188

1. INTRODUCTION

1.1 Mood Disorders

The term Mood Disorders refers to a set of mental conditions characterized by long-lasting alterations in emotional and motivational states, with detrimental consequences on the individual normal functioning (Rakofsky & Rapaport, 2018). The Diagnostic and Statistical Manual of Mental Disorders, Fourth Edition (DSM-IV) (American Psychiatric Association, 1994) classifies Mood Disorders into Depressive Disorders and Bipolar Disorders (BD), with the core clinical discriminating feature being the absence of preceding manic, mixed, or hypomanic episodes in the case of Depressive Disorders. However, the DSM Fifth Edition Text Revision (DSM-5-TR) (American Psychiatric Association, 2022) define a distinct chapter for "Bipolar and Related Disorders" not included in Mood Disorders to take into account the translational nature of BDs between depression and psychosis (Goodwin & Jamison, 1990).

1.1.1 Major Depressive Disorder

According to the DSM-5-TR, Major Depressive Disorder (MDD) is defined by the occurrence of distinct depressive episodes lasting at least two weeks, separated by remissions (American Psychiatric Association, 2022). For the diagnosis of MDD, at least one of two core symptoms (i.e., depressed mood and anhedonia) should be present. Along with them, at least other four symptoms are required, such as changes in appetite; sleep disturbances (i.e., insomnia or hypersomnia); changes in psychomotor activity (i.e., retardation or agitation); fatigue or loss of energy; feelings of worthlessness or exaggerate guilt; difficulties in thinking, making decisions, and concentrating; thoughts of death, suicidal ideation, or suicide attempts. As stated by the World Health Organization (WHO) World Mental Health Survey (Scott et al, 2018), the MDD prevalence is estimated at 10% globally, and more than 40% in prospective studies (Moffitt et al, 2010). The Global Burden of Disease Study (2022) further demonstrated the significant impact of mental illnesses on disability worldwide, with depressive disorders representing the largest percentage of mental illnesses years lived with disability (YLDs) (37%) (GBD Mental Disorders Collaborators, 2022). The first onset of MDD typically occurs around 20-25 years old with a median episode duration from 2 to 6 months in the general population (Marx et al, 2023). Of note, while remission is usually observed within 12 months and

about 10% of patients experience persistent depression (i.e., episodes longer more than 12 months) in community surveys, this rate increases up to 60% in primary and secondary care settings, with only a partial remission between episodes (Herrman et al, 2022; Marx et al, 2023) and a lack of response to antidepressant treatments in about 30% of cases (McIntyre et al, 2023). Another crucial aspect linked to the relevant burden of MDD is the high risk of mortality: compared to the general population, people affected by MDD show a greater prevalence of comorbid conditions, which contributes significantly to the early mortality associated with it (Plana-Ripoll et al, 2019). Also, suicide represents an important cause of premature death in MDD, with having a diagnose of MDD increasing the risk of committing suicide up to 19% (Chesney et al, 2014).

1.1.2 Bipolar Disorders

BDs can be defined as a set of chronic clinical conditions characterized by severe swings in mood and energy levels, leading to significant cognitive and functional impairments. The DSM-5 classifies BD into bipolar I disorder (BD-I) and bipolar II disorder (BD-II), which are differentiated from cyclothymia (American Psychiatric Association, 2022). BD-I is described by the history or the presence of a manic episode (i.e., an extended time of unusually high mood, levels of energy or goal-oriented activity that lead to noticeable functional deterioration). Even though depressive episodes or subclinical depression could be recognized in BD-I patients, they are not needed for the diagnosis of BD-I since mania in the absence of depression can be observed in about 5% of BD-I cases (i.e., unipolar mania) (Vieta et al, 2018). Conversely, BD-II is defined by the presence of at least one hypomanic episode (i.e., a milder manic episode that does not compromise functioning) and one major depressive episode. Notably, during the course of BD-II, the preeminent episodes are the depressive ones, raising important challenges for the clinical differential diagnosis between BD-II and MDD. However, some clinical features have been recognized as suggestive of bipolar depression and might be helpful in guiding diagnostic processes (e.g., early age of onset, the presence of hyperphagia, hypersomnia, and psychosis, high incidence of episodes, psychiatric comorbidity, and family history of psychiatric disorders) (McIntyre et al, 2020). Finally, cyclothymia refers to a distinct clinical condition from both BD-I and BD-II characterized by emotional instability lasting more than 2 years accompanied by symptoms of depression and hypomania that do not fit into the traditional definition of depressive and hypomanic

episodes. Importantly, the presence of a cyclothymic temperament has been demonstrated to significantly predict BD, especially BD-II, suggesting that it might be considered a prodromal condition to BD (Karam et al, 2023).

The estimated lifetime prevalence of BD is approximately 2.5% in worldwide epidemiological studies, with a median age of onset before 25 years old in both sexes (McGrath et al, 2023). The onset of BD during childhood or adolescence has been associated with high psychiatric comorbidities, such as attention-deficit/hyperactivity disorder (ADHD), substance abuse and anxiety disorders, and high risk of suicide (18–20% 5-year prevalence) (Cirone et al, 2021). Despite this evidence, recent meta-analytic findings reported a delay of about 6 years between the onset of the first episode and diagnosis, with a median duration of untreated episodes of 5.9 years. Notably, these time delays are shorter for BD-I patients with psychotic symptoms or manic polarity, which are, however, more unlikely to occur compared to depressive onsets (Scott et al, 2022). The clinical management and the diagnostic process of BD are further complicated by the presence of coexisting conditions, which are reported in about 90% of BD cases (Merikangas et al, 2007). They include both psychiatric disorders, with anxiety disorders showing the highest prevalence rates (70-90%) (McIntyre et al, 2020; Yapici Eser et al, 2018), but also medical conditions, including metabolic, endocrine, cardiovascular and cardiometabolic disorders, which are reported in 7.5% to 35.6% of BD cases (Onyeka et al, 2019). Comorbidity not only has been associated with a worse illness course (e.g., earlier onset of the disorder, higher suicidality risk, and treatment resistance) but also with premature death (McIntyre et al, 2020). Recent meta-analytic findings indicate that in individuals with BD, the risk of mortality due to medical conditions is up to 4-fold higher compared to the general population (Biazus et al, 2023). Among them, cardiovascular disorders are the primary cause of mortality due to medical conditions in BD, which is also reflected by the higher cardiovascular risk in BD patients and first-degree relatives compared to healthy individuals (Coello et al, 2019; Weiner et al, 2011). In addition to physical conditions, also suicidality significantly impacts the mortality rates in BD: in fact, the risk of committing suicide is 20% higher in BD cases compared to the general population (Gonda et al, 2012).

1.2 Sources of heterogeneity in Mood Disorders

The huge impact of mood disorders both at the social and economic levels asks for increasing efforts to improve diagnostic procedures and clinical management. However, despite being assigned to the same diagnostic category, patients within a specific condition show different patterns of disease progression that may require patient-tailored treatments. This is particularly evident for MDD, where the polythetic approach of current diagnostic systems uncovers a relevant heterogeneity in the clinical manifestations of the disorder, with up to 227 possible ways to meet diagnostic criteria (Zimmerman et al, 2015). Despite the use of screening tools that could aid clinicians in the diagnostic procedure, the lack of hierarchy or primacy among symptoms flatters the differences among markedly diverse clinical manifestations, which conversely are linked to distinct progression trajectories and may require specific treatments (Malhi & Mann, 2018). Also, BD is highly heterogeneous, as reflected by the overlapping symptomatology with schizophrenia (SZ) and MDD, and the varied clinical manifestations in terms of clinical outcomes, response to treatments, and comorbidities (Charney et al, 2017).

The observed heterogeneity at the phenotypic level is mainly ascribable to the complex genetic architecture of both BD and MDD, with strong evidence of genetic overlap with other psychiatric disorders (i.e., SZ, ADHD, and autism spectrum disorder [ASD]) (Devlin et al, 2013). Nevertheless, despite the relevant heritability estimates (37% for MDD, 70-90% for BD) (Gordovez & McMahon, 2020; Sullivan et al, 2000), these disorders are thought to be best described by a multifactorial model of gene-environment interactions (Misiak et al, 2018; Uher, 2008). Indeed, psychiatric disorders are defined as "complex traits", meaning that their aetiology stems from the amalgamation of genetic, environmental, and lifestyle factors (Gratten et al, 2014). This complexity supposedly indicates the presence of multiple disorder subtypes linked to specific aetiologies that, despite converging to the same diagnosis, are phenotypically variegated across the behavioural, cognitive, and clinical domains. An overview of the main source of heterogeneity within Mood Disorders is described in the next paragraphs.

1.2.1 Genetics and epigenetic factors

As previously mentioned, both MDD and BD are highly heritable, with genetic heritability contributing up to 85% of the risk of developing both disorders (Sullivan et

al, 2000). Large-scale genome-wide association studies (GWAS) identified up to 178 genetic risk loci associated with MDD, which were particularly enriched in brain regions known to be involved in depression, such as the hypothalamus, prefrontal cortices (PFC), and nucleus accumbens (Levey et al, 2021; the 23 and Me Research Team, 2019). However, one of the most debated issues concerns the selection of MDD cases, which is usually based on a broad range of definitions, including the International Classification of Diseases (ICD) codes but also self-reported questionnaires (Flint, 2023). Moreover, the heterogeneous nature of MDD significantly limits the strength of associations of genetic variants in GWAS, resulting in inconsistencies among studies (Levinson et al, 2014). By stratifying depression cases from the UKBiobank on a wide range of clinical features, a recent GWAS study reported subtype-specific heritability rates of single nucleotide polymorphisms (SNP) with genetic correlations among subtypes spanning from 0.5 to 0.86. These findings suggest that each phenotypic MDD subtype has a unique genetic vulnerability, which might be overlooked when considering MDD cases as a whole (Nguyen et al, 2022). Regarding BD, the largest GWAS carried out so far from the Psychiatric Genomic Consortium (PGC3) identified 68 loci associated with the disorder, most of them being enriched in synaptic and neuronal pathways (especially in PFC and hippocampi) and calcium channel signalling. Despite the small effects of individual SNPs (odd ratios spanning from 1.053 to 1.146), the cumulative SNPs heritability explained about 18% of phenotypic variance, confirming the polygenic nature of BD. By also exploring the genetic associations with other psychiatric disorders, the GPC3 GWAS provided evidence of shared genetic variation (i.e., pleiotropy) between BD and SZ (0.68) and MDD (0.44), which is indicative of a partially common genetic vulnerability (Mullins et al, 2021).

Together with common genetic variants, also structural variations (i.e., copy number variation [CNV]) and *de novo* mutations (i.e., genetic variants that are present in probands' genome but not in the parental one) have been detected in Mood Disorders. Considering MDD, whole-exome sequencing studies demonstrated that rare variants contributed only in a small proportion to the genetic risk for MDD, which conversely was largely explained by common SNPs (>8%) (Peterson et al, 2017). A different scenario was described for BD, where a significant enrichment of rare variants was reported. However, while most of these rare variants were detected in genes derived from SZ exome

meta-analysis, no significant enrichment was detected for genes derived from BD GWAS, possibly due to their small sample size compared to SZ GWAS (Palmer et al, 2022). Evidence from the analysis of CNVs partially aligns with findings from whole-exome sequencing studies, demonstrating that the CNV burden is significantly increased for BD subtypes (i.e., schizoaffective BD, BD-I, BD-II) compared to controls, while no significant differences were found when considering BD as a unique entity. Overall, these results suggest that rare variants do not heavily contribute to BD aetiology as in other strongly genetic-determined psychiatric disorders (e.g., SZ, ASD), but their relevance might be better captured by focusing on specific BD subtypes (Charney et al, 2019).

Despite the strong genetic component, not all the variance associated with MDD and BD is completely explained by genetic factors, indicating an additional contribution of environmental influences to the aetiology of Mood Disorders. However, the role of gene-environment interactions in psychiatric disorders is still a discussed topic given the several methodological issues raised in this field (e.g., small sample sizes, inappropriate modelling on confounding variables, and the relevant positive publication bias) (Duncan & Keller, 2011). One of the most studied gene-environment interactions in depression literature in the moderating effect of a polymorphism in the promoter region of the serotonin-transported gene (5-HTTLPR) on the relationship between exposure to stressful life events and depressive symptomatology. As demonstrated by Caspi et al (2003) in their seminal paper, individuals carrying one or two copies of the short allele in this polymorphic region are more at risk of depression and suicide in response to stressful situations compared to those homozygous for the long allele. However, evidence supporting the influence of 5-HTTLPR-by-stress interaction in the aetiology of depression is still controversial (Karg et al, 2011; Sharpley et al, 2014). The most probable explanation for these inconsistencies is the small effect of single candidate gene polymorphisms on the phenotypic variance, meaning that large and deeply genetically and environmentally profiled cohorts are needed to reach adequate statistical power (Duncan & Keller, 2011).

1.2.2 Structural neuroimaging correlates

The intricate genetic architecture and complex gene-environment combinations contributing to the aetiology of psychiatric disorders make it difficult to find a direct encoding between genes and clinical phenotypes. Conversely, focusing on intermediate

phenotypes (i.e., endophenotypes) allows us to explore the indirect effects of genetic vulnerability on clinical outcomes through other biological pathways more proximal to psychiatric manifestations. An example of such endophenotypes is the neural system since is more directly affected by genetic variations than the disorder itself (Meyer-Lindenberg & Weinberger, 2006).

With the advent of neuroimaging techniques, it was possible to investigate the neurobiological mechanisms involved in Mood Disorders, providing novel insights into disorder-specific but also transdiagnostic brain alterations. At the structural level, cortical thinning in the medial orbitofrontal cortices (OFC), anterior and posterior cingulate gyrus, and insular and temporal cortices are some of the most consistent findings in MDD (Schmaal et al, 2017). What unites these regions is their strong connections with the limbic system, which aligns with the one of most accepted neurobiological theories of depression focusing on cortico-limbic dysfunctions as a core pathophysiological mechanism (Mayberg, 1997). Of note, these alterations were observed in adult but not in adolescent MDD patients, who conversely were characterized by smaller surface areas in medial OFC, superior frontal gyrus (SFG), and primary sensory and motor areas (Schmaal et al, 2017) (Figure 1). Given that cortical thickness and surface area are associated with genetically independent developmental trajectories (Winkler et al, 2010), these findings suggest that different morphological alterations could be observed in the MDD population according to the individual developmental age. In line with this consideration, several studies investigating the brain-predicted age difference (i.e., the discrepancy between the individual age estimated from the brain morphological measures and the actual chronological age) reported an advanced brain aging from 1 to 4 years in MDD patients compared to controls. These effects seemed not be affected by individual clinical features (e.g., age of onset, recurrences, remission state, antidepressant use, severity of depression), suggesting that biological ageing could be a core pathophysiological mechanism of MDD that transcends the individual trajectories of the disorder (Han et al, 2021; Koutsouleris et al, 2014).

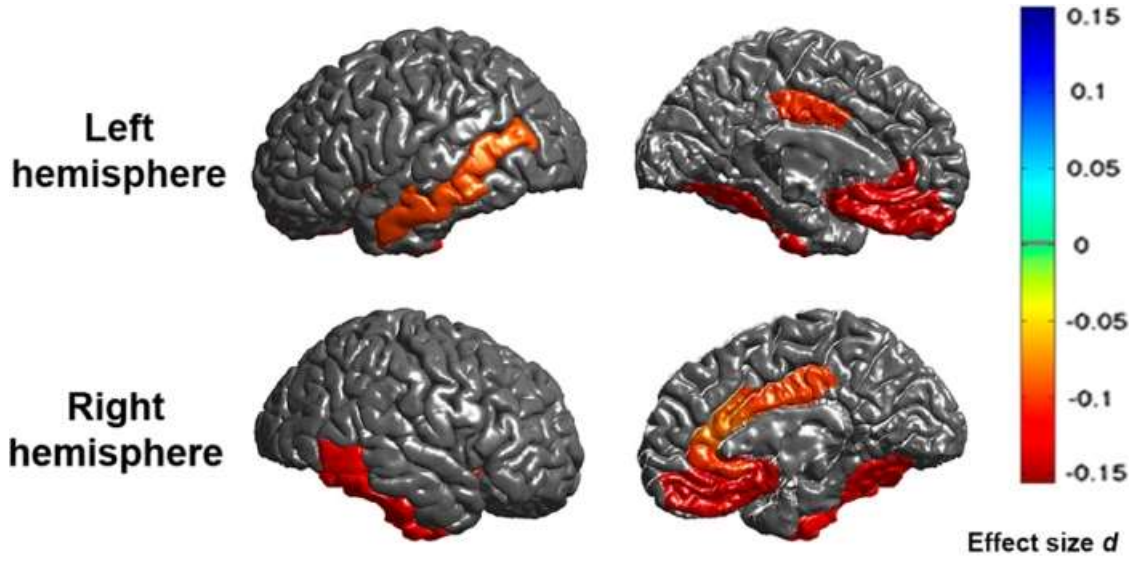

Figure 1. Cortical alterations in MDD patients compared to healthy controls. *Cohen's d effect sizes are plotted for each region of interest on the cortical surface of a template image. Reprinted from Schmaal et al (2017) (Open Access Source)*

Another well-known morphological brain alteration reported in MDD is hippocampal atrophy. Meta-analytic evidence from the Enhancing Neuro Imaging Genetics through Meta-Analysis (ENIGMA) consortium described a volumetric hippocampal reduction of about 1.24% in MDD patients compared to controls, which was more prominent in recurrent and early-onset individuals (Schmaal et al, 2016). Converging evidence was provided when focusing on subcortical shape metrics, demonstrating that these effects are circumscribed to specific hippocampal subfields, such as the subiculum and corpus ammonis (Ho et al, 2022). A possible explanation for these robust effects is proposed by the "neurotrophic hypothesis of depression". According to this hypothesis, the overactivation of the hypothalamic-pituitary-adrenal (HPA) axis typically reported in MDD induces an enhanced release of glucocorticoids, which in turn promote brain atrophy by altering the expression of neurotrophic factors (e.g., brain-derived neurotrophic factors [BDNF]) (Duman & Li, 2012). Among all the brain structures, the hippocampus seems to be specifically targeted by these processes given its enrichment of glucocorticoid receptors, which make it more vulnerable to the detrimental side effects of increased glucocorticoid production (e.g., dendritic shrinkage, neurogenesis blockage, and neural loss) (McEwen et al, 2015; Sapolsky et al, 1984). Indeed, increased hippocampal volumes and peripheral BDNF levels after antidepressant treatment has

been reported in animal and post-mortem studies (Boldrini et al, 2013; Santarelli et al, 2003), suggesting that neuronal plasticity might represent a candidate mechanism through which pharmacological but also biological interventions (e.g., Electro-Convulsive Treatment [ECT], transcranial magnetic stimulation [TMS]) exert their beneficial effects (Luan et al, 2020; Ozkan et al, 2024). More controversial are the results regarding the volumetric reduction of the amygdalae in MDD, with some studies providing evidence of reduced volumes (Kronenberg et al, 2009; Zhang et al, 2016), and others reporting volumetric enlargement or no significant changes compared to controls (Lorenzetti et al, 2010; Vassilopoulou et al, 2013). These inconsistencies might arise from the anatomical heterogeneity of the amygdalae, which are composed by several cellular nuclei specialized in different aspects of emotional processing (Labuschagne et al, 2024; Pitkänen et al, 1997). Using more precise and advanced techniques to capture localized effects in subcortical volumes, recent studies described a volumetric reduction in the basolateral amygdaloid complex in MDD patients, especially in those experiencing recurrences (Roddy et al, 2021; Yao et al, 2020). Given its role in memory consolidation and response to threats, this subfield is particularly sensible to chronic exposure to stress, which promotes plastic neural changes (e.g., spinogenesis, dendritic elongation) that affect its morphology and function (Roozendaal et al, 2009).

Regarding BD, evidence from cross-sectional structural neuroimaging studies indicates widespread cortical abnormalities, with the largest effects being reported in left pars opercularis, fusiform gyrus, and rostral middle frontal cortex (Hibar et al, 2018) (Figure 2). These effects were more pronounced in older patients and those with a longer duration of illness, suggesting a progressive neural deterioration accompanying the clinical and cognitive worsening of the disorder (a phenomenon known as “neuro progression”) (Berk et al, 2017). However, the extent to which this process is involved in BD is still questioned due to the lack of longitudinal studies and the consistent heterogeneity in brain alterations within the BD population (Martino et al, 2016). Considering the longitudinal evidence so far, multi-centre studies failed to detect widespread and progressive cortical thinning in BD relative to controls, except for faster cortical thinning in PFC with the increasing number of manic/hypomanic episodes. On the other hand, significant ventricular enlargement and subcortical volume reductions over time were observed in BD patients compared to controls (Abé et al, 2022; Abé et al,

2023). Several potential neurobiological mechanisms leading to neuroprogression have been proposed, such as alterations in glutamatergic and dopaminergic systems, inflammatory processes, oxidative stress and mitochondrial abnormalities (Berk et al, 2011), despite other contributing factors (e.g., lithium treatment, genetic vulnerability, and the incidence of mood episodes) has been shown to affect cortical structures (Abé et al, 2020; Cahn et al, 2021; Roberts et al, 2022).

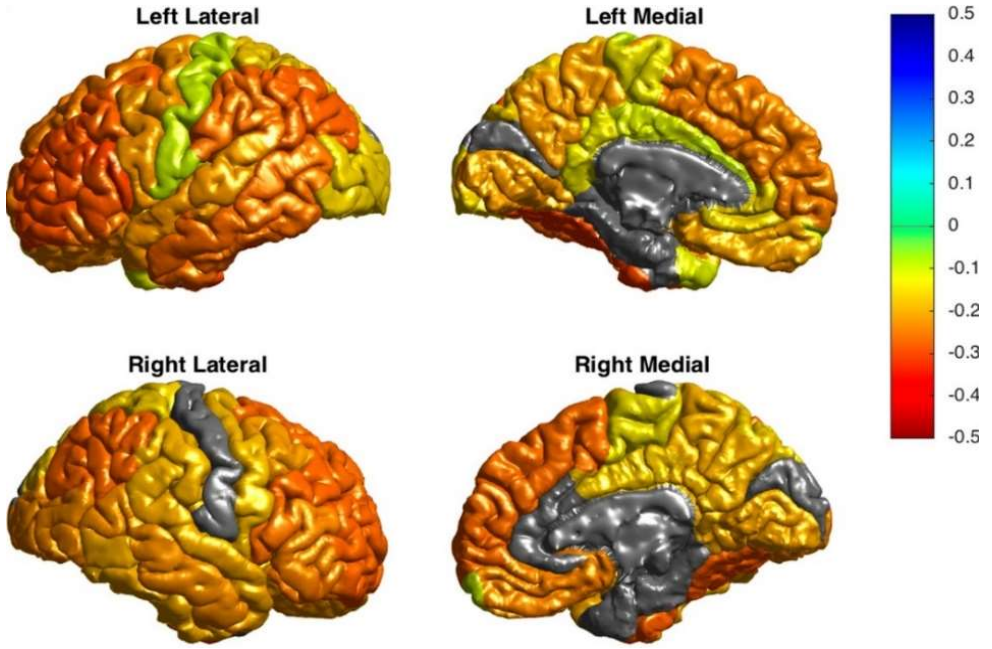

Figure 2. Cortical alterations in BD patients compared to healthy controls. *Cohen's d effect sizes are plotted for each region of interest on the cortical surface of a template image. Reprinted from Hibar et al (2018) (Open Access Source)*

The evidence of morphological cortical and subcortical alterations in MDD and BD is paralleled by findings from Diffusion Tensor Imaging (DTI) studies investigating the microstructural proprieties of white matter (WM) tracts. Most of these studies reported a widespread WM disruption in MDD patients relative to healthy controls, as reflected by lower fractional anisotropy (FA) and higher radial diffusivity (RD)[1] in interhemispheric, association, and commissural tracts (Chen et al, 2017; Van Velzen et al, 2020). These

[1] *Together with Axial Diffusivity (AD) and Mean Diffusivity (MD), FA and RD represent 2 measures of water diffusion that can be extracted from DTI to indirectly assess the integrity of WM tracts. Most common alterations are reflected by: decreased FA, being usually associated to microstructural damages due to demyelination; decreased AD, reflecting axonal damage; increased MD, indicating a reduction in membrane density usually linked to tissue degeneration; increased RD, suggesting incomplete myelination processes following axonal damage (Alexander et al., 2007).*

effects were mainly detected in the corpus callosum (CC) and the anterior corona radiata (CR), suggesting that MDD could be described as a "disconnection syndrome" in which both cortico-cortical and subcortical-cortical communications are affected (Liao et al, 2013). The fact that these alterations were primarily observed in adult and recurrent patients might be indicative of an incremental influence of stress on WM microstructure, probably consequent to the increased levels of glucocorticoids and neuroinflammatory processes in response to stressors (Gianaros et al, 2013; Howell et al, 2013).

Similar to MDD, structural disconnections involving WM tracts connecting frontal and limbic areas have been proposed as a candidate biomarker for BD (Phillips & Swartz, 2014; Vai et al, 2019). Nevertheless, increasing evidence from DTI studies suggests that these alterations are not limited to cingulate and amygdala-hippocampal connections (Benedetti et al, 2011a; Nortje et al, 2013; Vederine et al, 2011), but also to tracts external to the limbic system, including the CC and CR (Benedetti et al, 2011b; Favre et al, 2019; Leow et al, 2013; Repple et al, 2017). In particular, reduced callosal integrity was specifically associated with a history of psychotic features, suggesting that interhemispheric disconnection could represent a potential neurobiological correlate of psychosis in BD (Sarrazin et al, 2014). In line with this hypothesis, studies comparing the differences in WM integrity between BD and SZ consistently reported similar microstructural alterations in the CC, while disorder-specific dysconnectivity patterns were found in the cingulum and the anterior limb of CR (Squarcina et al, 2017; Zhao et al, 2022). Transdiagnostic studies, however, showed that almost overlapping alterations in the same WM tracts can be also found in MDD patients, indicating that the interhemispheric dysconnectivity might represent a shared neurobiological underpinning cutting across affective and psychotic disorders (Cui et al, 2020). In support of the dysconnectivity hypothesis (van den Heuvel & Sporns, 2019), recent studies have employed graph theory techniques to describe alterations in the neural "connectome" in terms of integration and segregation within and across brain networks (Bullmore & Sporns, 2009). A large multicentre study showed that the structural connectome of BD patients is characterized by longer characteristic path lengths (a measure of the level of integration within a network, where shorter paths reflect a better integration) and higher dysconnectivity within the frontoparietal network compared to controls (Nabulsi et al, 2022). Notably, a subsequent transdiagnostic study described a gradient in the global

efficiency within a common structural network between BD, MDD, and SZ, with SZ patients showing the lowest network efficiency. This network involved widespread connections, which allowed to differentiation of psychiatric patients from controls with moderate accuracies (0.54-0.60 accuracy range) (Repple et al, 2023). According to these findings, while alterations in long-range connections could be a neural marker shared across psychiatric disorders, dysconnections within the frontoparietal network might represent a disorder-specific signature of BD, possibly reflecting cognitive deficits and aberrant reward sensitivity commonly observed in these patients (Repple et al, 2023).

1.2.3 Functional neuroimaging correlates

The most widely used technique to investigate functional neural correlates is functional magnetic resonance imaging (fMRI), which captures changes in blood deoxyhemoglobin concentrations while performing a task (i.e., task-based fMRI) or at rest (i.e., resting-state fMRI [rs-fMRI]), providing an indirect measure of brain activity (Glover, 2011). The literature dealing with alterations in brain functions in Mood Disorders, however, presents conflicting findings. The small sample sizes, clinical heterogeneity, and technical differences in image acquisition and preprocessing represent the main reasons for these inconsistencies. The lack of consensus is particularly evident for task-based fMRI studies due to the differences in experimental designs and procedures (Pilmeyer et al, 2022). In line with these considerations, a meta-analysis of task-based fMRI studies in MDD failed to report any significant pooled difference between patients and controls, neither for emotional nor cognitive tasks (Müller et al, 2017). More consistent evidence has been reported for BD, since meta-analytic findings highlighted higher activations in the amygdala, hippocampus, caudate, temporal cortices, and middle frontal gyrus (MFG) in response to emotional stimuli compared to controls, while the inferior frontal gyrus (IFG) and anterior cingulate cortex (ACC) were hypoactivated (Ahmed et al, 2023). Of note, hyperactivations in the amygdala and hippocampus were observed in euthymic BD patients only, which suggests that dysfunctional cortico-limbic connections could represent a trait-marker of BD regardless of mood state (Vai et al, 2019). Together with emotional processing and regulation, also impairments in reward processing and cognitive functions have been investigated in BD through task-based fMRI. Results from the meta-analysis by Mesbah et al (2023) describe an overactivation in the left OFC during a reward task in BD patients compared to controls, which might

underlie the hypersensitivity to rewards commonly observed in these patients (Alloy et al, 2016). Regarding cognitive impairments, BD patients show an increased activation in the subgenual ACC and ventromedial PFC during working memory tasks relative to controls, both regions being involved in the integration of the cognitive and emotional aspects of external stimuli (Mesbah et al, 2023).

A second line of research focused on alterations in large-scale functional networks assessed through rs-fMRI. These networks can be described as complexes of brain regions that show highly synchronized neural activity (i.e., high temporal correlations) while performing a task or at rest, possibly reflecting a joint contribution in specific cognitive or emotional functions (Biswal et al, 1995; Greicius et al, 2003). Regarding Mood Disorders, rs-fMRI studies carried out so far highlighted the involvement of three main resting-state networks: the fronto-parietal network (FPN), the salience network (SN), and the default mode network (DMN). In normal conditions, these networks show patterns of reciprocal synchronization or desynchronization in response to external stimuli, while the aberrant involvement or disengagement of one of these has been recognized in many psychiatric disorders (Menon, 2011). The literature about functional alterations of these networks in MDD, however, reports inconsistent data. Whereas some studies described reduced activations in the FPN and heightened activations within the DMN in MDD patients compared to controls (Kaiser et al, 2015), a recent mega-analysis failed to replicate these effects while highlighting reduced connectivity between sensory networks and the SN (Javaheripour et al, 2021). As explained by the authors, these conflicting findings might arise from heterogeneities in medication status, symptom profiles, and depression severity (Javaheripour et al, 2021). Future studies focusing on specific depression subtypes and drug-naïve patients are needed to clarify this point. Inconsistencies in rs-fMRI studies were also raised for BD. Indeed, mixed results have been reported in the literature, with some studies describing patterns of hyper- or hypo-activations within and between the DMN, SN and FPN (Claeys et al, 2022), while others did not report any significant differences between patients and controls (Syan et al, 2018). One of the most plausible explanations for this lack of agreement is the heterogeneity in patients' mood states and clinical features (Syan et al, 2018). More consistent evidence has been reported from studies focusing on changes in neural activity in specific regions of interest (ROIs) and their functional connectivity (FC) with other brain regions.

Reduced local spontaneous neural activity at rest (i.e., the amplitude of low-frequency fluctuations [ALFF] and regional homogeneity [ReHo] (Yu-Feng et al, 2007; Zang et al, 2004)) in the medial temporal gyrus (MTG), posterior cingulate cortex (PCC), and precuneus was consistently found in bipolar depression, coupled with increases in the IFG and inferior parietal lobule (IPL) regardless of medication status (Claeys et al, 2022). Considering hypomania, seed-based connectivity analyses revealed diminished FC between the amygdala and OFC, as well as within the cingulum, which could possibly reflect impairments in inhibitory control and emotion regulatory mechanisms observed in these patients (Claeys et al, 2022). Taken together, these results suggest that alterations in large-scale brain networks, especially in the DMN, could represent a hallmark of BD, despite specific mood-related dysfunctions could be identified (Vai et al, 2019).

1.2.4 Inflammatory markers

In addition to the research of the neural correlates of Mood Disorders, the involvement of other body systems (e.g., immune, cardiovascular, metabolic systems) has also been explored, and the theory that attributes the aetiology of many psychiatric disorders to multisystem body alterations is gaining ground (Tian et al, 2023). Among them, disruptions in innate and adaptive immunity mechanisms have been described both in MDD and BD, exerting damaging effects on neural mechanisms (Wohleb et al, 2016).

The first evidence of a strict link between depression and inflammatory processes comes from animal studies, demonstrating that rodents injected with pro-inflammatory markers or lipopolysaccharide exhibit a complete range of behaviours typically ascribable to sickness (e.g., motor inactivity, lack of pleasure or interest, lethargy, social isolation) (Dantzer, 2001). These so-called "sickness behaviours" are considered a physiological response of the organism to face infections, but the great resemblance with depressive symptoms points to the role of immune-inflammatory processes in clinical depression (Miller & Raison, 2016). This hypothesis is further supported by the high comorbidity of depression with autoimmune and inflammatory disorders (Wohleb et al, 2016), but also considering the consequences of pro- and anti-inflammatory treatments on depressive symptomatology, with the first fostering while the latter ameliorating them (Marx et al, 2023).

The research carried out so far mainly focused on MDD, demonstrating that MDD patients are characterized by increased concentrations of several pro-inflammatory cytokines compared to controls (Poletti et al, 2024). However, the considerable technical and clinical heterogeneity in these studies (e.g., different assays for analytes quantification, patients' clinical characteristics) prevents concluding the specificity of such markers in MDD aetiology (Poletti et al, 2024). Some of the most consistently reported in the literature include interleukin (IL)-6, IL-4, IL-8, IL-10, tumour necrosis factor (TNF)-α, and C-reactive protein (CRP). Meta-analytic findings reported significantly higher concentrations of IL-6, CRP, and TNF in depressed patients compared to controls (Dowlati et al, 2010; Haapakoski et al, 2015), while peripheral levels of interferon (INF)-γ are decreased (Köhler et al, 2017). Importantly, it has been argued that different immune-inflammatory signatures could be associated with specific MDD subtypes. For example, Lamers et al (2013) reported that MDD patients with atypical features show increased peripheral concentrations of CRP, IL-6, and TNF-α compared to patients with melancholic MDD and controls. This group was also characterized by metabolic alterations, as indicated by the higher body mass index (BMI), waist circumference, triglycerides, and lower High-Density Lipoprotein (HDL) cholesterol. Conversely, heightened cortisol levels in the absence of immune-inflammatory activation were described in patients with melancholic depression relative to the non-melancholic ones and controls. However, the study of differences in immune-inflammatory markers between depression subtypes is still in its infancy, and larger sample sizes and a more robust consensus on the definition of depression subtypes are needed (Yang et al, 2018). Not only pro-inflammatory but also anti-inflammatory cytokines are increased in MDD. For instance, increased IL-10 concentrations have been described in MDD patients compared to controls (Köhler et al, 2017), but only in those taking antidepressant medications, suggesting a potential mediating role of pharmacological treatment in downgrading immune-inflammatory activation by sustaining IL-10 immunosuppressive function (Poletti et al, 2024).

Despite being less explored than MDD, similar alterations in immune-metabolic functions have been reported in BD as well. One of the most consistent findings concerns the increase of IL-6 peripheral concentrations in BD patients relative to controls. As highlighted by a recent meta-analysis, elevated concentrations of IL-6 have been also

reported not only during depressive and manic states but also in euthymia, pointing out the potential role of IL-6 as a trait marker of BD (Solmi et al, 2021). In addition, high IL-6 concentrations are significantly associated with cognitive impairments (Poletti et al, 2021a) and poor antidepressant response (Benedetti et al, 2017). Conversely, TNF-α and CRP have been hypothesized to be state-dependent (Solmi et al, 2021), despite several inconsistencies about the associations with depressive and/or manic states (Benedetti et al, 2020). Considering anti-inflammatory cytokines, only IL-4 seems to be associated with BD since several studies consistently reported an increase in its peripheral levels regardless of mood state (Modabbernia et al, 2013). Recently, particular attention has turned to the investigation of the role of chemokines in BD aetiology, with some preliminary findings of altered peripheral profiles in these patients. The most solid evidence so far is represented by increased concentrations of chemokine (C-C motif) ligand 11 (CCL11), CCL24, and C-X-C motif chemokine ligand 10 (CXCL10) in BD patients relative to controls, whereas peripheral levels of CXCL8 were found to be decreased (Barbosa et al, 2013; Brietzke et al, 2009). Of note, a recent study aimed at distinguishing MDD patients from BD based on immune-inflammatory peripheral markers uncovered that BD diagnosis is best predicted by increased concentrations of several chemokines (i.e., CCL3, CCL4, CCL5, and CCL11), suggesting that alterations in chemotactic cytokines are more relevant to BD aetiology with respect to MDD (Poletti et al, 2021b).

In addition to studies focusing on cytokine alterations, another line of research has explored the role of T cell subpopulations in modulating immune-inflammatory response in Mood Disorders. One of the most well-recognized theories in this field states that both BD and MDD are distinguished by deficient T cell production, but this phenomenon occurs at different ages in the two disorders. In early age, MDD patients exhibit a premature ageing (i.e., senescence) of T cells characterized by incomplete maturation of T helper (Th) 2, Th17, and natural killer (NK) cells (Grosse et al, 2016b). This deficiency tends to worsen with advancing age since it extents to T regulatory (Treg) cells and combines with increasing monocyte inflammation (Grosse et al, 2016a). On the other hand, young BD patients show a pattern of T cell deficiency partially overlapping with that observed in MDD during adulthood, but some T cell subpopulations go towards maturation over time (e.g., Th17) (Drexhage et al, 2011). The evolution of T cell

maturation in BD, however, is also influenced by mood states, which further complicates the description of a precise immune-inflammatory signature. This is particularly evident for Th17 and Treg cells, with some studies reporting elevations during both the active phases of the illness and euthymia (Breunis et al, 2003; Drexhage et al, 2011), while others describing reductions or even no significant differences in euthymic BD patients compared to controls (Drexhage et al, 2011; Vogels et al, 2017).

The alterations in immune-inflammatory markers observed at the peripheral levels have been demonstrated to affect inflammatory processes in the brain through several pathways: the *humoral pathway*, where cytokines pass through the blood-brain barrier by being transported by epithelial and endothelial cells; the *neural pathway*, in which immune markers binds to peripheral afferent nerves (e.g., vagus nerve) and mediate the bidirectional translation of inflammatory signalling between the brain and the periphery; the *cellular pathway*, characterized by the migration of activated immune cells (e.g., lymphocytes, monocytes, and dendritic cells) to the brain through blood vessels and the lymphatic system (Miller et al, 2013). Once reach the brain, cytokines significantly affect neural processes involved in mood regulation in several ways, including the reduction of monoamines availability in the synapses; switch of tryptophan metabolism into kynurenine; the rise of glutamate cytotoxicity; reduction of BDNF expression; and microglia activation (Poletti et al, 2024; Wohleb et al, 2016) (Figure 3). As a consequence of this, several fMRI studies provided evidence of inflammation-mediated functional alterations in brain regions associated with reward processing and motivation (e.g., ventral striatum, basal ganglia), and in the decoding of threatening stimuli and social rejection (e.g., insula, amygdala, dorsal ACC), promoting anhedonia and a state of hypervigilance (Miller et al, 2013; Miller & Raison, 2016). These changes in neural activity are paralleled by a reduction in WM integrity and grey matter (GM) hippocampal and prefrontal volumes, possibly reflecting impairments in myelination mechanisms and diminished glial and synaptic density (Benedetti et al, 2020).

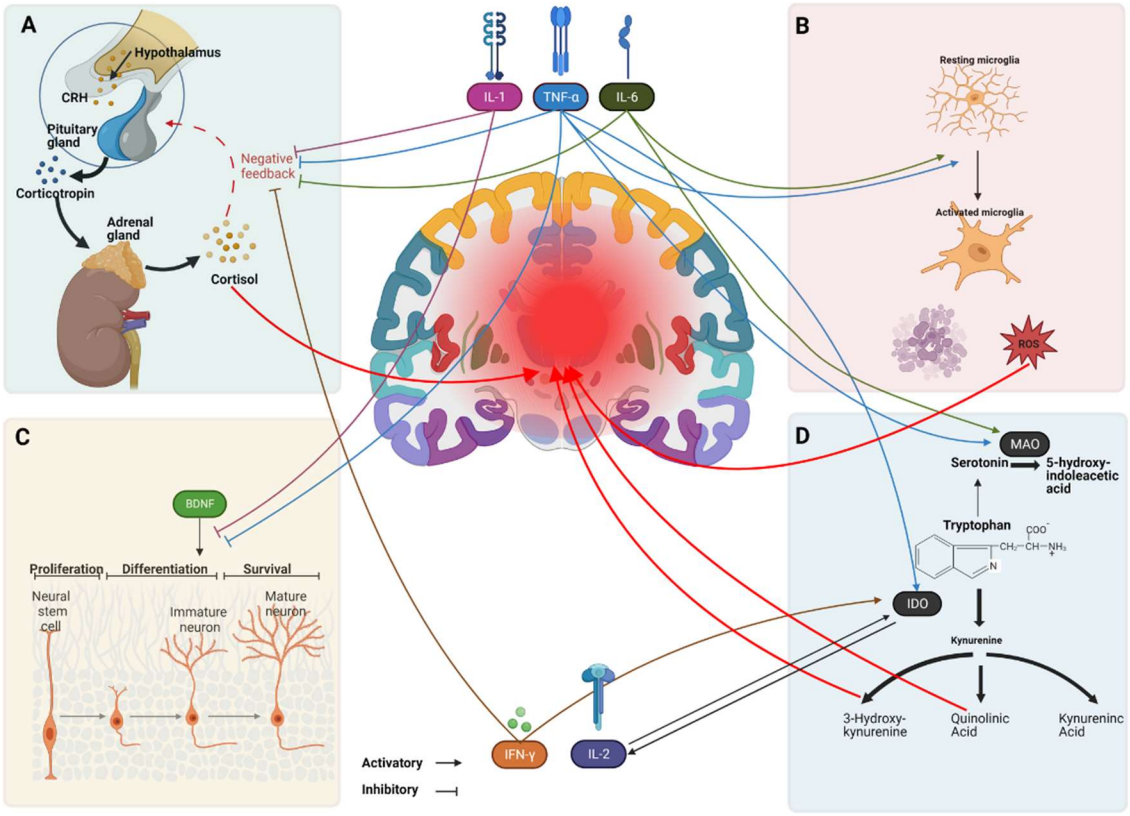

Figure 3. Immune-related neurobiological mechanisms involved in Mood Disorders. *The most widely recognized alterations concern A) HPA axis; B) microglial activation; C) alterations in synaptic plasticity; and D) switching of tryptophan metabolism into kynurenine. Reprinted from Poletti et al (2024) (Open Access Source).*

1.2.5 Environmental factors

As previously discussed in paragraph 1.2.1, environmental factors explain a relevant variance associated with Mood Disorders and, by interacting with the underlying genetic predisposition, contribute to their clinical manifestation (Duncan & Keller, 2011). Particularly relevant in this context is the role of stress, which has been extensively considered as one of the most impactful environmental factors advancing the onset of many psychiatric disorders (Sanacora & Yan, 2022). At the biological level, chronic exposure to stress induces a cascade of alterations in several body systems, especially in the HPA axis. The activation of this system in response to stress prompts the release of glucocorticoids into the blood circulation, which in turn promotes metabolic, cardiovascular, and neural changes aimed to efficiently face the stressor. While in physiological conditions the HPA self-regulates through a negative feedback loop, chronic exposure to stress impairs this mechanism, resulting in HPA hyper-activation and

uncontrolled glucocorticoid release (Russell & Lightman, 2019). At the neural levels, excessive glucocorticoid production inhibits the activation of signalling pathways involved in synaptic plasticity (e.g., BDNF), causing a loss of dendritic spines and branching and altered glutamatergic signalling (Sanacora & Yan, 2022). As previously stated in paragraph 1.2.2, these synaptic changes represent a plausible reason for the cortical and hippocampal atrophy described in MDD patients, also supported by evidence of decreased synapse number and function in the dorsolateral PFC in post-mortem studies (Kang et al, 2012). The functions of HPA axis are also affected by immune-inflammatory processes since a state of chronic inflammation is associated to resistance to glucocorticoids which, conversely, exert anti-inflammatory functions (Chrousos, 1995).

Among stressful life events, an extensive body of research has focused on Adverse Childhood Experiences (ACEs), which were first categorized by Felitti et al (1998) into i) *abuse* (physical, emotional, and sexual); ii) *neglect* (physical and emotional); iii) *household challenges* (e.g., domestic violence against the mother, substance abuse and mental illnesses in the family, parental separation). Indeed, exposure to ACEs has been consistently recognized as one of the major risk factors for many psychiatric disorders, doubling the likelihood of developing depression or other internalizing disorders later in life (Sahle et al, 2022). In MDD, the experience of early trauma has been associated with a worse clinical course of the disorder, such as a higher number of recurrences, treatment resistance (Nanni et al, 2012), higher suicidal risk (Dias de Mattos Souza et al, 2016), and medical comorbidities (Souama et al, 2023). Similar findings were also reported in BD, with traumatized patients being characterized by an earlier onset of the disease, suicidality (Daruy-Filho et al, 2011), longer duration of episodes, and higher risk of psychosis (Rowe & Perich, 2024). The occurrence of mood episodes both in MDD and BD seems to follow an incremental kindling-like progression: while the first affective episode manifests very closely to stressful events, the following ones can occur even in the absence of a clear stressor, reflecting a graded sensitization to stress (Carvalho et al, 2020). The damaging and durable consequences of ACEs could be explained by their effects on the neurodevelopmental changes occurring during sensitive periods. These time windows covering prenatal and early post-natal periods are characterized by an intense maturation and formation of the neural circuitry, making the brain particularly sensible to environmental changes. Therefore, the experience of ACEs can drastically

affect normal neural development by inhibiting synaptic pruning and branching, myelinization, hippocampal neurogenesis, and the expression of glucocorticoid receptors (Malave et al, 2022). In line with these considerations, it has been hypothesized that, under the same diagnostic label, traumatized patients represent a unique "ecophenotype" (i.e., a phenotype resulting from adaptation to environmental influences) with specific brain alterations and clinical characteristics (Teicher & Samson, 2013). For instance, abuse-specific changes in primary sensory cortices and WM tracts have been extensively reported in literature (e.g., exposure to parental verbal abuse has been associated with volumetric GM changes in the auditory cortex and reduced WM integrity of the arcuate fasciculus, whereas seeing episodes of domestic violence has been related to alterations in connectivity patterns between limbic and visual areas). From an evolutionary perspective, these modifications in brain morphology and connectivity might exert a protective function, reducing the access to consciousness to the experience of ACEs (Teicher et al, 2016).

In line with the aforementioned effects of stress on immune functions, several studies reported ACEs-related immune-inflammatory alterations in people exposed to childhood trauma. For example, higher peripheral concentrations of IL-6 and CRP have been described in ACEs-exposed children compared to the no-maltreated ones, and this inflammatory state remains stable into adulthood (Danese et al, 2011; Danese et al, 2007). This pro-inflammatory activation at the peripheral level is supposed to mediate the previously described ACEs-related alterations at the neural level. Indeed, it has been suggested that early exposure to adverse events could enhance the bidirectional exchange between peripheral inflammation and brain functions. On the one hand, ACEs impact cortico-amygdala circuits in a way aimed to enhance alertness and rapid response to potentially harmful stimuli. This activation induces a signalling cascade from the amygdala to the hypothalamus that ends with the norepinephrine-induced activation of monocytes and macrophages, which, in turn, modulate cortico-limbic activation through cytokines release. In the long run, this bidirectional cycle is believed to become self-fulfilling, with higher neural activations to threatening stimuli enhancing peripheral inflammatory processes and vice versa (Nusslock & Miller, 2016).

1.2.6 Clinical features: cognitive distortions in Mood Disorders

As previously mentioned, Mood Disorders can be described by variegated symptomatology characterized by affective, cognitive, and neurovegetative changes (Zimmerman et al, 2015). Among them, the study of how biased cognitive processes contribute to the onset and the maintenance of depressive symptoms has gained particular attention, laying also the foundation of cognitive-based therapies for depression (Beck & Dozois, 2011). Cognitive distortions in depressed patients were first described by Aaron Beck (1979), who defined them as biases in information processing leading to interpretations of the self and reality negatively. Based on the specific type of biased processes, cognitive distortions can be classified into: i) *paralogical*, reflecting the tendency of depressed people to focus on details of situations (i.e., selective abstraction) and generalizing conclusions from a single event (i.e., arbitrary inference and overgeneralization); ii) *stylistic*, referring to the proneness to magnify the negative aspects of a situation while minimizing the positive ones (i.e., exaggeration); iii) *semantic*, wherein people or situations are wrongly labelled or judged according to one's perception of them (i.e., inexact labelling) (Beck, 1979). Notably, what all the diverse types of cognitive distortions have in common is their automaticity (i.e., they occur without prior reasoning or reflection), plausibility (i.e., they are uncritically accepted as plausible by the patient), and perseveration (i.e., different types of situations can elicit the same cognitive distortion, promoting its repetition over time and experiences) (Beck, 1979).

The study of cognitive processes in depression laid the basis of Beck's cognitive model of depression. According to this theoretical model, how depressed patients perceive themselves and the world is influenced by internal mental representations called "schemas". A core feature of these mental inner structures is to be mood-congruent, meaning that they convey themes of loss, inadequacy, and exclusion that negatively shape patients' perceptions of themselves, the world, and the future (the so-called "cognitive triad"). As a consequence, the information processing of depressed people is biased toward the negative aspects of the self and the world and, consecutively, contributes to the maintenance of depressive mood (Beck, 2008). Most importantly, Beck (2008) attributes a fundamental role to ACEs in the formation of negative schemas, making individuals exposed to these experiences more vulnerable to developing depressive symptoms in response to stressful life events. Of note, these mood-congruent schemas are

supposed to persist latently even during remission and reactivate in the presence of negative events, which might explain recurrences of affective episodes in Mood Disorders (Figure 4).

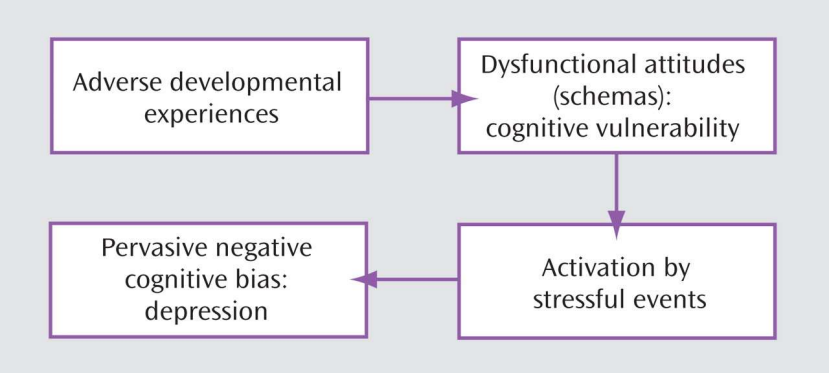

Figure 4. Schematic representation of Beck's cognitive model of depression. *Exposure to adverse events during childhood promotes the occurrence of a negative thinking style, which consolidates into cognitive schemas and increases vulnerability for depression; subsequent experience of stressful events activates the latent schemas, leading to the pervasive negative bias that underlies depression. Reprinted from Beck (2008) (Open Access Source).*

In line with these considerations, several studies demonstrated that early exposure to adverse events exacerbates cognitive distortions in BD (Poletti et al, 2014), MDD (Ghazanfari et al, 2018), and in the general population, possibly reflecting a maladaptive compensatory strategy to face with the negative aspects of potentially stressful situations (Mansueto & Cavallo, 2021). From a neurobiological perspective, it has been suggested that negative cognitive biases arise from aberrant bottom-up signalling from subcortical limbic structures that overcomes the reduced top-down cognitive control from high-ordered prefrontal regions (Disner et al, 2011). These alterations in brain networks are supposed to reflect stress-related neuroplastic changes: the exposure to traumatic or adverse events, indeed, leads to the consolidation of synaptic connections conveying emotionally relevant information, especially the negative one; these associations are further strengthen by subsequent stress-related plastic changes within the cortico-limbic circuit, promoting the inflexibility of cognitive biases (Price & Duman, 2020).

Despite the significant contribution of Beck's cognitive model to the investigation of the clinical, cognitive, and neurobiological features of depression, some criticisms have been levelled against the broadness and lack of specificity of its definition of "cognition" (Rief & Joormann, 2019). Indeed, recent advances in computational neuroscience have

proposed an integration of this theoretical framework with the more recent Bayesian neural models, which conceptualize the brain as an active generator of predictions about sensory inputs based on prior beliefs about the world (Knill & Pouget, 2004). This predictive processing is not only limited to external stimuli but also to interoceptive sensations, with a primary role of agranular visceromotor regions in generating autonomic, hormonal, and immunological predictions aimed to modulate body systems functions according to sensorial information (Barrett & Simmons, 2015). Extending this framework to Mood Disorders, it has been proposed that depressed people tend to anticipate negative events more frequently than positive ones and maintain negative expectations despite disconfirming positive information, resulting in chronic negative predictions and biased learning (Gilbert et al, 2022; Kube et al, 2020). Evidence supporting disrupted predictive processing in depression comes from neuroimaging and neurophysiological studies focusing on functional alterations associated with reward prediction errors. Dysregulated activations in the ventral striatum in response to reward feedback have been consistently reported in MDD, despite contradictory results regarding whether striatal dopaminergic signalling for reward prediction errors is blunted or increased (Kumar et al, 2018; Rutledge et al, 2017; Yaple et al, 2021). Considering BD, while hypo-manic symptoms have been associated with hypersensitivity to rewards, a consensus about the core mechanisms underlying depressive episodes is still limited (Nusslock & Alloy, 2017). Meta-analytic evidence of neuroimaging studies about reward anticipation in BD reported reduced activations within fronto-parietal regions during bipolar depression (similar to what has been described in MDD), but findings on abnormal activation in the ventral striatum are inconsistent, possibly due to heterogeneities in clinical populations, type of tasks and fMRI analyses (Long et al, 2022).

In an attempt to elucidate the neural underpinnings of distorted cognition in Mood Disorders, another line of research focused on the investigation of specific functional alterations in brain connectivity leading to different cognitive processes and depressive symptoms. An example of such endeavour is the work by Williams (2016), who identified 8 possible “biotypes” of depression, each of them being linked to unique dysfunctions at the network level. For instance, aberrant activation patterns within the DMN have been linked to a “rumination” biotype, whereas increased connectivity between the so-called

negative affective circuit and the DMN has been associated with the "negative bias" biotype (Williams, 2016). These findings suggest that not all depressed patients are characterized by the same distorted cognitive processes, but each patient might exhibit a neural-specific cognitive phenotype (e.g., rumination, mood-congruent bias, or reward insensitivity), which could benefit from targeted interventions (Tozzi & Zhang, 2024).

1.3 Computational approaches for neuro-biological phenotyping in Mood Disorders

Despite the extensive research into the biological, clinical, and environmental factors associated with Mood Disorders, a general consensus about the psychopathological and neurobiological mechanisms leading to mental illnesses is still lacking (Tiego et al, 2023). As briefly introduced in paragraph 1.2, the traditional classification of psychiatric disorders assumes that diagnostic categories are intrinsically homogeneous, meaning that all patients labelled with the same diagnosis are phenotypically and biologically similar (Feczko & Fair, 2020; Feczko et al, 2019). Consequently, the vast majority of studies in the psychiatric field have adopted a case-control approach, which involves the statistical comparison between a group of individuals with the trait of interest (i.e., psychiatric patients) against a control group. This approach, which largely relies on the homogeneity assumption, oversights two major problems commonly described in the study of psychiatric disorders: the comorbidity and the heterogeneity problem (Feczko et al, 2019). The comorbidity problem entails the high rates of co-occurrences of psychiatric conditions in the same individual, implying the existence of a shared underlying mechanism cutting across diagnostic boundaries (Caspi & Moffitt, 2018). The heterogeneity problem, instead, presumes that distinct combinations of biological pathways and environmental factors lead to the same diagnosis (a phenomenon called "equifinality" (Cicchetti & Rogosch, 1996)), resulting in phenotypic differences among individuals (Feczko et al, 2019).

In an attempt to address these problems, novel theoretical models alternative to the traditional psychiatric nosology have been proposed, such as the Research Domain Criteria (RDoC) (Insel, 2014) and the Hierarchical Taxonomy of Psychopathology

(HiTOP) (Kotov et al, 2017)[2]. A common rationale behind both these frameworks is to benefit from current advances in neuroscience and clinical research to unfold the mechanisms underlying mental disorders, which could inform future classification of mental illnesses to define new therapeutic targets (Michelini et al, 2021). This follows an emerging precision medicine approach to psychiatry, where endeavours to defy biomarkers for mental disorders can contribute to the improvement of personalized treatments (Fernandes et al, 2017). Although this approach has been promising in other fields of medicine (e.g., oncology (Prasad et al, 2016)), progress towards a "precision psychiatry" perspective has been relatively slow (Fernandes et al, 2017). A major obstacle to this achievement is represented by several weaknesses of the long-established case-control approach, which focuses on mean differences among groups. In fact, even in case of statistically significant differences, this approach does not guarantee their replicability nor reproducibility to other samples from the same population. This is particularly evident in complex disorders, where interactions among biological, behavioural, and environmental factors could be masked by classical univariate approaches that forsake accuracy in individual predictions in favour of explaining variance at the group level (Dwyer et al, 2018). To address these limitations, the advancing field of computational psychiatry (Huys et al, 2016; Wang & Krystal, 2014) has provided new mathematical tools to handle high-dimensional data, representing an opportunity to uncover complex relationships among them (Sanislow et al, 2019). Computational methods can be grouped into 2 main categories: theory-driven and data-driven approaches. While theory-driven approaches aim to define mechanistic and theoretical models of a specific phenomenon based on prior knowledge, data-driven approaches exploit machine learning (ML) techniques to build predictive models of clinically relevant outcomes (e.g., differential diagnosis, treatment response) (Huys et al, 2016). Given their primary focus on prediction at the single-subject level, ML techniques have been proposed as promising statistical

[2] *Launched by the National Institute of Mental Health (NIMH), the RDoC project proposes a dimensional approach to psychopathology, shifting the focus from diagnostic categories to basic "domains" of functioning that can be investigated through different levels of analysis (from genetic data to behavioural measures). The main goal of this framework is to uncover transdiagnostic subtypes of psychopathology linked to specific aetiopathological mechanisms, with a primary focus on alterations in brain (Insel, 2014). Conversely, the HiTOP model assumes the existence of a shared transdiagnostic liability dimension (i.e., p-factor) in which psychopathological dimensions are nested according to a hierarchical structure (Kotov et al., 2017).*

tools to tackle the limitations of group-level analyses and accelerate translation to precision psychiatry (Bzdok & Meyer-Lindenberg, 2018).

Broadly speaking, ML can be defined as computational methods that "automatically determines (i.e., learns) methods and parameters to reach an optimal solution to a problem" (Dwyer et al, 2018). Unlike theory-driven approaches, ML algorithms overlook any *a priori* theoretical assumptions but seek to unveil hidden structures within the data starting from the data themselves (Huys et al, 2016). The ability of a ML model to generalize predictions to new observations is evaluated through a two-step procedure called "cross-validation". During the "training" phase, the algorithm is applied to the subset of the data (i.e., training data) to learn characteristic patterns. In the following "testing" phase, the predictive performance of the trained model is tested on unseen data (i.e., test data). This procedure is repeated several times using different splits of the whole dataset to provide a reliable estimate of the model's generalizability (i.e., the degree to which a model fitted on a set of data makes accurate predictions on new observations) (Friedman et al, 2001). Although extremely varied, ML algorithms can be broadly classified into 2 main groups: supervised and unsupervised learning techniques. In supervised learning, the algorithm is trained on labelled data (e.g., behavioural, neuroimaging, genetic data) to predict categorical (i.e., classification) or continuous (i.e., regression) outcomes. In unsupervised learning, conversely, ML models aim to discover data-driven latent structures in the absence of explicit labels (Bzdok & Meyer-Lindenberg, 2018). Supervised learning approaches have been widely applied in psychiatry to solve different clinical problems, such as differential diagnosis and prediction of clinical and treatment outcomes (Dwyer et al, 2018). The translation of these findings in clinical practice, however, has been hampered by several limitations of these models. Above all, most of these applications assume the mutual exclusiveness of diagnostic categories, underestimating the comorbidity and heterogeneity problems (Huys et al, 2016). Moreover, the supervised nature of these approaches binds them to the definition of clinical labels regardless of their validity (Marquand et al, 2016). Consequently, unsupervised methods have been increasingly exploited to parse heterogeneity in psychiatric disorders and uncover new disease subtypes. The most widely used methods in this field are clustering algorithms, which aim to split the dataset into a specific number of partitions (i.e., clusters) so that observations assigned to the

same cluster are more similar to those belonging to other clusters. The similarity among data is usually defined according to a distance measure, such as the Euclidean distance (Marquand et al, 2016).

1.3.1 Applications of unsupervised learning methods in psychiatry

The direction to decompose heterogeneity through unsupervised approaches can be both top-down and bottom-up (Figure 5). The top-down approach aims to stratify patients according to their symptom profiles and then investigate the neurobiological correlates associated with each symptom-based subtype (Buch & Liston, 2021). However, most of these symptoms-based stratifications failed to provide reliable and reproducible subtypes, possibly due to the considerable overlap among disorders and longitudinal clinical evolution of symptoms during the course of illness (Lynch et al, 2020; Marquand et al, 2016). Bottom-up approaches, instead, start from developing stratification models from neuro-biological data and then investigate how the biologically derived subtypes are similar or different at the clinical or cognitive levels. The majority of the studies carried out in this field mainly implemented a "brain-first" approach, using functional or structural brain features to stratify patients into clinically meaningful subtypes (Buch & Liston, 2021). Within bottom-up approaches, 3 main strategies have been employed: categorical, dimensional, and hybrid approaches (Buch & Liston, 2021; Lynch et al, 2020).

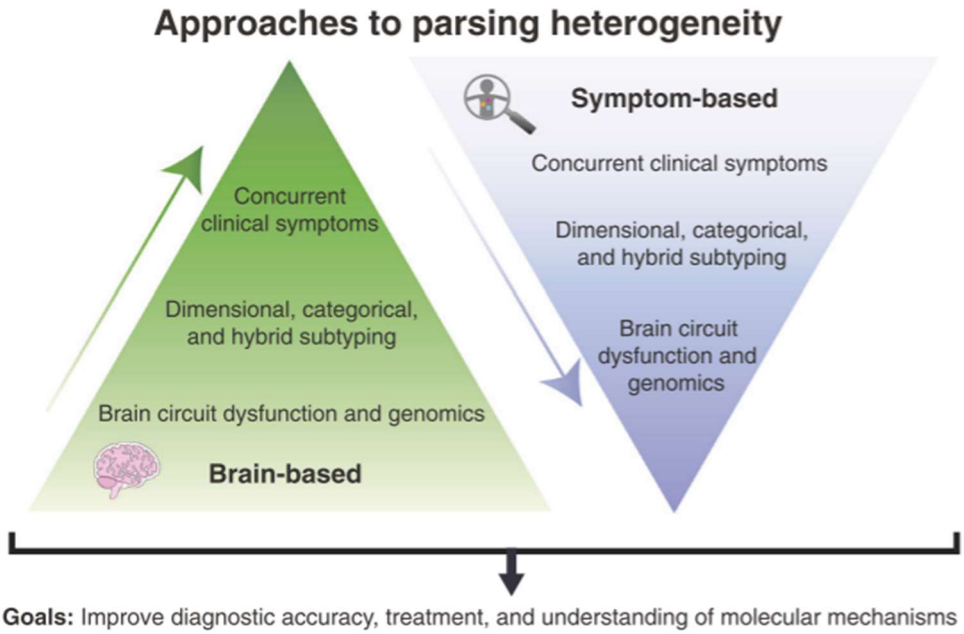

Figure 5. Approaches for disentangling heterogeneity in psychiatry. *Graphical representation of the "bottom-up" brain-based (left, green) and "top-down" symptom-based (right, blue) approaches to disentangle heterogeneity in psychiatric disorders. The main goals of both approaches are to improve diagnostic accuracy, treatment, and understanding of the neurobiological mechanisms underlying these disorders. Reprinted from Buch and Liston (2020) with permission from Springer Nature (License ID: 5852590731761)*

Categorical approaches aim to derive data-driven subgroups of patients using clustering algorithms and then evaluate how they differ in terms of symptom profiles or other clinically relevant outcomes (Lynch et al, 2020). One of the first instances of this approach is the work by Price et al (2017b) which aimed to cluster 68 MDD patients and 24 healthy controls based on FC patterns in response to a mood induction task. As a secondary aim, the authors investigated whether the discovered data-driven subgroups were differentially associated with clinically relevant variables. Using a community detection algorithm on FC paths, the 92 individuals could be clustered into 2 subgroups: the first one was characterized by higher FC within the ventral affective network, whereas the second exhibited an overall hypoconnectivity pattern. Importantly, the "hyperconnected" subgroup was largely represented by MDD patients (about 81%), suggesting a partial overlap between biological-derived categories and diagnostic labels. In addition, individuals assigned to this cluster exhibited higher scores of self-reported symptoms, lower positive mood during the induction task, and increased negative bias

during a separate affective information processing task. A 2-clusters solution was identified also in a subsequent study from the same group in which the previously described unsupervised approach was applied to resting-state FC (Price et al, 2017a). Although significantly associated with clinical symptoms, the identified clusters were neither biologically nor clinically overlapping with those discovered in the first study, suggesting that task-based and resting-state FC retain distinctive information that, collectively, could be useful for clinical purposes (Price et al, 2017a). Despite being less explored, some studies tried to derive data-driven subtypes using structural neuroimaging data. For instance, Cheng et al (2014) used a K-means clustering algorithm to stratify MDD patients and healthy controls based on extracted FA values from WM tracts, uncovering 2 different data-driven clusters. The first cluster exhibited higher FA values in the CC, corticospinal tract, and inferior fronto-occipital fasciculus (IFOF), whereas the second one was characterized by diminished WM integrity. In terms of clinical outcomes, the identified subgroups showed peculiar associations with depressive symptoms, indicating that differences in microstructural integrity could drive specific symptom profiles (Cheng et al, 2014). While the "brain-first" approach has been widely exploited to unveil the neurobiological heterogeneity in psychiatric disorders, another line of research focused on other types of biological data to answer the same question. Using peripheral concentrations of immune cell populations (i.e., neutrophils, monocytes, T-cells) as input features for a multivariate mixture modelling, Lynall et al (2020) uncovered 4 different subtypes of MDD patients reflecting distinct immune-inflammatory signatures. While 2 out of 4 subgroups exhibited an inflammatory profile characterized by high concentrations of IL-6 and CRP and more severe depressive symptomatology, the remaining clusters were distinguished by subsets of cell populations belonging to the myeloid and lymphoid lineage, respectively. These findings face the current "monolithic" perspective of the role of inflammation in the aetiology of MDD, providing evidence of multiple different immunophenotypes of depression reflecting specific immune-inflammatory mechanisms (Felger & Miller, 2020).

Instead of dividing individuals into separate categories, dimensional approaches focus on discovering latent continuous dimensions describing the association between brain features and clinical symptoms. In this way, each individual is assigned a score that quantifies the entity of such relationship, allowing the prediction of individual differences

in specific clinical or cognitive domains in a continuous and transdiagnostic manner (Buch & Liston, 2021; Lynch et al, 2020). These approaches make use of multivariate statistical approaches, such as canonical correlation analysis (CCA) and partial least squared (PLS), suited for investigating associations between multivariate and high-dimensional datasets (Mihalik et al, 2022). A pioneering work in this field is the one by Xia et al (2018), who used sparse CCA to derive linked dimensions of resting-state FC and psychopathological symptoms in a sample of 663 youths. Despite focusing on the general population, this study demonstrated the existence of 4 brain-behaviour dimensions reflecting specific combinations of symptoms (i.e., mood, psychosis, fear, and externalizing-related symptoms). Of note, the identified dimensions were largely replicated in an independent sample of 336 individuals, providing evidence of the generalizability of these findings to new observations. Similarly, Mihalik and Ferreira (2019) implemented CCA to investigate brain-behaviour association in youths, uncovering 2 different patterns of covariation reflecting resting-state functional alterations in the DMN, frontoparietal, and limbic networks: the first one exhibits a maximal association with externalizing symptoms, whereas the second one was largely associated with measures of well-being. It should be considered, though, that most of the included subjects were healthy, and only a few of them reported clinically relevant depressive symptoms. Considering clinical populations, Kebets et al (2019) investigated whether whole-brain resting-state FC patterns retain information to unveil multivariate dimensions of psychopathology cutting across several diagnostic categories (i.e., BD, ADHD, SZ, schizoaffective disorder, and healthy individuals). By implementing PLS correlation (PLSC) analysis, the authors discovered 3 transdiagnostic brain-behaviour latent variables reflecting, respectively, general psychopathology, cognitive deficits, and impulsivity. Of note, although each dimension was characterized by unique FC profiles, functional alterations in somatosensory, motor, and subcortical networks were shared across all dimensions, indicating that aberrant FC patterns within these networks are implicated both in clinical and cognitive features of psychiatric disorders. This approach was employed in a subsequent study of the same group to explore brain-behaviour multivariate dimensions of emotion dysregulation in a mixed sample of BD, ADHD, and borderline personality disorder patients, uncovering a significant latent variable linking emotion dysregulation with aberrant fALFF values in core regions of the cortico-limbic

circuit (e.g., amygdala, hippocampus, ventromedial and dorsolateral PFC) (Kebets et al, 2021).

Finally, some studies tried to combine categorical and dimensional approaches to benefit from the strengths of both strategies. This hybrid approach implies 2 steps: first, a multivariate method is modelled on neuroimaging and behavioural data to derive brain-behaviour continuous dimensions; then, a clustering algorithm is fitted in the derived dimensions to stratify patients into subgroups. The main advantage of the hybrid approach is to assign patients to unique groups, favouring the categorical reasoning typical of clinical practice, while keeping, at the same time, information about continuous variations in brain features and clinical symptoms (Lynch et al, 2020). One of the most influential studies within this line of research is the one conducted by Drysdale et al (2017). In this study, the authors first used CCA to derive multivariate associations between FC and depressive symptomology, identifying 2 distinct patterns of FC alterations associated, correspondingly, with anhedonia and anxiety-related symptoms. Then, hierarchical clustering was applied to the identified dimensions, uncovering 4 subtypes of MDD patients showing unique associations with clinical symptoms. Most importantly, 2 of the discovered clusters were also predictive of a better response to repetitive TMS compared to the others, highlighting the potential clinical utility of these subtypes in clinical practice. Despite promising, these findings were largely criticized for several methodological weaknesses that significantly hamper their reliability. Dinga et al (2019), by implementing the same pipeline in a different sample, obtained an optimal 3-cluster solution which, however, was not statistically significant. As suggested by the authors, the analytical pipeline proposed by Drysdale et al. (2017) is prone to overfitting (i.e., the model fits the training data excessively well, with the loss of generalizability to external data) due to the lack of appropriate strategies to avoid it (e.g., cross-validation, hold-out testing) (Dinga et al, 2019). A similar pipeline was implemented by Wang et al (2021a), who discovered 2 subtypes of MDD patients based on CCA-derived multivariate associations between network-based FC estimates and clinical symptoms: the first one was characterized by hyperconnectivity within the ventral attentive network and insomnia-related symptoms; the second cluster, instead, exhibited a reduced FC pattern within the subcortical and dorsal attentive networks coupled with anhedonia-related symptomology. However, similar to Drysdale et al. (2017), the authors did not test the

statistical significance of the identified subtypes. Only a few studies used hybrid approaches to discover transdiagnostic clusters based on brain features. For instance, Yang et al (2021) used a semi-supervised approach[3] to discover subtypes of MDD and BD patients based on structural neuroimaging data and then investigated how the data-driven clusters differentiated in terms of sociodemographic and psychopathological measures. This approach uncovered 2 brain-derived clusters of patients, with one of them being characterized by widespread cortical thickness reduction and a family history of psychiatric disorders. Notably, the distribution of MDD and BD patients was quite similar in the 2 clusters, suggesting that abnormalities in brain structure could unveil novel groupings of patients that transcend clinical diagnosis but might reflect other neurobiological mechanisms (e.g., shared genetic vulnerability) (Yang et al, 2021). The same approach was employed by Byrne et al (2022) to unravelling subtypes of psychiatric disorders (i.e. psychotic, depressive, and anxiety disorders) based on peripheral concentrations of inflammatory markers and receptors. The authors described a statistically significant 2-cluster solution cutting across diagnostic categories, with one cluster showing higher concentrations of TNF-α and IL-2 soluble receptors. In terms of clinical outcomes, patients assigned to this subgroup were unemployed, less educated, and more likely to have a past history of psychotic symptoms, reflecting a more severe disease course. However, the variability in the methods and protocols for immunoassay quantification significantly impacted on the quality of the quantified analytes (Byrne et al, 2022).

Overall, findings from neurobiological-based subtyping studies suggest the existence of different subtypes of depressed patients linked to specific neural and biological alterations, although relevant methodological differences (e.g., differences in MRI acquisitions and protocols, clinical characteristics of the investigated populations) substantially limit the reproducibility of stratification models among studies (Beijers et al, 2019; Buch & Liston, 2021). Most of all, despite the increasing efforts in improving the reproducibility of the discovered clusters, the related clinical implications are scarcely considered. Indeed, the high reproducibility of a stratification model does not guarantee

[3] *Unlike the supervised framework, in semi-supervised learning only some data are labelled, whereas the remaining observations are provided without labels. In psychiatric research, the labelled observations usually correspond to healthy controls, which are used as reference to derive patients' subtypes that are maximally separated from them (Varol et al., 2017)*

its clinical relevance, and both types of cluster validation (reproducibility and clinical utility) should be evaluated for a translation to a precision psychiatry perspective (Brucar et al, 2023).

2. AIM OF THE WORK

As introduced before, heterogeneity in Mood Disorders is shown at different levels of analyses (e.g., genetic, immune-metabolic, and neural), which hampers the understanding of the biological mechanisms leading to clinical outcomes. Characterizing the heterogeneous manifestations of these disorders based on multimodal data is crucial to understanding their aetiology and promoting tailored treatments. This deeply phenotyped characterization should also consider the interplay between neuro-biological correlates and environmental factors in modelling patient-specific disease trajectories, which might also transcend diagnostic categories. An example of such factors is exposure to childhood trauma, which has been shown to exacerbate depressive symptoms (e.g., negative cognitive biases) in BD and MDD by affecting both immune and neural systems. This project aims in particular at providing a neurobiological-driven stratification of Mood Disorders, with a specific focus on associations with cognitive distortions and the interplay between biological correlates and childhood trauma. To achieve this aim, an innovative unsupervised ML pipeline was implemented on multimodal brain imaging data as well as peripheral immune-inflammatory markers to investigate whether the learning of data-driven pathways could help to disentangle the clinical complexity of Mood Disorders. Neuroimaging data included i) measures of FC strength and spontaneous local neural activity extracted from rs-fMRI data, ii) regional measures of grey matter volumes and cortical thickness, and iii) tract-based DTI diffusivity indexes of WM integrity. Markers of peripheral inflammation encompassed i) subpopulations of T helper cells (Th), T cytotoxic, T regulatory, and NK cells quantified through fluorescence-activated cell sorting (FACS) flow cytometry immunophenotyping, and ii) immune-inflammatory profiles derived from peripheral cytokines, chemokines, and growth factors. As a secondary aim, multivariate associations with exposure to childhood trauma were explored in the discovered data-driven subgroups. Based on previous evidence, worse cognitive distortions are expected to be associated with ACEs in each subpopulation, with brain imaging patterns and/or immune-inflammatory signatures mediating this relationship.

3. RESULTS

3.1 Descriptive statistics

Descriptive statistics of the whole sample (N=344, 209 BD, 135 MDD) are reported in Table 1. No significant differences in age, sex, duration of illness, and pharmacological load were observed between MDD and BD. However, BD patients showed a significantly higher number of previous episodes compared to MDD ($q < 0.001$). BD and MDD patients were also comparable for HDRS-21 total score, as well as Cognition Questionnaire (CQ) and Childhood Trauma Questionnaire (CTQ) domains.

Table 1. Descriptive statistics of the whole sample

Variable	MDD (N=135)	BD (N=209)	t / U / χ2	p	q
Age	50.00 ± 14.50	48.00 ± 15.00	15640.5†	0.09	0.26
Sex	95 F; 40 M	133 F; 76 M	4.08§	0.17	0.39
Scanner	48 Gyroscan; 87 Igenia	144 Gyroscan; 65 Igenia	1.85§	**0.04**	0.26
No. of episodes	3.00 ± 3.00	7.00 ± 10.00	6098‡	**<0.001**	**<0.001***
Age of onset	31.00 ± 17.00	27.00 ± 16.00	16574‡	**0.01**	0.06
Duration of illness (years)	17.00 ± 16.00	17.00 ± 16.00	13139‡	0.28	0.47
Pharmacological load	4.00 ± 4.00	4.00 ± 3.00	14703‡	0.50	0.68
HDRS-21 total score	22.00 ± 9.00	22.00 ± 5.00	13965‡	0.87	0.87
CTQ physical abuse[a]	5.00 ± 1.75	5.00 ± 1.00	6729‡	0.63	0.74
CTQ emotional abuse[a]	8.00 ± 6.00	7.00 ± 5.00	7128‡	0.22	0.43
CTQ sexual abuse[a]	5.00 ± 0.00	5.00 ± 0.00	6726‡	0.55	0.68
CTQ physical neglect[a]	6.00 ± 4.00	6.00 ± 2.00	7360‡	0.08	0.26
CTQ emotional neglect[a]	13.00 ± 7.75	12.00 ± 8.00	6848‡	0.51	0.68
CTQ total score[a]	42.00 ± 18.00	38.00 ± 15.00	7489‡	0.05	0.26
CQ emotional impact[b]	4.00 ± 4.00	4.00 ± 4.00	5403.5‡	0.74	0.83
CQ attribution of causality[b]	5.00 ± 3.00	6.00 ± 3.00	4541.5‡	0.09	0.26
CQ generalization across time[b]	4.00 ± 4.00	4.00 ± 5.00	4791‡	0.27	0.47
CQ generalizzation across events[b]	6.00 ± 5.00	6.00 ± 4.00	5178‡	0.84	0.87
CQ perceived uncontrollability[b]	3.00 ± 3.00	4.00 ± 4.00	4646.5‡	0.15	0.36
CQ total score[b]	22.00 ± 16.00	23.00 ± 17.00	4830‡	0.31	0.48

Results are reported as mean ± standard deviation for continuous variables, whereas frequencies are reported for categorical variables. For non-normally distributed variables, results are reported as median ± interquantile range. Significant differences are reported in bold. Abbreviations: MDD, Major Depressive Disorder; BD, Bipolar Disorder; HDRS-21, Hamilton Depression Rating Scale – 21 items; CTQ, Childhood Trauma Questionnaire; CQ, Cognition

Questionnaire. [a]subsample of N=229 (106 MDD, 123 BD); [b]subsample of N=208 (87 MDD,121 BD); [†]parametric two-sample t-test; [‡]non-parametric Mann-Whitney U test; [§]chi-squared test; *FDR-corrected q<0.05.

3.2 Unsupervised data-driven stratification

3.2.1 Performances of the stability-based relative clustering stratification models

The first aim of the study was to investigate whether neuro-biological data (i.e., neuroimaging features and peripheral immune-inflammatory markers) could provide a meaningful transdiagnostic stratification of Mood Disorder patients. The performances of all the tested models are reported in Table 2 and Appendix 1. Except for the fALFF-based model, the stability-based relative clustering approach identified 2 clusters as the optimal clustering solution that minimizes normalized stability. All these models showed good accuracies in clusters' differentiation (accuracy range: 66.0%-84.8%), apart from the ReHo-based model that did not achieve a predictive accuracy above chance level (accuracy=40.9%). The best clustering performance was observed for the FC-based model, showing an accuracy in discriminating the identified clusters of 84.8% (normalized stability=0.15(0.02), accuracy=84.8%, silhouette score=0.29, Davies-Bouldin score=1.24). Of note, all the stratification models heavily deviate from the null hypothesis that clusters were generated from a single Gaussian distribution, except for fALFF model that did not survive to FDR correction for multiple comparisons.

Table 2. Clustering models' performance

Model	Algorithms	Clusters	Stability(error)	Acc	Sil	DB	q
FC	Kmeans + SVM	2	0.15(0.02)	84.8	0.29(2)	1.24(2)	<0.0001*
GM	Kmeans + SVM	2	0.17(0.01)	83.2	0.14(2)	2.14(2)	0.0007*
CT	Kmeans + SVM	2	0.18(0.02)	81.9	0.27(2)	1.51(2)	<0.0001*
RD	Kmeans + SVM	2	0.20(0.02)	80.1	0.17(2)	1.90(2)	0.0027*
FA	Kmeans + SVM	2	0.21(0.01)	79.2	0.20(2)	1.73(2)	<0.0001*
AD	Kmeans + SVM	2	0.21(0.01)	78.8	0.15(2)	2.11(2)	0.0004*
MD	Kmeans + SVM	2	0.24(0.02)	76.5	0.20(2)	1.84(2)	0.034*
Immune	Kmeans + EN	2	0.25(0.03)	75.4	0.40(2)	0.91(2)	<0.0001*
Multimodal	Multiview + SVM	2	0.27(0.04)	73.4	0.49(2)	0.76(2)	0.003*
FACS	Kmeans + EN	2	0.34(0.03)	66.0	0.15(2)	2.30(2)	<0.0001*
ReHo	Kmeans + SVM	2	0.59(0.04)	40.9	0.07(2)	3.21(3)	0.044*
fALFF	Kmeans + SVM	3	0.67(0.03)	31.6	0.10(2)	3.04(5)	0.209

For each feature, number of clusters, normalized stability measures, and accuracies (in percentage) are reported. For comparison, the number of clusters identified based on internal measures (i.e., Silhouette and Davies-Bouldin scores)

are reported in brackets. Models are sorted based on normalized stability measures, where lower values indicate a more stable clustering solution. FDR-corrected p-values obtained from 10,000 Monte-Carlo simulations are reported. Abbrevations: Acc, accuracy; Sil, Silhouette score; DB, Davies-Bouldin score; FC, functional connectivity; GM, grey matter; CT, cortical thickness; RD, radial diffusivity; FA, fractional anisotropy; AD, axial diffusivity; MD, mean diffusivity; FACS, fluorescence activated cell sorting; ReHo, regional homogeneity; fALFF, fractional amplitude of low frequency fluctuations; SVM, support vector machine; EN, elasticnet penalized regression. *FDR-corrected q<0.05.

3.2.2 Biological and clinical characterization of the FC-based stratification model

The demographic and clinical comparisons for the FC-based clusters are reported in Table 3. Patients belonging to Cluster 2 were characterized by higher CQ generalization across time (p = 0.044) and CQ perceived uncontrollability (p = 0.018) scores compared to those assigned to Cluster 1, although these comparisons did not survive to FDR correction. In terms of neuroimaging profiles, Cluster 1 was characterized by higher FC positive strength values in all the selected seeds compared to Cluster 2 (d = 0.82 - 2.79, q < 0.05) (Appendix 2). As shown in Figure 6A, the largest effect sizes were found in the cingulate gyrus, precuneus, and SFG. Conversely, Cluster 2 exhibited overall higher FC negative strength values compared to Cluster 1, despite the magnitude of the effect sizes was lower compared to FC positive strength (d = 0.41 - 1.57, q < 0.05) (Appendix 2). As depicted in Figure 6B, the largest effect sizes were observed for the dorsolateral MTG, dorsal and medial SFG, ventrolateral MFG, and precuneus.

Table 3. Clinical and demographic comparisons for the FC-based clusters

Variable	**Cluster 1 (N=50)**	**Cluster 2 (N=96)**	**t / U / χ2**	**p**	**q**
Age	48.00 ± 14.50	49.00 ± 14.25	2329‡	0.771	0.911
Sex	35 F; 15 M	64 F; 32 M	0.05§	0.824	0.911
Diagnosis	27 MDD; 23 BD	52 MDD; 44 BD	0§	1	1
Scanner	16 Gyroscan; 34 Igenia	34 Gyroscan; 16 Igenia	0.05§	0.819	0.911
No. of episodes	4.00 ± 3.75	5.50 ± 7.00	2087‡	0.194	0.510
Age of onset	30.00 ± 17.50	27.00 ± 15.00	2541.5‡	0.560	0.911
Duration of illness (years)	17.00 ± 18.50	19.00 ± 16.25	2235.5‡	0.498	0.911
Pharmacological load	4.00 ± 1.75	4.00 ± 4.00	2287.5‡	0.639	0.911
HDRS-21 total score	23.00 ± 7.00	21.00 ± 7.00	2602‡	0.405	0.850
CTQ physical abuse[a]	5.00 ± 1.00	5.00 ± 1.00	1436‡	0.297	0.693
CTQ emotional abuse[a]	6.00 ± 6.00	8.00 ± 6.00	1335‡	0.139	0.486
CTQ sexual abuse[a]	5.00 ± 0.00	5.00 ± 0.75	1350.5‡	0.052	0.318

CTQ physical neglect[a]	6.00 ± 3.00	6.00 ± 3.75	1604‡	0.979	1.000
CTQ emotional neglect[a]	12.00 ± 7.00	13.00 ± 8.50	1524‡	0.679	0.911
CTQ total score[a]	39.00 ± 16.50	40.50 ± 18.50	1495.5‡	0.568	0.911
CQ emotional impact[b]	4.00 ± 3.50	4.00 ± 4.00	1264‡	0.698	0.911
CQ attribution of causality[b]	5.00 ± 4.00	6.00 ± 3.00	1008‡	0.167	0.501
CQ generalization across time[b]	3.00 ± 3.00	4.00 ± 4.00	968‡	0.098	0.411
CQ generalization across events[b]	5.37 ± 2.92	6.59 ± 2.76	-2.06†	**0.044**	0.318
CQ perceived uncontrollability[b]	3.00 ± 3.00	4.00 ± 4.00	867‡	**0.018**	0.318
CQ total score[b]	21.00 ± 11.00	24.00 ± 14.00	934.5‡	0.061	0.318

Results are reported as mean ± standard deviation for continuous variables, whereas frequencies are reported for categorical variables. For non-normally distributed variables, results are reported as median ± interquantile range. Significant differences are reported in bold. Abbreviations: MDD, Major Depressive Disorder; BD, Bipolar Disorder; HDRS-21, Hamilton Depression Rating Scale – 21 items; CTQ, Childhood Trauma Questionnaire; CQ, Cognition Questionnaire. [a]subsample of N=121 (39 Cluster 1, 82 Cluster 2); [b]subsample of N=104 (35 Cluster 1, 69 Cluster 2); †parametric two-sample t-test; ‡non-parametric Mann-Whitney U test; §chi-squared test; *FDR-corrected q<0.05.

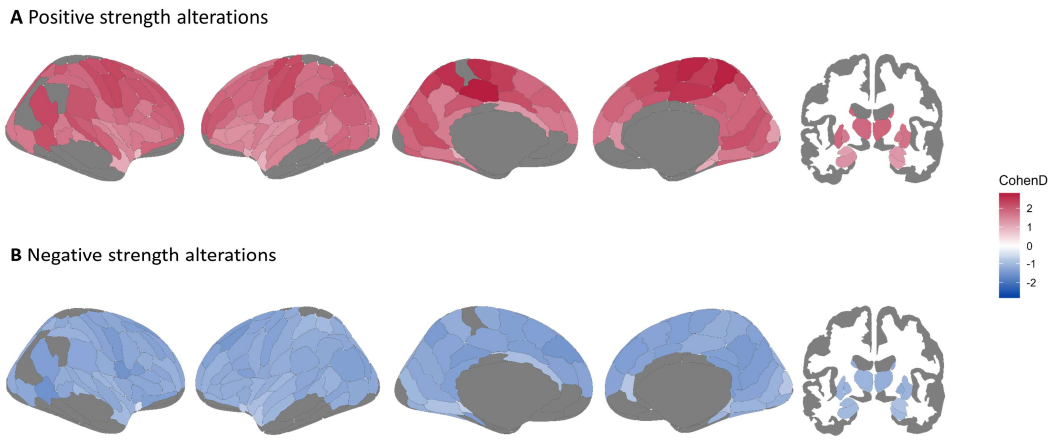

Figure 6. Cohen's d values describing the magnitude of differences in positive and negative strength values between the FC-based clusters. *Positive values (red) indicate higher values for Cluster 1 compared to Cluster 2, whereas negative values (blue) indicate higher values for Cluster 2 compared to Cluster 1.*

3.2.3 Biological and clinical characterization of the GM-based stratification model

Considering clusters derived from extracted GM volumes, no significant differences in demographic and clinical measures were found (Table 4). A widespread GM volumetric reduction was observed in Cluster 1 compared to Cluster 2 (d = 0.23-1.50, q < 0.05) (Appendix 3). As shown in Figure 7, the largest effect sizes were observed in the

right thalamus, transverse temporal gyrus (TTG), precuneus, PCC, middle occipital gyrus (MOG), as well as in the left medial frontal cortex (MFC) and parietal operculum.

Table 4. Clinical and demographic comparisons for clusters derived from extracted GM volumes

Variable	**Cluster 1 (N=150)**	**Cluster 2 (N=194)**	**t / U / χ2**	**p**	**q**
Age	49.00 ± 13.75	49.00 ± 16.00	14476‡	0.936	0.983
Sex	93 F; 57 M	135 F; 59 M	1.85§	0.173	0.881
Diagnosis	65 MDD; 85 BD	70 MDD; 124 BD	1.57§	0.210	0.881
Scanner	74 Gyroscan; 76 Igenia	118 Gyroscan; 76 Igenia	4.08§	0.044	0.881
No. of episodes	6.00 ± 7.00	5.5.00 ± 8.00	13820.5‡	0.423	0.983
Age of onset	30.00 ± 19.00	28.00 ± 15.00	15085.5‡	0.558	0.983
Duration of illness (years)	18.00 ± 16.50	17.00 ± 16.00	14531.5‡	0.984	0.984
Pharmacological load	4.00 ± 3.00	4.00 ± 3.00	15214.5‡	0.463	0.983
HDRS-21 total score	23.00 ± 6.75	22.00 ± 6.00	14099.5‡	0.880	0.983
CTQ physical abuse[a]	5.00 ± 2.00	5.00 ± 1.00	6828.5‡	0.502	0.983
CTQ emotional abuse[a]	7.50 ± 4.25	7.00 ± 5.00	7162‡	0.204	0.881
CTQ sexual abuse[a]	5.00 ± 0.00	5.00 ± 0.00	6584.5‡	0.884	0.983
CTQ physical neglect[a]	6.00 ± 4.00	6.00 ± 3.00	6467.5‡	0.891	0.983
CTQ emotional neglect[a]	13.00 ± 7.25	13.00 ± 8.00	6363‡	0.733	0.983
CTQ total score[a]	40.00 ± 18.25	39.00 ± 16.00	6646.5‡	0.802	0.983
CQ emotional impact[b]	4.00 ± 4.00	4.00 ± 4.00	5200‡	0.752	0.983
CQ attribution of causality[b]	5.00 ± 4.00	5.00 ± 3.00	5074‡	0.541	0.983
CQ generalization across time[b]	4.00 ± 4.00	4.00 ± 5.00	5220‡	0.788	0.983
CQ generalization across events[b]	7.00 ± 3.25	6.00 ± 4.00	5981‡	0.133	0.881
CQ perceived uncontrollability[b]	4.00 ± 3.00	3.00 ± 4.00	5512.5‡	0.680	0.983
CQ total score[b]	23.00 ± 15.00	22.00 ± 18.25	5440.5‡	0.700	0.983

Results are reported as mean ± standard deviation for continuous variables, whereas frequencies are reported for categorical variables. For non-normally distributed variables, results are reported as median ± interquantile range. Significant differences are reported in bold. Abbreviations: MDD, Major Depressive Disorder; BD, Bipolar Disorder; HDRS-21, Hamilton Depression Rating Scale – 21 items; CTQ, Childhood Trauma Questionnaire; CQ, Cognition Questionnaire. [a]subsample of N=229 (108 Cluster 1, 121 Cluster 2); [b]subsample of N=208 (92 Cluster 1, 116 Cluster 2); †parametric two-sample t-test; ‡non-parametric Mann-Whitney U test; §chi-squared test; *FDR-corrected q<0.05.

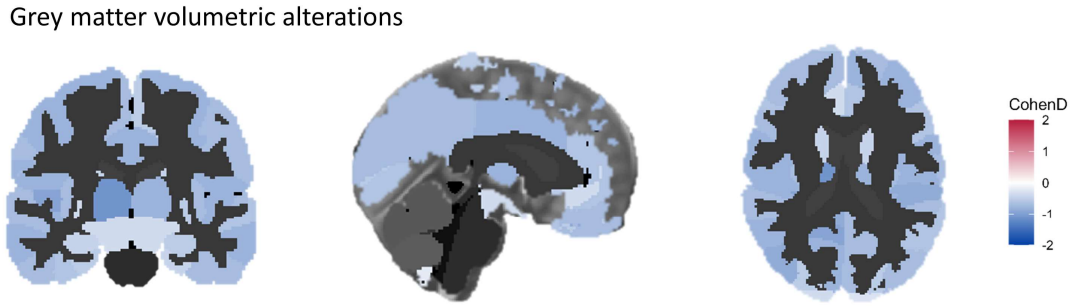

Figure 7. Cohen's d values describing the magnitude of differences in regional grey matter volumes between clusters. *Positive values (red) indicate higher values for Cluster 1 compared to Cluster 2, whereas negative values (blue) indicate higher values for Cluster 2 compared to Cluster 1.*

3.2.4 Biological and clinical characterization of the CT-based stratification model

Regarding clusters obtained from extracted cortical thickness (CT) values, no significant differences in demographic and clinical measures were reported (Table 5). Compared to Cluster 2, Cluster 1 was characterized by a widespread cortical thinning (d = 0.41-1.76, $q < 0.05$) (Appendix 4), with the largest effect sizes observed for the bilateral inferior parietal lobules, supramarginal gyrus, STG, and right MTG, SFG, fusiform gyrus, and precuneus (Figure 8).

Table 5. Clinical and demographic comparisons for clusters derived from cortical thickness

Variable	**Cluster 1 (N=149)**	**Cluster 2 (N=195)**	**t / U / χ2**	**p**	**q**
Age	48.00 ± 14.00	49.00 ± 16.00	13939‡	0.520	0.814
Sex	93 F; 56 M	135 F; 60 M	1.46§	0.226	0.792
Diagnosis	52 MDD: 97 BD	83 MDD; 112 BD	1.77§	0.183	0.792
Scanner	82 Gyroscan; 67 Igenia	110 Gyroscan; 85 Igenia	0.02§	0.885	0.937
No. of episodes	6.00 ± 7.00	5.00 ± 7.00	15049‡	0.567	0.814
Age of onset	28.00 ± 18.00	30.00 ± 17.00	13721.5‡	0.378	0.793
Duration of illness (years)	18.00 ± 17.00	17.00 ± 16.00	14974‡	0.625	0.821
Pharmacological load	5.00 ± 3.00	4.00 ± 3.00	15774‡	0.168	0.792
HDRS-21 total score	23.00 ± 6.00	22.00 ± 7.00	14806.5‡	0.493	0.814
CTQ physical abuse[a]	5.00 ± 2.00	5.00 ± 1.00	6688.5‡	0.684	0.845
CTQ emotional abuse[a]	7.00 ± 5.00	8.00 ± 6.25	5871.5‡	0.195	0.792
CTQ sexual abuse[a]	5.00 ± 0.00	5.00 ± 0.00	6205‡	0.375	0.793

CTQ physical neglect[a]	6.00 ± 3.00	6.00 ± 3.00	6244.5‡	0.582	0.814
CTQ emotional neglect[a]	13.00 ± 8.00	13.00 ± 7.25	6175.5‡	0.503	0.814
CTQ total score[a]	38.00 ± 15.00	41.00 ± 18.25	5779‡	0.149	0.792
CQ emotional impact[b]	4.00 ± 4.00	4.00 ± 4.00	5359.5‡	0.909	0.937
CQ attribution of causality[b]	5.50 ± 3.00	5.00 ± 4.00	5757.5‡	0.295	0.793
CQ generalization across time[b]	4.00 ± 4.75	4.00 ± 5.00	5420‡	0.798	0.931
CQ generalization across events[b]	7.00 ± 3.00	6.00 ± 4.00	6047‡	0.085	0.792
CQ perceived uncontrollability[b]	4.00 ± 3.00	4.00 ± 4.00	5276‡	0.937	0.937
CQ total score[b]	24.00 ± 15.00	22.00 ± 18.00	5634‡	0.369	0.793

Results are reported as mean ± standard deviation for continuous variables, whereas frequencies are reported for categorical variables. For non-normally distributed variables, results are reported as median ± interquantile range. Significant differences are reported in bold. Abbreviations: MDD, Major Depressive Disorder; BD, Bipolar Disorder; HDRS-21, Hamilton Depression Rating Scale – 21 items; CTQ, Childhood Trauma Questionnaire; CQ, Cognition Questionnaire. [a]subsample of N=229 (105 Cluster 1, 124 Cluster 2); [b]subsample of N=208 (90 Cluster 1, 118 Cluster 2); †parametric two-sample t-test; ‡non-parametric Mann-Whitney U test; §chi-squared test; *FDR-corrected q<0.05.

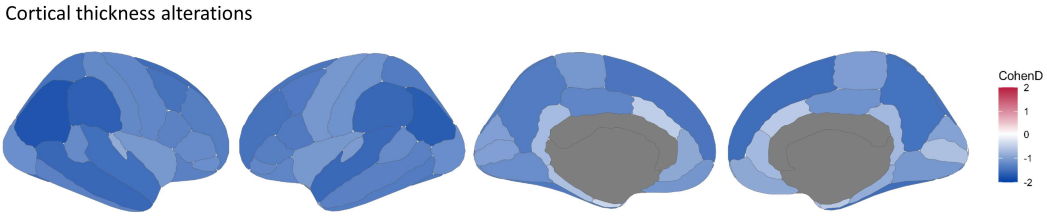

Figure 8. Cohen's d values describing the magnitude of differences in cortical thickness between clusters. *Positive values (red) indicate higher values for Cluster 1 compared to Cluster 2, whereas negative values (blue) indicate higher values for Cluster 2 compared to Cluster 1.*

3.2.5 Biological and clinical characterization of the DTI-based stratification models

Demographic and clinical comparisons for the AD-based clusters are reported in Table 6. Significant differences for sex (p = 0.019) and diagnosis (p = 0.036) were detected, with a higher proportion of males and MDD patients in Cluster 2. However, these comparisons did not survive to FDR correction. Compared to Cluster 2, Cluster 1 showed higher AD values in the majority of white matter tracts (d = 0.29-1.59, q < 0.05) (Appendix 5). AD values in the bilateral corona radiata, internal capsule, left superior longitudinal fasciculus (SLF) and superior fronto-occipital fasciculus (SFO) contributed the most to clusters' differentiation (Figure 9A).

Table 6. Clinical and demographic comparisons for the AD-based clusters

Variable	Cluster 1 (N=120)	Cluster 2 (N=155)	t / U / χ2	p	q
Age	49.50 ± 16.00	48.00 ± 14.00	9938.5‡	0.329	0.932
Sex	87 F; 33 M	90 F; 65 M	5.53§	**0.019**	0.377
Diagnosis	34 MDD; 86 BD	64 MDD; 91 BD	4.40§	**0.036**	0.377
Scanner	77 Gyroscan; 43 Igenia	92 Gyroscan; 63 Igenia	0.47§	0.491	0.932
No. of episodes	6.50 ± 8.00	5.00 ± 7.00	10271‡	0.136	0.932
Age of onset	28.00 ± 18.00	29.00 ± 15.50	9908.5‡	0.352	0.932
Duration of illness (years)	17.00 ± 16.25	18.00 ± 17.00	9102.5‡	0.763	0.941
Pharmacological load	4.00 ± 3.00	4.00 ± 3.00	9579‡	0.666	0.941
HDRS-21 total score	22.00 ± 6.00	23.00 ± 7.00	9286.5‡	0.984	0.993
CTQ physical abuse[a]	5.00 ± 1.00	5.00 ± 1.00	3762.5‡	0.673	0.941
CTQ emotional abuse[a]	7.00 ± 5.00	7.00 ± 5.00	3677‡	0.533	0.932
CTQ sexual abuse[a]	5.00 ± 0.00	5.00 ± 0.00	3945‡	0.807	0.941
CTQ physical neglect[a]	6.00 ± 3.00	6.00 ± 3.00	3984‡	0.770	0.941
CTQ emotional neglect[a]	12.00 ± 6.25	13.00 ± 8.00	3577.5‡	0.364	0.932
CTQ total score[a]	37.00 ± 14.00	39.50 ± 17.00	3614.5‡	0.425	0.932
CQ emotional impact[b]	3.00 ± 4.00	4.00 ± 4.00	2893.5‡	0.328	0.932
CQ attribution of causality[b]	5.00 ± 3.00	5.00 ± 4.00	3390‡	0.479	0.932
CQ generalization across time[b]	4.00 ± 5.5.00	5.00 ± 5.00	3184.5‡	0.993	0.993
CQ generalization across events[b]	6.00 ± 4.00	6.00 ± 4.00	2811.5‡	0.209	0.932
CQ perceived uncontrollability[b]	4.00 ± 3.00	3.00 ± 4.00	3156.5‡	0.933	0.993
CQ total score[b]	22.00 ± 17.50	23.00 ± 16.00	3030‡	0.610	0.941

Results are reported as mean ± standard deviation for continuous variables, whereas frequencies are reported for categorical variables. For non-normally distributed variables, results are reported as median ± interquantile range. Significant differences are reported in bold. Abbreviations: MDD, Major Depressive Disorder; BD, Bipolar Disorder; HDRS-21, Hamilton Depression Rating Scale – 21 items; CTQ, Childhood Trauma Questionnaire; CQ, Cognition Questionnaire. [a]subsample of N=180 (72 Cluster 1,108 Cluster 2); [b]subsample of N=164 (63 Cluster 1, 101 Cluster 2); †parametric two-sample t-test; ‡non-parametric Mann-Whitney U test; §chi-squared test; *FDR-corrected q<0.05.

Considering FA-based clusters, significant differences were observed for CTQ physical abuse (p = 0.012), CQ emotional impact (p = 0.028), and CQ attribution of causality (p = 0.046), with patients assigned to Cluster 2 showing higher scores on these variables in comparison with those belonging to Cluster 1. However, these significances

did not survive to FDR correction for multiple comparisons (Table 7). Compared to Cluster 2, Cluster 1 was characterized by higher FA values in all white matter tracts (d = 0.40-1.85, $q < 0.05$) (Appendix 6), with the largest effect sizes observed in the corpus callosum (CC) and bilateral corona radiata, internal capsule, and sagittal stratum (Figure 9B).

Table 7. Clinical and demographic comparisons for the FA-based clusters

Variable	**Cluster 1 (N=121)**	**Cluster 2 (N=154)**	**t / U / χ2**	**p**	**q**
Age	48.00 ± 15.00	49.00 ± 15.75	8918.50‡	0.543	0.723
Sex	78 F; 43 M	99 F; 55 M	0§	1	1
Diagnosis	35 MDD; 86 BD	63 MDD; 91 BD	3.74§	0.053	0.224
Scanner	81 Gyroscan; 40 Igenia	88 Gyroscan; 66 Igenia	2.35§	0.125	0.439
No. of episodes	6.00 ± 7.00	5.50 ± 7.75	9524.50‡	0.751	0.903
Age of onset	27.00 ± 18.00	29.00 ± 18.00	9158.00‡	0.809	0.903
Duration of illness (years)	17.00 ± 18.00	18.00 ± 15.75	8926.00‡	0.551	0.723
Pharmacological load	4.00 ± 3.00	4.00 ± 3.00	9166.50‡	0.817	0.903
HDRS-21 total score	23.00 ± 6.00	22.00 ± 7.00	9940.50‡	0.340	0.604
CTQ physical abuse[a]	5.00 ± 1.00	5.00 ± 2.00	3161.50‡	**0.012**	0.224
CTQ emotional abuse[a]	7.00 ± 4.00	7.00 ± 4.50	3473.50‡	0.202	0.530
CTQ sexual abuse[a]	5.00 ± 0.00	5.00 ± 0.00	3686.50‡	0.345	0.604
CTQ physical neglect[a]	6.00 ± 2.00	6.00 ± 3.50	3480.50‡	0.195	0.530
CTQ emotional neglect[a]	12.00 ± 10.00	13.00 ± 6.00	3610.00‡	0.389	0.629
CTQ total score[a]	37.00 ± 15.00	39.00 ± 15.00	3232.50‡	0.050	0.224
CQ emotional impact[b]	3.00 ± 5.00	4.00 ± 4.00	2670.00‡	**0.028**	0.224
CQ attribution of causality[b]	5.00 ± 3.75	6.00 ± 3.00	2729.00‡	**0.046**	0.224
CQ generalization across time[b]	4.00 ± 4.75	5.00 ± 5.00	3000.50‡	0.274	0.590
CQ generalization across events[b]	6.00 ± 4.00	7.00 ± 3.75	3105.00‡	0.456	0.683
CQ perceived uncontrollability[b]	3.00 ± 3.00	3.50 ± 4.00	3377.00‡	0.876	0.920
CQ total score[b]	21.00 ± 18.00	23.50 ± 15.50	3003.50‡	0.281	0.590

Results are reported as mean ± standard deviation for continuous variables, whereas frequencies are reported for categorical variables. For non-normally distributed variables, results are reported as median ± interquantile range. Significant differences are reported in bold. Abbreviations: MDD, Major Depressive Disorder; BD, Bipolar Disorder; HDRS-21, Hamilton Depression Rating Scale – 21 items; CTQ, Childhood Trauma Questionnaire; CQ, Cognition Questionnaire. [a]subsample of N=180 (73 Cluster 1, 107 Cluster 2); [b]subsample of N=164 (74 Cluster 1, 90 Cluster 2); †parametric two-sample t-test; ‡non-parametric Mann-Whitney U test; §chi-squared test; *FDR-corrected q<0.05.

Regarding the MD-based model, patients assigned to Cluster 2 exhibited higher CTQ physical abuse scores compared to those belonging to Cluster 1 (p = 0.025), despite not surviving to FDR correction (Table 8). In comparison to Cluster 1, all white matter tracts in Cluster 2 exhibited higher MD values (d = 0.28-1.62, q < 0.05) (Appendix 7). The largest effect sizes for clusters' separation were reported for the bilateral corona radiata, internal capsule, SLF, left cingulate gyrus and SFO (Figure 9C).

Table 8. Clinical and demographic comparisons for the MD-based clusters

Variable	**Cluster 1 (N=166)**	**Cluster 2 (N=109)**	**t / U / χ2**	**p**	**q**
Age	49.00 ± 14.00	49.00 ± 16.00	9502.50‡	0.480	0.776
Sex	112 F; 54 M	65 F; 44 M	1.44§	0.231	0.730
Diagnosis	66 MDD; 100 BD	32 MDD; 77 BD	2.67§	0.102	0.658
Scanner	99 Gyroscan; 67 Igenia	70 Gyroscan; 39 Igenia	0.41§	0.524	0.786
No. of episodes	5.00 ± 6.75	7.00 ± 8.00	7874.00‡	0.068	0.658
Age of onset	28.00 ± 19.00	28.00 ± 14.00	8799.00‡	0.701	0.796
Duration of illness (years)	17.00 ± 17.75	17.00 ± 16.00	9505.50‡	0.478	0.776
Pharmacological load	4.00 ± 3.00	4.00 ± 2.00	9621.50‡	0.368	0.730
HDRS-21 total score	22.00 ± 6.75	23.00 ± 6.00	8884.50‡	0.801	0.841
CTQ physical abuse[a]	5.00 ± 1.00	5.00 ± 2.00	3171.50‡	**0.025**	0.533
CTQ emotional abuse[a]	7.00 ± 5.00	7.00 ± 5.00	3950.00‡	0.720	0.796
CTQ sexual abuse[a]	5.00 ± 0.00	5.00 ± 0.00	3932.50‡	0.655	0.796
CTQ physical neglect[a]	6.00 ± 3.00	6.00 ± 3.00	4113.50‡	0.382	0.730
CTQ emotional neglect[a]	13.00 ± 8.50	12.00 ± 6.00	4134.50‡	0.369	0.730
CTQ total score[a]	38.00 ± 17.50	37.00 ± 13.00	3993.50‡	0.630	0.796
CQ emotional impact[b]	3.50 ± 4.00	4.00 ± 4.00	2870.00‡	0.592	0.796
CQ attribution of causality[b]	5.00 ± 4.00	6.00 ± 4.00	2584.50‡	0.125	0.658
CQ generalization across time[b]	4.00 ± 5.00	4.50 ± 5.00	2748.00‡	0.336	0.730
CQ generalization across events[b]	6.00 ± 4.00	7.00 ± 3.25	2683.00‡	0.235	0.730
CQ perceived uncontrollability[b]	3.50 ± 4.00	3.00 ± 3.00	3080.50‡	0.844	0.844
CQ total score[b]	22.00 ± 15.50	26.00 ± 17.00	2756.50‡	0.354	0.730

Results are reported as mean ± standard deviation for continuous variables, whereas frequencies are reported for categorical variables. For non-normally distributed variables, results are reported as median ± interquantile range. Significant differences are reported in bold. Abbreviations: MDD, Major Depressive Disorder; BD, Bipolar Disorder; HDRS-21, Hamilton Depression Rating Scale – 21 items; CTQ, Childhood Trauma Questionnaire; CQ, Cognition Questionnaire. [a]subsample of N=180 (111 Cluster 1, 69 Cluster 2); [b]subsample of N=164 (108 Cluster 1, 56 Cluster 2); †parametric two-sample t-test; ‡non-parametric Mann-Whitney U test; §chi-squared test; *FDR-corrected q<0.05.

Moving to the RD-based clusters, patients allocated to Cluster 1 were characterized by an earlier age of onset compared to those belonging to Cluster 2 (p = 0.03), despite not surviving to FDR correction (Table 9). Widespread higher RD values were detected in Cluster 2 in contrast to Cluster 1 (d = 0.34-1.74, q < 0.05) (Appendix 8), with the greatest contributions observed for the CC, bilateral corona radiata, internal capsule, and cingulate gyrus (Figure 9D).

Table 9. Clinical and demographic comparisons for the RD-based clusters

Variable	**Cluster 1 (N=137)**	**Cluster 2 (N=138)**	**t / U / χ2**	**p**	**q**
Age	47.00 ± 17.00	49.50 ± 13.00	8338‡	0.091	0.453
Sex	92 F; 45 M	85 F; 53 M	0.70§	0.403	0.904
Diagnosis	50 MDD; 87 BD	48 MDD; 90 BD	0.03§	0.864	0.904
Scanner	83 Gyroscan; 54 Igenia	86 Gyroscan; 52 Igenia	0.03§	0.864	0.904
No. of episodes	5.00 ± 7.00	6.00 ± 8.00	9050.5‡	0.540	0.904
Age of onset	27.00 ± 14.00	30.00 ± 16.00	8025‡	**0.030**	0.453
Duration of illness (years)	17.00 ± 17.00	17.00 ± 16.00	9719‡	0.687	0.904
Pharmacological load	4.00 ± 3.00	4.00 ± 2.00	10604.5‡	0.077	0.453
HDRS-21 total score	23.00 ± 6.00	22.00 ± 7.00	9650.5‡	0.765	0.904
CTQ physical abuse[a]	5.00 ± 1.00	5.00 ± 2.00	3460.5‡	0.051	0.453
CTQ emotional abuse[a]	7.00 ± 4.75	7.00 ± 5.00	4251‡	0.561	0.904
CTQ sexual abuse[a]	5.00 ± 0.00	5.00 ± 0.00	4021‡	0.904	0.904
CTQ physical neglect[a]	6.00 ± 3.00	6.00 ± 3.00	4111‡	0.856	0.904
CTQ emotional neglect[a]	13.00 ± 9.75	12.00 ± 6.00	4215‡	0.637	0.904
CTQ total score[a]	38.50 ± 16.00	37.00 ± 14.00	4101‡	0.885	0.904
CQ emotional impact[b]	4.00 ± 4.00	3.00 ± 4.00	3502‡	0.633	0.904
CQ attribution of causality[b]	5.00 ± 4.00	5.00 ± 3.50	3300.5‡	0.851	0.904
CQ generalization across time[b]	5.00 ± 5.00	4.00 ± 4.50	3672.5‡	0.298	0.893
CQ generalization across events[b]	6.00 ± 4.00	6.00 ± 4.00	3635.5‡	0.358	0.904
CQ perceived uncontrollability[b]	4.00 ± 4.00	3.00 ± 3.00	3841‡	0.108	0.453
CQ total score[b]	24.00 ± 16.00	21.00 ± 16.00	3743‡	0.205	0.717

Results are reported as mean ± standard deviation for continuous variables, whereas frequencies are reported for categorical variables. For non-normally distributed variables, results are reported as median ± interquantile range. Significant differences are reported in bold. Abbreviations: MDD, Major Depressive Disorder; BD, Bipolar Disorder; HDRS-21, Hamilton Depression Rating Scale – 21 items; CTQ, Childhood Trauma Questionnaire; CQ, Cognition

Questionnaire. [a]subsample of N=180 (90 Cluster 1, 90 Cluster 2); [b]subsample of N=164 (85 Cluster 1, 79 Cluster 2); [†]parametric two-sample t-test; [‡]non-parametric Mann-Whitney U test; [§]chi-squared test; *FDR-corrected q<0.05.

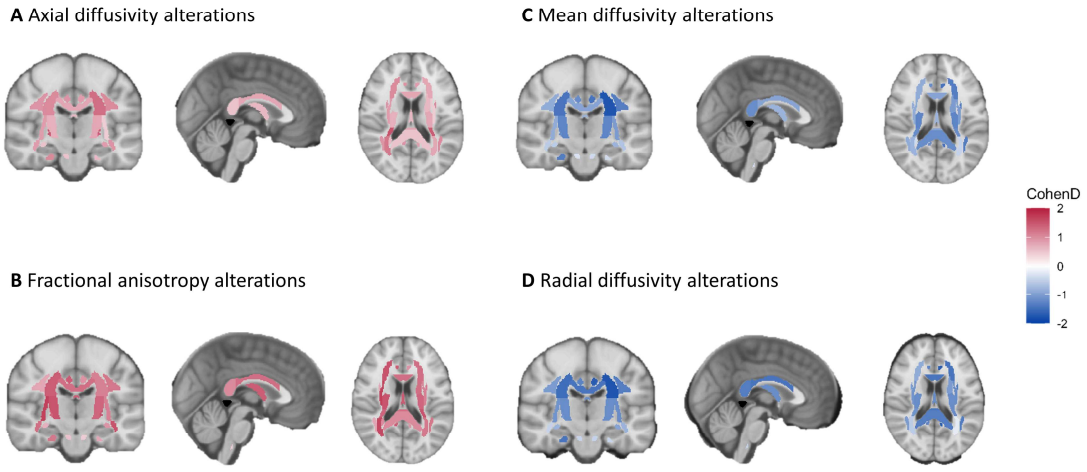

Figure 9. Cohen's d values describing the magnitude of differences in DTI diffusivity values between clusters. *A. Cohen's d values for AD-based clusters. B. Cohen's d values for FA-based clusters. C. Cohen's d values for MD-based clusters. D. Cohen's d values for RD-based clusters. Positive values (red) indicate higher values for Cluster 1 compared to Cluster 2, whereas negative values (blue) indicate higher values for Cluster 2 compared to Cluster 1.*

3.2.6 Biological and clinical characterization of the multimodal neuroimaging stratification model

Together with data-driven stratification models based on each neuroimaging feature in isolation, a multimodal approach was implemented to investigate whether the integration of different neuroimaging modalities could unveil novel data-driven groupings of patients that might be overlooked when focusing on a single neuroimaging modality. To achieve this aim, we implemented a multiview spectral clustering algorithm within the stability-based relative clustering validation pipeline, as described in the Methods.

The results of the demographic and clinical comparisons between the multimodal-based clusters are reported in Table 10. A significant difference was observed for CQ perceived uncontrollability ($p = 0.031$) and a trend toward significance for CQ total score ($p = 0.049$), with patients assigned to Cluster 1 showing higher scores compared to those assigned to Cluster 2. However, these comparisons did not survive to FDR correction. Considering differences in neuroimaging features, clusters' differentiation was mainly

guided by DTI extracted measures (d = 0.32-0.89, q < 0.05), followed by FC strength values which, however, did not survived to FDR correction for multiple comparisons (d = 0.19-0.51) (Appendix 10). As shown in Figure 10, Cluster 2 exhibited higher RD, MD, AD, and lower FA values compared to Cluster 1 in the vast majority of white matter tracts, suggesting a widespread dysconnectivity pattern.

Table 10. Clinical and demographic comparisons for the multimodal-derived clusters

Variable	**Cluster 1 (N=59)**	**Cluster 2 (N=57)**	**t / U / χ2**	**p**	**q**
Age	49.00 ± 13.50	47.00 ± 13.00	1871.5‡	0.295	0.707
Sex	38 F; 21 M	36 F; 21 M	0§	1	1
Diagnosis	26 MDD; 33 BD	30 MDD; 27 BD	0.54§	0.461	0.762
Scanner	27 Gyroscan; 32 Igenia	22 Gyroscan; 35 Igenia	0.35§	0.553	0.762
No. of episodes	6.00 ± 7.00	4.00 ± 7.00	1874.5‡	0.284	0.707
Age of onset	26.00 ± 17.00	27.00 ± 16.00	1799‡	0.517	0.762
Duration of illness (years)	18.00 ± 17.00	18.00 ± 15.00	1683.5‡	0.993	1.000
Pharmacological load	5.00 ± 2.50	4.00 ± 2.00	1771‡	0.617	0.762
HDRS-21 total score	21.80 ± 5.34	21.44 ± 6.31	0.33†	0.743	0.821
CTQ physical abuse[a]	5.00 ± 1.00	5.00 ± 2.00	1049‡	0.658	0.768
CTQ emotional abuse[a]	8.00 ± 6.50	7.00 ± 5.75	1177.5‡	0.554	0.762
CTQ sexual abuse[a]	5.00 ± 0.25	5.00 ± 0.00	1205.5‡	0.257	0.707
CTQ physical neglect[a]	6.00 ± 4.00	5.00 ± 3.00	1217‡	0.349	0.732
CTQ emotional neglect[a]	13.00 ± 10.25	12.00 ± 6.00	1207‡	0.419	0.762
CTQ total score[a]	39.50 ± 19.50	37.00 ± 14.00	1166.5‡	0.617	0.762
CQ emotional impact[b]	4.00 ± 6.00	3.00 ± 3.50	915.5‡	0.183	0.707
CQ attribution of causality[b]	6.00 ± 3.00	6.00 ± 3.00	884.5‡	0.303	0.707
CQ generalization across time[b]	5.00 ± 4.25	4.00 ± 3.50	935‡	0.127	0.667
CQ generalization across events[b]	7.03 ± 2.70	5.95 ± 2.82	1.73†	0.087	0.612
CQ perceived uncontrollability[b]	4.00 ± 5.00	3.00 ± 2.00	998.5‡	**0.031**	0.515
CQ total score[b]	24.50 ± 15.25	21.00 ± 12.00	981.0‡	**0.049**	0.515

Results are reported as mean ± standard deviation for continuous variables, whereas frequencies are reported for categorical variables. For non-normally distributed variables, results are reported as median ± interquantile range. Significant differences are reported in bold. Abbreviations: MDD, Major Depressive Disorder; BD, Bipolar Disorder; HDRS-21, Hamilton Depression Rating Scale – 21 items; CTQ, Childhood Trauma Questionnaire; CQ, Cognition Questionnaire. [a]subsample of N=94 (44 Cluster 1, 50 Cluster 2); [b]subsample of N=79 (40 Cluster 1, 39 Cluster 2); †parametric two-sample t-test; ‡non-parametric Mann-Whitney U test; §chi-squared test; *FDR-corrected q<0.05.

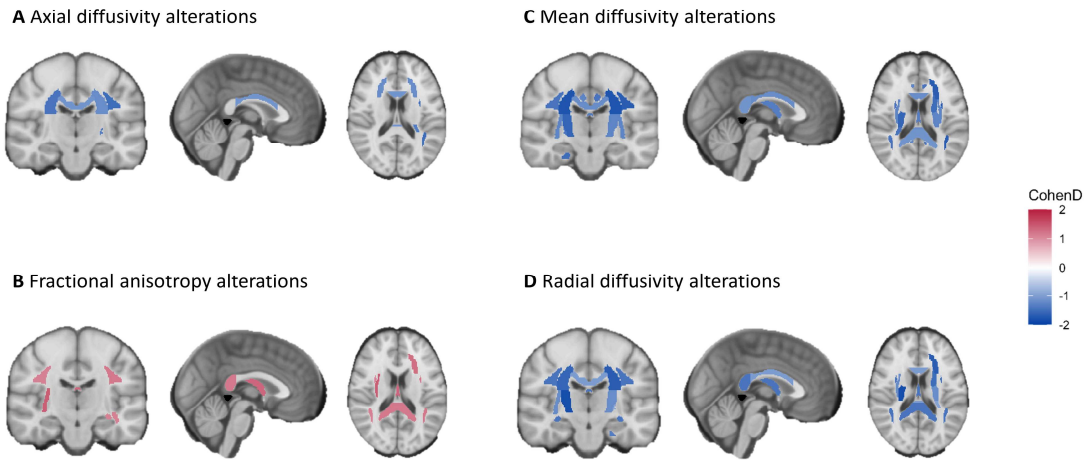

Figure 10. Cohen's d values describing the magnitude of differences in neuroimaging features between the multimodal-derived clusters. *A. Cohen's d values for axial diffusivity. B. Cohen's d values for fractional anisotropy. C. Cohen's d values for mean diffusivity. D. Cohen's d values for radial diffusivity. Positive values (red) indicate higher values for Cluster 1 compared to Cluster 2, whereas negative values (blue) indicate higher values for Cluster 2 compared to Cluster 1.*

3.2.7 Biological and clinical characterization of the FACS-based stratification model

Considering demographic and clinical characteristics of the FACS-derived clusters, a significant difference for diagnosis was detected, with a higher proportion of MDD patients assigned to Cluster 2 compared to Cluster 1 ($p = 0.022$). A significant between-clusters difference was observed for CTQ total score ($p = 0.049$), with patients belonging to Cluster 2 being characterized by higher scores relative to those allocated to Cluster 1. However, these comparisons did not survive to FDR correction (Table 11). Compared to Cluster 2, Cluster 1 showed increased number of CD8+/TEMRA/CM/Perf-GrzB+, NK cells/Perf-GrzB+, CD8+/EM/CM/Perf-GrzB+, CD3+/Tγδ/Perf-GrzB+, CD4+/TNF-α, NK cells/IL-17, CD8+/TNF-α, NK cells/TNF-α, CD8+/IL-17, CD4+/CM/CD69+, CD4+/IL-17, CD4+/Naive/CD69+, CD4+/EM/CD69+, CD4+/IL-2, CD8+/IL-2, and NK cells/GM-CSF ($d = 0.22$-1.56, $q < 0.05$). Conversely, patients belonging to Cluster 2 were characterized by higher frequencies of CD8+/TEMRA/Perf+GrzB+, CD8+/CM/Perf+GrzB+, CD8+/EM/Perf+GrzB+, NK cells/Perf+GrzB+, CD3+/Tγδ/Perf+GrzB+, CD8+/CM/Perf+GrzB-, CD3+/Tγδ/Perf+GrzB-, CD8+/EM/Perf+GrzB-, CD8+/TEMRA/Perf+GrzB-, NK cells/Perf+GrzB-,

CD8+/Naive/Perf+GrzB+, CD8+/Naive/Perf+GrzB-, CD4+/Naive/CD25+, and CD4+/CM/CD25+, CD4+/EM/CD25+ (d = 0.26-1.93, q < 0.05) (Figure 11 and Appendix 11).

Table 11. Clinical and demographic comparisons for the FACS-derived clusters

Variable	**Cluster 1 (N=41)**	**Cluster 2 (N=96)**	**t / U / χ2**	**p**	**q**
Age	51.00 ± 11.00	49.00 ± 12.25	1915.00‡	0.805	0.984
Diagnosis	18 MDD; 23 BD	64 MDD; 32 BD	5.28§	**0.022**	0.333
Sex	28 F; 13 M	71 F; 25 M	0.22§	0.638	0.984
No. of episodes	4.00 ± 5.00	4.50 ± 5.25	2027.00‡	0.781	0.984
Age of onset	26.00 ± 12.00	30.00 ± 20.00	1642.50‡	0.126	0.429
Duration of illness (years)	19.00 ± 19.00	17.00 ± 15.25	2291.50‡	0.129	0.429
Pharmacological load	4.00 ± 3.00	4.00 ± 3.00	1998.00‡	0.888	0.984
HDRS-21 total score	21.78 ± 5.86	21.80 ± 5.79	-0.02†	0.984	0.984
CTQ physical abuse[a]	5.00 ± 2.00	5.00 ± 2.00	1067.50‡	0.300	0.605
CTQ emotional abuse[a]	6.5.00 ± 6.00	7.00 ± 7.00	1000.00‡	0.168	0.481
CTQ sexual abuse[a]	5.00 ± 0.00	5.00 ± 0.00	1228.00‡	0.791	0.984
CTQ physical neglect[a]	6.00 ± 2.00	6.00 ± 4.00	1042.50‡	0.265	0.605
CTQ emotional neglect[a]	10.00 ± 7.25	13.00 ± 9.00	912.00‡	0.050	0.333
CTQ total score[a]	35.50 ± 14.50	40.00 ± 21.00	910.00‡	**0.049**	0.333
CQ emotional impact[b]	3.00 ± 4.00	4.50 ± 5.00	755.50‡	0.093	0.429
CQ attrbution of causality[b]	5.00 ± 4.00	5.00 ± 5.00	953.50‡	0.961	0.984
CQ generalization across time[b]	4.50 ± 5.00	4.00 ± 6.00	834.50‡	0.303	0.605
CQ generalization across events[b]	6.59 ± 2.60	6.68 ± 2.84	-0.15†	0.879	0.984
CQ perceived uncontrollability[b]	3.00 ± 4.00	4.00 ± 4.00	950.00‡	0.937	0.984
CQ total score[b]	22.00 ± 11.50	22.50 ± 19.25	911.50‡	0.694	0.984

Results are reported as mean ± standard deviation for continuous variables, whereas frequencies are reported for categorical variables. For non-normally distributed variables, results are reported as median ± interquantile range. Significant differences are reported in bold. Abbreviations: MDD, Major Depressive Disorder; BD, Bipolar Disorder; HDRS-21, Hamilton Depression Rating Scale – 21 items; CTQ, Childhood Trauma Questionnaire; CQ, Cognition Questionnaire. [a]subsample of N=107 (32 Cluster 1, 75 Cluster 2); [b]subsample of N=92 (32 Cluster 1, 60 Cluster 2); †parametric two-sample t-test; ‡non-parametric Mann-Whitney U test; §chi-squared test; *FDR-corrected q<0.05.

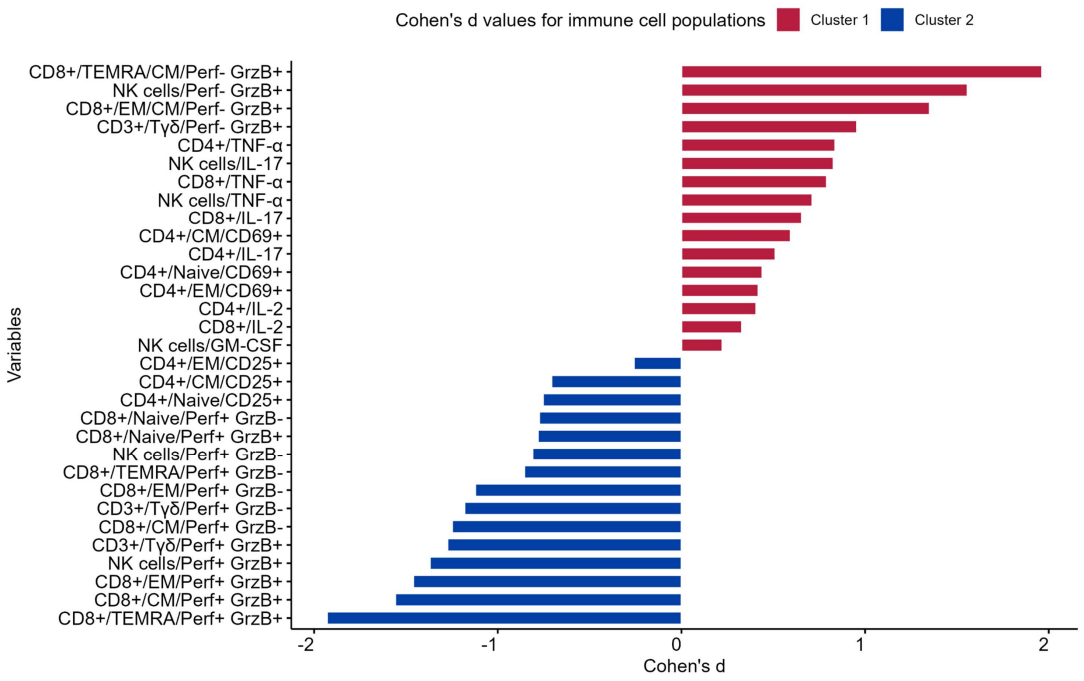

Figure 11. Cohen's d values describing the magnitude of differences in immune cell counts between clusters. *Positive values (red) indicate higher values for Cluster 1 compared to Cluster 2, whereas negative values (blue) indicate higher values for Cluster 2 compared to Cluster 1. Abbreviations: CM, central memory; EM, effective memory; GM-CSF; granulocyte macrophage colony stimulating factor; IL, interleukin; INF; interferon; TNF, tumor necrosis factor; Perf; perforin; GrzB; granzyme; TEMRA, T cells re-expressing CD45RA; NK, natural killer.*

3.2.8 Biological and clinical characterization of the stratification model based on immune-inflammatory profiles

The data-driven clusters derived from immune-inflammatory profiles showed significant differences in the majority of CQ domains, with patients assigned to Cluster 2 showing higher CQ generalization across time ($p = 0.001$, $q = 0.010$), CQ generalization across events ($p = 0.010$, $q = 0.048$), CQ perceived uncontrollability ($p = 0.003$, $q = 0.020$), and CQ total scores ($p < 0.001$, $q = 0.002$) compared to those belonging to Cluster 1 (Table 12). Considering the immune-inflammatory signatures associated to each cluster, Cluster 2 exhibited higher immune profiles z-scores compared to Cluster 1, reflecting an inflammatory status ($d = 0.15$-2.25, $q < 0.05$) (Figure 12 and Appendix 12).

Table 12. Clinical and demographic comparisons for the clusters derived from immune-inflammatory profiles.

Variable	Cluster 1 (N=115)	Cluster 2 (N=70)	t / U / $\chi 2$	p	q
Age	50.00 ± 13.00	49.50 ± 14.50	4103.5‡	0.825	0.889
Diagnosis	59 MDD; 56 BD	43 MDD; 27 BD	1.42§	0.233	0.358
Sex	76 F; 39 M	45 F; 25 M	0.01§	0.928	0.928
No. of episodes	4 ± 6.50	5.00 ± 3.00	4270.5‡	0.484	0.645
Age of onset	27.00 ± 17.00	29.50 ± 19.75	3818‡	0.558	0.698
Duration of illness (years)	18.00 ± 16.50	17.00 ± 16.25	4331.5‡	0.386	0.551
Pharmacological load	4.00 ± 3.00	5.00 ± 3.00	3475‡	0.115	0.256
HDRS-21 total score	21.79 ± 6.08	21.51 ± 5.59	0.32†	0.752	0.885
CTQ physical abuse[a]	5.00 ± 1.00	5.00 ± 1.25	2676‡	0.845	0.889
CTQ emotional abuse[a]	7.00 ± 5.57	8.00 ± 7.00	2285.5‡	0.172	0.287
CTQ sexual abuse[a]	5.00 ± 0.00	5.00 ± 0.25	2317‡	0.068	0.170
CTQ physical neglect[a]	6.00 ± 2.00	6.50 ± 4.00	2143.5‡	**0.047**	0.163
CTQ emotional neglect[a]	11.50 ± 9.00	13.00 ± 9.00	2315.5‡	0.172	0.287
CTQ total score[a]	37.00 ± 16.00	40.00 ± 21.75	2247‡	0.135	0.270
CQ emotional impact[b]	4.00 ± 4.50	4.00 ± 5.75	1668‡	0.057	0.163
CQ attribution of causality[b]	5.00 ± 4.00	6.00 ± 5.00	1660.5‡	0.055	0.163
CQ generalization across time[b]	4.00 ± 4.00	6.00 ± 5.00	1375.5‡	**0.001**	**0.010***
CQ generalization across events[b]	6.00 ± 4.00	8.00 ± 4.75	1520‡	**0.010**	**0.048***
CQ perceived uncontrollability[b]	2.00 ± 2.00	4.00 ± 5.00	1437.5‡	**0.003**	**0.020***
CQ total score[b]	20.00 ± 13.00	31.00 ± 15.75	1324.5‡	**<0.001**	**0.002***

Results are reported as mean ± standard deviation for continuous variables, whereas frequencies are reported for categorical variables. For non-normally distributed variables, results are reported as median ± interquantile range. Significant differences are reported in bold. Abbreviations: MDD, Major Depressive Disorder; BD, Bipolar Disorder; HDRS-21, Hamilton Depression Rating Scale – 21 items; CTQ, Childhood Trauma Questionnaire; CQ, Cognition Questionnaire. [a]subsample of N=150 (94 Cluster 1, 56 Cluster 2); [b]subsample of N=133 (83 Cluster 1, 40 Cluster 2); †parametric two-sample t-test; ‡non-parametric Mann-Whitney U test; §chi-squared test; *FDR-corrected q<0.05.

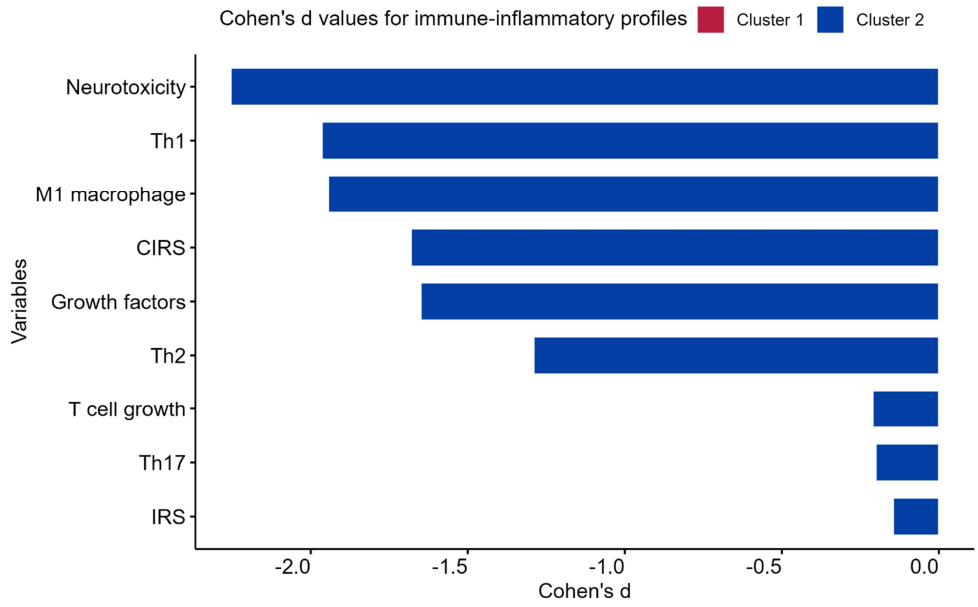

Figure 12. Cohen's d values describing the magnitude of differences in immune-inflammatory profiles between clusters. *Positive values (red) indicate higher values for Cluster 1 compared to Cluster 2, whereas negative values (blue) indicate higher values for Cluster 2 compared to Cluster 1. Abbreviations: Abbreviations: Th, T helper cells; CIRS, compensatory immunoregulatory system; IRS, immune-inflammatory response system.*

3.3 Differential multivariate neuro-biological-ACEs associations among clusters

To test whether the multivariate association between biological data and childhood trauma is differentially expressed between clusters, grouped PLS correlation (PLSC) analyses were implemented for each data-driven stratification model, considering the corresponding clusters' labels as grouping variable. Specifically, for each PLSC model, the biological data used as input features for clustering were considered as "biological" dataset, whereas CTQ domains were entered as "behavioural" variables (see Methods for additional details). Among all the stratification models, significant latent variable (LV) pairs surviving to FDR correction were obtained for FC-based (q = 0.01) and immune-based (q = 0.03) models, which accounted for the 39.3% and 76.0% of explained covariance, respectively.

3.3.1 Grouped PLSC results for the FC-based stratification model

Focusing on the significant LV pairs obtained from the FC-based stratification model, the contribution of neuroimaging features was largely driven by FC positive strength values, with the largest brain bootstrap ratios (BSR) observed for seeds in the caudal part of the cingulate gyrus, superior and inferior parietal lobules, insula, somatosensory cortex, as well as subcortical regions such as the lateral amygdala, thalamus, and basal ganglia (Figure 13A). Significant BSR were also observed for FC negative strengths values in the ventral and caudal cingulate gyrus, precentral gyrus, rostral and caudal SPL, dorsolateral putamen, and thalamus (Figure 13B). To investigate how the multivariate brain-ACEs relationship manifest across CTQ domains and clusters, a bootstrapping procedure with 5000 resamples was performed to compute 95% confidence intervals (CI) on brain-CTQ correlations (i.e., loadings) in each cluster. Loadings whose 95% CI do not include a correlation of 0 are indicative of CTQ domains highly and significantly contributing to the LV. As shown in Figure 8C, almost all CTQ domains significantly contributed to the brain-ACEs multivariate association in Cluster 1, whereas significant associations for CTQ emotional neglect and sexual abuse were found in Cluster 2. These results suggest that, although multivariate brain-ACEs relationships can be detected in both clusters, these associations are differentially expressed, with one cluster being characterized by a "multi-trauma" profile while the other showing a more "neglect-focused" signature. With the exception of CTQ sexual abuse in Cluster 2, the direction of the loadings of the CTQ domains was negative, meaning that higher exposure to childhood trauma is associated with decreased FC strength, and this effect is particularly evident in Cluster 1.

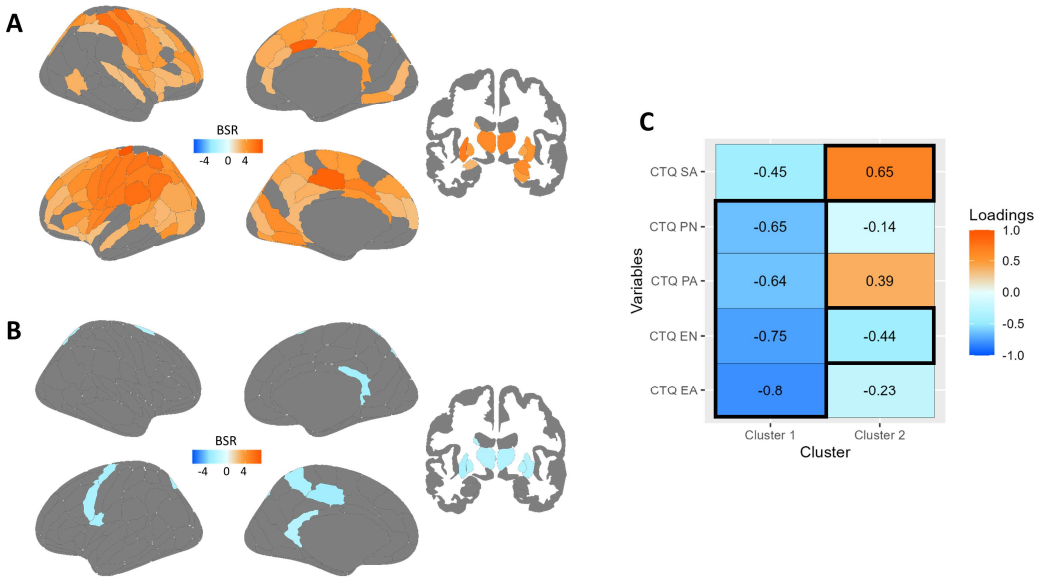

Figure 13. Differences in multivariate brain-ACEs relationships between the FC-based clusters. *A-B. Significant brain bootstrap ratios (BSRs) for positive (A) and negative (B) FC strength in each region. Brain regions with orange BSRs have correlations that have the same directionality shown in the heatmap in (C). Brain regions with blue BSRs have correlations in the opposite direction shown in the heatmap in (C). C. PLS correlations for each CTQ domain (row) and each cluster (columns). Loadings with black outline are those with 95% confidence intervals that do not include zero. Abbreviations: BSR, bootstrap ratio; CTQ, Childhood Trauma Questionnaire; SA, sexual abuse; PN, physical neglect; PA, physical abuse; EN, emotional neglect; EA, emotional abuse.*

3.3.2 Grouped PLSC results for the stratification model based on immune-inflammatory profiles

Considering the grouped PLSC results for the immune-based stratification model, all the immune-inflammatory profiles significantly drove the immune-ACEs multivariate relationship, with the higher contribution observed for the IRS profile (Figure 14A). Notably, all CTQ domains significantly contributed to the LV in Cluster 2, whereas in Cluster 1 significant contributions where observed for CTQ physical and sexual abuse. In both clusters, the direction of the loadings of CTQ domains was positive, indicating that the exposure to childhood trauma is associated with higher inflammation (Figure 14B).

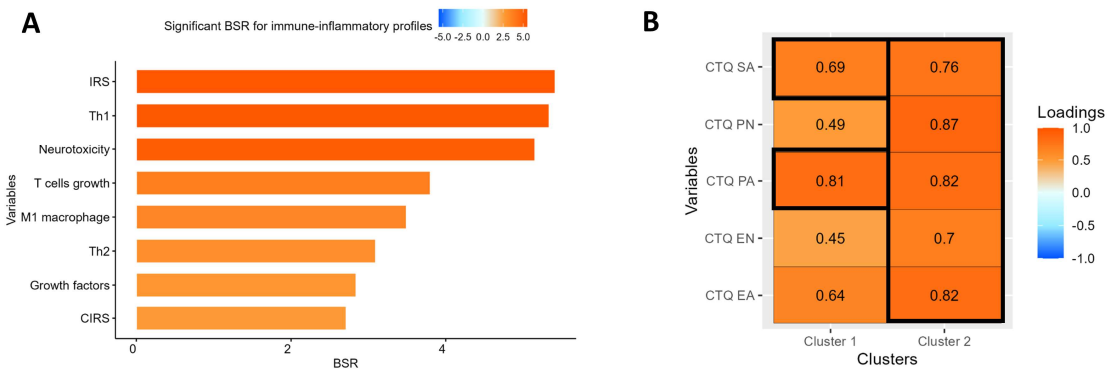

Figure 14. Differences in multivariate biological-trauma relationships between the immune-based clusters. *A. Significant bootstrap ratios (BSRs) for each immune-inflammatory profile. Immune-inflammatory profiles with orange BSRs have correlations that have the same directionality shown in the heatmap in (B). Immune-inflammatory profiles with blue BSRs have correlations in the opposite direction shown in the heatmap in (B). B. PLS correlations for each CTQ domain (row) and each cluster (columns). Loadings with black outline are those with 95% confidence intervals that do not include zero. Abbreviations: BSR, bootstrap ratio; Th, T helper cells; CIRS, compensatory immunoregulatory system; IRS, immune-inflammatory response system; CTQ, Childhood Trauma Questionnaire; SA, sexual abuse; PN, physical neglect; PA, physical abuse; EN, emotional neglect; EA, emotional abuse.*

3.4 General linear models and mediation analyses

Given the significant neuro-biological-ACEs multivariate associations, the final step was to explore whether, for each PLSC model, LV neuro-biological scores (i.e., FC positive and negative strength and immune-inflammatory profiles) differentially mediated the relationships between the LV CTQ scores and CQ domains in the FC-based and immune-inflammatory clusters.

3.4.1 Effect of FC strength on cognitive distortions in the FC-derived clusters

Considering the PLSC model for the FC-based clusters, the assumptions to perform the mediation analysis were assessed through multivariate and univariate general linear models (GLM) separated for each cluster, entering the LV FC scores as predictors, while CQ domains were considered as outcome variables (see Methods for additional details). Multivariate GLMs did not show significant multivariate effects for LV FC scores on CQ domains neither in Cluster 1 (Wilk's $\lambda = 0.88$, $F_{(5,27)} = 0.73$, p=0.609) nor in Cluster 2 (Wilk's $\lambda = 0.87$, $F_{(5,58)} = 1.71$, p=0.147). However, considering univariate results, a significant effect was observed in Cluster 2, with LV FC scores significantly and positively predicting CQ generalization across time ($b = 0.029$, $p = 0.031$; overall model

fit: R^2 = 0.07, RMSE = 0.90, $F_{(1,62)}$ = 4.87, p = 0.031). These findings laid the basis to perform a mediation model in Cluster 2 in which LV FC scores mediate the relationship between LV CTQ scores and CQ generalization across time.

Mediation analysis revealed a significant indirect effect of LV CTQ scores on CQ generalization across time through LV FC scores (a*b: b = 0.137, SE = 0.095, 90%CI [0.016; 0.318]). The total and the direct effects of LV CTQ scores on CQ generalization across time were not significant; however, the significant indirect effect support the mediation effect of LV FC scores. Specifically, LV CTQ scores significantly increased LV FC scores (path a: b = 4.7, 90%CI [2.433, 6.967], p = 0.001), whereas the effect of LV FC scores on CQ generalization across time is marginally significant (path b: b = 0.029, 90%CI[0.005, 0.054], p = 0.053). Overall, these results suggest that in Cluster 2 LV FC scores significantly mediate the relationship between LV CTQ scores on CQ generalization across time, despite the total effect is not significant (Figure 15).

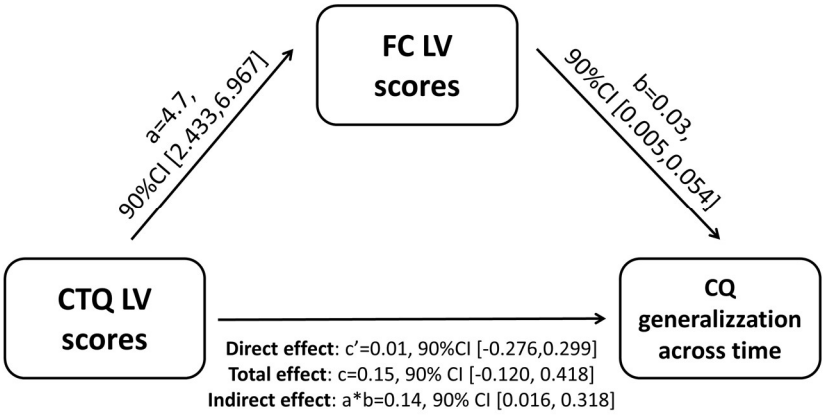

Figure 15. Mediation effect of FC LV scores in the relationship between CTQ LV scores and CQ generalization across time in Cluster 2*. Abbreviations: CQ, cognition questionnaire; CTQ, Childhood Trauma Questionnaire; FC, functional connectivity; LV, latent variable.*

3.4.2 Effect of inflammation on cognitive distortions in clusters derived from immune-inflammatory profiles

Similarly, the potential mediating effect of LV immune-inflammatory scores in the relationship between LV CTQ scores and CQ domains in the clusters derived from immune-inflammatory profiles was investigated. Multivariate GLMs did not show significant multivariate effects for PLS immune scores on CQ domains neither in Cluster

1 (Wilk's $\lambda = 0.97$, $F_{(5,70)} = 0.43$, $p = 0.826$) nor in Cluster 2 (Wilk's $\lambda = 0.85$, $F_{(5,38)} = 1.38$ $p = 0.254$). No significant effects were reported in subsequent univariate analyses, indicating that PLSC immune scores do not contribute to the prediction of CQ domains in the identified clusters.

4. DISCUSSION

This project aimed to investigate whether multimodal neuroimaging data and immune-inflammatory markers provide information for data-driven and clinically meaningful stratifications of Mood Disorder patients. To achieve this aim, we employed a novel and robust unsupervised ML pipeline that provides direct information about the stability and generalizability of the identified subgroups to unseen data. Reliable and stable clusters of depressed patients were identified based on neuroimaging data and immune-inflammatory markers, with accuracies in clusters' differentiation ranging from 41% to 85%. Considering the clinical validation of the discovered stratification models, clusters based on immune-inflammatory profiles showed significant differences in cognitive distortions, with patients characterized by high levels of peripheral inflammation exhibiting biased cognitive processes. In addition, differential multivariate neurobiological-ACEs associations emerged in the FC-based and immune-based clusters, alongside the mediating role of FC strength in the relationship between childhood trauma and overgeneralization across time in a specific subgroup of patients. To the best of our knowledge, this approach is innovative and has the potential to provide reliable prognostic data-driven models for the individualized prediction of long-term clinical outcomes in depressed patients.

4.1 Neuroimaging data provide information for stable data-driven stratifications of Mood Disorders

The results from unsupervised ML analyses suggest that, compared to immune-inflammatory profiles and immune cell subpopulations, neuroimaging data led to more stable clustering solutions, with the highest accuracy (84.8%) observed for the FC-based model. The utility of resting-state fMRI features in characterizing "biotypes" of depressed patients has been previously reported in the literature, suggesting that not only different

brain functional alterations might reflect specific subgroups of patients but could also associate with relevant clinical outcomes (e.g., response to treatments) (Liang et al, 2020; Tozzi & Zhang, 2024). The results of the current study contribute to this landscape by unveiling 2 subtypes of depressed patients characterized by hyper- and hypo-connectivity FC patterns, respectively. Considering the "hyper-connected" cluster (i.e., Cluster 1), a major contribution was found for the FC strength in the precuneus and posterior cingulate gyrus, both areas being involved in the DMN (Raichle et al, 2001). Conversely, the "hypo-connected" subtype (i.e., Cluster 2) showed a marked diminished FC strength in the medial temporal and superior frontal gyri. A similar stratification model was described by Liang et al (2020), demonstrating that patterns of reduced and increased FC within the DMN can categorize MDD patients into distinct subgroups. Importantly, patients characterized by hyper-activations within the DMN have been shown to exhibit emotional and cognitive deficits and benefit from behavioural therapies (Tozzi & Zhang, 2024). However, the results of our stratification model failed to provide evidence of significant differences in depression severity between the FC-based clusters, possibly due to the small sample size. It should be noted, though, that a worsened cognitive distortion profile was observed in patients assigned to the hypo-connected cluster compared to those belonging to the hyper-connected one, despite not surviving multiple comparisons. Functional alterations in the MTG and SFG have been consistently reported in BD and MDD (Zhang et al, 2024), and the strength of their connectivity has been demonstrated to be positively associated with an efficient suppression of intrusive thoughts in the general population (Lu et al, 2022). Hence, a diminished FC strength in these regions might reflect an impaired cognitive inhibition toward invasive thoughts, potentially contributing to a negative thinking style.

Data-driven subgroups derived from GM volumes and cortical thickness distinguished between patients with widespread GM volumetric and cortical reductions from those with a preserved neural structure with accuracies above 80%. This distinction between patients with preserved versus not-preserved GM patterns has been reported also in MDD and transdiagnostic populations, showing differential associations with cognitive functions (Pfarr et al, 2023; Yeung et al, 2021). Contrarily, no significant differences in clinically relevant outcomes were reported in our models. Nevertheless, it is possible that alterations in cortical and subcortical structures might reflect cognitive deficits in Mood

Disorders rather than impaired emotional processing or depression severity. Indeed, deviations from normal brain maturation have been linked with delays or precocity in cognitive abilities in the general population (Erus et al, 2015), which could be explained by individual differences in the activity of cholinergic, glutamatergic, and dopaminergic neurotransmitter systems in modelling cortical changes in adulthood and ageing (Lotter & Saberi, 2024). Alterations in these pathways have been consistently reported in both MDD and BD (Dulawa & Janowsky, 2019; Dunlop & Nemeroff, 2007; Ino et al, 2023; Moriguchi et al, 2019), also contributing to cognitive impairments in these patients (Colwell et al, 2022). Future studies investigating differences in cognitive functions in the discovered GM-based clusters might elucidate the association between differential brain structural patterns and compromised cognitive processes in depression.

Measures of WM integrity clustered depressed patients into 2 subgroups with accuracies ranging from 76.5% to 80.1%, reflecting the existence of stable and reliable clustering solutions. What emerged from these stratification models is that patients characterized by a widespread WM dysconnectivity pattern can be separated from those presenting a more preserved WM integrity, and this phenomenon can be captured by all WM diffusivity indexes. These results partially align with those of Liang et al (2019), who unveiled 3 subtypes of MDD patients based on FA values reflecting a gradient in WM alterations, especially in the CC and cingulate gyrus. It is worth noting that, despite being comparable for depressive symptoms, the subtypes discovered by Liang et al (2019) were characterized by distinct neurocognitive profiles, with patients showing widespread WM alterations exhibiting deficits in attention, memory, and executive functions. These findings, along with the absence of differences in the severity of depression and cognitive distortions in our DTI-based subtypes, suggest that WM abnormalities in depressed patients are more likely to drive impairments in cognitive functions rather than depressive symptomatology. Microstructural changes in the CC and cingulate gyrus have been previously associated with deficits in working memory and attention in depressed patients (Schermuly et al, 2010; Yamada et al, 2020), and a recent ML study demonstrated that WM integrity in frontal-limbic tracts predicts performance in information processing speed in late-onset depressed patients (Wang et al, 2021b). Another possible explanation for the absence of clinically relevant differences among DTI-based subtypes is that BD and MDD are distinguished by unique WM alterations that might be masked when

looking at them transdiagnostically. Indeed, while abnormalities in CC have been described in BD, SZ, and ASD, MDD patients exhibit a specific WM pattern distinguished from those observed in other psychiatric populations (Koshiyama et al, 2020). Moreover, supervised ML studies demonstrated that indexes of WM integrity differentiate BD from MDD with accuracies ranging from 56% to 78%, supporting the existence of specific WM signatures for each disorder (Calesella et al, 2024; Vai et al, 2019). In line with these considerations, we found that the AD-based clusters associate with the diagnosis (uncorrected p-value), with a higher proportion of MDD patients in the WM-compromised subgroup compared to the other. The investigation of WM-based subtypes separately for BD and MDD could provide additional insight into the association between WM, diagnostic categories, and clinical outcomes in depression.

The results of the multimodal stratification model partially overlap with those reported for the DTI-based models, achieving an optimal 2-clusters solution with an accuracy of 73.4%. The larger contribution of DTI indexes compared to other neuroimaging modalities in clusters' differentiation might be explained by the theoretical and computational mechanisms underlying the multiview spectral clustering algorithm: since the agreement of clustering labels across views represents the criterion to identify the optimal clustering solution, it is more likely to obtain similar grouping structures among highly correlated DTI measures rather than structural or functional neuroimaging features. However, the combination of all DTI modalities in the same stratification model unveiled a slightly different grouping of patients compared to those obtained from separated DTI measures. Specifically, the multimodal approach uncovered a subtype of depressed patients distinguished by low FA and high axial, radial, and mean diffusivity in the majority of WM tracts (i.e., Cluster 2). Despite being commonly considered as an index of axonal integrity, high AD values combined with decreased FA and increased MD are supposed to reflect the expansion of extracellular space and increase of water diffusion (Alves et al, 2015; Winklewski et al, 2018). Indeed, a widespread WM disruption seems to characterize patients belonging to this cluster, as also reflected by increased RD values (Winklewski et al, 2018). It should be also noticed that, despite not surviving to correction for multiple comparisons, patients assigned to this subgroup were distinguished by abnormal positive FC strength in the superior and inferior frontal gyri, motor cortex, and thalamus (see Appendix 11). Altered subcortical-somatosensory

resting-state FC has been proposed as a transdiagnostic neurobiological correlate of general psychopathology (i.e., *p* factor), possibly reflecting altered bodily self-consciousness and interoceptive mechanisms commonly reported in various psychiatric disorders (Kebets et al, 2019; Van Dam et al, 2017). These findings, coupled with evidence of altered WM integrity in projection fibres (e.g., corona radiata), suggest that patients assigned to this subtype could be characterized by altered sensory-motor processing possibly arising from an inefficient top-down control over lower-level mechanisms. Investigating these aspects in the future could therefore provide a more comprehensive clinical and symptomatic characterization of these patients. Conversely, an opposite WM pattern characterized by high FA and low diffusivity indices was observed in Cluster 1. Although FA is commonly considered as an index of well-preserved and dense WM structure, this interpretation has been recently criticized for being over-simplistic. In fact, in the case of demyelination processes or augmented membrane permeability (e.g., multiple sclerosis, ageing, or brain lesions), a reduction in all diffusivity indexes could be observed while unchanged FA (Figley et al, 2022). Indeed, the uncovered multimodal-based subgroups may reflect distinct patterns of WM alterations in depressed patients linked to differential underlying neurobiological mechanisms. The integration of DTI with more sophisticated measures of WM integrity (e.g., neurite orientation and density imaging [NODDI]) might yield more insights into how such mechanisms may contribute to different patterns of WM organization in Mood Disorders.

Unlike the FC-based model, stratification models based on fALFF and ReHo did not achieve stable and significant data-driven subtypes of depressed patients. These results suggest that the strength of functional connections among brain regions rather than their spontaneous neural activity at rest is more likely to capture neurobiological differences within the depressed population. This is in line with the current view of neuropsychiatric illnesses as “dysconnectivity disorders”, meaning that disturbances in the structural and functional brain connectome contribute to the aetiology of major brain disorders (Hansen et al, 2022; van den Heuvel & Sporns, 2019). Whereas FC provides information about the temporal synchronization of neural signals between distant brain areas, fALFF and ReHo can be considered as measures of intra-regional connectivity, which has been shown to be highly influenced by the network characteristics of the underlying structural

architecture. For instance, if voxels belonging to the same region show distinct structural connections with other voxels in the brain, their neural dynamics are expected to be different, resulting in a net decreased regional neural activity (Lee & Xue, 2017). Accordingly, fALFF and ReHo are not just indicators of localized neuronal activity, but they might also encapsulate network-level information that would be overlooked if the underlying structural topology is not taken into account (Lee & Xue, 2017). An integrative approach combining these measures with graph theory indexes of structural connectivity might elucidate the contribution of regional neural abnormalities in the aetiology of Mood Disorders.

4.2 Immune-inflammatory markers provide information for stable and clinically meaningful data-driven stratifications of Mood Disorders

The unsupervised stratification model based on immune-inflammatory profiles identified 2 subgroups of depressed patients distinguished by specific immune-inflammatory signatures with an accuracy of 75.4%. In particular, one cluster (i.e., Cluster 2) exhibited higher scores in all the immune-inflammatory profiles compared to the other (i.e., Cluster 1), suggesting an overall state of low-grade inflammation. In inspecting the clinical outcomes associated with each cluster, patients assigned to the inflamed cluster exhibited worse cognitive distortions compared to those belonging to the other cluster. Conversely, patients distinguished by a lower degree of inflammation did not display a specific clinical signature. The pivotal role of immune dysregulations in the aetiology of depression has been largely described in the literature (Dowlati et al, 2010; Haapakoski et al, 2015). However, not all depressed patients exhibit immune-inflammatory alterations, as suggested by the variability in the response to anti-inflammatory treatments (Kappelmann et al, 2018; Raison et al, 2013). Indeed, evidence of low-grade inflammation, as reflected by high peripheral concentrations of CRP, has been reported in almost 30% of depressed patients, suggesting the existence of a specific subtype of "inflamed depression" (Osimo et al, 2019). Our findings further support this evidence by demonstrating that, in a completely unsupervised way, peripheral immune-inflammatory signatures can distinguish between inflamed and uninflamed depressed patients with good accuracy. Among all the immune profiles, the neurotoxicity profile showed the highest contribution to clusters' differentiation. Elevated concentrations of pro-inflammatory cytokines (e.g., IL-1β, IL-6, and TNF-α) have been shown to significantly affect BDNF

production, resulting in impaired synaptic plasticity, neurogenesis, long-term potentiation and dendritic maturation (Bourgognon & Cavanagh, 2020; Miller & Raison, 2016; Wohleb et al, 2016). These neuroplastic changes have been suggested to alter glutamatergic signalling between subcortical limbic structures and prefrontal cortex, consequently leading to the emotional deficits and biases observed in depression (Price & Duman, 2020; Thompson et al, 2015). Moreover, associations between inflammation and negative affect have been demonstrated in healthy controls (Benson et al, 2017; Ghane et al, 2021), Mood Disorder patients (Niemegeers et al, 2019; Vai et al, 2022), and also depressed COVID-19 survivors (Benedetti et al, 2022), possibly mediated by the detrimental effects of pro-inflammatory cytokines in brain areas involved in emotion regulation (Vai et al, 2022). Taken together, the exacerbated negative thinking style observed in patients belonging to the more inflamed subgroup might reflect dysconnectivity within the prefrontal-mesolimbic circuitry induced by the neurotoxic effect of peripheral inflammation.

Considering the results of the FACS-based stratification model, depressed patients were separated into 2 subgroups with an accuracy of 66%. One cluster (i.e., Cluster 1) was associated with i) TEMRA and effector memory (EM) CD8+, Tγδ, and NK cells expressing granzyme; ii) CD4+, CD8+, and NK cells releasing TNF-α, IL-2, and IL-17; and iii) naïve and EM cells expressing CD69+. On the other hand, the other cluster (i.e., Cluster 2) exhibited higher frequencies of i) CM and EM CD8+, Tγδ, and NK cells expressing perforin or both perforin and granzyme and ii) naïve and memory cells expressing CD25+. Perforin and granzyme are secreted by cytotoxic lymphocytes and induce the apoptosis of the target cell: once released in the synaptic cleft, perforin can polymerize and create a channel that disrupts the cell membrane, allowing the trafficking of granzymes within the cell and the initiation of pro-apoptotic pathways and DNA degradation (Voskoboinik et al, 2015). However, knockout studies demonstrated that while perforin is essential for granule-dependent cell death, the effects of disrupting granzyme genes are much less severe (Kägi et al, 1994; Voskoboinik et al, 2015). Among brain cells, oligodendrocytes are known to be particularly susceptible to the deleterious proprieties of perforin (Scolding et al, 1990), and recent evidence demonstrated that high frequencies of cytotoxic T cells secreting perforin or both perforin and granzyme affect WM integrity in BD, possibly through myelin damage (Aggio et al, 2023). Indeed, the

subtypes derived from immune cell counts seem to reflect a subgroup of more cytotoxic and actively inflamed depressed patients and another subpopulation characterized by a less cell-damaging profile. Interestingly, Cluster 1, the one distinguished by cytotoxic T cells expressing only granzyme, exhibited high percentages of T cell subpopulations releasing IL-17, TNF-α, IL-2, and GM-CSF. These inflammatory mediators can be co-expressed by T cells, showing intercorrelated functions during inflammatory states. Specifically, a specific subtype of Th cells (i.e., Th17) produce IL-17 together with other pro-inflammatory factors such as GM-CSF and TNF-α, and its elevations have been recognized in several autoimmune disorders and inflammatory conditions (Korn et al, 2009). However, findings from animal studies suggest that, at the neural level, Th17 cells promote hippocampal neurogenesis (Niebling et al, 2014; Wolf et al, 2009), a mechanism that was associated with antidepressant-like effects in stressed mice (Brachman & Lehmann, 2015). In humans, the frequency of peripheral Th17 cells has been demonstrated to promote WM integrity both in healthy controls and BD patients, supporting their role in maintaining brain tropism (Poletti et al, 2017). Similar considerations were also reported in BD patients for cytokine-releasing NK cells, which were found to positively associate with indices of WM microstructural integrity and FC within the cortico-limbic circuit during an emotional processing task (Furlan et al, 2019). Moreover, IL-2 is produced early after T cell activation and is known to be essential for the generation and maintenance of Tregs which contribute to dampen the inflammatory response and restore homeostasis. Alterations in Treg populations have been reported both in MDD and BD patients (Poletti et al, 2024). The discovered FACS-based subtypes were also differentiated by the frequencies of activated T cells, with patients belonging to Cluster 1 showing a high percentage of T cells expressing CD69+, while those assigned to Cluster 2 exhibited an increased frequency of activated CD25+ T cells. The activation of T cells is characterized by distinct stages according to the different expressed markers. More specifically, CD69+ is expressed in the very early phase of T cell activation up to 2-3 hours after initial stimulation, and its activation modulates the releasing of pro-inflammatory markers (e.g., IL-17, IFN-γ, and IL-22) and the differentiation of Th and Treg cells (Cibrián & Sánchez-Madrid, 2017). CD25+, instead, is a constitutional element of the IL-2 receptor and its expression can be observed both in immune (e.g., activated lymphocytes and Treg cells) and non-immune cells (Peng et al, 2023). Considering Mood

Disorders, evidence of T lymphocyte activation was reported in both BD and MDD, despite with different signatures. In MDD, recent meta-analytic findings provided evidence of increased expression of CD25+ and HLA-DR + activated T cells, especially during depressive episodes (Sørensen et al, 2023). A more complex picture has been described in BD patients: while T cell activation seems to characterize the acute phases of the illness (Maes & Carvalho, 2018), a significant reduction in the expression of activation markers, including CD69+, has been observed in remitted BD patients, and this phenomenon is more pronounced in late-stage patients (Maes et al, 2021). It should be considered, though, that the frequency of mood episodes was treated as a confounding variable in our unsupervised stratification model. Although a difference in the proportion of MDD and BD patients in our FACS-based subgroups was detected at an uncorrected threshold, future investigations of the role of the stage and phase of illness are needed to clarify the differential contribution of T cell subpopulations to the aetiology of Mood Disorders.

4.3 Brain functional and immune-based clusters show specific multivariate associations with childhood trauma and cognitive distortions

Except for subgroups derived from immune-inflammatory profiles, little evidence was found for subtype differences at the group level in clinical and environmental measures such as depression severity, cognitive distortions, and exposure to ACEs. This suggests that neuro-biological subtypes alone may not be sufficient to uncover distinct phenotypic signatures in Mood Disorders. Rather, given the strict association between early stress and depressive symptomatology (Nusslock & Miller, 2016; Sanacora & Yan, 2022), especially cognitive distortions (Beck, 2008; Poletti et al, 2014), it is possible that subtype labels combined with subject-specific variation in exposure to childhood trauma are more sensitive in describing differences in negative thinking styles.

Among all the unsupervised stratification models, significant multivariate neurobiological-ACEs relationships were found for the FC-based and immune-based subtypes. Considering biotypes derived from FC strength, childhood trauma, as measured through CTQ, was negatively associated with FC strength in the aforementioned “hyper-connected” cluster (i.e., Cluster 1). A different relationship was observed in the “hypo-connected” cluster (i.e., Cluster 2), where only sexual abuse and emotional neglect were,

respectively, significantly positively and negatively correlated with FC strength. Therefore, the described multivariate brain-ACEs relationship might reflect a "multi-trauma" effect on FC that is specific to Cluster 1, whereas the same relationship was mainly guided by emotional neglect and sexual abuse in Cluster 2. The highest BSR encompassed brain regions that are known to be highly relevant for emotional, cognitive and social functioning, such as cortico-limbic structures (lateral amygdala, cingulate gyrus), as well as areas belonging to subcortical (thalamus, basal ganglia, and putamen), somatosensory (precentral gyrus), and ventral and dorsal attentive networks (insula, inferior and superior parietal lobules). Of note, the functional organization along thalamocortical and fronto-amygdala pathways, as well as regions belonging to the ventral attentive network (e.g., insula, anterior cingulate, and supplementary motor area) has been demonstrated to be highly influenced by cortical maturational changes occurring from childhood to adolescence, promoting the normative development of cognitive and affective functions (Casey et al, 2019; Dong et al, 2024; Luo et al, 2024; Park et al, 2024). The deprivation of adequate emotional stimulation during childhood significantly alters maturation processes in the developing brain by diminishing the production of neurotrophin and neurotransmitters which, ultimately, end with aberrant structural and functional neural organization (De Bellis, 2005; van der Kolk, 2003). The difference in the contribution of CTQ domains in the FC-based subtypes might underlie different biological or environmental factors that make an individual more or less vulnerable to the effect of early traumatic events. For instance, the BDNF Val66Met polymorphism has been shown to moderate the impact of childhood trauma on brain structure and function by affecting synaptic plasticity (Frodl et al, 2014; Gerritsen et al, 2012; Tian et al, 2021). Considering environmental factors, resilience and family environment contribute to mitigating the detrimental effects of exposure to childhood trauma (Bradley et al, 2013; Poole et al, 2017; Wingo et al, 2010). Future work examining these potential moderating variables in the identified subtypes may be important to better delineate risk or resilience profiles for each individual.

The presence of distinct underlying mechanisms explaining the differential impact of ACEs on FC in the uncovered subtypes is further supported by the results of the mediation analysis. In fact, the individual FC scores derived from PLSC analysis mediated the relationship between the subject-specific PLSC CTQ scores and generalization across

time only for patients assigned to Cluster 2. Overgeneralization of hopelessness represents a key feature of depressive symptomatology (Gamble et al, 2019), and also constitutes a core element of the "cognitive triad" described by Beck (1979). Although the experience of ACEs has been widely considered a risk factor for the development of negative thinking style both in psychiatric (Poletti et al, 2014) and general populations (Mansueto & Cavallo, 2021), the results of this study suggest that the tendency to overgeneralize negative events in the future might characterize a specific neurobiological subtype of depressed patients. Compared to Cluster 1, patients belonging to Cluster 2 were distinguished by a global hypo-connected pattern, which resulted in being mainly influenced by emotional neglect and sexual abuse in a multivariate fashion. Previous evidence highlighted a widespread FC reduction in MDD patients with a history of childhood neglect, with a major involvement of prefrontal, thalamic, limbic, and cerebellar regions (Wang et al, 2014). Moreover, increased activation in the left IPL during the recognition of negatively valenced stimuli in an emotional attention shifting task was reported in MDD patients with a history of sexual abuse, possibly reflecting abuse-related compromised representations of the peripersonal space and body schema (Skokauskas et al, 2015). In turn, aberrant functional activations involving the amygdala, ACC, as well as the fronto-parietal and salience networks has been linked to ruminative thinking in maltreated children and also depressed individuals (Abler et al, 2007; Hoffmann et al, 2018; Young et al, 2016). The results of this study further contribute to this scenario by providing additional evidence of the detrimental effects of ACEs on functional neural organization, highlighting also potential neurobiological mechanisms through which the exposure to childhood trauma contribute to cognitive vulnerability in depression.

Considering the results of PLSC analysis in the immune-based stratification model, the contribution of CTQ domains on the multivariate relationship was much significantly stronger in Cluster 2 (mainly characterized by a pro-inflammatory signature) compared to Cluster 1, which was mostly influenced by sexual and physical abuse. Although all the immune-inflammatory profiles significantly guided the immune-ACEs relationship, the IRS profile exhibited the highest contribution, followed by the Th1 and neurotoxicity profiles. Similar findings were previously reported in the literature, demonstrating that increased production of these immune profiles is linked to ACEs and stressful life events

in Mood Disorder patients (Almulla et al, 2024; Maes et al, 2022a). All these immune profiles reflect a state of immune activation, which aligns with the current evidence of positive associations between increased levels of pro-inflammatory markers and childhood trauma (Baumeister et al, 2016). However, the relationship between childhood adversities and inflammation seems to be contingent on the specific type of trauma, with sexual and physical abuse being significantly associated with increased production of IL-6, TNF-α, and CRP (Baumeister et al, 2016; Brown et al, 2021). The results of our stratification model provide further evidence in support of this claim, suggesting that different biological mechanisms within each immune-based subtype may underpin the variability observed in the relationship with childhood trauma.

Surprisingly, the subject-specific immune scores derived from PLSC analysis did not significantly predict cognitive distortions either in Cluster 1 or in Cluster 2. These results are partially in contrast with the evidence of significant group-level differences in CQ scores between the immune-based subtypes. A possible explanation for these findings is that the relationship between inflammation and cognitive distortion is not completely explained by childhood trauma alone but other underlying mechanisms could contribute to the association, such as inflammation-related alterations in threat- and reward-related neural circuits (Nusslock & Miller, 2016) or epigenetic modifications (Yuan et al, 2023). Future studies investigating these factors could elucidate the role of epigenetic and neuro-biological mechanisms in this relationship.

4.4 Strengths and limitations

One of the main strengths of this work is represented by the robust unsupervised data-driven approach implemented in ML analyses, providing stable and highly generalizable stratification models for the identification of neuro-biological subtypes of depressed patients. A major limitation of most studies that employ classical unsupervised clustering algorithms is the lack of external validation of the discovered subtypes to other datasets, limiting the generalizability of such groupings of patients to new observations. By translating the unsupervised framework into a supervised classification problem, a unique facet of this approach is the possibility to directly test the reliability and validity of the discovered clusters thanks to cross-validation. This is consistent with the increasing attention toward the definition of a biologically informed nosology of psychiatric

disorders, wherein efforts to define rigorous methodological approaches for the discovery of hidden groupings within a psychiatric population might assist in the definition of more effective and individualized treatment strategies (Brucar et al, 2023). Moreover, by assessing not only the reproducibility of the identified clusters but also their clinical relevance, the data-driven discovery of depression subtypes with different neurobiological-clinical relationships might provide important information for translational research to promote more favourable clinical outcomes according to individual characteristics. For instance, cognitive-behavioural therapies might be particularly effective in patients exhibiting worse negative thinking styles, especially in those with a history of childhood trauma (Cohen & Mannarino, 2015; Nemeroff et al, 2003). Conversely, patients characterized by a pro-inflammatory signature could benefit from treatments targeting immune-metabolic pathways (e.g., physical activity, diet, or anti-inflammatory interventions) (Gleeson et al, 2011; Kappelmann et al, 2018; Suneson et al, 2024). Finally, unlike the majority of stratification studies carried out so far that focused on a specific psychiatric population, a transdiagnostic approach cutting across depressed MDD and BD patients was implemented in this study, allowing the identification of data-driven subtypes that transcend the clinical diagnosis. Such an approach aligns with current efforts in psychiatry to promote novel taxonomies of psychiatric disorders that go beyond diagnostic categories in favour of shared and neurobiologically-informed cognitive, affective, and behavioural domains of functioning (Insel, 2014; Kotov et al, 2017). In this context, the unsupervised discovery of "biotypes" of depression might offer more robust and personalized insights into how alterations in neuro-biological pathways might have an impact on clinically relevant outcomes.

Some limitations should be underscored about this work. First, all the recruited patients were inpatients admitted to the same hospital, and thus the ability to generalize these findings to other samples might be limited. Although the implementation of a cross-validation framework with the unsupervised ML pipeline offers a reliable estimation of the external validity of clustering solutions (Landi et al, 2021), assessing the replicability of these stratification models in a completely independent validation set is crucial to test the real-world applications. Second, all patients were under pharmacological treatment at the time of the recruitment. Although the effect of pharmacological load was considered as a nuisance covariate in all the analyses, the potentially long-lasting effects of

antidepressant treatments both at the peripheral and neural levels might not have been completely controlled. In addition to this, relevant socio-demographic variables, such as the socioeconomic status, might have influenced the relationship between childhood trauma and biological data and should be considered as potential confounding variable in future studies. Third, clusters' comparisons were mainly focused on the neuro-biological signatures and the association with cognitive distortions (i.e., "hot" cognition), while extending this approach also to the investigation of the so-called "cold" cognition (e.g., executive functions, memory, attention, information processing and psychomotor speed) would provide a more comprehensive picture of cognitive dysfunctions in depression. Moreover, the clinical validation of these stratification models would benefit from the investigation of comorbidities and atypical features of depression, both representing important sources of heterogeneity. For instance, sleep disturbances, including both insomnia and hypersomnia, have been widely described both in MDD and BD, possibly reflecting specific functional alterations at the neural level (Geoffroy et al, 2018). Moreover, metabolic dysfunctions as well as comorbidity with cardiometabolic conditions has been reported in depression, representing a unique "immunometabolic" phenotype characterizing patients with high levels of peripheral inflammation (i.e., CRP > 1 mg/L and high BMI) (Sforzini et al, 2024). Future studies evaluating also these measures would provide valuable clinical insights for the discovered stratification models and accelerate a precision-medicine approach in depression. The presence of potential uncontrolled sources of noise in biological data represents another drawback that could have influenced the discovery of clustering solutions. However, it should be noticed that several preprocessing steps (e.g., ComBat harmonization, cross-validated confound regression) were performed to relax these issues. The absence of healthy controls represents another relevant limitation hampering the direct translation of these findings into clinical practice. Indeed, the discovery of biomarkers in the general population could be useful to detect high-risk individuals and promote screening and prevention strategies. Finally, we acknowledge that the lack of group-level differences or multivariate associations in some stratification models could also be due to the relatively small sample size. Future studies evaluating the validity of the discovered clustering solutions in larger cohorts are needed to improve the statistical power and the robustness of these findings.

4.5 Conclusions

In conclusion, the results of this project suggest that both neuroimaging features and immune-inflammatory markers provide useful information for a neurobiological-driven discovery of subtypes of depressed patients. The identified "biotypes" were distinguished by unique neural and immune-inflammatory signatures and exhibited differential associations with childhood trauma and cognitive distortions. Specifically, immune-inflammatory profiles led to a clinically relevant stratification of depressed patients associated with different profiles of biased cognitive processing, suggesting that immune-inflammatory signatures could be considered as promising biomarkers for individualized predictions of clinical outcomes in depressed patients. In line with the framework of inflammation-related sickness behaviours in depression, these findings possibly reflect the modulatory effects of pro-inflammatory mediators on cortico-limbic structures in promoting depressive thinking styles. On the other hand, the association between cognitive distortions and FC-based subtypes was better explained by the differential influence of childhood trauma in the discovered clusters, indicating the existence of multifaceted relationships between alterations at the neural level and depressive symptomatology. Future studies extending this approach by including genetic data (e.g., polygenic risk scores, gene expression) and other features of brain activity and structure (e.g., task-based fMRI, graph-theory measures) could provide a more in-depth comprehension of how biologically-driven subtypes may unravel heterogeneity at several levels of analyses, from genetics to the neural system.

5. MATERIALS AND METHODS

5.1 Participants

The total sample included 344 inpatients (135 MDD, 209 BD) consecutively admitted at the IRCCS San Raffaele Scientific Institute (Milan, Italy). All patients met DSM-5 criteria for MDD and BD, according to the Structured Clinical Interview for the Diagnosis of Axis I Disorders (SCID-5). To be included in the study, patients had to be 18-65 years old and meet the diagnostic criteria for a major depressive episode. The severity of depression was rated on the HDRS-21, and only patients with a total score higher than 8 were recruited (Hamilton, 1986). The HDRS-21 total score was calculated for all 21 items. To mitigate the possibility of false positives for BDs, only MDD patients without a family history of BD in their first-degree relatives were included in the study. Exclusion criteria for all patients were: major medical and neurological disorders, pregnancy, intellectual disability, and history of drug or alcohol abuse or dependency. MRI acquisitions were performed for all participants between 2.30 pm and 6.00 pm, whereas fasting blood sampling was performed between 7.00 am and 9.00. After a complete description of the study, written informed consent was obtained. All procedures contributing to this work comply with the ethical standards of the relevant national and institutional committees on human experimentation and with the Helsinki Declaration of 1975, as revised in 2008. The study was approved by the local ethical committee.

5.2 Assessment of childhood trauma and cognitive distortions

In a subsample of 229 patients (106 MDD, 123 BD), the exposure to ACE was assessed through the 28-item version of the CTQ (Bernstein et al, 2003), which has been widely used in the adult population to retrospectively assess the exposure to traumatic events during childhood, showing good psychometric proprieties (Cruz, 2023). The CTQ is composed of 5 subscales which investigate different aspects of childhood trauma: i) *physical abuse*, defined as physical violence on a child by an adult that could have caused harm or ended in injury; ii) *emotional abuse*, which represents any degrading or shameful actions taken by an adult against a child, including verbal attacks on the child's self-worth or overall health; iii) *sexual abuse*, indicating any kind of sexual relationship involving a minor and an adult; iv) *physical neglect*, reflected by the unwillingness of caregivers to adequately supply a child's fundamental needs (e.g., clothing, nourishment, warmth,

security, and medical care); v) *emotional neglect*, which indicates caregivers' inability to meet the primary emotional and psychological needs of a child (e.g., support, affection, feeling of belonging, and parenting). In the 28-item version of CTQ, each form of maltreatment is evaluated through 5 items, which substantially reduces the total number of items while maintaining reasonable reliability and coverage of the content (Bernstein et al, 2003). High scores in each subscale reflect a higher exposure to childhood maltreatment.

Cognitive distortions were evaluated through the administration of the CQ (Fennell & Campbell, 1984). Compared to other well-known scales which focus on general depressive thinking style (e.g., Dysfunctional Attitude Scale) (Weissman & Beck, 1978), the CQ has the main advantage of investigating different dimensions of cognitive distortions, providing a more fine-tuned evaluation of negative thinking in response to positive, neutral, and negative events (Fennell & Campbell, 1984). Five different dimensions can be derived: i) *emotional impact*, which reflects the perceived unpleasantness from adverse events and pleasure from the favourable ones; ii) *attribution of causality*, indicating the individual's inclination to self-blame for bad outcomes while assigning the causes for the good ones to external influences; iii) *generalization across time*, which represents the belief that undesirable events will keep occurring without any amelioration in the future; iv) *generalization across situations*, reflecting one's tendency to consider negative experiences to be representative of his/her life rather than isolated instances; v) *perceived uncontrollability*, indicating the degree to which a person thinks that proactive behaviours can ameliorate an adverse circumstance or maintain a favourable one. High scores in each domain are indicative of a high degree of that specific cognitive distortion.

5.3 MRI data acquisition and preprocessing

5.3.1 Data acquisition

The acquisition of T1-weighted, DTI, and rs-fMRI images was performed with two different 3.0 Tesla scanners. A sample of 192 patients (48 MDD, 144 BD) was acquired with Gyroscan Intera, Philips, Netherlands employing a 8 channels SENSE head coil (T1-weighted MPRAGE sequences: TR 25.00 ms, TE 4.6 ms, field of view FOV=230 mm,91 matrix=256×256, in-plane resolution 0.9×0.9 mm, yielding 220

transversal slices with a thickness of 0.8 mm). SE EPI sequences (TR/TE=9000/58 ms, FoV (mm) 232(ap), 126 (fh), 240.00 (rl); acquisition matrix = 112×85; voxel acquisition 2.14×2.73×2.3; 55 contiguous, with in-plane voxel size 1.88×1.88 mm; SENSE acceleration factor=2; 1 b0 and 35 non-collinear directions of the diffusion gradients; b value=900 s/mm2) were used. Finally, for 50 patients (22 MDD, 28 BD), a rs-fMRI acquisition was also performed, with the instruction to keep their eyes closed. Gradient-echo EPI sequences were acquired. The scanning sessions included 100 sequential T2*-weighted volumes (interleaved ascending transverse slices covering the whole brain), acquired using an EPI pulse sequence (TR = 2000 ms; TE = 30 ms; flip angle = 77°; field of view = 220 mm; number of slices = 32; slice thickness = 4 mm; matrix size = 64 x 63 reconstructed up to 64 x 64 pixels). Two dummy scans before fMRI acquisition allowed for obtaining longitudinal magnetization equilibrium. Total time acquisition was 3 min and 28 s.

A sample of 152 patients (87 MDD, 65 BD) was instead acquired with an Ingenia CX, Philips, The Netherlands using a 32-channel sensitivity encoding SENSE head coil (T1-weighted MPRAGE sequence: TR 8.00 ms, TE 3.7 ms, field of view FOV = 256 mm, matrix = 256 x 256, in-plane resolution 1 x 1 mm, yielding 182 transversal slices with a thickness of 1 mm). SE EPI sequences (EPI factor= 43; TR/TE=5900/78 ms, FoV (mm) 232 (ap), 129 (fh), 240.00 (rl); acquisition matrix 112×85; 56 contiguous, 2.3-mm thick axial slices reconstructed with in-plane pixel size 1.88×1.88 mm; SENSE acceleration factor= 2; Multiband acceleration factor= 2; ten b0 and 96 non-collinear directions of the diffusion gradients: 60 b values=2855 s/mm2, 6 b values=700 s/mm2, 30 b values=1000 s/mm2) were acquired. Fat saturation was performed to avoid chemical shift artefacts. Lastly, for 96 patients (57 MDD, 39 BD), a rs-fMRI acquisition was performed, with the instruction to keep their eyes closed. Gradient-echo EPI sequences were acquired. The scanning sessions comprised 200 sequential T2*-weighted volumes (interleaved ascending transverse slices covering the whole brain, tilted 30° downward concerning bicommissural line to reduce susceptibility artefacts in orbitofrontal region), acquired using an EPI pulse sequence (TR = 2000 ms; TE = 30 ms; flip angle = 85°; field of view = 192 mm; number of slices = 38; slice thickness = 3.7 mm; matrix size = 64 x 62 reconstructed up to 96 x 96 pixels). Six dummy scans before fMRI acquisition allowed

for obtaining longitudinal magnetization equilibrium. Total time acquisition was 6 min and 56 s.

5.3.2 Grey matter processing and features extraction

The processing of T1-weighted neuroanatomical images was performed through the Computational Anatomy Toolbox (CAT12) for statistical parametric mapping (SPM) software (Gaser & Dahnke, 2016). The main pre-processing steps involved: normalization in the Montreal Neurological Institute (MNI) space; tissue segmentation into GM, WM, and cerebrospinal fluid (CSF); check of spatial alignment and sample homogeneity to exclude outliers; spatial smoothing of each GM map with a 6 mm full width at half maximum Gaussian filter. Cortical thickness was computed for 68 regions derived from the Desikan-Killiany atlas (Desikan et al, 2006), while volumes of cortical and subcortical regions were extracted for 122 regions identified from the Neuromorphometrics atlas (http://Neuromorphometrics.com/). The total intracranial volume (TIV) was also computed.

5.3.3 DTI processing and features extraction

DTI pre-processing was performed using FMRIB Software Library (FSL) 6.0 tools (Smith et al, 2006; Smith et al, 2004; Woolrich et al, 2009). First, all images were corrected for the effects of eddy currents and head motion (Horsfield, 1999) and a brain mask was created using the Brain Extraction Tool (Smith, 2002) (S. M. Smith, 2002) to remove non-brain tissues from the image. Non-linear registration to a standard template (FMRIB58-FA, FMRIB Centre University of Oxford, Department of Clinical Neurology, John Radcliffe Hospital Headington, Oxford, United Kingdom) was performed, and a diffusion tensor model was fitted at each voxel to obtain voxel-wise maps of four diffusion indices: AD, RD, MD, and FA. The obtained images for all patients were then processed using FSL's Tract Based Spatial Statistics (TBSS, http://fsl.fmrib.ox.ac.uk/fsl/fslwiki/TBSS) analytic method and were aligned to the MNI space through the Non-Linear Image Registration Tool (FNIRT) (www.fmrib.ox.ac.uk/fsl/fnirt/index.html). For each DTI diffusion index, the maps of all subjects were merged into a common 4D image, and a "thinning" process was applied to create a skeletonized mean image representing the centres of all common tracts. A threshold of 0.2 was set for this image to control for intersubject variability and reduce the likelihood of a partial volume effect. Whole-brain tract-based average values for each

diffusion index were extracted according to ENIGMA-DTI protocols (http://enigma.ini.usc.edu/protocols/dtiprotocols/). Average FA values were calculated from voxels in each subject's white matter skeleton within 43 tract-wise ROIs, derived from the Johns Hopkins University (JHU) white matter parcellation atlas (Mori et al, 2008). The same procedure was performed for the extraction of tract-based average values of AD, RD and MD. All measures were separately calculated for the right and left hemispheres in each ROI, except for the body of corpus callosum (BCC), CC, fornix (FX), genu of corpus callosum (GCC) e splenium of corpus callosum (SCC).

5.3.4 rs-fMRI processing and features extraction

The T2*-weighted images were analysed using the Harmonized AnaLysis of Functional MRI pipeline (HALFpipe) version 1.2.1 (Waller et al, 2021). Pre-processing steps encompass motion correction, slice time correction, susceptibility distortion correction, coregistration, and spatial normalization to the *MNI152NLin2009cAsym* template. After the resampling of the images to the standard space, denoising was performed on the resampled images and included: spatial smoothing with a 6 mm full-width at half-maximum kernel; grand mean scaling of 10,000; ICA-AROMA to regress out motion artefacts due to head motion, WM, and CSF (Pruim et al, 2015a; Pruim et al, 2015b); and temporal filtering using a Gaussian weighted high-pass (width of 125 s) for FC and a frequency-based bandpass (low cut-off of 0.01 Hz and a high cut-off of 0.1 Hz) for measures of local neural activity. Moreover, physiological nuisance regressors were isolated for anatomical component correction (aCompCor) considering the top 5 principal components of CSF signal (Muschelli et al, 2014). Different rs-fMRI features were extracted from the pre-processed images, including the strength of positive and negative weights from ROI-to-ROI FC matrices, and measures of local neural activity for each ROI (i.e., fALFF and ReHo). Regarding ROI-to-ROI FC, time series from 263 ROIs were extracted, encompassing 246 cortical and subcortical ROIs from the Brainnettome atlas (Fan et al, 2016) and 17 cerebellar ROIs from the Buckner 17-network atlas (Buckner et al, 2011). ROIs with missing time series across participants were excluded, resulting in 186 ROIs for which pairwise ROI-to-ROI FC matrices were computed for each participant (for a complete list of the included ROIs, see Appendix 1). From the individual ROI-to-ROI FC matrices, positive (Spos) and negative (Sneg) strengths (i.e., the sum of positive and negative weights of links connected to a region) were computed for each

ROI using the Python-equivalent of the Brain Connectivity Toolbox (*bctpy*, https://github.com/aestrivex/bctpy), resulting in 186 Spos and 186 Sneg measures. For local activity measures, fALFF and ReHo values were extracted from the pre-processed images. fALFF reflects the intensity of spontaneous neural activity, and it was calculated by dividing the power in the low frequency range (0.01–0.1 Hz) by the power in the entire frequency range (Zou et al, 2008). ReHo measures the temporal synchronization of a voxel with its nearest neighbouring voxels, and is calculated using the Kendall's coefficient of concordance (Zang et al, 2004). Voxel-wise fALFF and ReHo maps for each participant were Z-standardized at the individual level, and the average fALFF and ReHo values across 186 ROIs were extracted.

5.3.5 ComBat harmonization

The hidden technical variability among scanners is a well-recognized source of biases when aggregating imaging data from multiple sources, with a potentially detrimental impact on the downstream neuroimaging analysis (Eshaghzadeh Torbati et al, 2021). In the field of genetics, this issue is frequently acknowledged as "batch effect" (Leek et al, 2010), and it has been recently described also in neuroimaging under the name of "scanner effect" (Fortin et al, 2017). Given that the neuroimaging data used in this study were acquired with 2 different scanners, a harmonization step using the ComBat algorithm (Johnson et al, 2007) was performed to control for any potential "scanner effect". ComBat is a harmonization method commonly used in genomics that relies on empirical Bayes to account for both additive and multiplicative "batch effects", and it has been subsequently adapted to DTI (Fortin et al, 2017), cortical thickness (Fortin et al, 2018), and rs-fMRI data (Yu et al, 2018), demonstrating to effectively remove unwanted and biologically-unrelated sources of variations. In this study, ComBat was applied to the extracted neuroimaging data using the neuroCombat Python package (https://github.com/Jfortin1/ComBatHarmonization/tree/master) before entering them in the unsupervised ML pipeline. Age, sex, diagnosis, and TIV (only for grey matter and cortical thickness features) were entered as biological covariates to be preserved from ComBat harmonization.

5.4 Immune-inflammatory markers

5.4.1 Luminex quantification

In a subsample of 185 patients (102 MDD, 98 BD), Bio-Plex Pro™ Human Chemokine 48-Plex assays (BIO-RAD) were used to isolate plasmatic concentrations of immune analytes, which were detected through the bead-based Luminex system according to xMAP technology (Luminex 200™ system, Merck Millipore). Analysed immune analytes included: IL-1α, IL-1β, IL-1 receptor antagonist (IL-1Ra), IL-2, IL-2Rα, IL-3, IL-4, IL-5, IL-6, IL-7, IL-8, IL-9, IL-10, IL-12(p40), IL-12(p70), IL-13, IL-15, IL-16, IL-17, IL-18, IFN-α2, IFN-γ, TNF-α, TNF-β, TNF-related apoptosis-inducing ligand (TRAIL), macrophage migration inhibitory factor (MIF), leukaemia inhibitory factor (LIF), MCP-1/CCL2, MIP-1α/CCL3, MIP-1β/CCL4, RANTES/CCL5, MCP-3/CCL7, Eotaxin/CCL11, CTACK/CCL27, CXCL1/ GRO-α, CXCL9/MIG, IP-10/CXCL10. Analysed growth factors encompassed: granulocyte macrophage colony stimulating factor (GM-CSF), macrophage colony stimulating factor (M-CSF), basic fibroblast growth factor (basic FGF), granulocyte colony stimulating factor (G-CSF), β-nerve growth factor (β-NGF), platelet-derived growth factor-BB (PDGF-BB), vascular endothelial growth factor (VEGF), stem cell factor (SCF), stem cell growth factor β (SCGF-β), macrophage migration inhibitory factor (MIF), hepatocyte growth factor (HGF). Median fluorescence intensities (MFI) of each analyte-specific immunoassay bead set were detected using the flow- and fluorescence-based Luminex 200™ detection platform (Luminex Corporation, Austin, TX, USA). Compared to observed concentrations, MFI values do not require a level of detection for censoring, allowing the quantification of immune analytes with low abundance (Breen et al, 2016). Since the interpolation of concentrations has been shown to introduce some biases for samples with values exceeding the serial standard curves, MFI values could provide more reliable estimates of these analytes, resulting in greater statistical power in subsequent statistical analyses (Breen et al, 2015; Breen et al, 2016). Since samples were analysed on different plates, the ComBat harmonization procedure (https://github.com/CoAxLab/pycombat) was performed on the log2-transformed MFI values to adjust for potential batch effects, considering diagnosis as a biological covariate to be preserved.

5.4.2 Immune-inflammatory profiles calculation

Instead of focusing on individual immune analytes, an increasing body of literature has moved the attention toward immune-inflammatory profiles based on cytokine production to unveil complex relationships between inflammatory processes and mood disorders (Rachayon et al, 2024). Research carried out so far demonstrated that these immune-inflammatory profiles are associated with the severity of depression (Maes et al, 2022b; Rachayon et al, 2024) and mediate the relationship between ACEs and depressive phenotype (Maes et al, 2022a), representing potential biomarkers of immune dysregulation in Mood Disorders. In this study, cytokine-based immune-inflammatory profiles reflecting the immune-inflammatory response system (IRS), the compensatory immunoregulatory system (CIRS), M1 macrophage, Th1, Th2, Th17, T cell growth, growth factors, and neurotoxicity were computed as composite scores based on Z-standardized values of the harmonized immune analytes (Maes et al, 2022a). A detailed definition of the derived immune-inflammatory profiles is reported in Table 13.

Table 13. Definition of immune-inflammatory profiles.

Immune profiles	**Members**
M1 macrophage	IL-1β, IL-1Ra, IL-6, TNF-α, IL-8, MIP-1α/CCL3
Th1	IL-2, INF-γ, IL-12(p40), IL-12(p70)
Th2	IL-4, IL-5, IL-9, IL-17
Th17	IL-6, IL-17
CIRS	IL-4, IL-1Ra, IL-10
IRS	IL-1β, IL-6, TNF-α, IL-8, MIP-1α/CCL3, IL-2, IFN-γ, IL-12(p70), IL-12(p40), IL-17, IL-15, G-CSF, GM-CSF, IP-10/CXCL10, RANTES/CCL5, MCP-1/CCL2
T cell growth	IL-4, IL-9, IL-12(p40), IL-12(p70), IL-15
Neurotoxicity	IL-1β, IL-6, TNF-α, IL-8, MIP-1α/CCL3, IL-2, IFN-γ, IL-12(p40), IL-12(p70), IL-17, IP-10/CXCL10, Eotaxin/CCL11, RANTES/CCL5, MCP-1/CCL2
Growth factors	PDGF-BB, VEGF, basic FGF

Each profile was computed as Z-unit based composite score of the corresponding immune analytes. Abbreviations: Th, T helper; CIRS, compensatory immunoregulatory system; IRS, immune-inflammatory response system; IL, interleukin; TNF, tumor necrosis factor; CCL, C motif ligand; INF, interferon; G-CSF, granulocyte colony stimulating factor; GM-CSF, granulocyte macrophage colony stimulating factor; CXCL, C motif chemokine ligand; PDGF-BB, platelet-derived growth factor-BB; VEGF, vascular endothelial growth factor; basic FGF, basic fibroblast growth factor.

5.5 Immunophenotyping

5.5.1 PBMCs isolation

Flow cytometry was performed on fresh peripheral blood mononuclear cells (PBMCs), which were isolated from whole blood stored in five 6mL EDTA-containing vials. Blood samples from all the vials were then located in a wide-mouth flask and then diluted with a 30mL Sodium Chloride (NaCl) 0.9% solution. To isolate PBMCs from other blood cells, a density gradient centrifugation with Ficoll-Paque PLUS (GE Healthcare, Uppsala, Sweden) with a density of 1.007 g/mL was employed. Given their higher density compared to other blood components, dead cells, granulocytes, and erythrocytes precipitate through the Ficoll layer, whereas monocytes and lymphocytes mount up at the plasma-gradient boundary.

Fifteen mL of Ficoll-Paque PLUS were moved into two 50 mL Eppendorf Conical Tubes, and gradually filled with diluted blood (30 mL per tube). To achieve an adequate isolation of blood components, the tubes were centrifuged for 30 minutes at 1800 rpm without pausing to prevent vortex effects. Using a sterile pipette, the surface layer composed of plasma and platelets was removed, preserving the layer of PBMCs intact. The supernatant was subsequently discharged from the PBMCs by moving them to a sterile Eppendorf Conical Tube (50 mL) and washing them twice in a regular saline solution at 1500 rpm for 10 minutes. The determination of cell viability was done by diluting PBMCs another time and staining them with 10µL of Trypan Blue (SigmaAldrich, St Louis, MO, USA). PBMCs were them inserted into a Bürker counting chamber to establish the number of living cells. PBMCs were then frozen using 90% Fetal Bovine Serum (FBS) and 10% dimethyl sulfoxide (DMSO). According to the total amount of available PBMCs, each sterile cryogenic vial was filled with 1 mL of the freezing medium and 10x106 PBMCs and placed in liquid nitrogen at -192°.

5.5.2 Flow-cytometry Multiparametric Analysis

After being removed from the liquid nitrogen, the PBMCs vials were thawed in a 37° water bath for 1-2 minutes to minimize any damage to the cell membranes. The freezing medium was then removed by centrifuging the vials for 7 minutes at 1500 rpm. Next, PBMCs were resuspended in 650µL of Roswell Park Memorial Institute (RPMI) 640 Biowhittaker medium, which contains 10% FBS Gibco, 1% L-Glutamine and 1%

Penicillin Streptomycin. Finally, PBMCs were transferred on a 96-well plate with 1x106 cells in each well. For immunophenotyping, 4 different *ad hoc* panels were produced, of which one included surface markers only, while the other three comprised both surface and intracellular markers: i) lymphocytes and mait cells (panel 1); ii) cytotoxic T-lymphocytes (CD8), NK and T γδ cells (panel 2); iii) T-lymphocytes and NK cells cytokines (panel 3); iv) T-regulatory lymphocytes (panel 4).

The correct dilution required for cell probing was determined by titrating antibodies. Since cytokines are generally produced at low levels in resting cells, a 2-hour stimulation was performed for panels 2 and 3, which included additional procedures and specific buffers in comparison to the standard surface antibody staining. The solution used to stimulate PBMCs consisted of phorbol 12-myristate 13-acetate (PMA) (30ng/mL) (Sigma-Aldrich) and Ionoyicin from Streptomyces Conglobatus (300ng/mL). For each panel, PBMCs were split into 2 separate 96-well plates: an unstimulated sample used as control, and a stimulated sample. Following stimulation, PBMCs were resuspended, and a previously diluted (1:100) 1.5µL of BD GolgiPlug protein transport inhibitor-containing Brefeldin A (BD Cytofix/Cytoperm Plus Kit with BD GolgiPlug) was added to each well to maintain the cytokines within the cells. Lastly, cells underwent an additional 2-hours incubation time at 37°C CO_2 and then washed with staining buffer by centrifuging them at 1200 rpm for 5 minutes, followed by the removal of the supernatant.

Once the stimulation finished, the staining protocol was implemented. First, cell viability was assessed by marking cells from each panel with the LIVE/DEAD Fixable Aqua Dead Cell Stain (1:100, LIVE/DEAD Fixable Aqua Dead Cell Stain Kit, Invitrogen, Thermo Fisher). After 20 minutes at 4°C, cells were washed by centrifuging them at 1200 rpm for 5 minutes, and the supernatant was eliminated. Then, panel-specific mixes of principal fluorochrome-conjugated antibodies were prepared and stored protected from light exposure at 4°C until needed. Different mixes were prepared for both surface and intracellular staining. For surface staining, a specific staining buffer suited to preserve cell viability and amplify the fluorochromes fluorescence signal intensities (Stain Buffer – FBS, BD Pharmingen) was used. Conversely, the choice of the buffers utilized for the preparation of intracellular staining mixes was adapted according to the panel: BD Perm/Wash Buffer was used for panel 2 and 3, while diluted (1:10 in distilled H2O) eBioscience Perm/Wash Buffer was chosen for panel 4. Once prepared, 100 µL of surface

antibodies mixes were added to the corresponding panel, and the 96-well plate was incubated for 20 minutes at 4°C in a dark room. Subsequently, a staining buffer was used at 1200 rpm for 5 minutes to wash the cells, and the supernatant was removed. Regarding panel 2 and 3, the Cytofix/Cytoperm Plus Fixation/Permeabilization set Kit was added (BD Biosciences); while the FoxP3-staining buffer set toolkit (eBioscience) was used for panel 4. Finally, 100 µL of the previously diluted buffers were included and a centrifugation at 1200 rpm for 5 minutes of the 96-well plate was performed. To perform analyses with the BD FACSymphony A5 Cell Analyzer (BD Biosciences), cells were re-suspend in 200 µl PBS 1X and relocated into 5 mL round-bottom polypropylene tubes (Falcon). Analyses were performed using the FlowJo v 10.7.1 software (Tree Star Inc, Ashland, Oregon, USA). The consistency of data acquired in separate sessions was evaluated before each experiment through an 8-peak Rainbow calibration particles (BioLegend) acquisition.

5.5.3 Gating strategies

The detection of the specific sub-populations for each cell type was performed through a hierarchical gating strategy on markers expression, morphology, and Fluorescence Minus One (FMO) controls, the populations of interest were identified and clustered one after the other by describing a gate (i.e., a graphical or numerical boundary) on the scatterplot determined by physical or markers properties. For all the panels, the first gating strategy's step involves the identification of the lymphocyte population gate based on cell morphology. More specifically, the Forward scatter (FSC-A) and the Side scatter (SSC-A) allow the differentiation of cells based on their size and granularity, respectively. Indeed, FSC-A allows to discriminate lymphocytes from monocytes because of the smaller size of lymphocytes compared to monocytes, whereas SSC-A is used to distinguish lymphocytes from both monocytes and granulocytes due to the reduced volumes of cytoplasmatic granules in lymphocytes. The subsequent gate was aimed to separate the live cells from the dead ones using the LIVE/DEAD Aqua stain. Given that the membrane of dead cells is damaged, the LIVE/DEAD Aqua stain can penetrate only the dead ones, allowing to separate them from live cells. For live cells only, single cells were identified through a geometrical gating. Finally, a specific hierarchical gating strategy was implemented for each panel by choosing a different marker each time according to the population of interest to be analysed.

The gating strategy used for panel 1 is depicted in Figure 16 and it was implemented only on surface staining. Starting from single cells, T-lymphocytes were detected and gated based on the expression of CD3 marker. Then, Tγδ lymphocytes were identified through the relative expression of CD3 and Vd1-Vd2 (CD3+Vd1-Vd2+). Once the CD3+ T cells were classified, a subsequent gating strategy based on the expression of TCR Va7.2 was performed for the differentiation of the Mucosal Associated Invariant T-cells (MAIT) (CD3+Vα7.2+) from the CD3+ non-MAIT T cells. Additional characterization of the MAIT cells was assessed based on the expression of CD161 (CD3+Vα7.2+CD161+). Considering the CD3+Vα7.2- population, an additional classification according to the expression of CD4 and CD8 to classify T helper (CD4+), cytotoxic T cells (CD8+), and double negative T cells (CD4-CD8-). Within both CD4+ and CD8+ populations, further gating was performed using the CD27 and CD45RA markers, allowing the differentiation of i) naïve cells (CD45RA+CD27+); ii) CM cells (CD45RA-CD27+); iii) EM cells (CD45RA-CD27-); iv) TEMRA cells (CD45RA+CD27-). Lastly, naïve cells, CM and EM cells were additionally differentiated based on their relative expression of both CD69 and CD25.

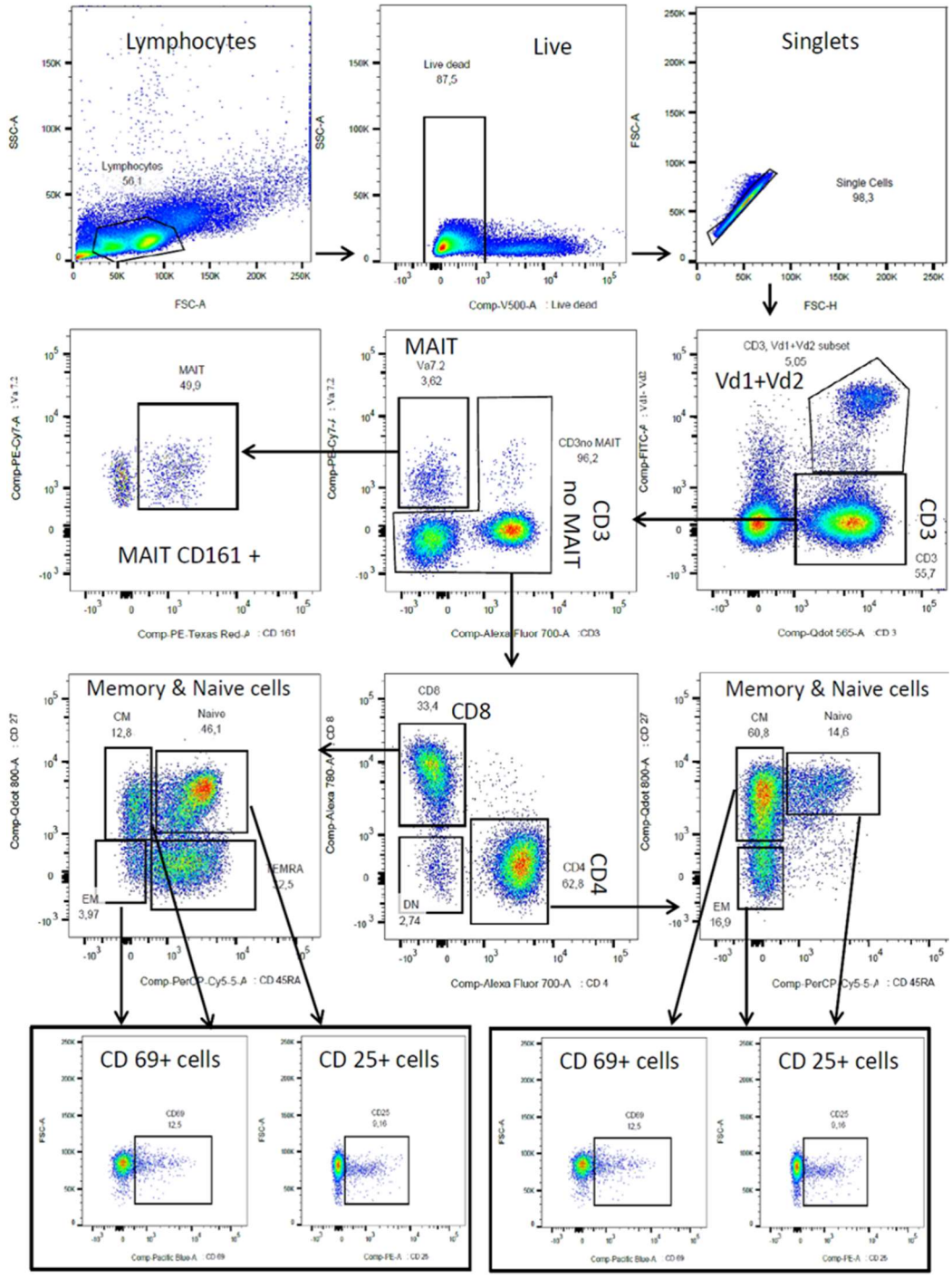

Figure 16. Gating strategy for Lymphocytes and Mait cells.

Panel 2 aims to determine the cytotoxic activity of NK cells, CD8+, and T ϒδ lymphocytes (Figure 17). Starting from single cells, both CD3 and CD56 markers were used for the gating of T lymphocytes (CD3+CD56-) and NK cells (CD3-CD56+). The

characterization of CD8+ lymphocytes was performed by considering the relative expression of CD4 and CD8, while Tϒδ lymphocytes were identified through the expression of Vd1 and Vd2. Furthermore, naïve, CM, EM, and TEMRA cells were further differentiated based on the expression of CD27 and CD45RA markers. Finally, the expression of both Granzyme (GrzB) and Perforin (Perf) was evaluated on NK cells, Tϒδ lymphocytes, and memory CD8+ T cells to investigate the activation of cytotoxic mechanisms and the secretion of granulocytes.

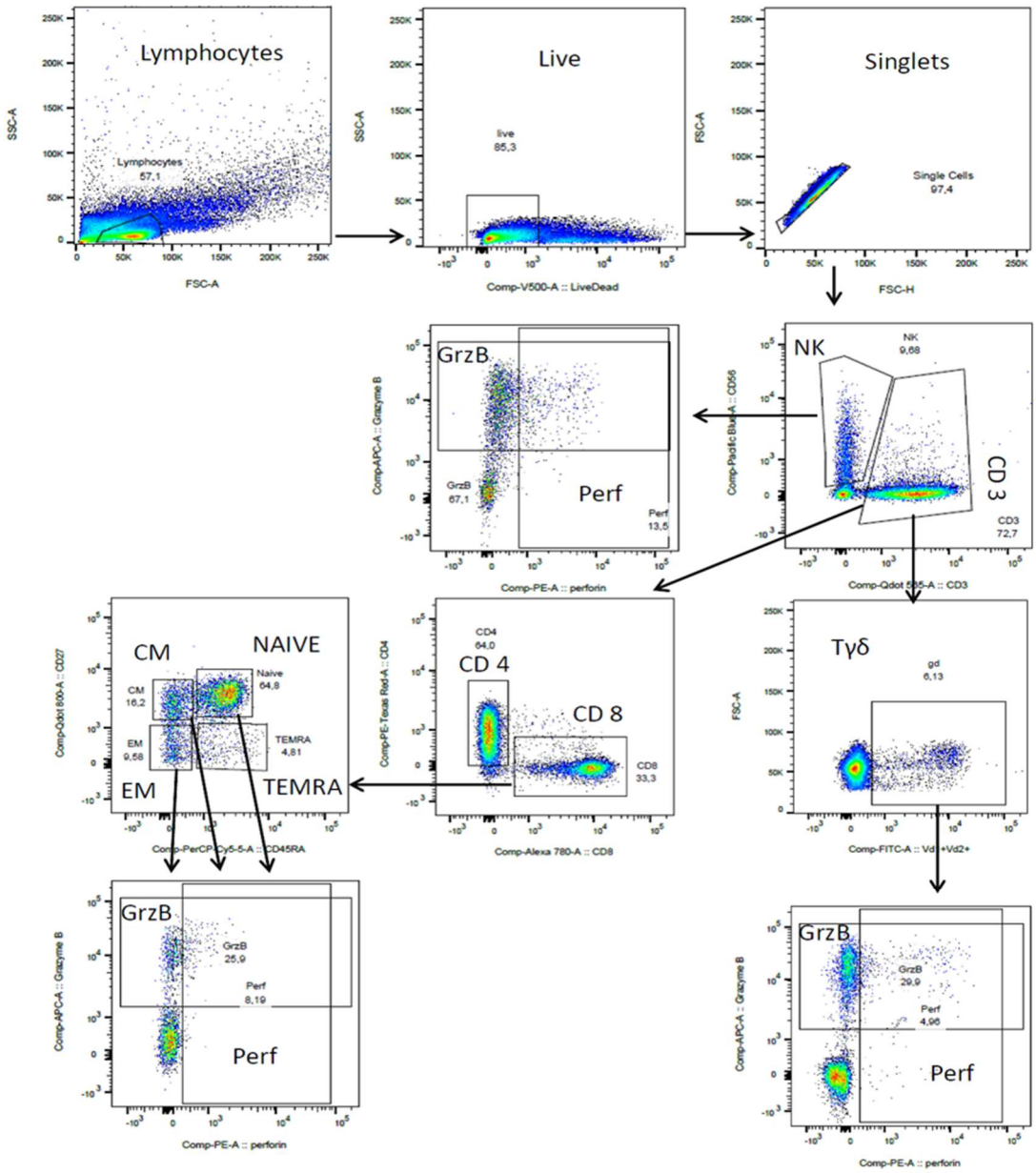

Figure 17. Gating strategy for Cytotoxic T-lymphocytes, NK, and T γδ panel

The gating strategy implemented for panel 3 assessed the secretion of different cytokines from both NK and T lymphocytes (Figure 18). Starting from the single cells population, CD3 and CD56 markers were used for the gating of both T lymphocytes (CD3+CD56-) and NK cells (CD3-CD56+). Within the CD3+ T lymphocytes, a further classification based on the expression of CD4 and CD8 was performed to detect T helper (CD4+) and cytotoxic T cells (CD8+). Lastly, the expression of GM-CSF, IL-2, IL-4, IL-17, INF-γ, and TNF-α was investigated in CD4+, CD8+, and NK cells.

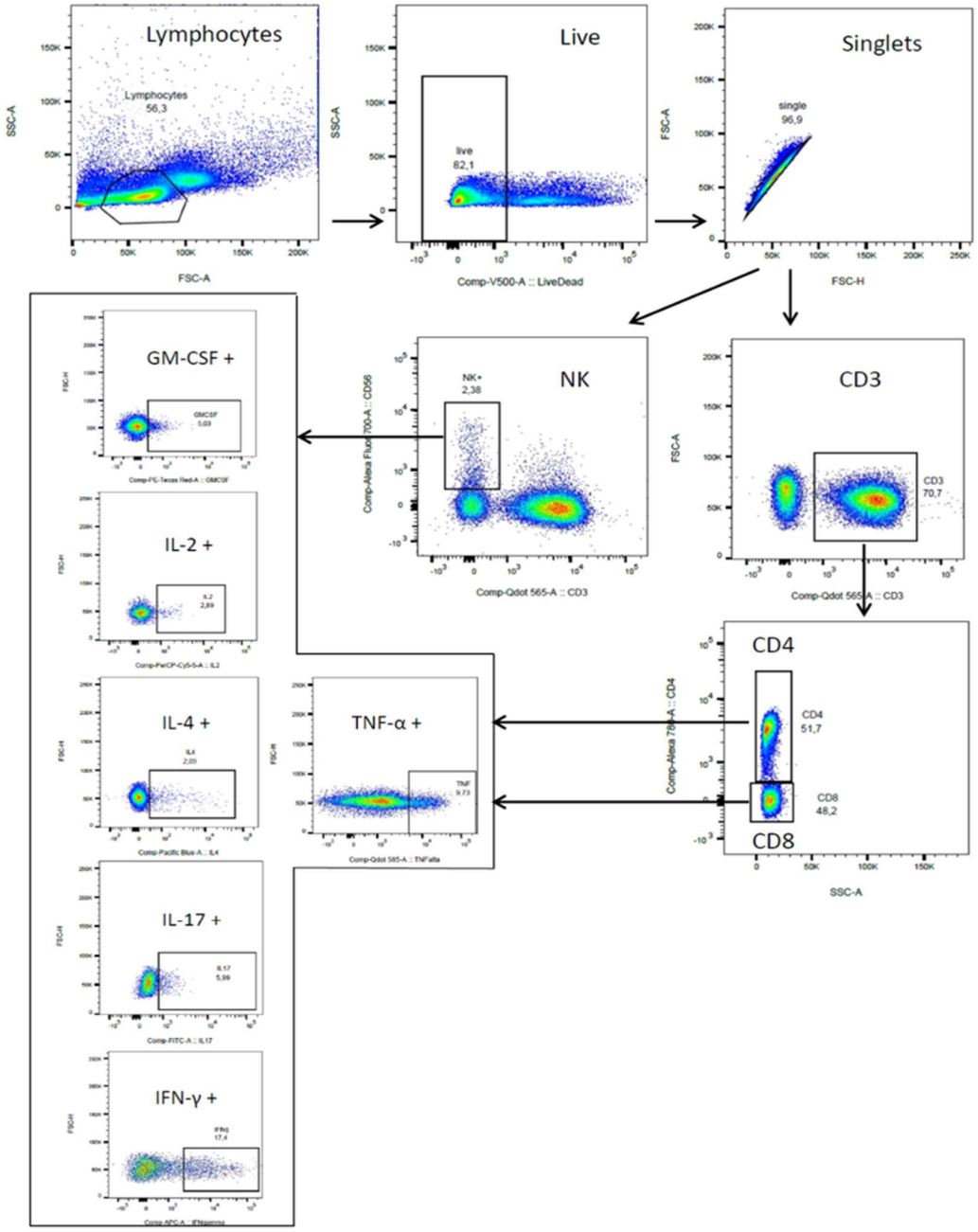

Figure 18. Gating strategy for T-lymphocytes and NK cells cytokines panel

Finally, the gating strategy implemented for panel 4 was designed to differentiate T regulatory lymphocytes (Figure 19). Considering the single cells populations, the T cells subpopulation expressing CD3 marker (CD3+) were isolated. An additional gate was defined to characterize Treg cells based on the expression of transcription factors FoxP3 and CD39. Lastly, the expression of CD49d marker was used to differentiate FoxP3+CD39+ Treg cells into activated (FoxP3+CD39+CD49d+) and un-activated (FoxP3+CD39+CD49d-).

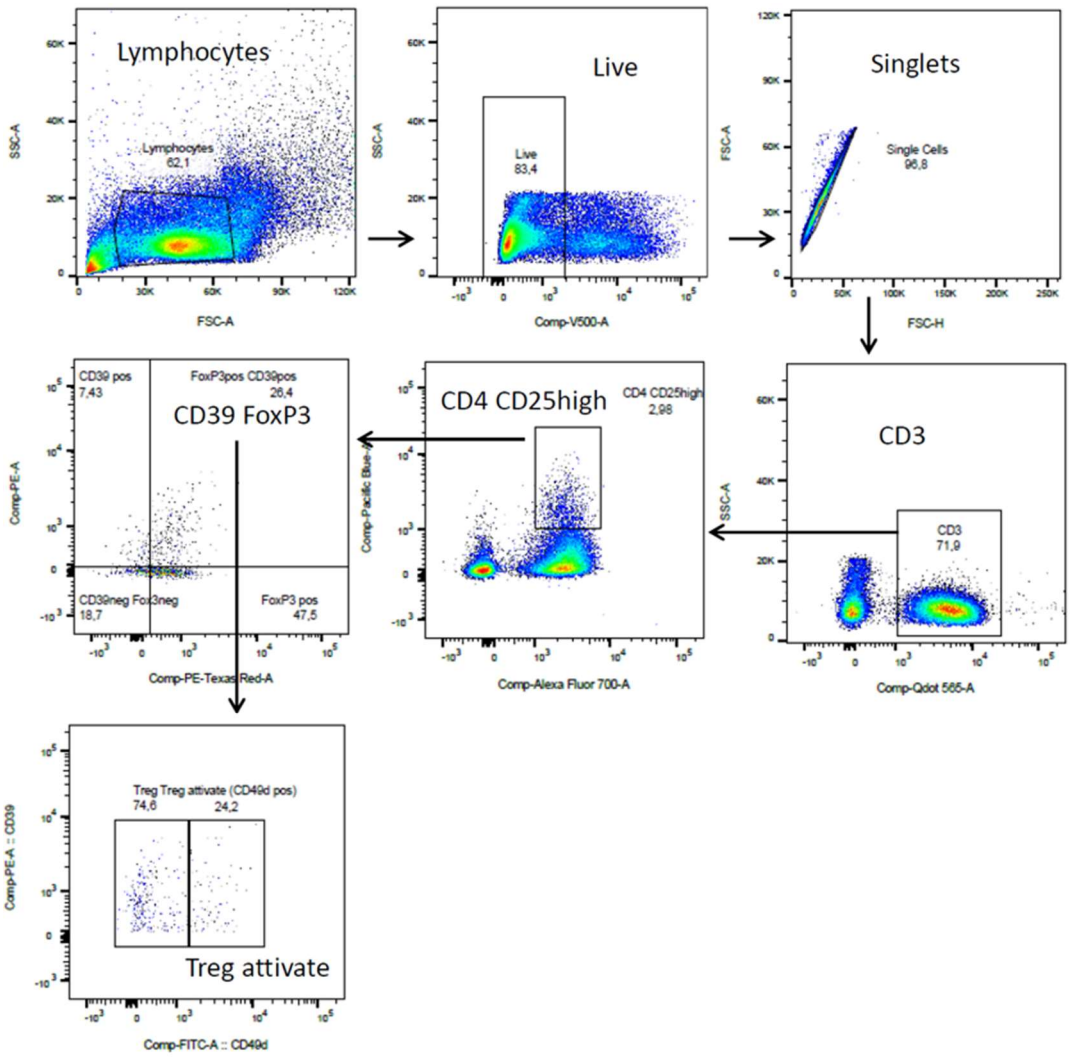

Figure 19. Gating strategy for T regulatory lymphocytes panel

A complete list of the immune cell populations used for unsupervised ML analyses is reported in Table 14.

Table 14. Immune cells populations for each panel used for ML analyses

PANEL 1	PANEL 2	PANEL 3	PANEL 4
CD4+/CM/CD25+	CD8+/CM/Perf- GrzB+	CD4+/GM-CSF	FoxP3- CD39+
CD4+/CM/CD69+	CD8+/CM/Perf+ GrzB+	CD4+/IFN-γ	FoxP3+ CD39+
CD4+/EM/CD25+	CD8+/CM/Perf+ GrzB-	CD4+/IL-2	Treg (CD49d+)
CD4+/EM/CD69+	CD8+/EM/CM/Perf- GrzB+	CD4+/IL-4	Treg (CD49d-)
CD4+/Naive/CD25+	CD8+/EM/Perf+ GrzB+	CD4+/IL-17	FoxP3+ CD39-
CD4+/Naive/CD69+	CD8+/EM/Perf+ GrzB-	CD4+/TNF-α	FoxP3- CD39-
CD8+/CM/CD25+	CD8+/Naive/Perf- GrzB+	CD8+/GM-CSF	
CD8+/CM/CD69+	CD8+/Naive/Perf+ GrzB+	CD8+/IFN-γ	
CD8+/EM/CD25+	CD8+/Naive/Perf+ GrzB-	CD8+/IL-2	
CD8+/EM/CD69+	CD8+/TEMRA/CM/Perf- GrzB+	CD8+/IL-4	
CD8+/Naive/CD25+	CD8+/TEMRA/Perf+ GrzB+	CD8+/IL-17	
CD8+/Naive/CD69+	CD8+/TEMRA/Perf+ GrzB-	CD8+/TNF-α	
Mait Cells CD161+	CD3+/Tγδ/Perf- GrzB+	NK cells/GM-CSF	
	CD3+/Tγδ/Perf+ GrzB+	NK cells/IFN-γ	
	CD3+/Tγδ/Perf+ GrzB-	NK cells/IL-2	
	NK cells/Perf- GrzB+	NK cells/IL-4	
	NK cells/Perf+ GrzB+	NK cells/IL-17	
	NK cells/Perf+ GrzB-	NK cells/TNF-α	

Abbreviations: CM, central memory; EM, effective memory; GM-CSF; granulocyte macrophage colony stimulating factor; IL, interleukin; INF; interferon; TNF, tumor necrosis factor; Treg; regulatory T cells; Perf; perforin; GrzB; granzyme; TEMRA, T cells re-expressing CD45RA; NK, natural killer.

5.6 Statistical analysis

A graphical representation of the statistical analysis plan is depicted in Figure 20.

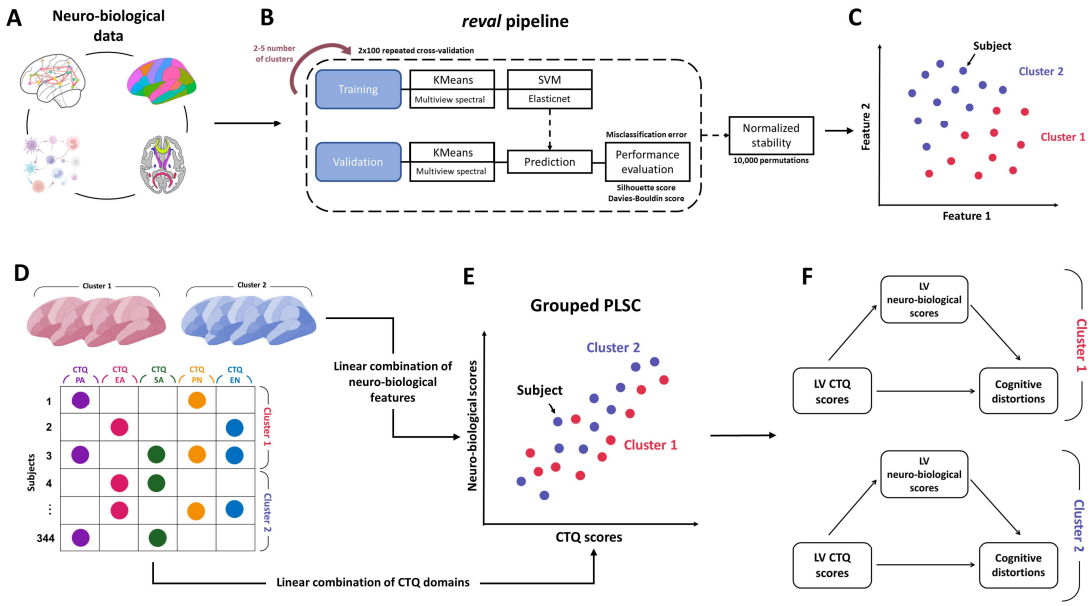

Figure 20. Graphic representation of the analysis pipeline. *A. Neuroimaging and immune-inflammatory markers (cytokines, chemokines, growth factors, and immune cell populations) were extracted for each patient. B-C. For each type of feature, a stability-based relative clustering approach was implemented. The best clustering solution was identified minimizing the misclassification error (i.e., normalized stability). D-E. For each stratification model, multivariate neurobiological-ACEs relationships were investigated through Partial Least Squared Correlation (PLSC) analyses, considering Childhood Trauma Questionnaire (CTQ) domains as the "behavioural" dataset and clusters' labels as the grouping structure. F. For significant latent variables (LV), mediation analyses were performed to investigate the mediating effect of LV neurobiological scores on the relationship between LV CTQ scores and Cognition Questionnaire (CQ) domains in the discovered clusters. Abbreviations: SVM, support vector machine; CTQ, Childhood Trauma Questionnaire; CQ, Cognition Questionnaire; PLSC, Partial Least Squared Correlation analysis; LV, latent variable.*

5.6.1 Unsupervised machine learning analyses

One of the main limitations of the most commonly used clustering algorithms is the absence of *a priori* knowledge, which makes challenging the assessment of the reliability of an identified clustering solution. Usually, the optimal number of clusters is selected through internal validation measures (e.g., elbow method, Silhouette score), which, however, are tied to the intrinsic characteristics of the data at hand (Friedman et al, 2001). Conversely, relative validation approaches (also called stability-based methods) determine the best clustering as the one that minimizes the distance among groupings of

observations identified in distinct datasets, providing a direct measure of how well a clustering solution replicates on new data (Lange et al, 2004; Tibshirani & Walther, 2005). In this study, a stability-based relative clustering validation algorithm (*reval* Python package) (Landi et al, 2021) was implemented for each type of input data to uncover biologically-driven subtypes of depressed patients. Based on the stability-based method proposed by Lange et al (2004), this approach has the main strength of translating the unsupervised nature of cluster analysis into a supervised learning framework, assessing the generalizability of clustering solutions to unseen observations through a cross-validation procedure. The main steps of the *reval* pipeline are depicted in Figure 20 B. First, the input dataset is split into separate training (X_{tr}) and validation (X_{ts}) sets. A clustering algorithm A_k is independently applied on X_{tr} and X_{ts} to derive clusters' labels for each set (i.e., Y_{tr} and Y_{ts}). Second, a supervised classification algorithm Φ is trained on [X_{tr} , Y_{tr}] and fitted to X_{ts}. The predicted labels in the test set (Φ (X_{ts})) are then compared with the original Y_{ts}. By iterating over different number of clusters, the optimal clustering solution is selected as the one that minimize the prediction error between Y_{ts} and Φ (X_{ts}) in cross-validation. In this context, the misclassification error is defined through the 0-1 loss, also known as normalized Hamming distance (1):

$$d_{S_k}(\Phi\ (X_{ts}), Y_{ts}) = \min_{\sigma \in S_k} \frac{1}{n} \sum_{i=1}^{n} 1\{\Phi\ (X_{ts_i})\ \neq \sigma(Y_{ts_i})\} \tag{1}$$

where S_k indicates the set of all the possible permutations. To account for the non-uniqueness of clusters' labels, Y_{ts} are permuted *n* times, and the specific permutation that minimizes the distance is denoted by $\sigma(Y_{ts_i})$[4]. The stability index is then defined as the average of the distances across all the possible X_{tr} and X_{ts} splits (2):

$$S(A_k) = E_{X_{tr}, X_{ts}}[d_{S_k}(\Phi(X_{ts}), Y_{ts})] \tag{2}$$

[4] *The identification of the permuted labels that minimize the misclassification error is performed through the Kuhn-Munkres algorithm. However, contrary to the original definition of Lange el al (2004), in reval the permutation is*

The stability index values range from 0 to 1, where lower values reflect more stable clustering solutions (Lange et al, 2004). Given that this measure tends to scale with the number of clusters, the stability described in (2) is divided by the stability obtained from random labelling (i.e., normalized stability) (3):

$$\bar{S}\,(A_k) = \frac{S(A_k)}{S(R_k)} \tag{3}$$

where $\bar{S}$ represents the normalized stability $S(R_k)$ and R_k the stability obtained from the random label guessing (Lange et al, 2004). The accuracy of the selected clustering solution is defined as 1 - $\bar{S}$.

For the present study, the *reval* algorithm was improved by embedding preprocessing steps (i.e., features standardization and confound regression for nuisance variables) into the cross-validation framework, minimizing data leakage between training and test sets (GitHub repository: https://github.com/fede-colombo/NeuReval). For all the models, the input features were standardized by removing the mean and scaling to unit variance. Then, the confounding effects of age, sex, pharmacological load, and frequency of previous episodes were removed from the input features through linear regression. For neuroimaging data, age-by-sex interaction and the squared of age were considered as confounding variables to account for potential non-linear effects of age (Alfaro-Almagro et al, 2021). Moreover, only for GM volumes and cortical thickness, TIV was also entered as a covariate. All these steps were fitted on the training set and then applied to the test set. A 2-fold cross-validation scheme (50% training, 50% test) was employed to account for size imbalances resulting from training-test sets splitting (Landi et al, 2021), and it was repeated 100 times to ensure the robustness of the identified clustering solution. Whereas K-Means was implemented as a clustering algorithm for all the models, different classifiers were employed considering the specific type of input features. Specifically, support vector machine (SVM) was considered as a supervised classifier in neuroimaging-based models, whereas elasticnet penalized regression was employed in the inflammatory-based (i.e., FACS and immune-inflammatory profiles) models (for a

performed on the clustering labels Y_{ts} instead of the classifier labels $\Phi\,(X_{ts})$ to ensure that the grouping structure within the training set in maintained in the test set (Landi et al, 2021).

detailed description of each algorithm, see Appendix 2). Moreover, a grid search procedure was performed in the training set to optimize the hyperparameters for both clustering and classifier algorithms, using the minimization of the normalized stability as the criterion to select the optimal ones. These included i) K-Means initialization (i.e., random or k-means++); ii) the soft-margin *C* (range: 0.01, 0.1, 1, 10, 100, 1000) and the type of kernel (i.e., linear or radial basis function) for SVM; iii) the regularization strength (λ range values: 0.01, 0.1, 1, 10, 100, 1000) and the trade-off between L1 and L2 regularizations (α range values: 0, 0.25, 0.5, 0.75, 1) for elasticnet penalized regression. The entire process was iterated over a number of clusters from 2 to 5, and the clustering solution achieving the minimum normalized stability throughout cross-validation was selected.

To investigate whether the combination of different neuroimaging modalities could provide a more informative stratification model compared to a single-modality approach, a multiview spectral clustering algorithm was embedded within the *reval* pipeline (GitHub repository: https://github.com/fede-colombo/Multiview_NeuReval). In multiview frameworks, different feature sets called *views* can be entered within the clustering algorithm, which can be separately used to derive clusters. The rationale behind this approach is that the grouping structure identified in one view should agree with the one derived from another view. Consequently, the best clustering solution is the one that assigns an observation to the same cluster regardless of the specific view (Kumar & Daumé, 2011). This approach largely relies on the core idea of *co-training*, which was initially proposed in semi-supervised frameworks to derive clusters of unlabelled data using information from labelled observations (Blum & Mitchell, 1998). The co-training approach relies on 3 assumptions: i) *sufficiency*, meaning that each view is sufficient to derive clusters by itself; ii) *compatibility*, denoting that, if an observation is labelled with high confidence in one view, clusters' labels derived from the other views should not disagree with this labelling; iii) *conditional independence*, which means that, given the cluster label, the information derived from one view is conditionally independent of the others (Blum & Mitchell, 1998). Whereas in semi-supervised learning the labelled data are used to drive the agreement between clusters' labels derived from different views, in unsupervised learning the grouping structure obtained from one view is used to inform the clustering processing in another view and vice versa (Kumar & Daumé, 2011). In this

study, the multiview approach was applied to a spectral clustering algorithm as implemented in *mvlearn* Python package (Perry et al, 2021). Derived from graph theory, spectral clustering aims to detect clusters of nodes (i.e., observations) from a graph considering the edges linking them as a measure of similarity, allowing to capture groupings of complex or arbitrary shapes within the data (von Luxburg, 2007). Moreover, unlike the multiview K-Means algorithm, multiview spectral clustering can be applied to more than 2 views, making it particularly suitable for analysing multiple types of data (Kumar & Daumé, 2011). For the multimodal stratification model, each neuroimaging feature set was entered in *reval* as separate views, considering multiview spectral clustering as the clustering algorithm and SVM as the classifier. Notably, only neuroimaging features that resulted in stable clustering solutions (i.e., misclassification error above chance level) in single-feature models were considered. As for the models based on individual features, *reval* was run with a 2-fold cross-validation scheme repeated 100 times, iterating over a number of clusters from 2 to 5. Age, sex, age squared, age-by-sex interaction, frequency of previous episodes, pharmacological load, and TIV (only for grey matter volumes and cortical thickness) were considered as confounding variables. Hyperparameters to be tuned included i) the affinity metric used to build the affinity matrix (i.e., radial basis function or nearest neighbors) for multiview spectral clustering; ii) the soft-margin *C* (range: 0.01, 0.1, 1, 10, 100, 1000) and the type of kernel (i.e., linear or radial basis function) for SVM.

In addition to normalized stability, the silhouette score and Davies-Bouldin index[5] were computed for each stratification model to investigate the degree of agreement between clustering solutions obtained through a stability-based approach and those identified through internal validity indices. In this case, K-Means (for single-feature models) or multiview spectral clustering (for the multimodal model) were applied on the entire dataset considering the same range of number of clusters used in *reval* (i.e., 2-5 clusters), and the clustering solution that maximized the silhouette score or minimized

[5] The silhouette score combines information about the cohesion (i.e., the degree to which one observation is similar to the other observations in the same cluster) and separation (i.e., the degree of separation between an observation and those assigned to other clusters). Its values range from -1 to 1, where values near to 1 reflect well-separated clusters, while values close to 0 suggest overlapping clusters. Negative values indicate incorrectly classified observations (Rousseeuw, 1987). The Davies-Bouldin index is defined as the average similarity (i.e., within-cluster to between-cluster ratio) of each cluster with its nearest cluster. The minimum value is 0, where lower values reflect a well-separated clustering solution (Bouldin, 1979).

the Davies-Bouldin index was considered as the optimal one. Finally, to verify whether the identified clustering solutions reflect the existence of true clusters within the data, a Monte Carlo simulation approach was implemented to test if the obtained clusters derive from a single multivariate Gaussian distribution. To do this, the *sigclust* method with 10,000 simulations (Huang et al, 2015) was applied to each feature set, considering the same standardization and correction for nuisance covariates implemented in *reval.* Only stratification models that passed false-discovery rate (FDR) $q<0.05$ threshold were deemed as significant.

5.6.2. Clinical and neurobiological characterization of the clusters

For each significant stratification model, subtypes were tested for differences in age, diagnosis, sex, number of previous episodes, age of onset, duration of illness, pharmacological load, HDRS-21 total score, CTQ and CQ total scores and domains. Two-sample t-tests were performed for continuous variables, whereas chi-square tests were implemented for categorical variables. In the case of non-normally distributed variables as assessed through the Shapiro-Wilk test, non-parametric Mann-Whitney U tests were applied. The same approach was employed to investigate differences between clusters in the biological features used for clustering. For these latter comparisons, Cohen's d effects sizes were also calculated and multiple comparison corrections were achieved at FDR $q<0.05$. In addition to univariate comparisons, grouped PLSC analyses were performed to investigate whether the multivariate relationship between biological data and measures of exposure to childhood trauma is different between clusters (Figure 20 D-E). PLSC is a multivariate technique that aims to maximize the covariation between 2 different datasets (e.g., biological and behavioural data). The optimal relationship between the datasets is described by latent variables (LV) pairs, which represent linear combinations of the original data that maximally explain covariation in the dataset and that are uncorrelated with other biological-behavioural LV pairs (Krishnan et al, 2011). When information about group membership is provided, the covariance matrix is calculated separately for each of them, allowing the investigation of differences in biological-behavioural multivariate relationships between groups (Krishnan et al, 2011). In this study, grouped PLSC analyses were implemented for each significant stratification model, considering the biological data used as input features for clustering as the "biological" dataset, CTQ domain scores as the "behavioural" dataset, and clusters' labels

as the grouping structure. Before being entered into PLSC analyses, each biological dataset was corrected for the same nuisance covariates considered for *reval* analysis, whereas the confounding effects of age and sex were removed from CTQ domains. For each PLSC model, permutation testing (5000 permutations) was performed to assess the statistical significance of the LV pairs, and only LV pairs that passed FDR $q<0.05$ were considered significant. BSR and 95% CI biological-CTQ correlations were estimated through 5000 bootstrap resampling. BSRs were computed by dividing the correlation coefficient for each biological variable by its bootstrapped standard deviation, and they can roughly be considered as Z-scores reflecting the reliability of that biological variable for contributing to the identified LV pair (Krishnan et al, 2011). Only BSRs>|2| were judged as important in guiding the neurobiological-ACEs relationships, whereas CTQ loadings with 95% CI that do not include zero were deemed as significant. To account for the high dimensionality of biological data, BSRs were converted into p-values and multiple comparison correction was performed with FDR $q<0.05$ (Kebets et al, 2019). All grouped PLSC analyses were implemented within the myPLS MATLAB toolbox (https://github.com/danizoeller/myPLS/).

Finally, in the case of significant LV pairs, the interplay between neuro-biological data, childhood trauma, and cognitive distortions in the discovered clusters was investigated with the following analyses. First, multivariate GLMs were implemented separately for each cluster considering LV neuro-biological scores as independent variables and CQ domains as dependent variables. Univariate analyses were also performed within each cluster to explore the differential effect of LV neuro-biological scores on each CQ domain. For each model, the statistical significance was assessed using parametric estimates of the predictor variables, calculated by the least squares method. For those CQ domains that were significantly predicted by LV neuro-biological scores, mediation models were performed with the PROCESS macro for SPSS (Hayes, 2012), considering LV CTQ scores as independent variables, LV neuro-biological scores as mediator, and CQ domain as dependent variable. A 5000 bootstrap resampling procedure was implemented for significance testing and computing 90% CI (Figure 20F).

REFERENCES

Abé C, Ching CR, Liberg B, Lebedev AV, Agartz I, Akudjedu TN, Alda M, Alnæs D, Alonso-Lana S, Benedetti F (2022) Longitudinal structural brain changes in bipolar disorder: a multicenter neuroimaging study of 1232 individuals by the ENIGMA bipolar disorder working group. *Biol Psychiatry* **91:** 582-592

Abé C, Liberg B, Klahn AL, Petrovic P, Landén M (2023) Mania-related effects on structural brain changes in bipolar disorder–a narrative review of the evidence. *Mol Psychiatry* **28:** 2674-2682

Abé C, Liberg B, Song J, Bergen SE, Petrovic P, Ekman CJ, Sellgren CM, Ingvar M, Landén M (2020) Longitudinal cortical thickness changes in bipolar disorder and the relationship to genetic risk, mania, and lithium use. *Biol Psychiatry* **87:** 271-281

Abler B, Erk S, Herwig U, Walter H (2007) Anticipation of aversive stimuli activates extended amygdala in unipolar depression. *J Psychiatr Res* **41:** 511-522

Aggio V, Fabbella L, Poletti S, Lorenzi C, Finardi A, Colombo C, Zanardi R, Furlan R, Benedetti F (2023) Circulating cytotoxic immune cell composition, activation status and toxins expression associate with white matter microstructure in bipolar disorder. *Sci Rep* **13:** 22209

Ahmed YB, Al-Bzour AN, Alzghoul SM, Ibrahim RB, Al-Khalili AA, Ghayda'a N, Hamza AI, Al-Zamer YS, Alhayek K, Kofahi R (2023) Limbic and cortical regions as functional biomarkers associated with emotion regulation in bipolar disorder: A meta-analysis of neuroimaging studies. *J Affect Disord* **323:** 506-513

Alexander AL, Lee JE, Lazar M, Field AS (2007) Diffusion Tensor Imaging of the Brain. *Neurotherapeutics* **4:** 316-329

Alfaro-Almagro F, McCarthy P, Afyouni S, Andersson JLR, Bastiani M, Miller KL, Nichols TE, Smith SM (2021) Confound modelling in UK Biobank brain imaging. *Neuroimage* **224:** 117002

Alloy LB, Olino T, Freed RD, Nusslock R (2016) Role of reward sensitivity and processing in major depressive and bipolar spectrum disorders. *Behav Ther* **47:** 600-621

Almulla AF, Algon AAA, Maes M (2024) Adverse childhood experiences and recent negative events are associated with activated immune and growth factor pathways, the phenome of first episode major depression and suicidal behaviors. *Psychiatry Res* **334:** 115812

Alves GS, Oertel Knöchel V, Knöchel C, Carvalho AF, Pantel J, Engelhardt E, Laks J (2015) Integrating Retrogenesis Theory to Alzheimer's Disease Pathology: Insight from DTI-TBSS Investigation of the White Matter Microstructural Integrity. *BioMed research international* **2015:** 291658

American Psychiatric Association (1994) *Diagnostic and statistical manual of mental disorders, 4th ed*, Arlington, VA, US: American Psychiatric Publishing, Inc.

American Psychiatric Association (2022) Diagnostic and Statistical Manual of Mental Disorders, Fifth Edition, Text Revision. *Washington, DC*

Arthur D, Vassilvitskii S. (2006) k-means++: The advantages of careful seeding. Stanford.

Barbosa IG, Rocha NP, Bauer ME, De Miranda AS, Huguet RB, Reis HJ, Zunszain PA, Horowitz MA, Pariante CM, Teixeira AL (2013) Chemokines in bipolar disorder: trait or state? *Eur Arch Psychiatry Clin Neurosci* **263:** 159-165

Barrett LF, Simmons WK (2015) Interoceptive predictions in the brain. *Nat Rev Neurosci* **16:** 419-429

Baumeister D, Akhtar R, Ciufolini S, Pariante CM, Mondelli V (2016) Childhood trauma and adulthood inflammation: a meta-analysis of peripheral C-reactive protein, interleukin-6 and tumour necrosis factor-α. *Mol Psychiatry* **21:** 642-649

Beck AT (1979) *Cognitive therapy of depression*: Guilford press.

Beck AT (2008) The evolution of the cognitive model of depression and its neurobiological correlates. *Am J Psychiatry* **165:** 969-977

Beck AT, Dozois DJ (2011) Cognitive therapy: current status and future directions. *Annu Rev Med* **62:** 397-409

Beijers L, Wardenaar KJ, van Loo HM, Schoevers RA (2019) Data-driven biological subtypes of depression: systematic review of biological approaches to depression subtyping. *Mol Psychiatry* **24:** 888-900

Benedetti F, Absinta M, Rocca MA, Radaelli D, Poletti S, Bernasconi A, Dallaspezia S, Pagani E, Falini A, Copetti M (2011a) Tract-specific white matter structural disruption in patients with bipolar disorder. *Bipolar disorders* **13:** 414-424

Benedetti F, Aggio V, Pratesi ML, Greco G, Furlan R (2020) Neuroinflammation in Bipolar Depression. *Frontiers in Psychiatry* **11**

Benedetti F, Palladini M, D'Orsi G, Furlan R, Ciceri F, Rovere-Querini P, Mazza MG (2022) Mood-congruent negative thinking styles and cognitive vulnerability in depressed COVID-19 survivors: A comparison with major depressive disorder. *J Affect Disord* **308:** 554-561

Benedetti F, Poletti S, Hoogenboezem TA, Locatelli C, de Wit H, Wijkhuijs AJ, Colombo C, Drexhage HA (2017) Higher baseline proinflammatory cytokines mark poor antidepressant response in bipolar disorder. *The Journal of clinical psychiatry* **78:** 4015

Benedetti F, Yeh P-H, Bellani M, Radaelli D, Nicoletti MA, Poletti S, Falini A, Dallaspezia S, Colombo C, Scotti G (2011b) Disruption of white matter integrity in bipolar depression as a possible structural marker of illness. *Biol Psychiatry* **69:** 309-317

Benson S, Brinkhoff A, Lueg L, Roderigo T, Kribben A, Wilde B, Witzke O, Engler H, Schedlowski M, Elsenbruch S (2017) Effects of acute systemic inflammation on the interplay between sad mood and affective cognition. *Transl Psychiatry* **7:** 1281

Berk M, Kapczinski F, Andreazza AC, Dean OM, Giorlando F, Maes M, Yücel M, Gama CS, Dodd S, Dean B (2011) Pathways underlying neuroprogression in bipolar disorder: focus on inflammation, oxidative stress and neurotrophic factors. *Neurosci Biobehav Rev* **35:** 804-817

Berk M, Post R, Ratheesh A, Gliddon E, Singh A, Vieta E, Carvalho AF, Ashton MM, Berk L, Cotton SM (2017) Staging in bipolar disorder: from theoretical framework to clinical utility. *World Psychiatry* **16:** 236-244

Bernstein DP, Stein JA, Newcomb MD, Walker E, Pogge D, Ahluvalia T, Stokes J, Handelsman L, Medrano M, Desmond D (2003) Development and validation of a brief screening version of the Childhood Trauma Questionnaire. *Child Abuse Negl* **27:** 169-190

Biazus TB, Beraldi GH, Tokeshi L, Rotenberg LdS, Dragioti E, Carvalho AF, Solmi M, Lafer B (2023) All-cause and cause-specific mortality among people with bipolar disorder: a large-scale systematic review and meta-analysis. *Mol Psychiatry* **28:** 2508-2524

Biswal B, Zerrin Yetkin F, Haughton VM, Hyde JS (1995) Functional connectivity in the motor cortex of resting human brain using echo-planar MRI. *Magn Reson Med* **34:** 537-541

Blum A, Mitchell T (1998) Combining labeled and unlabeled data with co-training. In *Proceedings of the eleventh annual conference on Computational learning theory*, pp 92-100.

Boldrini M, Santiago AN, Hen R, Dwork AJ, Rosoklija GB, Tamir H, Arango V, John Mann J (2013) Hippocampal granule neuron number and dentate gyrus volume in antidepressant-treated and untreated major depression. *Neuropsychopharmacology* **38:** 1068-1077

Bourgognon J-M, Cavanagh J (2020) The role of cytokines in modulating learning and memory and brain plasticity. *Brain and Neuroscience Advances* **4:** 2398212820979802

Brachman RA, Lehmann ML (2015) Lymphocytes from chronically stressed mice confer antidepressant-like effects to naive mice. **35:** 1530-1538

Bradley B, Davis TA, Wingo AP, Mercer KB, Ressler KJ (2013) Family environment and adult resilience: contributions of positive parenting and the oxytocin receptor gene. *European journal of psychotraumatology* **4:** 21659

Breen EJ, Polaskova V, Khan A (2015) Bead-based multiplex immuno-assays for cytokines, chemokines, growth factors and other analytes: median fluorescence intensities versus their derived absolute concentration values for statistical analysis. *Cytokine* **71:** 188-198

Breen EJ, Tan W, Khan A (2016) The statistical value of raw fluorescence signal in Luminex xMAP based multiplex immunoassays. *Sci Rep* **6:** 26996

Breunis MN, Kupka RW, Nolen WA, Suppes T, Denicoff KD, Leverich GS, Post RM, Drexhage HA (2003) High numbers of circulating activated T cells and raised levels of serum IL-2 receptor in bipolar disorder. *Biol Psychiatry* **53:** 157-165

Brietzke E, Kauer-Sant'Anna M, Teixeira AL, Kapczinski F (2009) Abnormalities in serum chemokine levels in euthymic patients with bipolar disorder. *Brain Behav Immun* **23:** 1079-1082

Brown M, Worrell C, Pariante CM (2021) Inflammation and early life stress: An updated review of childhood trauma and inflammatory markers in adulthood. *Pharmacol Biochem Behav* **211:** 173291

Brucar LR, Feczko E, Fair DA, Zilverstand A (2023) Current approaches in computational psychiatry for the data-driven identification of brain-based subtypes. *Biol Psychiatry* **93:** 704-716

Buch AM, Liston C (2021) Dissecting diagnostic heterogeneity in depression by integrating neuroimaging and genetics. *Neuropsychopharmacology* **46:** 156-175

Buckner RL, Krienen FM, Castellanos A, Diaz JC, Yeo BT (2011) The organization of the human cerebellum estimated by intrinsic functional connectivity. *J Neurophysiol* **106:** 2322-2345

Bullmore E, Sporns O (2009) Complex brain networks: graph theoretical analysis of structural and functional systems. *Nature reviews neuroscience* **10:** 186-198

Byrne JF, Healy C, Mongan D (2022) Transdiagnostic inflammatory subgroups among psychiatric disorders and their relevance to role functioning: a nested case-control study of the ALSPAC cohort. **12:** 377

Bzdok D, Meyer-Lindenberg A (2018) Machine learning for precision psychiatry: opportunities and challenges. *Biological Psychiatry: Cognitive Neuroscience and Neuroimaging* **3:** 223-230

Cahn AJ, Keramatian K, Frysch C, Yatham LN, Chakrabarty T (2021) Longitudinal grey matter changes following first episode mania in bipolar I disorder: a systematic review. *J Affect Disord* **291:** 198-208

Calesella F, Colombo F, Bravi B, Fortaner-Uyà L, Monopoli C, Poletti S, Tassi E, Maggioni E, Brambilla P, Colombo C, Bollettini I, Benedetti F, Vai B (2024) A machine learning pipeline for efficient differentiation between bipolar and major depressive disorder based on multimodal structural neuroimaging. *Neuroscience Applied* **3:** 103931

Carvalho AF, Firth J, Vieta E (2020) Bipolar Disorder. *N Engl J Med* **383:** 58-66

Casey BJ, Heller AS, Gee DG, Cohen AO (2019) Development of the emotional brain. *Neurosci Lett* **693:** 29-34

Caspi A, Moffitt TE (2018) All for One and One for All: Mental Disorders in One Dimension. *Am J Psychiatry* **175:** 831-844

Caspi A, Sugden K, Moffitt TE, Taylor A, Craig IW, Harrington H, McClay J, Mill J, Martin J, Braithwaite A (2003) Influence of life stress on depression: moderation by a polymorphism in the 5-HTT gene. *Science* **301:** 386-389

Charney A, Ruderfer D, Stahl E, Moran J, Chambert K, Belliveau R, Forty L, Gordon-Smith K, Di Florio A, Lee P (2017) Evidence for genetic heterogeneity between clinical subtypes of bipolar disorder. *Transl Psychiatry* **7:** e993-e993

Charney AW, Stahl EA, Green EK, Chen C-Y, Moran JL, Chambert K, Belliveau Jr RA, Forty L, Gordon-Smith K, Lee PH (2019) Contribution of rare copy number variants to bipolar disorder risk is limited to schizoaffective cases. *Biol Psychiatry* **86:** 110-119

Chen G, Guo Y, Zhu H, Kuang W, Bi F, Ai H, Gu Z, Huang X, Lui S, Gong Q (2017) Intrinsic disruption of white matter microarchitecture in first-episode, drug-naive major depressive disorder: A voxel-based meta-analysis of diffusion tensor imaging. *Prog Neuropsychopharmacol Biol Psychiatry* **76:** 179-187

Cheng Y, Xu J, Yu H, Nie B, Li N, Luo C, Li H, Liu F, Bai Y, Shan B, Xu L, Xu X (2014) Delineation of early and later adult onset depression by diffusion tensor imaging. *PLoS One* **9:** e112307

Chesney E, Goodwin GM, Fazel S (2014) Risks of all-cause and suicide mortality in mental disorders: a meta-review. *World psychiatry* **13:** 153-160

Chrousos GP (1995) The hypothalamic-pituitary-adrenal axis and immune-mediated inflammation. *N Engl J Med* **332:** 1351-1362

Cibrián D, Sánchez-Madrid F (2017) CD69: from activation marker to metabolic gatekeeper. *Eur J Immunol* **47:** 946-953

Cicchetti D, Rogosch FA (1996) Equifinality and multifinality in developmental psychopathology. *Dev Psychopathol* **8:** 597-600

Cirone C, Secci I, Favole I, Ricci F, Amianto F, Davico C, Vitiello B (2021) What do we know about the long-term course of early onset bipolar disorder? A review of the current evidence. *Brain sciences* **11:** 341

Claeys EH, Mantingh T, Morrens M, Yalin N, Stokes PR (2022) Resting-state fMRI in depressive and (hypo) manic mood states in bipolar disorders: A systematic review. *Prog Neuropsychopharmacol Biol Psychiatry* **113:** 110465

Coello K, Kjærstad HL, Stanislaus S, Melbye S, Faurholt-Jepsen M, Miskowiak KW, McIntyre RS, Vinberg M, Kessing LV, Munkholm K (2019) Thirty-year cardiovascular risk score in patients with newly diagnosed bipolar disorder and their unaffected first-degree relatives. *Aust N Z J Psychiatry* **53:** 651-662

Cohen JA, Mannarino AP (2015) Trauma-focused Cognitive Behavior Therapy for Traumatized Children and Families. *Child Adolesc Psychiatr Clin N Am* **24:** 557-570

Colwell MJ, Tagomori H, Chapman S, Gillespie AL, Cowen PJ, Harmer CJ, Murphy SE (2022) Pharmacological targeting of cognitive impairment in depression: recent developments and challenges in human clinical research. *Transl Psychiatry* **12:** 484

Cristianini N, Shawe-Taylor J (2000) *An introduction to support vector machines and other kernel-based learning methods*: Cambridge university press.

Cruz D (2023) Childhood Trauma Questionnaire-Short Form: Evaluation of factor structure and measurement invariance. *Journal of Child & Adolescent Trauma* **16:** 1099-1108

Cui Y, Dong J, Yang Y, Yu H, Li W, Liu Y, Si J, Xie S, Sui J, Lv L (2020) White matter microstructural differences across major depressive disorder, bipolar disorder and schizophrenia: A tract-based spatial statistics study. *J Affect Disord* **260:** 281-286

Danese A, Caspi A, Williams B, Ambler A, Sugden K, Mika J, Werts H, Freeman J, Pariante CM, Moffitt TE, Arseneault L (2011) Biological embedding of stress through inflammation processes in childhood. *Mol Psychiatry* **16:** 244-246

Danese A, Pariante CM, Caspi A, Taylor A, Poulton R (2007) Childhood maltreatment predicts adult inflammation in a life-course study. *Proc Natl Acad Sci U S A* **104:** 1319-1324

Dantzer R (2001) Cytokine-induced sickness behavior: where do we stand? *Brain Behav Immun* **15:** 7-24

Daruy-Filho L, Brietzke E, Lafer B, Grassi-Oliveira R (2011) Childhood maltreatment and clinical outcomes of bipolar disorder. *Acta Psychiatr Scand* **124:** 427-434

Davies DL, Bouldin DW (1979) A Cluster Separation Measure. *IEEE Transactions on Pattern Analysis and Machine Intelligence* **PAMI-1:** 224-227

De Bellis MD (2005) The psychobiology of neglect. *Child maltreatment* **10:** 150-172

Desikan RS, Ségonne F, Fischl B, Quinn BT, Dickerson BC, Blacker D, Buckner RL, Dale AM, Maguire RP, Hyman BT (2006) An automated labeling system for subdividing the human cerebral cortex on MRI scans into gyral based regions of interest. *Neuroimage* **31:** 968-980

Devlin B, Kelsoe JR, Sklar P, Daly MJ, O'Donovan MC, Craddock N, Sullivan PF, Smoller JW, Kendler KS (2013) Genetic relationship between five psychiatric disorders estimated from genome-wide SNPs. *Nat Genet* **45:** 984-994

Dias de Mattos Souza L, Lopez Molina M, Azevedo da Silva R, Jansen K (2016) History of childhood trauma as risk factors to suicide risk in major depression. *Psychiatry Res* **246:** 612-616

Dinga R, Schmaal L, Penninx BW, van Tol MJ, Veltman DJ, van Velzen L, Mennes M, van der Wee NJ, Marquand AF (2019) Evaluating the evidence for biotypes of depression: Methodological replication and extension of. *NeuroImage: Clinical* **22:** 101796

Disner SG, Beevers CG, Haigh EA, Beck AT (2011) Neural mechanisms of the cognitive model of depression. *Nature Reviews Neuroscience* **12:** 467-477

Dong H-M, Zhang X-H, Labache L, Zhang S, Ooi LQR, Yeo BTT, Margulies DS, Holmes AJ, Zuo X-N (2024) Ventral attention network connectivity is linked to cortical maturation and cognitive ability in childhood. *Nat Neurosci*

Dowlati Y, Herrmann N, Swardfager W, Liu H, Sham L, Reim EK, Lanctôt KL (2010) A Meta-Analysis of Cytokines in Major Depression. *Biol Psychiatry* **67:** 446-457

Drexhage RC, Hoogenboezem TH, Versnel MA, Berghout A, Nolen WA, Drexhage HA (2011) The activation of monocyte and T cell networks in patients with bipolar disorder. *Brain Behav Immun* **25:** 1206-1213

Drysdale AT, Grosenick L, Downar J, Dunlop K, Mansouri F, Meng Y, Fetcho RN, Zebley B, Oathes DJ, Etkin A (2017) Resting-state connectivity biomarkers define neurophysiological subtypes of depression. *Nat Med* **23:** 28-38

Dulawa SC, Janowsky DS (2019) Cholinergic regulation of mood: from basic and clinical studies to emerging therapeutics. *Mol Psychiatry* **24:** 694-709

Duman RS, Li N (2012) A neurotrophic hypothesis of depression: role of synaptogenesis in the actions of NMDA receptor antagonists. *Philosophical Transactions of the Royal Society B: Biological Sciences* **367:** 2475-2484

Duncan LE, Keller MC (2011) A critical review of the first 10 years of candidate gene-by-environment interaction research in psychiatry. *Am J Psychiatry* **168:** 1041-1049

Dunlop BW, Nemeroff CB (2007) The role of dopamine in the pathophysiology of depression. *Arch Gen Psychiatry* **64:** 327-337

Dwyer DB, Falkai P, Koutsouleris N (2018) Machine Learning Approaches for Clinical Psychology and Psychiatry. *Annu Rev Clin Psychol* **14:** 91-118

Erus G, Battapady H, Satterthwaite TD, Hakonarson H, Gur RE, Davatzikos C, Gur RC (2015) Imaging patterns of brain development and their relationship to cognition. *Cereb Cortex* **25:** 1676-1684

Eshaghzadeh Torbati M, Minhas DS, Ahmad G, O'Connor EE, Muschelli J, Laymon CM, Yang Z, Cohen AD, Aizenstein HJ, Klunk WE, Christian BT, Hwang SJ, Crainiceanu CM, Tudorascu DL (2021) A multi-scanner neuroimaging data harmonization using RAVEL and ComBat. *Neuroimage* **245:** 118703

Fan L, Li H, Zhuo J, Zhang Y, Wang J, Chen L, Yang Z, Chu C, Xie S, Laird AR (2016) The human brainnetome atlas: a new brain atlas based on connectional architecture. *Cereb Cortex* **26:** 3508-3526

Favre P, Pauling M, Stout J, Hozer F, Sarrazin S, Abé C, Alda M, Alloza C, Alonso-Lana S, Andreassen OA (2019) Widespread white matter microstructural abnormalities in bipolar disorder: evidence from mega-and meta-analyses across 3033 individuals. *Neuropsychopharmacology* **44:** 2285-2293

Feczko E, Fair DA (2020) Methods and Challenges for Assessing Heterogeneity. *Biol Psychiatry* **88:** 9-17

Feczko E, Miranda-Dominguez O, Marr M, Graham AM, Nigg JT, Fair DA (2019) The heterogeneity problem: Approaches to identify psychiatric subtypes. *TiCS* **23:** 584-601

Felger JC, Miller AH (2020) Identifying Immunophenotypes of Inflammation in Depression: Dismantling the Monolith. *Biol Psychiatry* **88:** 136-138

Felitti VJ, Anda RF, Nordenberg D, Williamson DF, Spitz AM, Edwards V, Koss MP, Marks JS (1998) Relationship of childhood abuse and household dysfunction to many of the leading causes of death in adults. The Adverse Childhood Experiences (ACE) Study. *Am J Prev Med* **14:** 245-258

Fennell MJ, Campbell EA (1984) The Cognitions Questionnaire: Specific thinking errors in depression. *Br J Clin Psychol* **23:** 81-92

Fernandes BS, Williams LM, Steiner J, Leboyer M, Carvalho AF, Berk M (2017) The new field of 'precision psychiatry'. *BMC Med* **15:** 80

Figley CR, Uddin MN, Wong K, Kornelsen J, Puig J, Figley TD (2022) Potential Pitfalls of Using Fractional Anisotropy, Axial Diffusivity, and Radial Diffusivity as Biomarkers of Cerebral White Matter Microstructure. *Front Neurosci* **15**

Flint J (2023) The genetic basis of major depressive disorder. *Mol Psychiatry* **28:** 2254-2265

Fortin J-P, Cullen N, Sheline YI, Taylor WD, Aselcioglu I, Cook PA, Adams P, Cooper C, Fava M, McGrath PJ (2018) Harmonization of cortical thickness measurements across scanners and sites. *Neuroimage* **167:** 104-120

Fortin J-P, Parker D, Tunç B, Watanabe T, Elliott MA, Ruparel K, Roalf DR, Satterthwaite TD, Gur RC, Gur RE, Schultz RT, Verma R, Shinohara RT (2017) Harmonization of multi-site diffusion tensor imaging data. *Neuroimage* **161:** 149-170

Friedman J, Hastie T, Tibshirani R (2001) *The elements of statistical learning*, Vol. 1: Springer series in statistics New York.

Frodl T, Skokauskas N, Frey EM, Morris D, Gill M, Carballedo A (2014) BDNF Val66Met genotype interacts with childhood adversity and influences the formation of hippocampal subfields. *Hum Brain Mapp* **35:** 5776-5783

Furlan R, Melloni E, Finardi A, Vai B, Di Toro S, Aggio V, Battistini L, Borsellino G, Manfredi E, Falini A, Colombo C, Poletti S, Benedetti F (2019) Natural killer cells protect white matter integrity in bipolar disorder. *Brain Behav Immun* **81:** 410-421

Gamble B, Moreau D, Tippett LJ, Addis DR (2019) Specificity of Future Thinking in Depression: A Meta-Analysis. *Perspect Psychol Sci* **14:** 816-834

Gaser C, Dahnke R (2016) CAT-a computational anatomy toolbox for the analysis of structural MRI data. *Hbm* **2016:** 336-348

GBD Mental Disorders Collaborators (2022) Global, regional, and national burden of 12 mental disorders in 204 countries and territories, 1990–2019: a systematic analysis for the Global Burden of Disease Study 2019. *The Lancet Psychiatry* **9:** 137-150

Geoffroy PA, Hoertel N, Etain B, Bellivier F, Delorme R, Limosin F, Peyre H (2018) Insomnia and hypersomnia in major depressive episode: Prevalence, sociodemographic characteristics and psychiatric comorbidity in a population-based study. *J Affect Disord* **226:** 132-141

Gerritsen L, Tendolkar I, Franke B, Vasquez AA, Kooijman S, Buitelaar J, Fernández G, Rijpkema M (2012) BDNF Val66Met genotype modulates the effect of childhood

adversity on subgenual anterior cingulate cortex volume in healthy subjects. *Mol Psychiatry* **17:** 597-603

Ghane M, Sullivan-Toole H, DelGiacco AC, Richey JA (2021) Subjective arousal and perceived control clarify heterogeneity in inflammatory and affective outcomes. *Brain, Behavior, & Immunity - Health* **18:** 100341

Ghazanfari F, Rezaei M, Rezaei F (2018) The mediating role of repetitive negative thinking and experiential avoidance on the relationship between childhood trauma and depression. *Arch Psychiatr Nurs* **32:** 432-438

Gianaros PJ, Marsland AL, Sheu LK, Erickson KI, Verstynen TD (2013) Inflammatory pathways link socioeconomic inequalities to white matter architecture. *Cereb Cortex* **23:** 2058-2071

Gilbert JR, Wusinich C, Zarate Jr CA (2022) A predictive coding framework for understanding major depression. *Front Hum Neurosci*

Gleeson M, Bishop NC, Stensel DJ, Lindley MR, Mastana SS, Nimmo MA (2011) The anti-inflammatory effects of exercise: mechanisms and implications for the prevention and treatment of disease. *Nature Reviews Immunology* **11:** 607-615

Glover GH (2011) Overview of functional magnetic resonance imaging. *Neurosurgery Clinics* **22:** 133-139

Gonda X, Pompili M, Serafini G, Montebovi F, Campi S, Dome P, Duleba T, Girardi P, Rihmer Z (2012) Suicidal behavior in bipolar disorder: epidemiology, characteristics and major risk factors. *J Affect Disord* **143:** 16-26

Goodwin F, Jamison K (1990) Manic-depressive illness. Oxford University Press. *New York* **567**

Gordovez FJA, McMahon FJ (2020) The genetics of bipolar disorder. *Mol Psychiatry* **25:** 544-559

Gratten J, Wray NR, Keller MC, Visscher PM (2014) Large-scale genomics unveils the genetic architecture of psychiatric disorders. *Nat Neurosci* **17:** 782-790

Greicius MD, Krasnow B, Reiss AL, Menon V (2003) Functional connectivity in the resting brain: a network analysis of the default mode hypothesis. *Proceedings of the national academy of sciences* **100:** 253-258

Grosse L, Carvalho LA, Birkenhager TK, Hoogendijk WJ, Kushner SA, Drexhage HA, Bergink V (2016a) Circulating cytotoxic T cells and natural killer cells as potential predictors for antidepressant response in melancholic depression. Restoration of T regulatory cell populations after antidepressant therapy. *Psychopharmacology (Berl)* **233:** 1679-1688

Grosse L, Hoogenboezem T, Ambrée O, Bellingrath S, Jörgens S, de Wit HJ, Wijkhuijs AM, Arolt V, Drexhage HA (2016b) Deficiencies of the T and natural killer cell system in major depressive disorder: T regulatory cell defects are associated with inflammatory monocyte activation. *Brain Behav Immun* **54:** 38-44

Haapakoski R, Mathieu J, Ebmeier KP, Alenius H, Kivimäki M (2015) Cumulative meta-analysis of interleukins 6 and 1β, tumour necrosis factor α and C-reactive protein in patients with major depressive disorder. *Brain Behav Immun* **49:** 206-215

Hamilton M (1986) The Hamilton rating scale for depression. In *Assessment of depression*, pp 143-152. Springer

Han LK, Dinga R, Hahn T, Ching CR, Eyler LT, Aftanas L, Aghajani M, Aleman A, Baune BT, Berger K (2021) Brain aging in major depressive disorder: results from the ENIGMA major depressive disorder working group. *Mol Psychiatry* **26:** 5124-5139

Hansen JY, Shafiei G, Vogel JW, Smart K, Bearden CE, Hoogman M, Franke B, van Rooij D, Buitelaar J, McDonald CR, Sisodiya SM, Schmaal L, Veltman DJ, van den Heuvel OA, Stein DJ, van Erp TGM, Ching CRK, Andreassen OA, Hajek T, Opel N, Modinos G, Aleman A, van der Werf Y, Jahanshad N, Thomopoulos SI, Thompson PM, Carson RE, Dagher A, Misic B (2022) Local molecular and global connectomic contributions to cross-disorder cortical abnormalities. *Nature communications* **13:** 4682

Hayes AF (2012) PROCESS : A Versatile Computational Tool for Observed Variable Mediation , Moderation , and Conditional Process Modeling 1.

Herrman H, Patel V, Kieling C, Berk M, Buchweitz C, Cuijpers P, Furukawa TA, Kessler RC, Kohrt BA, Maj M (2022) Time for united action on depression: a Lancet–World Psychiatric Association Commission. *The Lancet* **399:** 957-1022

Hibar D, Westlye LT, Doan NT, Jahanshad N, Cheung J, Ching CR, Versace A, Bilderbeck A, Uhlmann A, Mwangi B (2018) Cortical abnormalities in bipolar disorder: an MRI analysis of 6503 individuals from the ENIGMA Bipolar Disorder Working Group. *Mol Psychiatry* **23:** 932-942

Ho TC, Gutman B, Pozzi E, Grabe HJ, Hosten N, Wittfeld K, Völzke H, Baune B, Dannlowski U, Förster K, Grotegerd D, Redlich R, Jansen A, Kircher T, Krug A, Meinert S, Nenadic I, Opel N, Dinga R, Veltman DJ, Schnell K, Veer I, Walter H, Gotlib IH, Sacchet MD, Aleman A, Groenewold NA, Stein DJ, Li M, Walter M, Ching CRK, Jahanshad N, Ragothaman A, Isaev D, Zavaliangos-Petropulu A, Thompson PM, Sämann PG, Schmaal L (2022) Subcortical shape alterations in major depressive disorder: Findings from the ENIGMA major depressive disorder working group. *Hum Brain Mapp* **43:** 341-351

Hoffmann F, Viding E, Puetz VB, Gerin MI, Sethi A, Rankin G, McCrory EJ (2018) Evidence for Depressogenic Spontaneous Thoughts and Altered Resting-State Connectivity in Adolescents With a Maltreatment History. *J Am Acad Child Adolesc Psychiatry* **57:** 687-695.e684

Horsfield MA (1999) Mapping eddy current induced fields for the correction of diffusion-weighted echo planar images. *Magn Reson Imaging* **17:** 1335-1345

Howell BR, McCormack KM, Grand AP, Sawyer NT, Zhang X, Maestripieri D, Hu X, Sanchez MM (2013) Brain white matter microstructure alterations in adolescent rhesus monkeys exposed to early life stress: associations with high cortisol during infancy. *Biology of mood & anxiety disorders* **3:** 1-14

Huang H, Liu Y, Yuan M, Marron J (2015) Statistical significance of clustering using soft thresholding. *Journal of Computational and Graphical Statistics* **24:** 975-993

Huys QJ, Maia TV, Frank MJ (2016) Computational psychiatry as a bridge from neuroscience to clinical applications. *Nat Neurosci* **19:** 404-413

Ino H, Honda S, Yamada K, Horita N, Tsugawa S, Yoshida K, Noda Y, Meyer JH, Mimura M, Nakajima S, Moriguchi S (2023) Glutamatergic Neurometabolite Levels in Bipolar Disorder: A Systematic Review and Meta-analysis of Proton Magnetic Resonance Spectroscopy Studies. *Biological psychiatry Cognitive neuroscience and neuroimaging* **8:** 140-150

Insel TR (2014) The NIMH Research Domain Criteria (RDoC) Project: precision medicine for psychiatry. *Am J Psychiatry* **171:** 395-397

James G, Witten D, Hastie T, Tibshirani R, Taylor J (2023) *An introduction to statistical learning: With applications in python*: Springer Nature.

Javaheripour N, Li M, Chand T, Krug A, Kircher T, Dannlowski U, Nenadić I, Hamilton JP, Sacchet MD, Gotlib IH (2021) Altered resting-state functional connectome in major

depressive disorder: a mega-analysis from the PsyMRI consortium. *Transl Psychiatry* **11:** 511

Johnson WE, Li C, Rabinovic A (2007) Adjusting batch effects in microarray expression data using empirical Bayes methods. *Biostatistics* **8:** 118-127

Kägi D, Ledermann B, Bürki K, Seiler P, Odermatt B, Olsen KJ, Podack ER, Zinkernagel RM, Hengartner H (1994) Cytotoxicity mediated by T cells and natural killer cells is greatly impaired in perforin-deficient mice. *Nature* **369:** 31-37

Kaiser RH, Andrews-Hanna JR, Wager TD, Pizzagalli DA (2015) Large-scale network dysfunction in major depressive disorder: a meta-analysis of resting-state functional connectivity. *JAMA psychiatry* **72:** 603-611

Kang HJ, Voleti B, Hajszan T, Rajkowska G, Stockmeier CA, Licznerski P, Lepack A, Majik MS, Jeong LS, Banasr M, Son H, Duman RS (2012) Decreased expression of synapse-related genes and loss of synapses in major depressive disorder. *Nat Med* **18:** 1413-1417

Kappelmann N, Lewis G, Dantzer R, Jones PB, Khandaker GM (2018) Antidepressant activity of anti-cytokine treatment: a systematic review and meta-analysis of clinical trials of chronic inflammatory conditions. *Mol Psychiatry* **23:** 335-343

Karam EG, Saab D, Jabbour S, Karam GE, Hantouche E, Angst J (2023) The role of affective temperaments in bipolar disorder: the solid role of the cyclothymic, the contentious role of the hyperthymic, and the neglected role of the irritable temperaments. *Eur Psychiatry* **66:** e37

Karg K, Burmeister M, Shedden K, Sen S (2011) The serotonin transporter promoter variant (5-HTTLPR), stress, and depression meta-analysis revisited: evidence of genetic moderation. *Arch Gen Psychiatry* **68:** 444-454

Kebets V, Favre P, Houenou J, Polosan M, Perroud N, Aubry JM, Van De Ville D (2021) Fronto-limbic neural variability as a transdiagnostic correlate of emotion dysregulation. **11:** 545

Kebets V, Holmes AJ, Orban C, Tang S, Li J, Sun N, Kong R, Poldrack RA, Yeo BTT (2019) Somatosensory-Motor Dysconnectivity Spans Multiple Transdiagnostic Dimensions of Psychopathology. *Biol Psychiatry* **86:** 779-791

Knill DC, Pouget A (2004) The Bayesian brain: the role of uncertainty in neural coding and computation. *Trends Neurosci* **27:** 712-719

Köhler CA, Freitas TH, Maes Md, De Andrade N, Liu CS, Fernandes BS, Stubbs B, Solmi M, Veronese N, Herrmann N (2017) Peripheral cytokine and chemokine alterations in depression: a meta-analysis of 82 studies. *Acta Psychiatr Scand* **135:** 373-387

Korn T, Bettelli E, Oukka M, Kuchroo VK (2009) IL-17 and Th17 Cells. *Annu Rev Immunol* **27:** 485-517

Koshiyama D, Fukunaga M, Okada N, Morita K, Nemoto K, Usui K, Yamamori H, Yasuda Y, Fujimoto M, Kudo N, Azechi H, Watanabe Y, Hashimoto N, Narita H, Kusumi I, Ohi K, Shimada T, Kataoka Y, Yamamoto M, Ozaki N, Okada G, Okamoto Y, Harada K, Matsuo K, Yamasue H, Abe O, Hashimoto R, Takahashi T, Hori T, Nakataki M, Onitsuka T, Holleran L, Jahanshad N, van Erp TGM, Turner J, Donohoe G, Thompson PM, Kasai K, Hashimoto R, Cocoro (2020) White matter microstructural alterations across four major psychiatric disorders: mega-analysis study in 2937 individuals. *Mol Psychiatry* **25:** 883-895

Kotov R, Krueger RF, Watson D, Achenbach TM, Althoff RR, Bagby RM, Brown TA, Carpenter WT, Caspi A, Clark LA, Eaton NR, Forbes MK (2017) The Hierarchical Taxonomy of Psychopathology (HiTOP): A dimensional alternative to traditional nosologies. **126:** 454-477

Koutsouleris N, Davatzikos C, Borgwardt S, Gaser C, Bottlender R, Frodl T, Falkai P, Riecher-Rössler A, Möller H-J, Reiser M (2014) Accelerated brain aging in schizophrenia and beyond: a neuroanatomical marker of psychiatric disorders. *Schizophr Bull* **40:** 1140-1153

Krishnan A, Williams LJ, McIntosh AR, Abdi H (2011) Partial Least Squares (PLS) methods for neuroimaging: A tutorial and review. *Neuroimage* **56:** 455-475

Kronenberg G, van Elst LT, Regen F, Deuschle M, Heuser I, Colla M (2009) Reduced amygdala volume in newly admitted psychiatric in-patients with unipolar major depression. *J Psychiatr Res* **43:** 1112-1117

Kube T, Schwarting R, Rozenkrantz L, Glombiewski JA, Rief W (2020) Distorted cognitive processes in major depression: a predictive processing perspective. *Biol Psychiatry* **87:** 388-398

Kumar A, Daumé H (2011) A co-training approach for multi-view spectral clustering. In *Proceedings of the 28th international conference on machine learning (ICML-11)*, pp 393-400.

Kumar P, Goer F, Murray L, Dillon DG, Beltzer ML, Cohen AL, Brooks NH, Pizzagalli DA (2018) Impaired reward prediction error encoding and striatal-midbrain connectivity in depression. *Neuropsychopharmacology* **43:** 1581-1588

Labuschagne I, Dominguez JF, Grace S, Mizzi S, Henry JD, Peters C, Rabinak CA, Sinclair E, Lorenzetti V, Terrett G (2024) Specialization of amygdala subregions in emotion processing. *Hum Brain Mapp* **45:** e26673

Lamers F, Vogelzangs N, Merikangas K, De Jonge P, Beekman A, Penninx B (2013) Evidence for a differential role of HPA-axis function, inflammation and metabolic syndrome in melancholic versus atypical depression. *Mol Psychiatry* **18:** 692-699

Landi I, Mandelli V, Lombardo MV (2021) reval: A Python package to determine best clustering solutions with stability-based relative clustering validation. *Patterns* **2:** 100228

Lange T, Roth V, Braun ML, Buhmann JM (2004) Stability-based validation of clustering solutions. *Neural Comput* **16:** 1299-1323

Lee T-W, Xue S-W (2017) Linking graph features of anatomical architecture to regional brain activity: A multi-modal MRI study. *Neurosci Lett* **651:** 123-127

Leek JT, Scharpf RB, Bravo HC, Simcha D, Langmead B, Johnson WE, Geman D, Baggerly K, Irizarry RA (2010) Tackling the widespread and critical impact of batch effects in high-throughput data. *Nature Reviews Genetics* **11:** 733-739

Leow A, Ajilore O, Zhan L, Arienzo D, GadElkarim J, Zhang A, Moody T, Van Horn J, Feusner J, Kumar A (2013) Impaired inter-hemispheric integration in bipolar disorder revealed with brain network analyses. *Biol Psychiatry* **73:** 183-193

Levey DF, Stein MB, Wendt FR, Pathak GA, Zhou H, Aslan M, Quaden R, Harrington KM, Nuñez YZ, Overstreet C (2021) Bi-ancestral depression GWAS in the Million Veteran Program and meta-analysis in> 1.2 million individuals highlight new therapeutic directions. *Nat Neurosci* **24:** 954-963

Levinson DF, Mostafavi S, Milaneschi Y, Rivera M, Ripke S, Wray NR, Sullivan PF (2014) Genetic studies of major depressive disorder: why are there no genome-wide association study findings and what can we do about it? *Biol Psychiatry* **76:** 510-512

Liang S, Deng W, Li X, Greenshaw AJ, Wang Q, Li M, Ma X, Bai T-J, Bo Q-J, Cao J (2020) Biotypes of major depressive disorder: neuroimaging evidence from resting-state default mode network patterns. *NeuroImage: Clinical* **28:** 102514

Liang S, Wang Q, Kong X, Deng W, Yang X, Li X, Zhang Z, Zhang J, Zhang C, Li X-m, Ma X, Shao J, Greenshaw AJ, Li T (2019) White Matter Abnormalities in Major Depression Biotypes Identified by Diffusion Tensor Imaging. *Neurosci Bull* **35:** 867-876

Liao Y, Huang X, Wu Q, Yang C, Kuang W, Du M, Lui S, Yue Q, Chan RC, Kemp GJ (2013) Is depression a disconnection syndrome? Meta-analysis of diffusion tensor imaging studies in patients with MDD. *J Psychiatry Neurosci* **38:** 49-56

Long X, Wang X, Tian F, Cao Y, Xie H, Jia Z (2022) Altered brain activation during reward anticipation in bipolar disorder. *Transl Psychiatry* **12:** 1-10

Lorenzetti V, Allen NB, Whittle S, Yücel M (2010) Amygdala volumes in a sample of current depressed and remitted depressed patients and healthy controls. *J Affect Disord* **120:** 112-119

Lotter LD, Saberi A (2024) Regional patterns of human cortex development correlate with underlying neurobiology. **15:** 7987

Lu F, Yang W, Wei D, Sun J, Zhang Q, Qiu J (2022) Superior frontal gyrus and middle temporal gyrus connectivity mediates the relationship between neuroticism and thought suppression. **16:** 1400-1409

Luan S, Zhou B, Wu Q, Wan H, Li H (2020) Brain-derived neurotrophic factor blood levels after electroconvulsive therapy in patients with major depressive disorder: a systematic review and meta-analysis. *Asian J Psychiatr* **51:** 101983

Luo AC, Sydnor VJ, Pines A, Larsen B, Alexander-Bloch AF, Cieslak M, Covitz S, Chen AA, Esper NB, Feczko E, Franco AR, Gur RE, Gur RC, Houghton A, Hu F, Keller AS, Kiar G, Mehta K, Salum GA, Tapera T, Xu T, Zhao C, Salo T, Fair DA, Shinohara RT, Milham MP, Satterthwaite TD (2024) Functional connectivity development along the sensorimotor-association axis enhances the cortical hierarchy. *Nature communications* **15:** 3511

Lynall M-E, Turner L, Bhatti J, Cavanagh J, de Boer P, Mondelli V, Jones D, Drevets WC, Cowen P, Harrison NA (2020) Peripheral blood cell–stratified subgroups of inflamed depression. *Biol Psychiatry* **88:** 185-196

Lynch CJ, Gunning FM, Liston C (2020) Causes and Consequences of Diagnostic Heterogeneity in Depression: Paths to Discovering Novel Biological Depression Subtypes. *Biol Psychiatry* **88:** 83-94

Maes M, Carvalho AF (2018) The Compensatory Immune-Regulatory Reflex System (CIRS) in Depression and Bipolar Disorder. *Mol Neurobiol* **55:** 8885-8903

Maes M, Nani JV, Noto C, Rizzo L, Hayashi MAF, Brietzke E (2021) Impairments in Peripheral Blood T Effector and T Regulatory Lymphocytes in Bipolar Disorder Are Associated with Staging of Illness and Anti-cytomegalovirus IgG Levels. *Mol Neurobiol* **58:** 229-242

Maes M, Rachayon M, Jirakran K, Sodsai P, Klinchanhom S, Debnath M (2022a) Adverse Childhood Experiences Predict the Phenome of Affective Disorders and These Effects Are Mediated by Staging, Neuroimmunotoxic and Growth Factor Profiles. **11**

Maes M, Rachayon M, Jirakran K, Sodsai P, Klinchanhom S, Gałecki P (2022b) The Immune Profile of Major Dysmood Disorder: Proof of Concept and Mechanism Using the Precision Nomothetic Psychiatry Approach. **11**

Malave L, van Dijk MT, Anacker C (2022) Early life adversity shapes neural circuit function during sensitive postnatal developmental periods. **12:** 306

Malhi GS, Mann JJ (2018) Depression. *Lancet* **392:** 2299-2312

Mansueto G, Cavallo C (2021) Adverse childhood experiences and repetitive negative thinking in adulthood: A systematic review. **28:** 557-568

Marquand AF, Wolfers T, Mennes M, Buitelaar J, Beckmann CF (2016) Beyond lumping and splitting: a review of computational approaches for stratifying psychiatric disorders. *Biological Psychiatry: Cognitive Neuroscience and Neuroimaging* **1:** 433-447

Martino DJ, Samamé C, Marengo E, Igoa A, Strejilevich SA (2016) A critical overview of the clinical evidence supporting the concept of neuroprogression in bipolar disorder. *Psychiatry Res* **235:** 1-6

Marx W, Penninx BW, Solmi M, Furukawa TA, Firth J, Carvalho AF, Berk M (2023) Major depressive disorder. *Nature Reviews Disease Primers* **9:** 44

Mayberg HS (1997) Limbic-cortical dysregulation: a proposed model of depression. *The Journal of neuropsychiatry and clinical neurosciences* **9:** 471-481

McEwen BS, Bowles NP, Gray JD, Hill MN, Hunter RG, Karatsoreos IN, Nasca C (2015) Mechanisms of stress in the brain. *Nat Neurosci* **18:** 1353-1363

McGrath JJ, Al-Hamzawi A, Alonso J, Altwaijri Y, Andrade LH, Bromet EJ, Bruffaerts R, de Almeida JMC, Chardoul S, Chiu WT (2023) Age of onset and cumulative risk of mental disorders: a cross-national analysis of population surveys from 29 countries. *The Lancet Psychiatry* **10:** 668-681

McIntyre RS, Alsuwaidan M, Baune BT, Berk M, Demyttenaere K, Goldberg JF, Gorwood P, Ho R, Kasper S, Kennedy SH (2023) Treatment-resistant depression: definition, prevalence, detection, management, and investigational interventions. *World Psychiatry* **22:** 394-412

McIntyre RS, Berk M, Brietzke E, Goldstein BI, López-Jaramillo C, Kessing LV, Malhi GS, Nierenberg AA, Rosenblat JD, Majeed A (2020) Bipolar disorders. *The Lancet* **396:** 1841-1856

Menon V (2011) Large-scale brain networks and psychopathology: a unifying triple network model. *TiCS* **15:** 483-506

Merikangas KR, Akiskal HS, Angst J, Greenberg PE, Hirschfeld RM, Petukhova M, Kessler RC (2007) Lifetime and 12-month prevalence of bipolar spectrum disorder in the National Comorbidity Survey replication. *Arch Gen Psychiatry* **64:** 543-552

Mesbah R, Koenders MA, van der Wee NJ, Giltay EJ, van Hemert AM, de Leeuw M (2023) Association between the fronto-limbic network and cognitive and emotional functioning in individuals with bipolar disorder: a systematic review and meta-analysis. *JAMA psychiatry*

Meyer-Lindenberg A, Weinberger DR (2006) Intermediate phenotypes and genetic mechanisms of psychiatric disorders. *Nature reviews neuroscience* **7:** 818-827

Michelini G, Palumbo IM, DeYoung CG, Latzman RD, Kotov R (2021) Linking RDoC and HiTOP: A new interface for advancing psychiatric nosology and neuroscience. *Clin Psychol Rev* **86:** 102025

Mihalik A, Chapman J, Adams RA, Winter NR, Ferreira FS, Shawe-Taylor J, Mourão-Miranda J (2022) Canonical Correlation Analysis and Partial Least Squares for Identifying Brain-Behavior Associations: A Tutorial and a Comparative Study. *Biological psychiatry Cognitive neuroscience and neuroimaging* **7:** 1055-1067

Mihalik A, Ferreira FS (2019) Brain-behaviour modes of covariation in healthy and clinically depressed young people. **9:** 11536

Miller AH, Haroon E, Raison CL, Felger JC (2013) Cytokine targets in the brain: impact on neurotransmitters and neurocircuits. *Depress Anxiety* **30:** 297-306

Miller AH, Raison CL (2016) The role of inflammation in depression: from evolutionary imperative to modern treatment target. *Nature reviews immunology* **16:** 22-34

Misiak B, Stramecki F, Gawęda Ł, Prochwicz K, Sąsiadek MM, Moustafa AA, Frydecka D (2018) Interactions between variation in candidate genes and environmental factors in the etiology of schizophrenia and bipolar disorder: a systematic review. *Mol Neurobiol* **55:** 5075-5100

Modabbernia A, Taslimi S, Brietzke E, Ashrafi M (2013) Cytokine alterations in bipolar disorder: a meta-analysis of 30 studies. *Biol Psychiatry* **74:** 15-25

Moffitt TE, Caspi A, Taylor A, Kokaua J, Milne BJ, Polanczyk G, Poulton R (2010) How common are common mental disorders? Evidence that lifetime prevalence rates are doubled by prospective versus retrospective ascertainment. *Psychol Med* **40:** 899-909

Mori S, Oishi K, Jiang H, Jiang L, Li X, Akhter K, Hua K, Faria AV, Mahmood A, Woods R (2008) Stereotaxic white matter atlas based on diffusion tensor imaging in an ICBM template. *Neuroimage* **40:** 570-582

Moriguchi S, Takamiya A, Noda Y, Horita N, Wada M, Tsugawa S, Plitman E, Sano Y, Tarumi R, ElSalhy M, Katayama N, Ogyu K, Miyazaki T, Kishimoto T, Graff-Guerrero A, Meyer JH, Blumberger DM, Daskalakis ZJ, Mimura M, Nakajima S (2019) Glutamatergic neurometabolite levels in major depressive disorder: a systematic review and meta-analysis of proton magnetic resonance spectroscopy studies. *Mol Psychiatry* **24:** 952-964

Müller VI, Cieslik EC, Serbanescu I, Laird AR, Fox PT, Eickhoff SB (2017) Altered brain activity in unipolar depression revisited: meta-analyses of neuroimaging studies. *JAMA psychiatry* **74:** 47-55

Mullins N, Forstner AJ, O'Connell KS, Coombes B, Coleman JR, Qiao Z, Als TD, Bigdeli TB, Børte S, Bryois J (2021) Genome-wide association study of more than 40,000 bipolar disorder cases provides new insights into the underlying biology. *Nat Genet* **53:** 817-829

Muschelli J, Nebel MB, Caffo BS, Barber AD, Pekar JJ, Mostofsky SH (2014) Reduction of motion-related artifacts in resting state fMRI using aCompCor. *Neuroimage* **96:** 22-35

Nabulsi L, McPhilemy G, O'Donoghue S, Cannon DM, Kilmartin L, O'Hora D, Sarrazin S, Poupon C, D'Albis M-A, Versace A (2022) Aberrant subnetwork and hub

dysconnectivity in adult bipolar disorder: A multicenter graph theory analysis. *Cereb Cortex* **32:** 2254-2264

Nanni V, Uher R, Danese A (2012) Childhood maltreatment predicts unfavorable course of illness and treatment outcome in depression: a meta-analysis. *Am J Psychiatry* **169:** 141-151

Nemeroff CB, Heim CM, Thase ME, Klein DN, Rush AJ, Schatzberg AF, Ninan PT, McCullough JP, Jr., Weiss PM, Dunner DL, Rothbaum BO, Kornstein S, Keitner G, Keller MB (2003) Differential responses to psychotherapy versus pharmacotherapy in patients with chronic forms of major depression and childhood trauma. *Proc Natl Acad Sci U S A* **100:** 14293-14296

Nguyen T-D, Harder A, Xiong Y, Kowalec K, Hägg S, Cai N, Kuja-Halkola R, Dalman C, Sullivan PF, Lu Y (2022) Genetic heterogeneity and subtypes of major depression. *Mol Psychiatry* **27:** 1667-1675

Niebling J, A ER, Schallenberg S, Kretschmer K, Kempermann G (2014) Myelin-specific T helper 17 cells promote adult hippocampal neurogenesis through indirect mechanisms. *F1000Research* **3:** 169

Niemegeers P, De Boer P, Schuermans J, Dumont GJ, Coppens V, Spittaels K, Claes S, Sabbe BG, Morrens M (2019) Digging deeper in the differential effects of inflammatory and psychosocial stressors in remitted depression: effects on cognitive functioning. *J Affect Disord* **245:** 356-363

Nortje G, Stein DJ, Radua J, Mataix-Cols D, Horn N (2013) Systematic review and voxel-based meta-analysis of diffusion tensor imaging studies in bipolar disorder. *J Affect Disord* **150:** 192-200

Nusslock R, Alloy LB (2017) Reward processing and mood-related symptoms: An RDoC and translational neuroscience perspective. *J Affect Disord* **216:** 3-16

Nusslock R, Miller GE (2016) Early-life adversity and physical and emotional health across the lifespan: A neuroimmune network hypothesis. *Biol Psychiatry* **80:** 23-32

Onyeka IN, Collier Høegh M, Nåheim Eien EM, Nwaru BI, Melle I (2019) Comorbidity of physical disorders among patients with severe mental illness with and without substance use disorders: a systematic review and meta-analysis. *Journal of dual diagnosis* **15:** 192-206

Osimo EF, Baxter LJ, Lewis G, Jones PB, Khandaker GM (2019) Prevalence of low-grade inflammation in depression: a systematic review and meta-analysis of CRP levels. *Psychol Med* **49:** 1958-1970

Ozkan BN, Bozali K, Boylu ME, Velioglu HA, Aktas S, Kirpinar I, Guler EM (2024) Altered blood parameters in "major depression" patients receiving repetitive transcranial magnetic stimulation (rTMS) therapy: a randomized case-control study. *Transl Psychiatry* **14:** 264

Palmer DS, Howrigan DP, Chapman SB, Adolfsson R, Bass N, Blackwood D, Boks MP, Chen C-Y, Churchhouse C, Corvin AP (2022) Exome sequencing in bipolar disorder identifies AKAP11 as a risk gene shared with schizophrenia. *Nat Genet* **54:** 541-547

Park S, Haak KV, Oldham S, Cho H, Byeon K, Park B-y, Thomson P, Chen H, Gao W, Xu T, Valk S, Milham MP, Bernhardt B, Di Martino A, Hong S-J (2024) A shifting role of thalamocortical connectivity in the emergence of cortical functional organization. *Nat Neurosci* **27:** 1609-1619

Peng Y, Tao Y, Zhang Y, Wang J, Yang J, Wang Y (2023) CD25: A potential tumor therapeutic target. *Int J Cancer* **152:** 1290-1303

Perry R, Mischler G, Guo R, Lee T, Chang A, Koul A, Franz C, Richard H, Carmichael I, Ablin P (2021) mvlearn: Multiview machine learning in python. *Journal of Machine Learning Research* **22:** 1-7

Peterson RE, Cai N, Bigdeli TB, Li Y, Reimers M, Nikulova A, Webb BT, Bacanu S-A, Riley BP, Flint J (2017) The genetic architecture of major depressive disorder in Han Chinese women. *JAMA psychiatry* **74:** 162-168

Pfarr J-K, Meller T, Brosch K, Stein F, Thomas-Odenthal F, Evermann U, Wroblewski A, Ringwald KG, Hahn T, Meinert S, Winter A, Thiel K, Flinkenflügel K, Jansen A, Krug A, Dannlowski U, Kircher T, Gaser C, Nenadić I (2023) Data-driven multivariate identification of gyrification patterns in a transdiagnostic patient cohort: A cluster analysis approach. *Neuroimage* **281:** 120349

Phillips ML, Swartz HA (2014) A critical appraisal of neuroimaging studies of bipolar disorder: toward a new conceptualization of underlying neural circuitry and a road map for future research. *Am J Psychiatry* **171:** 829-843

Pilmeyer J, Huijbers W, Lamerichs R, Jansen JF, Breeuwer M, Zinger S (2022) Functional MRI in major depressive disorder: A review of findings, limitations, and future prospects. *J Neuroimaging* **32:** 582-595

Pitkänen A, Savander V, LeDoux JE (1997) Organization of intra-amygdaloid circuitries in the rat: an emerging framework for understanding functions of the amygdala. *Trends Neurosci* **20:** 517-523

Plana-Ripoll O, Pedersen CB, Agerbo E, Holtz Y, Erlangsen A, Canudas-Romo V, Andersen PK, Charlson FJ, Christensen MK, Erskine HE (2019) A comprehensive analysis of mortality-related health metrics associated with mental disorders: a nationwide, register-based cohort study. *The Lancet* **394:** 1827-1835

Poletti S, Colombo C, Benedetti F (2014) Adverse childhood experiences worsen cognitive distortion during adult bipolar depression. *Compr Psychiatry* **55:** 1803-1808

Poletti S, de Wit H, Mazza E, Wijkhuijs AJM, Locatelli C, Aggio V, Colombo C, Benedetti F, Drexhage HA (2017) Th17 cells correlate positively to the structural and functional integrity of the brain in bipolar depression and healthy controls. *Brain Behav Immun* **61:** 317-325

Poletti S, Mazza MG, Benedetti F (2024) Inflammatory mediators in major depression and bipolar disorder. *Transl Psychiatry* **14:** 247

Poletti S, Mazza MG, Calesella F, Vai B, Lorenzi C, Manfredi E, Colombo C, Zanardi R, Benedetti F (2021a) Circulating inflammatory markers impact cognitive functions in bipolar depression. *J Psychiatr Res* **140:** 110-116

Poletti S, Vai B, Mazza MG, Zanardi R, Lorenzi C, Calesella F, Cazzetta S, Branchi I, Colombo C, Furlan R (2021b) A peripheral inflammatory signature discriminates bipolar from unipolar depression: a machine learning approach. *Prog Neuropsychopharmacol Biol Psychiatry* **105:** 110136

Poole JC, Dobson KS, Pusch D (2017) Childhood adversity and adult depression: The protective role of psychological resilience. *Child Abuse Negl* **64:** 89-100

Prasad V, Fojo T, Brada M (2016) Precision oncology: origins, optimism, and potential. *Lancet Oncol* **17:** e81-e86

Price RB, Duman R (2020) Neuroplasticity in cognitive and psychological mechanisms of depression: an integrative model. *Mol Psychiatry* **25:** 530-543

Price RB, Gates K, Kraynak TE, Thase ME, Siegle GJ (2017a) Data-driven subgroups in depression derived from directed functional connectivity paths at rest. *Neuropsychopharmacology* **42:** 2623-2632

Price RB, Lane S, Gates K, Kraynak TE, Horner MS, Thase ME, Siegle GJ (2017b) Parsing Heterogeneity in the Brain Connectivity of Depressed and Healthy Adults During Positive Mood. *Biol Psychiatry* **81:** 347-357

Pruim RH, Mennes M, Buitelaar JK, Beckmann CF (2015a) Evaluation of ICA-AROMA and alternative strategies for motion artifact removal in resting state fMRI. *Neuroimage* **112:** 278-287

Pruim RH, Mennes M, van Rooij D, Llera A, Buitelaar JK, Beckmann CF (2015b) ICA-AROMA: A robust ICA-based strategy for removing motion artifacts from fMRI data. *Neuroimage* **112:** 267-277

Rachayon M, Jirakran K, Sodsai P, Sughondhabirom A, Maes M (2024) T cell activation and deficits in T regulatory cells are associated with major depressive disorder and severity of depression. *Sci Rep* **14:** 11177

Raichle ME, MacLeod AM, Snyder AZ, Powers WJ, Gusnard DA, Shulman GL (2001) A default mode of brain function. *Proceedings of the national academy of sciences* **98:** 676-682

Raison CL, Rutherford RE, Woolwine BJ, Shuo C, Schettler P, Drake DF, Haroon E, Miller AH (2013) A randomized controlled trial of the tumor necrosis factor antagonist infliximab for treatment-resistant depression: the role of baseline inflammatory biomarkers. *JAMA psychiatry* **70:** 31-41

Rakofsky J, Rapaport M (2018) Mood Disorders. *Continuum (Minneapolis, Minn)* **24:** 804-827

Repple J, Gruber M, Mauritz M, de Lange SC, Winter NR, Opel N, Goltermann J, Meinert S, Grotegerd D, Leehr EJ (2023) Shared and specific patterns of structural brain connectivity across affective and psychotic disorders. *Biol Psychiatry* **93:** 178-186

Repple J, Meinert S, Grotegerd D, Kugel H, Redlich R, Dohm K, Zaremba D, Opel N, Buerger C, Förster K (2017) A voxel-based diffusion tensor imaging study in unipolar and bipolar depression. *Bipolar disorders* **19:** 23-31

Rief W, Joormann J (2019) Revisiting the Cognitive Model of Depression: The Role of Expectations. *Clinical Psychology in Europe* **1**

Roberts G, Lenroot R, Overs B, Fullerton J, Leung V, Ridgway K, Stuart A, Frankland A, Levy F, Hadzi-Pavlovic D (2022) Accelerated cortical thinning and volume reduction

over time in young people at high genetic risk for bipolar disorder. *Psychol Med* **52:** 1344-1355

Roddy D, Kelly JR, Farrell C, Doolin K, Roman E, Nasa A, Frodl T, Harkin A, O'Mara S, O'Hanlon E (2021) Amygdala substructure volumes in major depressive disorder. *NeuroImage: Clinical* **31:** 102781

Roozendaal B, McEwen BS, Chattarji S (2009) Stress, memory and the amygdala. *Nature Reviews Neuroscience* **10:** 423-433

Rousseeuw PJ (1987) Silhouettes: A graphical aid to the interpretation and validation of cluster analysis. *Journal of Computational and Applied Mathematics* **20:** 53-65

Rowe AL, Perich T (2024) Bipolar disorder and cumulative trauma: A systematic review of prevalence and illness outcomes. **80:** 692-713

Russell G, Lightman S (2019) The human stress response. **15:** 525-534

Rutledge RB, Moutoussis M, Smittenaar P, Zeidman P, Taylor T, Hrynkiewicz L, Lam J, Skandali N, Siegel JZ, Ousdal OT (2017) Association of neural and emotional impacts of reward prediction errors with major depression. *JAMA psychiatry* **74:** 790-797

Sahle BW, Reavley NJ, Li W, Morgan AJ, Yap MBH, Reupert A, Jorm AF (2022) The association between adverse childhood experiences and common mental disorders and suicidality: an umbrella review of systematic reviews and meta-analyses. *Eur Child Adolesc Psychiatry* **31:** 1489-1499

Sanacora G, Yan Z (2022) The stressed synapse 2.0: pathophysiological mechanisms in stress-related neuropsychiatric disorders. **23:** 86-103

Sanislow CA, Ferrante M, Pacheco J, Rudorfer MV, Morris SE (2019) Advancing Translational Research Using NIMH Research Domain Criteria and Computational Methods. *Neuron* **101:** 779-782

Santarelli L, Saxe M, Gross C, Surget A, Battaglia F, Dulawa S, Weisstaub N, Lee J, Duman R, Arancio O (2003) Requirement of hippocampal neurogenesis for the behavioral effects of antidepressants. *Science* **301:** 805-809

Sapolsky RM, Krey LC, McEwen BS (1984) Glucocorticoid-sensitive hippocampal neurons are involved in terminating the adrenocortical stress response. *Proceedings of the National Academy of Sciences* **81:** 6174-6177

Sarrazin S, Poupon C, Linke J, Wessa M, Phillips M, Delavest M, Versace A, Almeida J, Guevara P, Duclap D (2014) A multicenter tractography study of deep white matter tracts in bipolar I disorder: psychotic features and interhemispheric disconnectivity. *JAMA psychiatry* **71:** 388-396

Schermuly I, Fellgiebel A, Wagner S, Yakushev I, Stoeter P, Schmitt R, Knickenberg RJ, Bleichner F, Beutel ME (2010) Association between cingulum bundle structure and cognitive performance: an observational study in major depression. *Eur Psychiatry* **25:** 355-360

Schmaal L, Hibar D, Sämann PG, Hall G, Baune B, Jahanshad N, Cheung J, Van Erp T, Bos D, Ikram MA (2017) Cortical abnormalities in adults and adolescents with major depression based on brain scans from 20 cohorts worldwide in the ENIGMA Major Depressive Disorder Working Group. *Mol Psychiatry* **22:** 900-909

Schmaal L, Veltman DJ, van Erp TG, Sämann P, Frodl T, Jahanshad N, Loehrer E, Tiemeier H, Hofman A, Niessen W (2016) Subcortical brain alterations in major depressive disorder: findings from the ENIGMA Major Depressive Disorder working group. *Mol Psychiatry* **21:** 806-812

Scolding NJ, Jones J, Compston DA, Morgan BP (1990) Oligodendrocyte susceptibility to injury by T-cell perforin. *Immunology* **70:** 6-10

Scott J, Graham A, Yung A, Morgan C, Bellivier F, Etain B (2022) A systematic review and meta-analysis of delayed help-seeking, delayed diagnosis and duration of untreated illness in bipolar disorders. *Acta Psychiatr Scand* **146:** 389-405

Scott KM, de Jonge P, Stein DJ, Kessler RC (2018) *Mental disorders around the world: Facts and figures from the WHO World Mental Health surveys*: Cambridge University Press.

Sforzini L, Marizzoni M, Bottanelli C (2024) Transcriptomic profiles in major depressive disorder: the role of immunometabolic and cell-cycle-related pathways in depression with different levels of inflammation.

Sharpley CF, Palanisamy SK, Glyde NS, Dillingham PW, Agnew LL (2014) An update on the interaction between the serotonin transporter promoter variant (5-HTTLPR), stress and depression, plus an exploration of non-confirming findings. *Behav Brain Res* **273:** 89-105

Skokauskas N, Carballedo A, Fagan A, Frodl T (2015) The role of sexual abuse on functional neuroimaging markers associated with major depressive disorder. *World J Biol Psychiatry* **16:** 513-520

Smith SM (2002) Fast robust automated brain extraction. *Hum Brain Mapp* **17:** 143-155

Smith SM, Jenkinson M, Johansen-Berg H, Rueckert D, Nichols TE, Mackay CE, Watkins KE, Ciccarelli O, Cader MZ, Matthews PM (2006) Tract-based spatial statistics: voxelwise analysis of multi-subject diffusion data. *Neuroimage* **31:** 1487-1505

Smith SM, Jenkinson M, Woolrich MW, Beckmann CF, Behrens TEJ, Johansen-Berg H, Bannister PR, De Luca M, Drobnjak I, Flitney DE, Niazy RK, Saunders J, Vickers J, Zhang Y, De Stefano N, Brady JM, Matthews PM (2004) Advances in functional and structural MR image analysis and implementation as FSL. *Neuroimage* **23:** S208-S219

Solmi M, Sharma MS, Osimo EF, Fornaro M, Bortolato B, Croatto G, Miola A, Vieta E, Pariante CM, Smith L (2021) Peripheral levels of C-reactive protein, tumor necrosis factor-α, interleukin-6, and interleukin-1β across the mood spectrum in bipolar disorder: a meta-analysis of mean differences and variability. *Brain Behav Immun* **97:** 193-203

Sørensen NV, Frandsen BH, Orlovska-Waast S, Buus TB, Ødum N, Christensen RH, Benros ME (2023) Immune cell composition in unipolar depression: a comprehensive systematic review and meta-analysis. *Mol Psychiatry* **28:** 391-401

Souama C, Lamers F, Milaneschi Y, Vinkers CH, Defina S, Garvert L, Stein F, Woofenden T, Brosch K, Dannlowski U, Galenkamp H, de Graaf R, Jaddoe VWV, Lok A, van Rijn BB, Völzke H, Cecil CAM, Felix JF, Grabe HJ, Kircher T, Lekadir K, Have MT, Walton E, Penninx B (2023) Depression, cardiometabolic disease, and their co-occurrence after childhood maltreatment: an individual participant data meta-analysis including over 200,000 participants. *BMC Med* **21:** 93

Squarcina L, Bellani M, Rossetti MG, Perlini C, Delvecchio G, Dusi N, Barillari M, Ruggeri M, Altamura CA, Bertoldo A (2017) Similar white matter changes in schizophrenia and bipolar disorder: A tract-based spatial statistics study. *PLoS One* **12:** e0178089

Sullivan PF, Neale MC, Kendler KS (2000) Genetic epidemiology of major depression: review and meta-analysis. *Am J Psychiatry* **157:** 1552-1562

Suneson K, Söderberg Veibäck G, Lindahl J, Tjernberg J, Ståhl D, Ventorp S, Ängeby F, Lundblad K, Wolkowitz OM, Lindqvist D (2024) Omega-3 fatty acids for inflamed depression – A match/mismatch study. *Brain Behav Immun* **118:** 192-201

Syan SK, Smith M, Frey BN, Remtulla R, Kapczinski F, Hall GB, Minuzzi L (2018) Resting-state functional connectivity in individuals with bipolar disorder during clinical remission: a systematic review. *J Psychiatry Neurosci* **43:** 298-316

Teicher MH, Samson JA (2013) Childhood maltreatment and psychopathology: A case for ecophenotypic variants as clinically and neurobiologically distinct subtypes. *Am J Psychiatry* **170:** 1114-1133

Teicher MH, Samson JA, Anderson CM, Ohashi K (2016) The effects of childhood maltreatment on brain structure, function and connectivity. *Nature Reviews Neuroscience* **17:** 652-666

the 23 and Me Research Team (2019) Genome-wide meta-analysis of depression identifies 102 independent variants and highlights the importance of the prefrontal brain regions. *Nat Neurosci* **22:** 343-352

Thompson SM, Kallarackal AJ, Kvarta MD, Van Dyke AM, LeGates TA, Cai X (2015) An excitatory synapse hypothesis of depression. *Trends Neurosci* **38:** 279-294

Tian T, Li J, Zhang G, Wang J, Liu D, Wan C, Fang J, Wu D, Zhou Y, Zhu W (2021) Effects of childhood trauma experience and BDNF Val66Met polymorphism on brain plasticity relate to emotion regulation. *Behav Brain Res* **398:** 112949

Tian YE, Di Biase MA, Mosley PE, Lupton MK, Xia Y, Fripp J, Breakspear M, Cropley V, Zalesky A (2023) Evaluation of brain-body health in individuals with common neuropsychiatric disorders. *JAMA psychiatry* **80:** 567-576

Tibshirani R, Walther G (2005) Cluster validation by prediction strength. *Journal of Computational and Graphical Statistics* **14:** 511-528

Tiego J, Martin EA, DeYoung CG, Hagan K (2023) Precision behavioral phenotyping as a strategy for uncovering the biological correlates of psychopathology. **1:** 304-315

Tozzi L, Zhang X (2024) Personalized brain circuit scores identify clinically distinct biotypes in depression and anxiety. **30:** 2076-2087

Uher R (2008) The implications of gene–environment interactions in depression: will cause inform cure? *Mol Psychiatry* **13:** 1070-1078

Vai B, Bertocchi C, Benedetti F (2019) Cortico-limbic connectivity as a possible biomarker for bipolar disorder: where are we now? *Expert Rev Neurother* **19:** 159-172

Vai B, Palladini M, Lorenzi C, Zanardi R, Poletti S, Aggio V, Benedetti F (2022) Interleukin 6 associates with reduced grey matter volume and resting-state connectivity in the anterior cingulate cortex in bipolar patients. *Brain, Behavior, & Immunity - Health* **26:** 100522

Van Dam NT, O'Connor D, Marcelle ET, Ho EJ, Cameron Craddock R, Tobe RH, Gabbay V, Hudziak JJ, Xavier Castellanos F, Leventhal BL, Milham MP (2017) Data-Driven Phenotypic Categorization for Neurobiological Analyses: Beyond DSM-5 Labels. *Biol Psychiatry* **81:** 484-494

van den Heuvel MP, Sporns O (2019) A cross-disorder connectome landscape of brain dysconnectivity. *Nature reviews neuroscience* **20:** 435-446

van der Kolk BA (2003) The neurobiology of childhood trauma and abuse. *Child and Adolescent Psychiatric Clinics* **12:** 293-317

Van Velzen LS, Kelly S, Isaev D, Aleman A, Aftanas LI, Bauer J, Baune BT, Brak IV, Carballedo A, Connolly CG (2020) White matter disturbances in major depressive disorder: a coordinated analysis across 20 international cohorts in the ENIGMA MDD working group. *Mol Psychiatry* **25:** 1511-1525

Varol E, Sotiras A, Davatzikos C (2017) HYDRA: Revealing heterogeneity of imaging and genetic patterns through a multiple max-margin discriminative analysis framework. *Neuroimage* **145:** 346-364

Vassilopoulou K, Papathanasiou M, Michopoulos I, Boufidou F, Oulis P, Kelekis N, Rizos E, Nikolaou C, Pantelis C, Velakoulis D (2013) A magnetic resonance imaging study of hippocampal, amygdala and subgenual prefrontal cortex volumes in major depression subtypes: melancholic versus psychotic depression. *J Affect Disord* **146:** 197-204

Vederine F-E, Wessa M, Leboyer M, Houenou J (2011) A meta-analysis of whole-brain diffusion tensor imaging studies in bipolar disorder. *Prog Neuropsychopharmacol Biol Psychiatry* **35:** 1820-1826

Vieta E, Berk M, Schulze TG, Carvalho AF, Suppes T, Calabrese JR, Gao K, Miskowiak KW, Grande I (2018) Bipolar disorders. *Nature reviews Disease primers* **4:** 1-16

Vogels RJ, Koenders MA, Van Rossum EF, Spijker AT, Drexhage HA (2017) T cell deficits and overexpression of hepatocyte growth factor in anti-inflammatory circulating monocytes of middle-aged patients with bipolar disorder characterized by a high prevalence of the metabolic syndrome. *Frontiers in psychiatry* **8:** 34

von Luxburg U (2007) A tutorial on spectral clustering. *Statistics and Computing* **17:** 395-416

Voskoboinik I, Whisstock JC, Trapani JA (2015) Perforin and granzymes: function, dysfunction and human pathology. *Nature Reviews Immunology* **15:** 388-400

Waller L, Erk S, Pozzi E, Toenders YJ, Haswell CC, Büttner M, Thompson PM, Schmaal L, Morey RA, Walter H (2021) ENIGMA HALFpipe: Interactive, reproducible, and efficient analysis for resting-state and task-based fMRI data. *bioRxiv*

Wang L, Dai Z, Peng H, Tan L, Ding Y, He Z, Zhang Y, Xia M, Li Z, Li W, Cai Y, Lu S, Liao M, Zhang L, Wu W, He Y, Li L (2014) Overlapping and segregated resting-state functional connectivity in patients with major depressive disorder with and without childhood neglect. *Hum Brain Mapp* **35:** 1154-1166

Wang X-J, Krystal JH (2014) Computational psychiatry. *Neuron* **84:** 638-654

Wang Y, Tang S, Zhang L, Bu X, Lu L, Li H, Gao Y, Hu X, Kuang W, Jia Z, Sweeney JA, Gong Q, Huang X (2021a) Data-driven clustering differentiates subtypes of major depressive disorder with distinct brain connectivity and symptom features. *BJPsych* **219:** 606-613

Wang Z, Yuan Y, Jiang Y, You J, Zhang Z (2021b) Identification of specific neural circuit underlying the key cognitive deficit of remitted late-onset depression: A multi-modal MRI and machine learning study. *Prog Neuropsychopharmacol Biol Psychiatry* **108:** 110192

Weiner M, Warren L, Fiedorowicz JG (2011) Cardiovascular morbidity and mortality in bipolar disorder. *Annals of clinical psychiatry: official journal of the American Academy of Clinical Psychiatrists* **23:** 40

Weissman AN, Beck AT (1978) Development and validation of the dysfunctional attitude scale: a preliminary investigation.

Williams LM (2016) Precision psychiatry: a neural circuit taxonomy for depression and anxiety. *The Lancet Psychiatry* **3:** 472-480

Wingo AP, Wrenn G, Pelletier T, Gutman AR, Bradley B, Ressler KJ (2010) Moderating effects of resilience on depression in individuals with a history of childhood abuse or trauma exposure. *J Affect Disord* **126:** 411-414

Winkler AM, Kochunov P, Blangero J, Almasy L, Zilles K, Fox PT, Duggirala R, Glahn DC (2010) Cortical thickness or grey matter volume? The importance of selecting the phenotype for imaging genetics studies. *Neuroimage* **53:** 1135-1146

Winklewski PJ, Sabisz A, Naumczyk P, Jodzio K, Szurowska E, Szarmach A (2018) Understanding the physiopathology behind axial and radial diffusivity changes—what do we know? *Front Neurol* **9:** 92

Wohleb ES, Franklin T, Iwata M, Duman RS (2016) Integrating neuroimmune systems in the neurobiology of depression. *Nature Reviews Neuroscience* **17:** 497-511

Wolf SA, Steiner B, Akpinarli A, Kammertoens T, Nassenstein C, Braun A, Blankenstein T, Kempermann G (2009) CD4-Positive T Lymphocytes Provide a Neuroimmunological Link in the Control of Adult Hippocampal Neurogenesis1. *The Journal of Immunology* **182:** 3979-3984

Woolrich MW, Jbabdi S, Patenaude B, Chappell M, Makni S, Behrens T, Beckmann C, Jenkinson M, Smith SM (2009) Bayesian analysis of neuroimaging data in FSL. *Neuroimage* **45:** S173-186

Xia CH, Ma Z, Ciric R, Gu S, Betzel RF, Kaczkurkin AN, Calkins ME, Cook PA, García de la Garza A, Vandekar SN, Cui Z, Moore TM, Roalf DR, Ruparel K, Wolf DH, Davatzikos C, Gur RC, Gur RE, Shinohara RT, Bassett DS (2018) Linked dimensions of psychopathology and connectivity in functional brain networks. **9:** 3003

Yamada S, Takahashi S, Ohoshi Y, Ishida T, Tsuji T, Shinosaki K, Terada M, Ukai S (2020) Widespread white matter microstructural abnormalities and cognitive impairment in schizophrenia, bipolar disorder, and major depressive disorder: Tract-based spatial statistics study. *Psychiatry research Neuroimaging* **298:** 111045

Yang C, Tiemessen KM, Bosker FJ, Wardenaar KJ, Lie J, Schoevers RA (2018) Interleukin, tumor necrosis factor-α and C-reactive protein profiles in melancholic and non-melancholic depression: a systematic review. *J Psychosom Res* **111:** 58-68

Yang T, Frangou S, Lam RW (2021) Probing the clinical and brain structural boundaries of bipolar and major depressive disorder. **11:** 48

Yao Z, Fu Y, Wu J, Zhang W, Yu Y, Zhang Z, Wu X, Wang Y, Hu B (2020) Morphological changes in subregions of hippocampus and amygdala in major depressive disorder patients. *Brain imaging and behavior* **14:** 653-667

Yapici Eser H, Kacar AS, Kilciksiz CM, Yalcinay-Inan M, Ongur D (2018) Prevalence and associated features of anxiety disorder comorbidity in bipolar disorder: a meta-analysis and meta-regression study. *Frontiers in psychiatry* **9:** 229

Yaple ZA, Tolomeo S, Yu R (2021) Abnormal prediction error processing in schizophrenia and depression. *Hum Brain Mapp* **42:** 3547-3560

Yeung HW, Shen X, Stolicyn A, De Nooij L, Harris MA, Romaniuk L, Buchanan CR, Waiter GD, Sandu AL, McNeil CJ (2021) Spectral clustering based on structural magnetic resonance imaging and its relationship with major depressive disorder and cognitive ability. *Eur J Neurosci* **54:** 6281-6303

Young KD, Siegle GJ, Bodurka J, Drevets WC (2016) Amygdala Activity During Autobiographical Memory Recall in Depressed and Vulnerable Individuals: Association With Symptom Severity and Autobiographical Overgenerality. *Am J Psychiatry* **173:** 78-89

Yu-Feng Z, Yong H, Chao-Zhe Z, Qing-Jiu C, Man-Qiu S, Meng L, Li-Xia T, Tian-Zi J, Yu-Feng W (2007) Altered baseline brain activity in children with ADHD revealed by resting-state functional MRI. *Brain Dev* **29:** 83-91

Yu M, Linn KA, Cook PA, Phillips ML, McInnis M, Fava M, Trivedi MH, Weissman MM, Shinohara RT, Sheline YI (2018) Statistical harmonization corrects site effects in functional connectivity measurements from multi-site fMRI data. *Hum Brain Mapp* **39:** 4213-4227

Yuan M, Yang B, Rothschild G, Mann JJ, Sanford LD, Tang X, Huang C, Wang C, Zhang W (2023) Epigenetic regulation in major depression and other stress-related disorders: molecular mechanisms, clinical relevance and therapeutic potential. *Signal Transduction and Targeted Therapy* **8:** 309

Zang Y, Jiang T, Lu Y, He Y, Tian L (2004) Regional homogeneity approach to fMRI data analysis. *Neuroimage* **22:** 394-400

Zhang H, Li L, Wu M, Chen Z, Hu X, Chen Y, Zhu H, Jia Z, Gong Q (2016) Brain gray matter alterations in first episodes of depression: a meta-analysis of whole-brain studies. *Neurosci Biobehav Rev* **60:** 43-50

Zhang L, Qin K, Pan N, Xu H, Gong Q (2024) Shared and distinct patterns of default mode network dysfunction in major depressive disorder and bipolar disorder: A comparative meta-analysis. *J Affect Disord*

Zimmerman M, Ellison W, Young D, Chelminski I, Dalrymple K (2015) How many different ways do patients meet the diagnostic criteria for major depressive disorder? Compr Psychiatry 56: 29-34

Zou H, Hastie T (2005) Regularization and variable selection via the elastic net. Journal of the Royal Statistical Society Series B: Statistical Methodology 67: 301-320

Zou Q-H, Zhu C-Z, Yang Y, Zuo X-N, Long X-Y, Cao Q-J, Wang Y-F, Zang Y-F (2008) An improved approach to detection of amplitude of low-frequency fluctuation (ALFF) for resting-state fMRI: fractional ALFF. J Neurosci Methods 172: 137-141

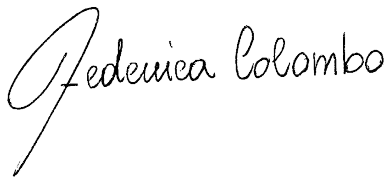

APPENDIX

Appendix 1. List of the selected ROIs for fMRI features

Brainnettome label	**ROI label**
A8m L	SFG medial frontal area 8 L
A8m R	SFG medial frontal area 8 R
A8dl L	SFG dorsolateral frontal area 8 L
A8dl R	SFG dorsolateral frontal area 8 R
A9l L	SFG lateral area 9 L
A9l R	SFG lateral area 9 R
A6dl L	SFG dorsolateral area 6 L
A6dl R	SFG dorsolateral area 6 R
A6m L	SFG medial area 6 L
A6m R	SFG medial area 6 R
A9m L	SFG medial area 9 L
A9m R	SFG medial area 9 R
A10m L	SFG medial area 10 L
A10m R	SFG medial area 10 R
A9/46d L	MFG dorsal area 9/46 L
A9/46d R	MFG dorsal area 9/46 R
IFJ L	MFG inferior frontal junction L
IFJ R	MFG inferior frontal junction R
A46 L	MFG middle frontal area 46 L
A46 R	MFG middle frontal area 46 L
A9/46v L	MFG ventral area 9/46 L
A9/46v R	MFG ventral area 9/46 R
A8vl L	MFG ventrolateral area 8 L
A8vl R	MFG ventrolateral area 8 R
A6vl L	MFG ventrolateral area 6 L
A6vl R	MFG ventrolateral area 6 R
A44d L	IFG dorsolateral area 44 L
A44d R	IFG dorsolateral area 44 L
IFS L	IFG inferior frontal sulcus L
IFS R	IFG inferior frontal sulcus R
A45c L	IFG caudal area 45 L
A45c R	IFG caudal area 45 R
A45r L	IFG rostral area 45 L
A45r R	IFG rostral area 45 R
A44op L	IFG opercular area 44 L
A44op R	IFG opercular area 44 R
A44v L	IFG ventral area 44 L

A44v R	IFG ventral area 44 L
A12/47l L	OrG lateral area 12/47 L
A12/47l R	OrG lateral area 12/47 R
A4hf L	PreCG area 4 head and face L
A4hf R	PreCG area 4 head and face R
A6cdl L	PreCG caudal dorsolat area 6 L
A6cdl R	PreCG caudal dorsolat area 6 R
A4ul L	PreCG area 4 upper limb 4 L
A4ul R	PreCG area 4 upper limb 4 R
A4tl L	PreCG area 4 tongue and larynx L
A4tl R	PreCG area 4 tongue and larynx R
A6cvl L	PreCG caudal ventrolateral area 6 L
A6cvl R	PreCG caudal ventrolateral area 6 R
A1/2/3ll R	ParaCL area 1/2/3 lower limb R
A4ll L	ParaCL area 4 lower limb L
A4ll R	ParaCL area 4 lower limb R
A41/42 L	STG area 41/42 L
A41/42 R	STG area 41/42 R
TE1.0/TE1.2 L	STG TE 1.0/1.2 L
TE1.0/TE1.2 R	STG TE 1.0/1.2 R
A22c L	STG caudal area 22 L
A22c R	STG caudal area 22 R
A38l L	STG lateral area 38 L
A38l R	STG lateral area 38 R
A22r L	STG rostral area 22 L
A22r R	STG rostral area 22 R
A37dl L	MTG dorsolateral area 37 L
A37dl R	MTG dorsolateral area 37 R
A37vl L	ITG ventrolateral area 37 L
A37mv L	FusGy medioventral area 37 L
A37mv R	FusGy medioventral area 37 R
TL L	ParHipGy lateral post PH area L
TL R	ParHipGy lateral post PH area R
TH L	ParHipGy Tharea medialPHG L
TH R	ParHipGy Tharea medialPHG R
rpSTS L	PostSupTempSulc rostropost sup temp sulc L
rpSTS R	PostSupTempSulc rostropost sup temp sulc R
cpSTS L	PostSupTempSulc caudopost sup temp sulc L
cpSTS R	PostSupTempSulc caudopost sup temp sulc R
A7r L	SPL rostral area 7 L
A7r R	SPL rostral area 7 R

A7c L	SPL caudal area 7 L
A7c R	SPL caudal area 7 R
A5l L	SPL lateral area 5 L
A5l R	SPL lateral area 5 R
A7ip L	SPL intrapariet area 7 L
A7ip R	SPL intrapariet area 7 R
A39c L	IPL caudal area 39 L
A39rd L	IPL rostrodorsal area 39 L
A40rd L	IPL rostrodorsal area 40 L
A40rd R	IPL rostrodorsal area 40 R
A40c L	IPL caudal area 40 L
A39rv L	IPL rostroventral area 39 L
A39rv R	IPL rostroventral area 39 R
A40rv L	IPL rostroventral area 40 L
A40rv R	IPL rostroventral area 40 R
A7m L	PreCun medial area 7 L
A7m R	PreCun medial area 7 R
A5m L	PreCun medial area 5 L
A5m R	PreCun medial area 5 R
dmPOS L	PreCun dorsomed parietocc sulcus L
dmPOS R	PreCun dorsomed parietocc sulcus R
A31 L	PreCun area 31 L
A31 R	PreCun area 31 R
A1/2/3ulhf L	PostCGy area 1/2/3 head and face L
A1/2/3ulhf R	PostCGy area 1/2/3 head and face R
A1/2/3tonIa L	PostCGy area 1/2/3 tongue and larynx L
A1/2/3tonIa R	PostCGy area 1/2/3 tongue and larynx R
A2 L	PostCGy lateral area 2 L
A2 R	PostCGy lateral area 2 R
G L	InsL hypergranular insular L
G R	InsL hypergranular insular R
vIa L	InsL ventral agranular insular L
vIa R	InsL ventral agranular insular R
dIa L	InsL dorsolat agranular insular L
dIa R	InsL dorsolat agranular insular R
vId/vIg L	InsL ventral granular insular L
vId/vIg R	InsL ventral granular insular R
dIg L	InsL dorsolat granular insular L
dIg R	InsL dorsolat granular insular R
dId L	InsL dorsal dysgranular insular L
dId R	InsL dorsal dysgranular insular R

A23d L	CingGy dorsal area 23 L
A23d R	CingGy dorsal area 23 R
A24rv L	CingGy rostroventral area 24 L
A32p L	CingGy pregenual area 32 L
A32p R	CingGy pregenual area 32 R
A23v L	CingGy ventral area 23 L
A23v R	CingGy ventral area 23 R
A24cd L	CingGy caudodorsal area 24 L
A24cd R	CingGy caudodorsal area 24 R
A23c L	CingGy caudal area 23 L
A23c R	CingGy caudal area 23 R
A32sg R	CingGy subgenual area 32 R
cLinG L	MedVentOC caudal lingual gyrus L
cLinG R	MedVentOC caudal lingual gyrus R
rCunG L	MedVentOC rostral cuneus gyrus L
rCunG R	MedVentOC rostral cuneus gyrus R
cCunG R	MedVentOC caudal cuneus gyrus R
rLinG L	MedVentOC rostral lingual gyrus L
rLinG R	MedVentOC rostral lingual gyrus R
vmPOS L	MedVentOC ventromed parietocc sulcus L
vmPOS R	MedVentOC ventromed parietocc sulcus R
mOccG L	LatOC middle occip gyrus L
mOccG R	LatOC middle occip gyrus R
V5/MT+ L	LatOC V5/MT area L
V5/MT+ R	LatOC V5/MT area R
msOccG L	LatOC med sup occ gyrus L
msOccG R	LatOC med sup occ gyrus R
lsOccG L	LatOC lat sup occ gyrus L
lsOccG R	LatOC lat sup occ gyrus R
lAmyg L	Amy lateral amygdala L
lAmyg R	Amy lateral amygdala R
rHipp L	Hipp rostral hipp L
rHipp R	Hipp rostral hipp R
cHipp L	Hipp caudal hipp L
cHipp R	Hipp caudal hipp R
vCa L	BasGang ventral caudate L
vCa R	BasGang ventral caudate R
GP L	BasGang globus pallidus L
GP R	BasGang globus pallidus R
NAC L	BasGang nucleus accumbens L
vmPu L	BasGang ventromedial putamen L

vmPu R	BasGang ventromedial putamen R
dCa L	BasGang dorsal caudate L
dCa R	BasGang dorsal caudate R
dlPu L	BasGang dorsolat putamen L
dlPu R	BasGang dorsolat putamen R
mPFtha L	Thal medial prefront thalamus L
mPFtha R	Thal medial prefront thalamus R
mPMtha L	Thal premotor thalamus L
mPMtha R	Thal premotor thalamus R
Stha L	Thal sensory thalamus L
Stha R	Thal sensory thalamus R
rTtha L	Thal rostral temp thalamus L
rTtha R	Thal rostral temp thalamus R
PPtha L	Thal posterior parietal thalamus L
PPtha R	Thal posterior parietal thalamus R
Otha L	Thal occipital thalamus L
Otha R	Thal occipital thalamus R
cTtha L	Thal caudal temporal thalamus L
cTtha R	Thal caudal temporal thalamus R
lPFtha L	Thal lateral prefrontal thalamus L
lPFtha R	Thal lateral prefrontal thalamus R
Buckner2011 17Networks 1	Buckner cerebellar networks 1
Buckner2011 17Networks 2	Buckner cerebellar networks 2
Buckner2011 17Networks 4	Buckner cerebellar networks 4
Buckner2011 17Networks 5	Buckner cerebellar networks 5
Buckner2011 17Networks 9	Buckner cerebellar networks 9

For each Brainnetome label the corresponding region of interest (ROI) is reported Abbrevations: SFG, superior frontal gyrus; MFG, medial frontal gyrus; IFG; inferior frontal gyrus; OrG, orbital gyrus; PreCG, precentral gyrus; ParaCL, paracentral lobule; STG, superior temporal gyrus; MTG, medial temporal gyrus; ITG, inferior temporal gyrus; FusGy, fusiform gyrus; ParHipGy, hippocampal part of the cingulate gyrus; PostSupTempSulc, posterior and superior temporal sulcus; SPL, superior parietal lobule; IPL, inferior parietal lobule; PreCun, precuneus; PostCGy, posterior cingulate gyrus; Ins, insula; CingCy, cingulate gyrus; MedVenOC, medial ventral occipital cortex; LatOC, lateral occipital cortex; Amy, amygdala; Hipp, hippocampus; BasGang, basal ganglia; Thal, thalamus; L, left; R, right.

Appendix 2. ML algorithms used in single-feature stratification models

For all single-feature stratification models, K-means was chosen as data-driven approach to be implemented in *reval*. K-means is one of the most popular clustering algorithm that aims to partitioning the dataset at hand according to a specific number of *K* clusters. The main goal of this approach is to find the clustering solution that minimize the within-cluster variance according to the following equation:

$$\underset{C_1,\ldots,C_K}{\text{minimize}}\left(\sum_{k=1}^{K} W(C_k)\right)$$

(1)

Where C_k represents the observations assigned to a specific cluster K and W(C_k) the corresponding internal variance. K-means is commonly defined as a distance-based clustering approach, meaning that the assignment of each observation to a cluster is based on the distance between an observation and clusters' centroids (i.e., mean of the observations previously assigned to a given cluster). Different distance measures can be used, but the most frequently implemented is the squared Euclidean distance. Consequently, the W(C_k) is computed as follow:

$$W(C_k) = \frac{1}{|C_K|}\sum_{i,i' \in Ck}\sum_{j=1}^{p}\left(x_{ij} - x_{i'j}\right)^2$$

(2)

where p is the number of features and x_{ij} stands for the value of the jth feature for the ith observation. In other words, the within-cluster variance W(C_k) is calculated as the sum of all the pairwise squared Euclidean distances between the observations assigned to the Kth cluster divided by the number of the observations belonging to the Kth cluster. From a computational point of view, finding an optimal solution to this optimization problem is demanding due to the huge number of ways in which a dataset can be split into clusters. However, the usual application of K-means relies on a simple algorithm that is able to achieve a local optimum (i.e., the optimal solution within a subset of potential solutions) (James et al, 2023). The K-means algorithm works as follows. First, each observation is randomly assigned to one of the K clusters. Then, for each cluster, a centroid is computed, and the Euclidean distance of each observation to every K centroids is calculated. Consequently, each observation is reassigned to the cluster whose centroid is the closest. This procedure continues iteratively until observations' assignments do not change, indicating that a local minimum has been reached. However, one of the major drawback of this algorithm is that the identification of the local minimum is largely influenced by the initial clusters' assignments. Hence, the algorithm should be run several times with different initial random assignments and the solution with the lowest within-cluster

variance should be considered as the optimal one (James et al, 2023). Another variant of this approach called *k-means++* (Arthur & Vassilvitskii, 2006) tries to overcome this issue by randomly assigning the first centroid and then choosing the remaining centroids according to the largest squared distance. Compared to the classical k-means algorithm, *k-means++* improves the separation among centroids, which results in an optimal solution that is closer to a global minimum (Arthur & Vassilvitskii, 2006).

Regarding supervised ML classifiers, 2 different algorithms were implemented in *reval* according to the different type of input features: SVM and elasticnet penalized regression. SVM is a supervised ML algorithm that aims to identify a hyperplane (i.e., a subspace of the original space of dimension $p - 1$, where p represents the number of features in the original space) that best separates the labelled observations (Cristianini & Shawe-Taylor, 2000). During the training phase, SVM used the labeled observation to define the hyperplane that best discriminates between 2 or more classes, which is subsequently used to predict the labels of new data. However, within a given dataset, a potential infinite number of hyperplanes can be defined to separate the observations into classes. SVM identifies the optimal hyperplane as the one with the maximal margin (that is, the minimal distance from the observations to the hyperplane). According to this definition, the optimal hyperplane is also called *maximal margin hyperplane*, whereas the observations closest to the hyperplane are denoted as *support vectors*. The general idea behind this approach is that if a hyperplane is able to maximize the distance between observations belonging to different classes in the training dataset, it should behave similarly also in test set. It should be considered, though, that a supervised ML algorithm that relies on the maximal margin criterion will always correctly classify observations in the training set, making it extremely sensitive to the individual observations. This might increase the risk of overfitting, meaning that the algorithm also learns noise within the dataset that impairs its classification accuracy in the test set. Even though counterintuitive, it could be beneficial to let the algorithm misclassify some observations in the training set in order to improve the generalizability of predictions on unseen data. The trade-off between misclassification and generalizability is determined by the hyperparameter C: for high C values, SVM identifies a larger margin, thus being more tolerant against misclassifications; for low C values, SVM identifies a smaller margin, increasing the cost of making misclassifications. Another characteristic of SVM is to be

adapted to work on non-linearly separable datasets through the so-called *kernel trick.* The rationale behind this approach is that data that are non-linearly separable in their original space can be linearly separated in a higher-order space (Cristianini & Shawe-Taylor, 2000). The kernel trick allows to implicitly transform the original space into a higher-dimensional space by computing the pairwise similarity between observations, making it particularly suitable to deal high-dimensional data (e.g., neuroimaging).

Whereas SVM was employed in neuroimaging-based models, elasticnet penalized regression was implemented for stratification models based on immune peripheral markers (i.e., immune-inflammatory profiles and FACS). Elasticnet is a penalization term that can be added to the regression loss function to improve the performance of the model in case of high-dimensional and highly correlated predictors (Zou & Hastie, 2005). Specifically, elasticnet tries to find a trade-off between 2 commonly used regularization terms: L1 and L2. The L1 regularization force a shrinkage of regression coefficients toward zero, making it particularly suitable for feature selection and produce sparse models (i.e., a predictive model in which only a subset of predictors is included). However, in case in which predictors are highly correlated (i.e., multicollinearity), the L1 penalization tends to include only some of them in the model, resulting in a suboptimal solution. Conversely, the L2 penalization term shrinks the coefficients of the model very close to zero, allowing to deal with multicollinearity despite being less useful to improve the sparsity of the model. The elasticnet regularization tries to combine the strengths of both L1 and L2 through the optimization of 2 hyperparameters called λ and α. Elasticnet regularization can be defined in the following way:

$$P_\alpha(\beta) = \lambda\left(\sum_{j=1}^{p}\left(\frac{(1-\alpha)}{2}\beta_j^2 + \alpha\left|\beta_j\right|\right)\right) \quad (3)$$

where β_j represents the jth regression coefficient for j ranging from 1 to p number of predictors. The λ hyperparameter controls the amount of shrinkage of regression coefficients: the higher the λ value, the higher the shrinkage of coefficients toward zero. The α hyperparameter, instead, manages the balance between L1 and L2 penalty terms:

when α = 0, the elasticnet converts to L2 penalty, whereas it becomes equivalent to L1 in case of α = 1.

Appendix 3. Normalized stability plots for each clustering model

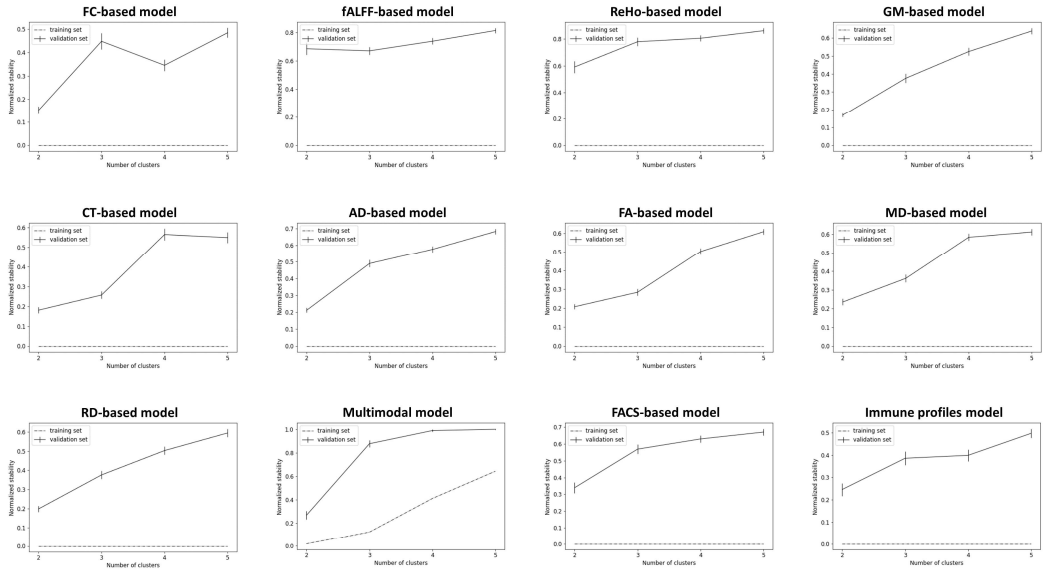

Solid lines represent the validation normalized stability with 95% confidence intervals. Dashed lines indicate the stability during training. Abbrevations: FC, functional connectivity; fALFF, fractional amplitude of low frequency fluctuations; ReHo, regional homogeneity; GM, grey matter; CT, cortical thickness; AD, axial diffusivity; FA, fractional anisotropy; MD, mean diffusivity; RD, radial diffusivity; FACS, fluorescence activated cell sorting.

Appendix 4. Differences in positive and negative strength values for each region between the FC-based clusters

Variable	Cluster 1 (N = 50)	Cluster 2 (N =96)	t / U	d	p	q
Spos A8m R	59.37 ± 28.56	33.86 ± 11.76	4397‡	2.15	<0.001	<0.001*
Spos A8dl L	45.94 ± 22.1	27.4 ± 13.54	4032‡	1.59	<0.001	<0.001*
Spos A8dl R	48.25 ± 22.3	26.56 ± 10.62	4054‡	1.70	<0.001	<0.001*
Spos A9l L	41.9 ± 18.54	25.75 ± 10.71	3798‡	1.26	<0.001	<0.001*
Spos A9l R	46.1 ± 21.56	27.12 ± 9.7	3988‡	1.53	<0.001	<0.001*
Spos A6dl L	53.78 ± 29.14	29.16 ± 12.19	4150‡	1.73	<0.001	<0.001*
Spos A6dl R	57.38 ± 28.97	28.02 ± 10.98	4390‡	2.16	<0.001	<0.001*
Spos A6m L	65.25 ± 23.96	34.66 ± 13.11	4524‡	2.36	<0.001	<0.001*
Spos A6m R	67.05 ± 27.01	32.34 ± 13.17	4590‡	2.54	<0.001	<0.001*
Spos A9m L	52.93 ± 29.15	28.63 ± 11.3	4318‡	1.96	<0.001	<0.001*
Spos A9m R	54.83 ± 26.69	31.67 ± 13.56	4307‡	1.92	<0.001	<0.001*

Spos A10m L	47.64 ± 20.2	28.39 ± 12.87	4080‡	1.62	<0.001	<0.001*
Spos A10m R	47.76 ± 20.89	31.64 ± 13.4	4143‡	1.67	<0.001	<0.001*
Spos A9.46d L	54.01 ± 25.83	29.94 ± 15	4244‡	1.90	<0.001	<0.001*
Spos A9.46d R	55.99 ± 22.49	29.9 ± 14.18	4449‡	2.13	<0.001	<0.001*
Spos IFJ L	49.52 ± 25.45	28.43 ± 10.03	4234‡	1.84	<0.001	<0.001*
Spos IFJ R	51.55 ± 20.56	27.95 ± 10.87	4414‡	2.10	<0.001	<0.001*
Spos A46 L	54.76 ± 21.76	26.77 ± 14.93	4413‡	2.12	<0.001	<0.001*
Spos A46 R	53.73 ± 20.8	28 ± 12.87	4355‡	2.03	<0.001	<0.001*
Spos A9.46v L	54.98 ± 23.49	28.72 ± 12.31	4325‡	2.02	<0.001	<0.001*
Spos A9.46v R	56.07 ± 19.65	27.14 ± 13.2	4288‡	1.98	<0.001	<0.001*
Spos A8vl L	51.33 ± 28.39	28.43 ± 11.72	4277‡	1.86	<0.001	<0.001*
Spos A8vl R	55.07 ± 25.6	27.99 ± 12.11	4318‡	2.05	<0.001	<0.001*
Spos A6vl L	52.74 ± 27.9	29.55 ± 12.22	4362‡	2.00	<0.001	<0.001*
Spos A6vl R	53.53 ± 27.03	28.4 ± 13.15	4426‡	2.03	<0.001	<0.001*
Spos A44d L	47.72 ± 26.32	28.01 ± 10.43	4078‡	1.64	<0.001	<0.001*
Spos A44d R	48.85 ± 25.76	27.82 ± 13.62	4118‡	1.63	<0.001	<0.001*
Spos IFS L	47.1 ± 25.02	25.75 ± 11.38	4217‡	1.80	<0.001	<0.001*
Spos IFS R	51.74 ± 26.61	27.63 ± 12.77	4289‡	1.92	<0.001	<0.001*
Spos A45c L	43.19 ± 26.44	24.67 ± 8.58	3901‡	1.48	<0.001	<0.001*
Spos A45c R	50.49 ± 26.84	30.27 ± 11.6	4168‡	1.75	<0.001	<0.001*
Spos A45r L	42.28 ± 23.93	26.92 ± 10.17	3895‡	1.39	<0.001	<0.001*
Spos A45r R	48.73 ± 22.56	27.12 ± 11.73	4109‡	1.69	<0.001	<0.001*
Spos A44op L	44.47 ± 20.76	28.06 ± 11.5	3945‡	1.37	<0.001	<0.001*
Spos A44op R	47.51 ± 22.22	29.36 ± 13.18	4055‡	1.53	<0.001	<0.001*
Spos A44v L	47.46 ± 19.47	27.69 ± 12.25	4035‡	1.57	<0.001	<0.001*
Spos A44v R	49.09 ± 26.22	27.61 ± 14.37	4182‡	1.77	<0.001	<0.001*
Spos A12.47l L	47.31 ± 20.37	29.55 ± 11.21	4128‡	1.53	<0.001	<0.001*
Spos A12.47l R	51.59 ± 23.15	28.82 ± 11.63	4268‡	1.90	<0.001	<0.001*
Spos A4hf L	60.59 ± 20.26	37.63 ± 14.13	4495‡	2.18	<0.001	<0.001*
Spos A4hf R	55.38 ± 21.01	33.72 ± 11.62	4569‡	2.28	<0.001	<0.001*
Spos A6cdl L	61.8 ± 23.63	32.38 ± 13.63	4550‡	2.32	<0.001	<0.001*
Spos A6cdl R	64.27 ± 23.75	33.3 ± 15.76	4498‡	2.27	<0.001	<0.001*
Spos A4ul L	59.33 ± 25.44	29.8 ± 14.27	4465‡	2.18	<0.001	<0.001*
Spos A4ul R	58.09 ± 27.05	32.63 ± 15.05	4480‡	2.14	<0.001	<0.001*
Spos A4tl L	47.05 ± 22.93	30.16 ± 14.96	3890‡	1.33	<0.001	<0.001*
Spos A4tl R	54.79 ± 25.14	29.98 ± 12.99	4287‡	1.84	<0.001	<0.001*
Spos A6cvl L	56.6 ± 23.78	33.11 ± 11.84	4221‡	1.80	<0.001	<0.001*
Spos A6cvl R	62.24 ± 22.61	32.04 ± 14.44	4331‡	2.03	<0.001	<0.001*
Spos A1.2.3ll R	63.27 ± 23.45	31.8 ± 13.54	4510‡	2.37	<0.001	<0.001*
Spos A4ll L	61.36 ± 22.97	31.74 ± 13.92	4610‡	2.59	<0.001	<0.001*
Spos A4ll R	65.12 ± 20.21	32.39 ± 15.37	4650‡	2.69	<0.001	<0.001*

Spos A41.42 L	59.87 ± 26.64	33.98 ± 14.29	4372‡	2.02	<0.001	<0.001*
Spos A41.42 R	59.34 ± 25.37	33.23 ± 14.49	4305‡	1.98	<0.001	<0.001*
Spos TE1.0.TE1.2 L	56.28 ± 23.51	33.53 ± 13.65	4116‡	1.58	<0.001	<0.001*
Spos TE1.0.TE1.2 R	56.21 ± 27.06	34.62 ± 13.45	4337‡	1.94	<0.001	<0.001*
Spos A22c L	50.71 ± 25.86	28.29 ± 13.95	4142‡	1.66	<0.001	<0.001*
Spos A22c R	56.61 ± 22.63	30.9 ± 13.04	4453‡	2.14	<0.001	<0.001*
Spos A38l L	37.78 ± 20.68	24.87 ± 9.65	3522‡	0.96	<0.001	<0.001*
Spos A38l R	38.99 ± 23.62	29.8 ± 14.95	3516‡	1.05	<0.001	<0.001*
Spos A22r L	48.63 ± 26.82	28.81 ± 14.23	3944‡	1.51	<0.001	<0.001*
Spos A22r R	43.69 ± 19.42	25.87 ± 11.3	3953‡	1.46	<0.001	<0.001*
Spos A37dl L	53.3 ± 17.13	30.93 ± 11.64	4348‡	1.86	<0.001	<0.001*
Spos A37dl R	55.19 ± 19.47	29.8 ± 12.91	4446‡	2.14	<0.001	<0.001*
Spos A37vl L	53.38 ± 17.55	28.12 ± 13.54	4315‡	1.89	<0.001	<0.001*
Spos A37mv L	63.62 ± 23.57	37.01 ± 14.8	4381‡	2.10	<0.001	<0.001*
Spos A37mv R	61.41 ± 23.85	35.34 ± 14.04	4312‡	1.96	<0.001	<0.001*
Spos TL L	35.96 ± 18.03	21.61 ± 10.21	4085‡	1.56	<0.001	<0.001*
Spos TL R	33.34 ± 17.4	24.42 ± 12.31	3587‡	1.02	<0.001	<0.001*
Spos TH L	33.16 ± 20.28	21.99 ± 12.01	3538‡	0.97	<0.001	<0.001*
Spos TH R	37.83 ± 26.04	23.17 ± 9.95	3539‡	1.15	<0.001	<0.001*
Spos rpSTS L	40.78 ± 24.76	27.05 ± 9.68	3820‡	1.35	<0.001	<0.001*
Spos rpSTS R	46.24 ± 25.91	27.96 ± 12.4	4170‡	1.71	<0.001	<0.001*
Spos cpSTS L	48.1 ± 17.9	29.23 ± 14.28	4083‡	1.57	<0.001	<0.001*
Spos cpSTS R	49.19 ± 15.49	28.13 ± 13.26	4110‡	1.60	<0.001	<0.001*
Spos A7r L	55.72 ± 28.96	28.34 ± 16.28	4244‡	1.83	<0.001	<0.001*
Spos A7r R	60.22 ± 23.4	30.05 ± 15.96	4435‡	2.20	<0.001	<0.001*
Spos A7c L	56.45 ± 27.02	31.38 ± 17.53	4322‡	1.91	<0.001	<0.001*
Spos A7c R	57.63 ± 22.03	29.51 ± 13.81	4409‡	2.10	<0.001	<0.001*
Spos A5l L	54.89 ± 26	31.56 ± 13.36	4280‡	1.87	<0.001	<0.001*
Spos A5l R	57.07 ± 22.58	31.77 ± 12.45	4399‡	2.07	<0.001	<0.001*
Spos A7ip L	56.19 ± 23.34	29.91 ± 14.46	4399‡	2.04	<0.001	<0.001*
Spos A7ip R	57.04 ± 25.67	29.28 ± 14.86	4260‡	1.90	<0.001	<0.001*
Spos A39c L	56.94 ± 22.9	32.55 ± 14.22	4245‡	1.84	<0.001	<0.001*
Spos A39rd L	56.12 ± 29.32	29.21 ± 10.89	4368‡	2.10	<0.001	<0.001*
Spos A40rd L	53.2 ± 26.81	31.44 ± 16.51	4200‡	1.77	<0.001	<0.001*
Spos A40rd R	55.53 ± 24.32	31.38 ± 16.81	4269‡	1.81	<0.001	<0.001*
Spos A40c L	49.16 ± 18.31	28.42 ± 11.37	4395‡	1.97	<0.001	<0.001*
Spos A39rv L	54.69 ± 22.52	31.8 ± 10.79	4325‡	1.94	<0.001	<0.001*
Spos A39rv R	52.19 ± 18.99	29.38 ± 11.46	4510‡	2.24	<0.001	<0.001*
Spos A40rv L	61.31 ± 28.26	33.03 ± 15.08	4398‡	2.08	<0.001	<0.001*
Spos A40rv R	59.92 ± 24.02	33.34 ± 13	4383‡	2.10	<0.001	<0.001*
Spos A7m L	63.46 ± 22.12	32.73 ± 14.62	4547‡	2.41	<0.001	<0.001*

Spos A7m R	60.11 ± 21.51	33.39 ± 12.91	4468‡	2.26	<0.001	<0.001*
Spos A5m L	67.21 ± 22.93	37.57 ± 15.38	4633‡	2.55	<0.001	<0.001*
Spos A5m R	68.58 ± 23.43	37.47 ± 17.04	4711‡	2.74	<0.001	<0.001*
Spos dmPOS L	54.51 ± 15.44	34.48 ± 11.62	4386‡	1.98	<0.001	<0.001*
Spos dmPOS R	54.24 ± 21.26	34.93 ± 12.81	4331‡	1.90	<0.001	<0.001*
Spos A31 L	51.31 ± 19.23	32.74 ± 14.18	4135‡	1.58	<0.001	<0.001*
Spos A31 R	52.91 ± 18.41	33.58 ± 12.05	4339‡	1.90	<0.001	<0.001*
Spos A1.2.3ulhf L	62.44 ± 23.55	37.66 ± 12.59	4529‡	2.25	<0.001	<0.001*
Spos A1.2.3ulhf R	62.51 ± 30.12	35.56 ± 11.77	4485‡	2.22	<0.001	<0.001*
Spos A1.2.3tonIa L	59.09 ± 24.17	36.94 ± 15.24	4162‡	1.70	<0.001	<0.001*
Spos A1.2.3tonIa R	58.45 ± 23.72	33.51 ± 15.89	4122‡	1.69	<0.001	<0.001*
Spos A2 L	53.86 ± 25.39	29.16 ± 12.03	4179‡	1.73	<0.001	<0.001*
Spos A2 R	56.78 ± 26.16	33.27 ± 15.6	4268‡	1.86	<0.001	<0.001*
Spos G L	48.14 ± 17.28	29.73 ± 12.63	3948‡	1.38	<0.001	<0.001*
Spos G R	41.97 ± 22.13	25.84 ± 11.53	4076‡	1.50	<0.001	<0.001*
Spos vIa L	34.95 ± 15.37	23.29 ± 11.19	3621‡	1.02	<0.001	<0.001*
Spos vIa R	33.45 ± 27.16	21.59 ± 12.04	3225‡	0.82	<0.001	<0.001*
Spos dIa L	42.12 ± 23.55	28.4 ± 9.29	3998‡	1.44	<0.001	<0.001*
Spos dIa R	46.07 ± 26.66	26.22 ± 12.55	4083‡	1.65	<0.001	<0.001*
Spos vId.vIg L	44.21 ± 19.7	27.13 ± 10.51	3899‡	1.37	<0.001	<0.001*
Spos vId.vIg R	50.51 ± 25.44	28.81 ± 11.63	3903‡	1.48	<0.001	<0.001*
Spos dIg L	44.56 ± 18.52	27.58 ± 12.28	3929‡	1.35	<0.001	<0.001*
Spos dIg R	44.45 ± 30.07	27.51 ± 11.27	3846‡	1.39	<0.001	<0.001*
Spos dId L	51.35 ± 17.85	30.37 ± 10.14	4036‡	1.61	<0.001	<0.001*
Spos dId R	47.9 ± 22.84	29.56 ± 12.18	4105‡	1.57	<0.001	<0.001*
Spos A23d L	53.82 ± 20.65	32.49 ± 13.95	4411‡	2.07	<0.001	<0.001*
Spos A23d R	53.39 ± 18.51	31.71 ± 11.13	4333‡	1.98	<0.001	<0.001*
Spos A24rv L	43.05 ± 24.31	23.54 ± 13.39	3847‡	1.29	<0.001	<0.001*
Spos A32p L	50.49 ± 24.58	31.84 ± 12.11	4098‡	1.67	<0.001	<0.001*
Spos A32p R	52.76 ± 27.75	29.73 ± 13.28	4095‡	1.73	<0.001	<0.001*
Spos A23v L	50.94 ± 19.41	33.61 ± 15.3	4095‡	1.59	<0.001	<0.001*
Spos A23v R	55.52 ± 18.2	34.03 ± 15.41	4293‡	1.85	<0.001	<0.001*
Spos A24cd L	56.31 ± 24.48	31.37 ± 12.07	4465‡	2.17	<0.001	<0.001*
Spos A24cd R	53.41 ± 22.18	31.17 ± 13.31	4456‡	2.09	<0.001	<0.001*
Spos A23c L	65.28 ± 20.97	33.78 ± 12.12	4652‡	2.79	<0.001	<0.001*
Spos A23c R	65.62 ± 23.68	33.79 ± 11.35	4586‡	2.50	<0.001	<0.001*
Spos A32sg R	39.33 ± 23.11	25.5 ± 12.33	3801‡	1.32	<0.001	<0.001*
Spos cLinG L	59.15 ± 22.51	33.68 ± 15.89	4328‡	1.98	<0.001	<0.001*
Spos cLinG R	57.95 ± 23.01	32.06 ± 17.31	4263‡	1.84	<0.001	<0.001*
Spos rCunG L	62.33 ± 23.55	38.14 ± 14.81	4269‡	1.90	<0.001	<0.001*
Spos rCunG R	60.56 ± 29.47	39.26 ± 14.79	4396‡	2.00	<0.001	<0.001*

Spos cCunG R	49.77 ± 32.43	32.27 ± 17.57	3685‡	1.19	<0.001	<0.001*
Spos rLinG L	53.88 ± 23.24	32.95 ± 14.56	4040‡	1.62	<0.001	<0.001*
Spos rLinG R	53.82 ± 28.41	33.04 ± 12.18	4015‡	1.61	<0.001	<0.001*
Spos vmPOS L	61.26 ± 17.95	39.33 ± 11.7	4515‡	2.19	<0.001	<0.001*
Spos vmPOS R	59.87 ± 18.5	39.94 ± 13.69	4490‡	2.13	<0.001	<0.001*
Spos mOccG L	50.57 ± 30.21	30.8 ± 12.7	4127‡	1.66	<0.001	<0.001*
Spos mOccG R	50.44 ± 23.89	30.27 ± 11.63	4090‡	1.67	<0.001	<0.001*
Spos V5.MT. L	59.22 ± 25.74	33.52 ± 14.4	4175‡	1.80	<0.001	<0.001*
Spos V5.MT. R	57.3 ± 27.47	31.24 ± 14.04	4107‡	1.67	<0.001	<0.001*
Spos msOccG L	55.36 ± 24.05	32.6 ± 13.57	4034‡	1.60	<0.001	<0.001*
Spos msOccG R	53.25 ± 28.75	33.34 ± 14.25	4114‡	1.63	<0.001	<0.001*
Spos lsOccG L	64.17 ± 23.89	35.05 ± 14.38	4447‡	2.19	<0.001	<0.001*
Spos lsOccG R	59.64 ± 25.38	35.05 ± 15.36	4403‡	2.05	<0.001	<0.001*
Spos lAmyg L	28.27 ± 17.4	19.83 ± 11.54	3684‡	1.15	<0.001	<0.001*
Spos lAmyg R	33.55 ± 20.42	19.38 ± 9.3	3772‡	1.30	<0.001	<0.001*
Spos rHipp L	40.08 ± 18.82	25.95 ± 12.49	3766‡	1.16	<0.001	<0.001*
Spos rHipp R	31.49 ± 20.85	23.9 ± 9.9	3315‡	0.88	<0.001	<0.001*
Spos cHipp L	44.67 ± 20.17	27.99 ± 14.07	4034‡	1.48	<0.001	<0.001*
Spos cHipp R	44.77 ± 19.94	28.93 ± 11.15	4031‡	1.51	<0.001	<0.001*
Spos vCa L	40.13 ± 21.28	23.59 ± 10.74	4252‡	1.76	<0.001	<0.001*
Spos vCa R	40.45 ± 16.76	23.55 ± 10.17	4274‡	1.77	<0.001	<0.001*
Spos GP L	42.77 ± 24.18	23.89 ± 11.33	4102‡	1.69	<0.001	<0.001*
Spos GP R	42.6 ± 17.51	23.72 ± 12.64	4120‡	1.64	<0.001	<0.001*
Spos NAC L	35.15 ± 17.96	20.77 ± 9.34	4141‡	1.52	<0.001	<0.001*
Spos vmPu L	48.51 ± 20.9	26.07 ± 10.39	4241‡	1.90	<0.001	<0.001*
Spos vmPu R	43.36 ± 21.44	23.66 ± 11.26	4131‡	1.77	<0.001	<0.001*
Spos dCa L	49.28 ± 18.01	25.42 ± 10.83	4365‡	1.99	<0.001	<0.001*
Spos dCa R	49.43 ± 21.36	25.93 ± 11.9	4268‡	1.88	<0.001	<0.001*
Spos dlPu L	50.53 ± 26.58	28.16 ± 13.75	4245‡	1.82	<0.001	<0.001*
Spos dlPu R	52.44 ± 23.73	28.53 ± 13	4146‡	1.68	<0.001	<0.001*
Spos mPFtha L	55.28 ± 16.26	27.59 ± 13.1	4591‡	2.43	<0.001	<0.001*
Spos mPFtha R	57.02 ± 14.43	29.63 ± 11.16	4643‡	2.55	<0.001	<0.001*
Spos mPMtha L	23.53 ± 17.65	16.2 ± 10.26	3491‡	1.04	<0.001	<0.001*
Spos mPMtha R	43.12 ± 16.19	22.69 ± 11.7	4242‡	1.73	<0.001	<0.001*
Spos Stha L	36.73 ± 16.68	20.16 ± 11.72	4049‡	1.49	<0.001	<0.001*
Spos Stha R	39.75 ± 19.02	20.04 ± 11.81	4071‡	1.55	<0.001	<0.001*
Spos rTtha L	51.68 ± 22.73	26.26 ± 9.21	4271‡	1.93	<0.001	<0.001*
Spos rTtha R	39.82 ± 22.33	23.25 ± 10.26	3891‡	1.40	<0.001	<0.001*
Spos PPtha L	49.39 ± 18.1	27.48 ± 14.1	4467‡	2.14	<0.001	<0.001*
Spos PPtha R	56.05 ± 21.57	27.23 ± 9.94	4505‡	2.35	<0.001	<0.001*
Spos Otha L	48.31 ± 20.62	23.89 ± 14.23	4423‡	2.06	<0.001	<0.001*

Spos Otha R	41.77 ± 20.85	23.6 ± 9.95	4308‡	1.89	<0.001	<0.001*
Spos cTtha L	46.91 ± 16.3	25.5 ± 14.71	4399‡	1.95	<0.001	<0.001*
Spos cTtha R	42.41 ± 19.33	23.43 ± 13.73	4100‡	1.61	<0.001	<0.001*
Spos lPFtha L	46.06 ± 16.44	28.97 ± 11.55	4319‡	1.77	<0.001	<0.001*
Spos lPFtha R	57.29 ± 17.19	29.59 ± 12.47	4529‡	2.27	<0.001	<0.001*
Spos Buckner2011 17Networks 1	45.39 ± 26.34	24.59 ± 14.74	3840‡	1.33	<0.001	<0.001*
Spos Buckner2011 17Networks 2	40.05 ± 19.86	22.8 ± 13.19	4011‡	1.48	<0.001	<0.001*
Spos Buckner2011 17Networks 4	61.28 ± 24.32	32.55 ± 16.03	4369‡	2.05	<0.001	<0.001*
Spos Buckner2011 17Networks 5	26.51 ± 22.31	17.09 ± 11.91	3400‡	0.89	<0.001	<0.001*
Spos Buckner2011 17Networks 9	52.35 ± 23.68	26.16 ± 14.49	4332‡	2.00	<0.001	<0.001*
Sneg A8m L	0.61 ± 1.97	5.84 ± 6.47	402‡	-1.37	<0.001	<0.001*
Sneg A8m R	0.46 ± 1.25	5.37 ± 6.02	360‡	-1.31	<0.001	<0.001*
Sneg A8dl L	1.29 ± 2.52	7.85 ± 6.12	414‡	-1.43	<0.001	<0.001*
Sneg A8dl R	1.39 ± 2.97	8.46 ± 7.56	418‡	-1.47	<0.001	<0.001*
Sneg A9l L	2.19 ± 3.24	8.04 ± 6.34	635‡	-1.24	<0.001	<0.001*
Sneg A9l R	1.29 ± 2.46	7.91 ± 6.67	513‡	-1.43	<0.001	<0.001*
Sneg A6dl L	0.54 ± 1.04	5.06 ± 4.58	369‡	-1.35	<0.001	<0.001*
Sneg A6dl R	0.44 ± 1.2	5.47 ± 7.25	387‡	-1.34	<0.001	<0.001*
Sneg A6m L	0.41 ± 0.94	4.54 ± 3.95	383‡	-1.35	<0.001	<0.001*
Sneg A6m R	0.42 ± 0.87	4.7 ± 4.85	316‡	-1.39	<0.001	<0.001*
Sneg A9m L	0.81 ± 2.05	5.91 ± 5.88	365‡	-1.53	<0.001	<0.001*
Sneg A9m R	0.68 ± 1.73	5.21 ± 5.51	411‡	-1.41	<0.001	<0.001*
Sneg A10m L	1.04 ± 1.73	7.66 ± 5.92	511‡	-1.32	<0.001	<0.001*
Sneg A10m R	1.46 ± 2.67	7.97 ± 7.31	559‡	-1.32	<0.001	<0.001*
Sneg A9.46d L	0.72 ± 1.15	4.98 ± 4.15	367‡	-1.35	<0.001	<0.001*
Sneg A9.46d R	0.58 ± 1.2	5.23 ± 6.64	325‡	-1.30	<0.001	<0.001*
Sneg IFJ L	1.2 ± 2.32	6.43 ± 5.8	486‡	-1.27	<0.001	<0.001*
Sneg IFJ R	0.66 ± 1.66	6.03 ± 6.41	564‡	-1.22	<0.001	<0.001*
Sneg A46 L	0.48 ± 1.75	5.79 ± 6.16	515‡	-1.20	<0.001	<0.001*
Sneg A46 R	0.87 ± 1.56	6.66 ± 6.42	389‡	-1.26	<0.001	<0.001*
Sneg A9.46v L	1.08 ± 2.06	6.7 ± 6.14	593‡	-1.15	<0.001	<0.001*
Sneg A9.46v R	1.28 ± 2	7.11 ± 5.85	573‡	-1.15	<0.001	<0.001*
Sneg A8vl L	1.43 ± 2.27	6.51 ± 7.74	412‡	-1.49	<0.001	<0.001*
Sneg A8vl R	0.98 ± 1.5	7.58 ± 7.05	506‡	-1.35	<0.001	<0.001*
Sneg A6vl L	0.7 ± 1.86	5.72 ± 5.66	545‡	-1.29	<0.001	<0.001*
Sneg A6vl R	0.76 ± 1.75	6.5 ± 7.08	366‡	-1.39	<0.001	<0.001*
Sneg A44d L	0.96 ± 1.34	5.63 ± 6.97	530‡	-1.30	<0.001	<0.001*
Sneg A44d R	0.76 ± 2.14	5.72 ± 6.5	490‡	-1.18	<0.001	<0.001*
Sneg IFS L	0.91 ± 2.03	5.57 ± 5.26	546‡	-1.23	<0.001	<0.001*
Sneg IFS R	1.17 ± 1.77	5.87 ± 5.53	467‡	-1.27	<0.001	<0.001*
Sneg A45c L	1.58 ± 3.28	7.14 ± 5.88	744‡	-1.20	<0.001	<0.001*

Sneg A45c R	0.98 ± 2.55	6.6 ± 6.63	454‡	-1.28	<0.001	<0.001*
Sneg A45r L	1.48 ± 3.29	6.28 ± 6.4	702‡	-1.21	<0.001	<0.001*
Sneg A45r R	0.91 ± 2.31	6.64 ± 7.2	578‡	-1.19	<0.001	<0.001*
Sneg A44op L	1.23 ± 2.98	6.25 ± 5.43	659‡	-1.21	<0.001	<0.001*
Sneg A44op R	1.78 ± 2.41	7.64 ± 6.07	600‡	-1.29	<0.001	<0.001*
Sneg A44v L	1.44 ± 3.22	8.22 ± 8.44	559‡	-1.39	<0.001	<0.001*
Sneg A44v R	1.38 ± 2.99	8.17 ± 6.93	475‡	-1.43	<0.001	<0.001*
Sneg A12.47l L	0.99 ± 1.7	5 ± 5.27	657‡	-1.15	<0.001	<0.001*
Sneg A12.47l R	0.67 ± 1.4	5.55 ± 4.42	262‡	-1.37	<0.001	<0.001*
Sneg A4hf L	0.41 ± 1.21	3.67 ± 3.87	500‡	-1.34	<0.001	<0.001*
Sneg A4hf R	0.45 ± 1.1	4.71 ± 5.46	405‡	-1.45	<0.001	<0.001*
Sneg A6cdl L	0.56 ± 1.11	4.61 ± 4.78	376‡	-1.34	<0.001	<0.001*
Sneg A6cdl R	0.43 ± 0.84	4.6 ± 5.75	361‡	-1.25	<0.001	<0.001*
Sneg A4ul L	0.56 ± 1.34	4.96 ± 4.55	558‡	-1.21	<0.001	<0.001*
Sneg A4ul R	0.52 ± 1.37	4.75 ± 5.33	448‡	-1.31	<0.001	<0.001*
Sneg A4tl L	1.75 ± 2.59	6.11 ± 5.41	697‡	-1.25	<0.001	<0.001*
Sneg A4tl R	1.02 ± 1.8	7.22 ± 5.05	290‡	-1.55	<0.001	<0.001*
Sneg A6cvl L	0.91 ± 2.07	5.6 ± 6.16	475‡	-1.19	<0.001	<0.001*
Sneg A6cvl R	0.6 ± 1.81	5.46 ± 6.5	437‡	-1.27	<0.001	<0.001*
Sneg A1.2.3ll R	0.66 ± 1.07	3.54 ± 3.91	499‡	-1.18	<0.001	<0.001*
Sneg A4ll L	0.6 ± 1.3	4.87 ± 4.87	380‡	-1.24	<0.001	<0.001*
Sneg A4ll R	0.45 ± 0.8	4.64 ± 4.78	338‡	-1.38	<0.001	<0.001*
Sneg A41.42 L	0.41 ± 1.08	4.38 ± 4.52	477‡	-1.27	<0.001	<0.001*
Sneg A41.42 R	0.32 ± 0.7	3.8 ± 5.03	442‡	-1.16	<0.001	<0.001*
Sneg TE1.0.TE1.2 L	0.49 ± 1.32	4.44 ± 6.01	599‡	-1.14	<0.001	<0.001*
Sneg TE1.0.TE1.2 R	0.43 ± 0.96	4.51 ± 4.81	412‡	-1.25	<0.001	<0.001*
Sneg A22c L	0.71 ± 1.56	4.59 ± 5.36	606.5‡	-1.31	<0.001	<0.001*
Sneg A22c R	0.5 ± 0.82	3.85 ± 6.18	462‡	-1.23	<0.001	<0.001*
Sneg A38l L	1.34 ± 3.65	5.41 ± 5.53	929‡	-0.82	<0.001	<0.001*
Sneg A38l R	0.8 ± 2.31	3.9 ± 4.86	937‡	-1.01	<0.001	<0.001*
Sneg A22r L	0.68 ± 1.6	3.69 ± 4.74	713‡	-1.07	<0.001	<0.001*
Sneg A22r R	0.77 ± 2.17	4.69 ± 5.43	815‡	-1.03	<0.001	<0.001*
Sneg A37dl L	0.56 ± 1.15	5.24 ± 4.86	485‡	-1.31	<0.001	<0.001*
Sneg A37dl R	0.53 ± 1.09	6.67 ± 7.19	316‡	-1.57	<0.001	<0.001*
Sneg A37vl L	0.8 ± 0.89	5.12 ± 5.49	473‡	-1.19	<0.001	<0.001*
Sneg A37mv L	0.38 ± 0.9	3.65 ± 5.42	460‡	-1.20	<0.001	<0.001*
Sneg A37mv R	0.48 ± 1.1	4.6 ± 6.24	493‡	-1.25	<0.001	<0.001*
Sneg TL L	1.03 ± 2.29	5.58 ± 5.03	481‡	-1.42	<0.001	<0.001*
Sneg TL R	1.5 ± 3.69	5.51 ± 5.08	893‡	-1.08	<0.001	<0.001*
Sneg TH L	1.6 ± 2.95	6.47 ± 6.16	944‡	-0.69	<0.001	<0.001*
Sneg TH R	1.78 ± 3.37	6.38 ± 5.42	1048‡	-0.88	<0.001	<0.001*

Sneg rpSTS L	1.13 ± 3.1	5.77 ± 5.15	766‡	-1.16	<0.001	<0.001*
Sneg rpSTS R	0.97 ± 1.89	5.46 ± 5.81	535‡	-1.27	<0.001	<0.001*
Sneg cpSTS L	0.61 ± 1.57	5.21 ± 4.83	680‡	-1.13	<0.001	<0.001*
Sneg cpSTS R	0.64 ± 1.83	5.26 ± 5.85	604‡	-1.18	<0.001	<0.001*
Sneg A7r L	0.88 ± 1.66	6.42 ± 7.33	450‡	-1.41	<0.001	<0.001*
Sneg A7r R	0.66 ± 1.37	5.82 ± 7.33	416‡	-1.35	<0.001	<0.001*
Sneg A7c L	0.83 ± 1.78	5.51 ± 7.7	699‡	-1.18	<0.001	<0.001*
Sneg A7c R	0.76 ± 1.51	5.9 ± 6.77	462‡	-1.39	<0.001	<0.001*
Sneg A5l L	0.64 ± 1.82	4.63 ± 6.57	661‡	-1.01	<0.001	<0.001*
Sneg A5l R	0.75 ± 1.5	5.52 ± 6.38	472‡	-1.25	<0.001	<0.001*
Sneg A7ip L	0.58 ± 2.15	4.54 ± 6.38	554‡	-1.17	<0.001	<0.001*
Sneg A7ip R	0.56 ± 1.48	5.62 ± 6.46	593‡	-1.11	<0.001	<0.001*
Sneg A39c L	0.64 ± 1.64	6.06 ± 5.97	432‡	-1.36	<0.001	<0.001*
Sneg A39rd L	1.02 ± 2.24	6.27 ± 6.59	521‡	-1.26	<0.001	<0.001*
Sneg A40rd L	1.09 ± 1.96	6.13 ± 6.2	599‡	-1.22	<0.001	<0.001*
Sneg A40rd R	1.01 ± 1.27	5.52 ± 7.82	574‡	-1.13	<0.001	<0.001*
Sneg A40c L	0.93 ± 1.66	6.74 ± 7.67	425‡	-1.25	<0.001	<0.001*
Sneg A39rv L	1.04 ± 2.78	7.6 ± 7.22	541‡	-1.35	<0.001	<0.001*
Sneg A39rv R	0.91 ± 1.96	7.18 ± 6.4	423‡	-1.39	<0.001	<0.001*
Sneg A40rv L	0.58 ± 0.96	5.22 ± 6.72	517‡	-1.28	<0.001	<0.001*
Sneg A40rv R	0.72 ± 1.39	5.64 ± 9	497‡	-1.29	<0.001	<0.001*
Sneg A7m L	0.53 ± 1.3	6.24 ± 5.83	286‡	-1.44	<0.001	<0.001*
Sneg A7m R	0.79 ± 1.31	5.92 ± 5.82	371‡	-1.35	<0.001	<0.001*
Sneg A5m L	0.41 ± 0.62	3.3 ± 3.88	324‡	-1.18	<0.001	<0.001*
Sneg A5m R	0.45 ± 0.84	3.22 ± 4.53	299‡	-1.23	<0.001	<0.001*
Sneg dmPOS L	0.76 ± 1.38	6.13 ± 6.72	548‡	-1.24	<0.001	<0.001*
Sneg dmPOS R	0.88 ± 1.74	6.25 ± 5.6	504‡	-1.42	<0.001	<0.001*
Sneg A31 L	1.22 ± 2.7	8.02 ± 6.89	642‡	-1.31	<0.001	<0.001*
Sneg A31 R	1.4 ± 2.41	8.45 ± 6.33	464‡	-1.46	<0.001	<0.001*
Sneg A1.2.3ulhf L	0.47 ± 1.17	3.93 ± 5.69	466‡	-1.20	<0.001	<0.001*
Sneg A1.2.3ulhf R	0.39 ± 1	4.39 ± 5.24	419‡	-1.33	<0.001	<0.001*
Sneg A1.2.3tonIa L	0.75 ± 1.42	4.77 ± 5.02	620‡	-1.18	<0.001	<0.001*
Sneg A1.2.3tonIa R	0.72 ± 1.65	5.42 ± 6.04	567‡	-1.21	<0.001	<0.001*
Sneg A2 L	0.92 ± 2.38	5.33 ± 6.14	712‡	-1.04	<0.001	<0.001*
Sneg A2 R	0.57 ± 1.42	5.64 ± 8.06	565‡	-1.22	<0.001	<0.001*
Sneg G L	0.87 ± 1.28	3.76 ± 4.77	751‡	-1.05	<0.001	<0.001*
Sneg G R	1.03 ± 1.59	4.46 ± 4.46	641‡	-1.07	<0.001	<0.001*
Sneg vIa L	1.27 ± 2.32	4.62 ± 4.47	1016‡	-0.78	<0.001	<0.001*
Sneg vIa R	1.9 ± 3.61	5.07 ± 5.46	1400‡	-0.41	<0.001	<0.001*
Sneg dIa L	1.21 ± 1.79	5.47 ± 4.05	615‡	-1.23	<0.001	<0.001*
Sneg dIa R	1.52 ± 2.55	6.81 ± 4.62	555‡	-1.33	<0.001	<0.001*

Sneg vId.vIg L	1.16 ± 1.93	4.91 ± 6.59	741‡	-0.95	<0.001	<0.001*
Sneg vId.vIg R	0.77 ± 1.31	4.44 ± 4.46	638‡	-1.13	<0.001	<0.001*
Sneg dIg L	0.96 ± 2.02	4.71 ± 4.85	725.5‡	-1.20	<0.001	<0.001*
Sneg dIg R	0.63 ± 1.8	5.24 ± 4.55	644‡	-1.06	<0.001	<0.001*
Sneg dId L	1.21 ± 2.34	5.76 ± 5.89	697‡	-1.11	<0.001	<0.001*
Sneg dId R	1.1 ± 2.35	5.97 ± 5.6	605‡	-1.24	<0.001	<0.001*
Sneg A23d L	0.89 ± 1.88	7.34 ± 6.43	371‡	-1.44	<0.001	<0.001*
Sneg A23d R	0.98 ± 2.35	6.23 ± 6.32	382‡	-1.36	<0.001	<0.001*
Sneg A24rv L	1.31 ± 2.55	4.39 ± 4.76	958‡	-0.94	<0.001	<0.001*
Sneg A32p L	0.67 ± 1.36	5.37 ± 4.56	479‡	-1.35	<0.001	<0.001*
Sneg A32p R	0.85 ± 1.42	6.28 ± 6.49	502‡	-1.32	<0.001	<0.001*
Sneg A23v L	1.1 ± 2.47	6.73 ± 7.22	528‡	-1.36	<0.001	<0.001*
Sneg A23v R	0.97 ± 1.47	6.2 ± 6.83	450‡	-1.42	<0.001	<0.001*
Sneg A24cd L	0.81 ± 1.51	4.87 ± 5.81	448‡	-1.38	<0.001	<0.001*
Sneg A24cd R	0.82 ± 1.56	4.61 ± 4.53	486‡	-1.37	<0.001	<0.001*
Sneg A23c L	0.32 ± 0.43	2.52 ± 2.9	403‡	-1.32	<0.001	<0.001*
Sneg A23c R	0.45 ± 0.67	2.94 ± 3.12	513‡	-1.20	<0.001	<0.001*
Sneg A32sg R	1.65 ± 2.91	5.7 ± 5.53	897‡	-0.82	<0.001	<0.001*
Sneg cLinG L	0.43 ± 1.04	4.47 ± 4.66	468‡	-1.16	<0.001	<0.001*
Sneg cLinG R	0.43 ± 1.33	5.17 ± 6.62	564‡	-1.17	<0.001	<0.001*
Sneg rCunG L	0.32 ± 0.88	4.11 ± 5.3	547‡	-1.05	<0.001	<0.001*
Sneg rCunG R	0.36 ± 0.89	4.25 ± 5.75	584‡	-1.13	<0.001	<0.001*
Sneg cCunG R	0.78 ± 2.46	5.37 ± 5.58	878‡	-0.80	<0.001	<0.001*
Sneg rLinG L	0.46 ± 1.45	4.96 ± 6.76	793‡	-0.89	<0.001	<0.001*
Sneg rLinG R	0.52 ± 2.04	5.46 ± 7.13	708‡	-1.09	<0.001	<0.001*
Sneg vmPOS L	0.44 ± 1.06	4.28 ± 5.63	423‡	-1.27	<0.001	<0.001*
Sneg vmPOS R	0.5 ± 1.31	4.89 ± 5.5	455‡	-1.32	<0.001	<0.001*
Sneg mOccG L	0.99 ± 1.94	6.08 ± 5.75	510‡	-1.26	<0.001	<0.001*
Sneg mOccG R	0.75 ± 2.45	6.86 ± 7.27	638‡	-1.20	<0.001	<0.001*
Sneg V5.MT. L	0.49 ± 1.99	6.3 ± 6.68	578‡	-1.24	<0.001	<0.001*
Sneg V5.MT. R	0.78 ± 1.57	6.31 ± 7.16	627‡	-1.26	<0.001	<0.001*
Sneg msOccG L	0.88 ± 1.85	5.7 ± 6.03	532‡	-1.22	<0.001	<0.001*
Sneg msOccG R	1 ± 2.05	5.89 ± 5.26	633‡	-1.15	<0.001	<0.001*
Sneg lsOccG L	0.45 ± 1.26	4.54 ± 5.55	522‡	-1.18	<0.001	<0.001*
Sneg lsOccG R	0.44 ± 1.18	4.36 ± 6.82	526‡	-1.16	<0.001	<0.001*
Sneg lAmyg L	1.32 ± 2.29	3.8 ± 4.18	885‡	-1.02	<0.001	<0.001*
Sneg lAmyg R	1.09 ± 2.42	4.34 ± 4.77	957‡	-0.87	<0.001	<0.001*
Sneg rHipp L	0.98 ± 2.48	4.09 ± 4.84	886‡	-0.89	<0.001	<0.001*
Sneg rHipp R	2.22 ± 4.39	5.96 ± 5.36	1029‡	-0.92	<0.001	<0.001*
Sneg cHipp L	1.12 ± 1.42	4.85 ± 4.83	653‡	-1.13	<0.001	<0.001*
Sneg cHipp R	0.99 ± 1.56	4.44 ± 4.31	568‡	-1.08	<0.001	<0.001*

Sneg vCa L	0.95 ± 1.25	4.25 ± 3.66	524‡	-1.26	<0.001	<0.001*
Sneg vCa R	0.87 ± 1.15	3.81 ± 4.28	483‡	-1.29	<0.001	<0.001*
Sneg GP L	0.53 ± 1.4	3.94 ± 4.19	758‡	-1.04	<0.001	<0.001*
Sneg GP R	0.51 ± 1.03	3.75 ± 4.4	629‡	-1.21	<0.001	<0.001*
Sneg NAC L	1.03 ± 1.52	4.05 ± 3.98	682‡	-1.15	<0.001	<0.001*
Sneg vmPu L	0.52 ± 0.68	3.58 ± 3.74	535‡	-1.14	<0.001	<0.001*
Sneg vmPu R	0.67 ± 1.36	3.93 ± 4.27	614.5‡	-1.30	<0.001	<0.001*
Sneg dCa L	0.51 ± 1.14	4.28 ± 5.33	585‡	-1.15	<0.001	<0.001*
Sneg dCa R	0.54 ± 1.91	4.7 ± 4.36	617‡	-1.11	<0.001	<0.001*
Sneg dlPu L	0.46 ± 0.87	3.58 ± 4.37	698‡	-1.03	<0.001	<0.001*
Sneg dlPu R	0.44 ± 1.33	2.84 ± 2.83	771‡	-0.88	<0.001	<0.001*
Sneg mPFtha L	0.41 ± 0.7	3.17 ± 4.24	410‡	-1.12	<0.001	<0.001*
Sneg mPFtha R	0.35 ± 0.52	3.3 ± 5.33	356.5‡	-1.21	<0.001	<0.001*
Sneg mPMtha L	1.89 ± 2.57	4.38 ± 4.5	1138‡	-0.80	<0.001	<0.001*
Sneg mPMtha R	0.48 ± 0.82	3.02 ± 3.11	411‡	-1.25	<0.001	<0.001*
Sneg Stha L	0.83 ± 1.32	3.89 ± 3.49	585‡	-1.00	<0.001	<0.001*
Sneg Stha R	0.64 ± 1.62	3.81 ± 4.05	634‡	-1.20	<0.001	<0.001*
Sneg rTtha L	0.56 ± 1.04	4.56 ± 5.83	323‡	-1.36	<0.001	<0.001*
Sneg rTtha R	0.99 ± 2.47	4.55 ± 6.93	818‡	-0.97	<0.001	<0.001*
Sneg PPtha L	0.33 ± 0.76	2.78 ± 4.27	551‡	-0.99	<0.001	<0.001*
Sneg PPtha R	0.31 ± 0.88	3.01 ± 4.13	485‡	-1.11	<0.001	<0.001*
Sneg Otha L	0.47 ± 0.79	3.83 ± 4.87	299‡	-1.32	<0.001	<0.001*
Sneg Otha R	0.67 ± 1.52	4.26 ± 5.99	563‡	-1.23	<0.001	<0.001*
Sneg cTtha L	0.7 ± 1.38	4.49 ± 5.2	572.5‡	-1.12	<0.001	<0.001*
Sneg cTtha R	1.26 ± 2.09	5.56 ± 6.12	751‡	-1.06	<0.001	<0.001*
Sneg lPFtha L	0.53 ± 1.06	2.87 ± 4.68	698.5‡	-0.89	<0.001	<0.001*
Sneg lPFtha R	0.31 ± 0.72	3.34 ± 4.76	448‡	-1.17	<0.001	<0.001*
Sneg Buckner2011 17Networks 1	0.69 ± 2.21	5.27 ± 5.38	809‡	-0.90	<0.001	<0.001*
Sneg Buckner2011 17Networks 2	0.86 ± 1.73	3.86 ± 4.36	710‡	-1.11	<0.001	<0.001*
Sneg Buckner2011 17Networks 4	0.3 ± 0.89	2.28 ± 3.06	618‡	-1.05	<0.001	<0.001*
Sneg Buckner2011 17Networks 5	2.03 ± 2.81	4.3 ± 5.07	1222‡	-0.60	<0.001	<0.001*
Sneg Buckner2011 17Networks 9	0.47 ± 0.82	2.79 ± 4.1	565‡	-1.01	<0.001	<0.001*

Results are reported as mean ± standard deviation. For non-normally distributed variables, results are reported as median ± interquantile range. Cohen's d values are reported for each region derived from Brainnetome atlas. Abbreviations: Spos, positive strength; Sneg, negative strength; R, right; L; left. †parametric two-sample t-test; ‡non-parametric Mann-Whitney U test; *FDR-corrected q<0.05.

Appendix 5. Differences in grey matter volumes for each region between the GM-based clusters.

Variable	Cluster 1 (N = 150)	Cluster 2 (N = 194)	t / U	d	p	q
Accumbens Area R	0.32 ± 0.06	0.33 ± 0.06	11857‡	-0.33	0.003	0.004*
Accumbens Area L	0.37 ± 0.06	0.38 ± 0.05	12228.5‡	-0.30	0.011	0.012*
Amygdala R	0.81 ± 0.09	0.85 ± 0.09	-4.59†	-0.50	<0.001	<0.001*
Amygdala L	0.82 ± 0.09	0.87 ± 0.09	-5.2†	-0.57	<0.001	<0.001*
Caudate R	2.67 ± 0.44	2.84 ± 0.43	10853‡	-0.42	<0.001	<0.001*
Caudate L	2.62 ± 0.43	2.77 ± 0.4	10808.5‡	-0.45	<0.001	<0.001*
Cerebellum Exterior R	39.85 ± 5.72	40.62 ± 6.03	12893‡	-0.21	0.070	0.074
Cerebellum Exterior L	39.7 ± 5.99	40.61 ± 5.27	12676‡	-0.23	0.041	0.043*
Hippocampus R	3.02 ± 0.31	3.14 ± 0.3	-3.76†	-0.41	<0.001	<0.001*
Hippocampus L	2.8 ± 0.3	2.95 ± 0.29	-4.83†	-0.53	<0.001	<0.001*
Pallidum R	0.16 ± 0.09	0.15 ± 0.1	15304‡	-0.05	0.410	0.42
Pallidum L	0.19 ± 0.09	0.18 ± 0.09	13729.5‡	-0.15	0.370	0.386
Putamen R	3.18 ± 0.58	3.37 ± 0.61	11831‡	-0.36	0.003	0.003*
Putamen L	3.35 ± 0.61	3.55 ± 0.56	10510‡	-0.51	<0.001	<0.001*
Thalamus Proper R	4.33 ± 0.59	4.98 ± 0.64	-9.82†	-1.05	<0.001	<0.001*
Thalamus Proper L	4.54 ± 0.6	4.99 ± 0.58	-6.94†	-0.76	<0.001	<0.001*
VentralDC R	0.86 ± 0.16	0.9 ± 0.14	11654.5‡	-0.36	0.002	0.002*
VentralDC L	0.87 ± 0.15	0.91 ± 0.15	11329‡	-0.39	<0.001	<0.001*
Optic Chiasm R	0.09 ± 0.03	0.09 ± 0.03	0.89†	-0.10	0.374	0.387
Cerebellar Vermal Lobules I-V	3.49 ± 0.57	3.41 ± 0.47	14957.5‡	-0.06	0.656	0.656
Cerebellar Vermal Lobules VI-VII	1.69 ± 0.24	1.66 ± 0.27	15230.5‡	-0.05	0.457	0.465
Cerebellar Vermal Lobules VIII-X	2.07 ± 0.31	2.09 ± 0.32	14066‡	-0.07	0.597	0.602
Basal Forebrain R	0.36 ± 0.06	0.38 ± 0.07	10254.5‡	-0.57	<0.001	<0.001*
Basal Forebrain L	0.35 ± 0.07	0.37 ± 0.07	10217‡	-0.56	<0.001	<0.001*
Anterior cingulate gyrus R	2.87 ± 0.58	3.07 ± 0.7	11448‡	-0.38	<0.001	<0.001*
Anterior cingulate gyrus L	3.35 ± 0.67	3.67 ± 0.65	9418‡	-0.64	<0.001	<0.001*
Anterior insula R	3.26 ± 0.54	3.51 ± 0.61	8625.5‡	-0.76	<0.001	<0.001*
Anterior insula L	3.3 ± 0.54	3.54 ± 0.61	9142.5‡	-0.64	<0.001	<0.001*
Anterior orbital gyrus R	1.38 ± 0.26	1.48 ± 0.26	9797‡	-0.60	<0.001	<0.001*
Anterior orbital gyrus L	1.28 ± 0.21	1.37 ± 0.25	9457‡	-0.67	<0.001	<0.001*
Angular gyrus R	7.6 ± 1.39	8.33 ± 1.45	8652‡	-0.77	<0.001	<0.001*
Angular gyrus L	6.49 ± 1.22	7.05 ± 1.2	9623‡	-0.63	<0.001	<0.001*
Calcarine cortex R	2.2 ± 0.34	2.41 ± 0.46	9787‡	-0.56	<0.001	<0.001*
Calcarine cortex L	2.22 ± 0.43	2.42 ± 0.52	10622‡	-0.50	<0.001	<0.001*
Central operculum R	2.84 ± 0.5	3.22 ± 0.61	8508.5‡	-0.75	<0.001	<0.001*
Central operculum L	2.82 ± 0.46	3.17 ± 0.67	8113‡	-0.79	<0.001	<0.001*
Cuneus R	3.44 ± 0.64	3.81 ± 0.76	8408‡	-0.79	<0.001	<0.001*

Cuneus L	3.23 ± 0.57	3.52 ± 0.68	9209‡	-0.69	<0.001	<0.001*
Ententorhinal area R	1.81 ± 0.31	1.92 ± 0.26	10162.5‡	-0.56	<0.001	<0.001*
Ententorhinal area L	1.74 ± 0.21	1.87 ± 0.2	-5.62†	-0.62	<0.001	<0.001*
Frontal operculum R	1.35 ± 0.26	1.49 ± 0.3	8569‡	-0.74	<0.001	<0.001*
Frontal operculum L	1.31 ± 0.26	1.45 ± 0.29	8571.5‡	-0.75	<0.001	<0.001*
Frontal pole R	2.94 ± 0.51	3.17 ± 0.52	10294‡	-0.50	<0.001	<0.001*
Frontal pole L	2.7 ± 0.41	2.93 ± 0.39	-5.24†	-0.57	<0.001	<0.001*
Fusiform gyrus R	5.95 ± 0.96	6.41 ± 0.94	9525.5‡	-0.63	<0.001	<0.001*
Fusiform gyrus L	5.66 ± 0.96	6.15 ± 0.83	8951‡	-0.72	<0.001	<0.001*
Gyrus rectus R	1.69 ± 0.32	1.84 ± 0.34	10019‡	-0.54	<0.001	<0.001*
Gyrus rectus L	1.65 ± 0.24	1.81 ± 0.29	9112‡	-0.67	<0.001	<0.001*
Inferior occipital gyrus R	4.73 ± 0.74	5 ± 0.83	9520‡	-0.65	<0.001	<0.001*
Inferior occipital gyrus L	4.54 ± 0.67	4.9 ± 0.89	9179‡	-0.70	<0.001	<0.001*
Inferior temporal gyrus R	9.48 ± 1.17	10.27 ± 1.17	-6.19†	-0.67	<0.001	<0.001*
Inferior temporal gyrus L	9.23 ± 1.72	10.02 ± 1.5	9319‡	-0.67	<0.001	<0.001*
Lingual gyrus R	6.62 ± 1.05	7.09 ± 1.07	9954‡	-0.59	<0.001	<0.001*
Lingual gyrus L	6.17 ± 0.95	6.51 ± 1	9926‡	-0.58	<0.001	<0.001*
Lateral orbital gyrus R	1.63 ± 0.31	1.79 ± 0.29	9277‡	-0.63	<0.001	<0.001*
Lateral orbital gyrus L	1.73 ± 0.24	1.83 ± 0.37	10402‡	-0.54	<0.001	<0.001*
Middle cingulate gyrus R	3.22 ± 0.54	3.53 ± 0.62	8885‡	-0.73	<0.001	<0.001*
Middle cingulate gyrus L	3.13 ± 0.5	3.4 ± 0.56	8683‡	-0.73	<0.001	<0.001*
Medial frontal cortex R	1.26 ± 0.27	1.43 ± 0.29	8776‡	-0.69	<0.001	<0.001*
Medial frontal cortex L	1.3 ± 0.23	1.47 ± 0.32	8048‡	-0.82	<0.001	<0.001*
Middle frontal gyrus R	13.26 ± 2.07	14.53 ± 2.54	8863‡	-0.69	<0.001	<0.001*
Middle frontal gyrus L	13.18 ± 2.16	14.72 ± 2.32	8416‡	-0.74	<0.001	<0.001*
Middle occipital gyrus R	3.66 ± 0.52	4.1 ± 0.55	-7.56†	-0.82	<0.001	<0.001*
Middle occipital gyrus L	4.24 ± 0.62	4.67 ± 0.57	-6.53†	-0.72	<0.001	<0.001*
Medial orbital gyrus R	3.18 ± 0.53	3.43 ± 0.51	9525‡	-0.61	<0.001	<0.001*
Medial orbital gyrus L	3.36 ± 0.44	3.63 ± 0.53	8805.5‡	-0.73	<0.001	<0.001*
Postcentral gyrus medial segment R	0.73 ± 0.19	0.79 ± 0.19	10864‡	-0.47	<0.001	<0.001*
Postcentral gyrus medial segment L	0.72 ± 0.17	0.76 ± 0.16	11793‡	-0.38	0.003	0.003*
Precentral gyrus medial segment R	1.84 ± 0.37	2.03 ± 0.4	9078‡	-0.70	<0.001	<0.001*
Precentral gyrus medial segment L	1.89 ± 0.35	2.01 ± 0.35	10488‡	-0.51	<0.001	<0.001*
Superior frontal gyrus medial segment R	5.56 ± 1.19	6.16 ± 1.12	8819‡	-0.71	<0.001	<0.001*
Superior frontal gyrus medial segment L	4.79 ± 0.83	5.26 ± 0.79	8182‡	-0.79	<0.001	<0.001*
Middle temporal gyrus R	11.01 ± 1.78	12.02 ± 1.81	8655‡	-0.76	<0.001	<0.001*
Middle temporal gyrus L	10.47 ± 1.86	11.46 ± 1.8	8843‡	-0.75	<0.001	<0.001*
Occipital pole R	2.56 ± 0.49	2.69 ± 0.54	11949‡	-0.35	0.004	0.005*
Occipital pole L	2.77 ± 0.53	2.84 ± 0.59	12061‡	-0.31	0.007	0.007*
Occipital fusiform gyrus R	2.96 ± 0.48	3.15 ± 0.48	9459‡	-0.65	<0.001	<0.001*
Occipital fusiform gyrus L	3.07 ± 0.51	3.26 ± 0.52	9643.5‡	-0.60	<0.001	<0.001*

Opercular part of the inferior frontal gyrus R	2.28 ± 0.41	2.57 ± 0.5	8790‡	-0.72	<0.001	<0.001*
Opercular part of the inferior frontal gyrus L	2.21 ± 0.38	2.37 ± 0.5	9744‡	-0.62	<0.001	<0.001*
Orbital part of the inferior frontal gyrus R	1.01 ± 0.2	1.12 ± 0.26	8585‡	-0.74	<0.001	<0.001*
Orbital part of the inferior frontal gyrus L	1.16 ± 0.26	1.27 ± 0.29	10115‡	-0.54	<0.001	<0.001*
Posterior cingulate gyrus R	2.91 ± 0.46	3.23 ± 0.5	7933‡	-0.83	<0.001	<0.001*
Posterior cingulate gyrus L	3.29 ± 0.5	3.67 ± 0.61	8615‡	-0.72	<0.001	<0.001*
Precuneus R	8.14 ± 1.26	9.13 ± 1.34	7481‡	-0.91	<0.001	<0.001*
Precuneus L	8.19 ± 1.27	9.05 ± 1.47	8676‡	-0.71	<0.001	<0.001*
Pparahippocampal gyrus R	2.65 ± 0.29	2.78 ± 0.27	-4.45†	-0.49	<0.001	<0.001*
Parahippocampal gyrus L	2.76 ± 0.37	2.9 ± 0.4	10758‡	-0.48	<0.001	<0.001*
Posterior insula R	1.73 ± 0.31	1.9 ± 0.31	8862‡	-0.70	<0.001	<0.001*
Posterior insula L	1.63 ± 0.3	1.79 ± 0.33	8787.5‡	-0.71	<0.001	<0.001*
Parietal operculum R	1.34 ± 0.3	1.55 ± 0.4	8331‡	-0.76	<0.001	<0.001*
Parietal operculum L	1.64 ± 0.33	1.9 ± 0.41	7848‡	-0.81	<0.001	<0.001*
Postcentral gyrus R	7.13 ± 1.2	7.86 ± 1.23	8612‡	-0.75	<0.001	<0.001*
Postcentral gyrus L	7.86 ± 1.29	8.53 ± 1.35	9089‡	-0.69	<0.001	<0.001*
Posterior orbital gyrus R	2.17 ± 0.37	2.4 ± 0.49	9268‡	-0.66	<0.001	<0.001*
Posterior orbital gyrus L	2.31 ± 0.4	2.51 ± 0.42	10253‡	-0.49	<0.001	<0.001*
Planum polare R	1.26 ± 0.24	1.43 ± 0.26	8156.5‡	-0.78	<0.001	<0.001*
Planum polare L	1.43 ± 0.28	1.61 ± 0.29	7892‡	-0.79	<0.001	<0.001*
Precentral gyrus R	8.99 ± 1.41	9.83 ± 1.47	8598‡	-0.76	<0.001	<0.001*
Precentral gyrus L	9.1 ± 1.43	9.76 ± 1.68	8788‡	-0.74	<0.001	<0.001*
Planum temporale R	1.36 ± 0.26	1.51 ± 0.3	8787‡	-0.69	<0.001	<0.001*
Planum temporale L	1.43 ± 0.3	1.64 ± 0.43	9263‡	-0.65	<0.001	<0.001*
Subcallosal area R	0.9 ± 0.17	0.98 ± 0.21	9919‡	-0.57	<0.001	<0.001*
Subcallosal area L	0.94 ± 0.14	1.02 ± 0.16	-4.73†	-0.51	<0.001	<0.001*
Superior frontal gyrus R	10.9 ± 2.1	11.79 ± 1.94	9566‡	-0.65	<0.001	<0.001*
Superior frontal gyrus L	11.03 ± 2.05	11.92 ± 2.1	9263‡	-0.69	<0.001	<0.001*
Supplementary motor cortex R	3.78 ± 0.65	4.28 ± 0.68	8461‡	-0.76	<0.001	<0.001*
Supplementary motor cortex L	4.01 ± 0.75	4.44 ± 0.8	9004‡	-0.70	<0.001	<0.001*
Supramarginal gyrus R	5.76 ± 1.15	6.5 ± 1.24	8915‡	-0.71	<0.001	<0.001*
Supramarginal gyrus L	6.36 ± 1.18	6.87 ± 1.16	9524‡	-0.62	<0.001	<0.001*
Superior occipital gyrus R	2.91 ± 0.46	3.09 ± 0.56	10310‡	-0.54	<0.001	<0.001*
Superior occipital gyrus L	2.46 ± 0.42	2.61 ± 0.48	10326‡	-0.53	<0.001	<0.001*
Superior parietal lobule R	7.48 ± 0.94	7.98 ± 0.99	-4.77†	-0.52	<0.001	<0.001*
Superior parietal lobule L	7.8 ± 0.99	8.5 ± 1.11	-6.16†	-0.66	<0.001	<0.001*
Superior temporal gyrus R	5.38 ± 1.03	5.89 ± 0.94	9086‡	-0.67	<0.001	<0.001*
Superior temporal gyrus L	5.11 ± 0.72	5.55 ± 0.69	-5.76†	-0.63	<0.001	<0.001*
Temporal pole R	7.26 ± 1.18	7.68 ± 1.19	10531‡	-0.48	<0.001	<0.001*
Temporal pole L	7.17 ± 1.22	7.74 ± 1.26	9661‡	-0.61	<0.001	<0.001*
Triangular part of the inferior frontal gyrus R	2.55 ± 0.35	2.78 ± 0.4	-5.69†	-0.61	<0.001	<0.001*

Triangular part of the inferior frontal gyrus L	2.54 ± 0.47	2.79 ± 0.57	9726‡	-0.59	<0.001	<0.001*
Transverse temporal gyrus R	0.85 ± 0.22	0.99 ± 0.21	7260‡	-0.93	<0.001	<0.001*
Transverse temporal gyrus L	0.94 ± 0.23	1.11 ± 0.24	8120‡	-0.76	<0.001	<0.001*

Results are reported as mean ± standard deviation. For non-normally distributed variables, results are reported as median ± interquantile range. Cohen's d values are reported for each region derived from Neuromorphometrics atlas. Abbreviations: R, right; L; left. †parametric two-sample t-test; ‡non-parametric Mann-Whitney U test; *FDR-corrected q<0.05.

Appendix 6 Differences in cortical thickness for each region between the CT-based clusters.

Variable	Cluster 1 (N = 149)	Cluster 2 (N = 195)	t / U	d	p	q
bankssts L	2.26 ± 0.12	2.41 ± 0.12	-11.14†	-1.21	<0.001	<0.001*
bankssts R	2.32 ± 0.15	2.44 ± 0.15	5673.5‡	-1.20	<0.001	<0.001*
caudalanteriorcingulate L	2.32 ± 0.21	2.42 ± 0.2	-4.59†	-0.50	<0.001	<0.001*
caudalanteriorcingulate R	2.24 ± 0.19	2.34 ± 0.18	-5.01†	-0.55	<0.001	<0.001*
caudalmiddlefrontal L	2.28 ± 0.15	2.45 ± 0.18	4389.5‡	-1.38	<0.001	<0.001*
caudalmiddlefrontal R	2.27 ± 0.19	2.46 ± 0.19	4222‡	-1.45	<0.001	<0.001*
cuneus L	1.8 ± 0.18	1.9 ± 0.15	6949‡	-1.00	<0.001	<0.001*
cuneus R	1.8 ± 0.14	1.92 ± 0.15	6876.5‡	-0.96	<0.001	<0.001*
entorhinal L	3.33 ± 0.41	3.42 ± 0.35	11413‡	-0.41	<0.001	<0.001*
entorhinal R	3.36 ± 0.44	3.49 ± 0.41	10426‡	-0.55	<0.001	<0.001*
fusiform L	2.37 ± 0.1	2.51 ± 0.1	-12.79†	-1.39	<0.001	<0.001*
fusiform R	2.4 ± 0.13	2.55 ± 0.16	4036‡	-1.50	<0.001	<0.001*
inferiorparietal L	2.22 ± 0.09	2.37 ± 0.09	-15.27†	-1.67	<0.001	<0.001*
inferiorparietal R	2.22 ± 0.12	2.38 ± 0.12	2705‡	-1.76	<0.001	<0.001*
inferiortemporal L	2.48 ± 0.11	2.62 ± 0.1	-12.34†	-1.36	<0.001	<0.001*
inferiortemporal R	2.53 ± 0.13	2.69 ± 0.13	5154‡	-1.30	<0.001	<0.001*
isthmuscingulate L	2.18 ± 0.16	2.29 ± 0.15	-6.46†	-0.71	<0.001	<0.001*
isthmuscingulate R	2.16 ± 0.16	2.27 ± 0.17	-6.81†	-0.73	<0.001	<0.001*
lateraloccipital L	2.02 ± 0.15	2.15 ± 0.13	5755.5‡	-1.17	<0.001	<0.001*
lateraloccipital R	2.06 ± 0.13	2.18 ± 0.13	5554‡	-1.16	<0.001	<0.001*
lateralorbitofrontal L	2.5 ± 0.11	2.63 ± 0.1	-11.36†	-1.26	<0.001	<0.001*
lateralorbitofrontal R	2.4 ± 0.11	2.53 ± 0.1	-11.94†	-1.31	<0.001	<0.001*
lingual L	1.91 ± 0.11	2.04 ± 0.11	-10.83†	-1.18	<0.001	<0.001*
lingual R	1.92 ± 0.12	2.04 ± 0.15	6320‡	-1.08	<0.001	<0.001*
medialorbitofrontal L	2.24 ± 0.12	2.36 ± 0.11	-10.04†	-1.10	<0.001	<0.001*
medialorbitofrontal R	2.3 ± 0.12	2.4 ± 0.1	-8.05†	-0.89	<0.001	<0.001*
middletemporal L	2.51 ± 0.12	2.67 ± 0.12	-11.84†	-1.30	<0.001	<0.001*
middletemporal R	2.52 ± 0.12	2.7 ± 0.11	-14.12†	-1.56	<0.001	<0.001*
parahippocampal L	2.12 ± 0.19	2.24 ± 0.18	-5.95†	-0.65	<0.001	<0.001*
parahippocampal R	2.22 ± 0.19	2.37 ± 0.18	-7.63†	-0.83	<0.001	<0.001*
paracentral L	2.11 ± 0.16	2.25 ± 0.16	5894‡	-1.08	<0.001	<0.001*

paracentral R	2.1 ± 0.16	2.24 ± 0.19	6590.5‡	-1.02	<0.001	<0.001*
parsopercularis L	2.33 ± 0.17	2.49 ± 0.15	4857.5‡	-1.37	<0.001	<0.001*
parsopercularis R	2.31 ± 0.13	2.47 ± 0.12	-11.74†	-1.28	<0.001	<0.001*
parsorbitalis L	2.33 ± 0.18	2.48 ± 0.17	5508‡	-1.23	<0.001	<0.001*
parsorbitalis R	2.32 ± 0.2	2.49 ± 0.18	5954‡	-1.17	<0.001	<0.001*
parstriangularis L	2.23 ± 0.14	2.36 ± 0.15	4950‡	-1.32	<0.001	<0.001*
parstriangularis R	2.22 ± 0.13	2.37 ± 0.12	-10.84†	-1.20	<0.001	<0.001*
pericalcarine L	1.63 ± 0.13	1.76 ± 0.12	-9†	-0.99	<0.001	<0.001*
pericalcarine R	1.67 ± 0.17	1.77 ± 0.17	9140.5‡	-0.65	<0.001	<0.001*
postcentral L	1.89 ± 0.13	2.02 ± 0.18	5937‡	-1.13	<0.001	<0.001*
postcentral R	1.9 ± 0.15	2.06 ± 0.17	5395‡	-1.23	<0.001	<0.001*
posteriorcingulate L	2.17 ± 0.1	2.3 ± 0.1	-11.41†	-1.25	<0.001	<0.001*
posteriorcingulate R	2.14 ± 0.12	2.27 ± 0.12	-10.29†	-1.12	<0.001	<0.001*
precentral L	2.14 ± 0.16	2.3 ± 0.22	5910‡	-1.09	<0.001	<0.001*
precentral R	2.14 ± 0.19	2.31 ± 0.19	5187.5‡	-1.23	<0.001	<0.001*
precuneus L	2.19 ± 0.1	2.31 ± 0.08	-12.26†	-1.36	<0.001	<0.001*
precuneus R	2.17 ± 0.13	2.32 ± 0.14	4057‡	-1.46	<0.001	<0.001*
rostralanteriorcingulate L	2.46 ± 0.16	2.59 ± 0.13	-8.04†	-0.89	<0.001	<0.001*
rostralanteriorcingulate R	2.54 ± 0.14	2.64 ± 0.14	-6.54†	-0.71	<0.001	<0.001*
rostralmiddlefrontal L	2.15 ± 0.14	2.28 ± 0.12	4350.5‡	-1.45	<0.001	<0.001*
rostralmiddlefrontal R	2.15 ± 0.14	2.27 ± 0.11	4850‡	-1.34	<0.001	<0.001*
superiorfrontal L	2.4 ± 0.16	2.58 ± 0.17	4418.5‡	-1.41	<0.001	<0.001*
superiorfrontal R	2.4 ± 0.16	2.58 ± 0.17	3786.5‡	-1.51	<0.001	<0.001*
superiorparietal L	2.03 ± 0.12	2.16 ± 0.15	4390‡	-1.35	<0.001	<0.001*
superiorparietal R	2.02 ± 0.12	2.16 ± 0.12	4182.5‡	-1.44	<0.001	<0.001*
superiortemporal L	2.43 ± 0.14	2.63 ± 0.12	-14.05†	-1.55	<0.001	<0.001*
superiortemporal R	2.48 ± 0.13	2.67 ± 0.13	-13.52†	-1.48	<0.001	<0.001*
supramarginal L	2.25 ± 0.14	2.4 ± 0.13	3837‡	-1.56	<0.001	<0.001*
supramarginal R	2.26 ± 0.13	2.41 ± 0.13	3306‡	-1.65	<0.001	<0.001*
frontalpole L	2.23 ± 0.19	2.42 ± 0.19	-9.17†	-1.00	<0.001	<0.001*
frontalpole R	2.2 ± 0.19	2.36 ± 0.18	-7.79†	-0.85	<0.001	<0.001*
temporalpole L	3.41 ± 0.4	3.65 ± 0.31	7603‡	-0.95	<0.001	<0.001*
temporalpole R	3.52 ± 0.35	3.72 ± 0.36	8915‡	-0.73	<0.001	<0.001*
transversetemporal L	2.02 ± 0.2	2.2 ± 0.26	6561‡	-1.03	<0.001	<0.001*
transversetemporal R	2.08 ± 0.18	2.23 ± 0.18	-7.97†	-0.87	<0.001	<0.001*
insula L	2.94 ± 0.22	3.1 ± 0.21	6559‡	-1.07	<0.001	<0.001*
insula R	2.93 ± 0.25	3.11 ± 0.21	6780‡	-1.06	<0.001	<0.001*

Results are reported as mean ± standard deviation. For non-normally distributed variables, results are reported as median ± interquantile range. Cohen's d values are reported for each region derived from the Desikian-Killiany atlas. Abbreviations: R, right; L; left. †parametric two-sample t-test; ‡non-parametric Mann-Whitney U test; *FDR-corrected $q<0.05$.

Appendix 7. Differences in axial diffusivity values for each tract between the AD-based clusters

Variable	Cluster 1 (N = 120)	Cluster 2 (N = 155)	t / U	d	p	q
ACR L	0.001 ± 0	0.001 ± 0	13695‡	0.87	<0.001	<0.001*
ACR R	0.001 ± 0	0.001 ± 0	5.53†	0.67	<0.001	<0.001*
ALIC L	0.001 ± 0	0.001 ± 0	13249.5‡	0.63	<0.001	<0.001*
ALIC R	0.001 ± 0	0.001 ± 0	12760‡	0.55	<0.001	<0.001*
BCC	0.002 ± 0	0.002 ± 0	3.86†	0.48	<0.001	<0.001*
CC	0.002 ± 0	0.002 ± 0	13108‡	0.73	<0.001	<0.001*
CGC L	0.001 ± 0	0.001 ± 0	6.43†	0.78	<0.001	<0.001*
CGC R	0.001 ± 0	0.001 ± 0	7.51†	0.91	<0.001	<0.001*
CGH L	0.001 ± 0	0.001 ± 0	12689‡	0.54	<0.001	<0.001*
CGH R	0.001 ± 0	0.001 ± 0	11903‡	0.45	<0.001	<0.001*
CR L	0.001 ± 0	0.001 ± 0	16271‡	1.59	<0.001	<0.001*
CR R	0.001 ± 0	0.001 ± 0	15886‡	1.45	<0.001	<0.001*
CST L	0.001 ± 0	0.001 ± 0	8904.5‡	-0.07	0.55	0.56
CST R	0.001 ± 0	0.001 ± 0	9395‡	-0.07	0.89	0.89
EC L	0.001 ± 0	0.001 ± 0	6.69†	0.82	<0.001	<0.001*
EC R	0.001 ± 0	0.001 ± 0	11251‡	0.38	0.00	0.00
FX	0.002 ± 0	0.002 ± 0	3.7†	0.45	<0.001	<0.001*
FX ST L	0.001 ± 0	0.001 ± 0	6.21†	0.76	<0.001	<0.001*
FX ST R	0.001 ± 0	0.001 ± 0	13581‡	0.84	<0.001	<0.001*
GCC	0.002 ± 0	0.001 ± 0	5.91†	0.71	<0.001	<0.001*
IC L	0.001 ± 0	0.001 ± 0	11.98†	1.47	<0.001	<0.001*
IC R	0.001 ± 0	0.001 ± 0	15030‡	1.19	<0.001	<0.001*
IFO L	0.001 ± 0	0.001 ± 0	11048‡	0.29	0.01	0.01
IFO R	0.001 ± 0	0.001 ± 0	4.39†	0.54	<0.001	<0.001*
PCR L	0.001 ± 0	0.001 ± 0	14187‡	1.02	<0.001	<0.001*
PCR R	0.001 ± 0	0.001 ± 0	14863‡	1.14	<0.001	<0.001*
PLIC L	0.001 ± 0	0.001 ± 0	10.63†	1.31	<0.001	<0.001*
PLIC R	0.001 ± 0	0.001 ± 0	5.41†	0.66	<0.001	<0.001*
PTR L	0.002 ± 0	0.001 ± 0	12778‡	0.68	<0.001	<0.001*
PTR R	0.002 ± 0	0.001 ± 0	13448‡	0.73	<0.001	<0.001*
RLIC L	0.001 ± 0	0.001 ± 0	14243‡	0.92	<0.001	<0.001*
RLIC R	0.001 ± 0	0.001 ± 0	15312‡	1.25	<0.001	<0.001*
SCC	0.002 ± 0	0.002 ± 0	12198‡	0.58	<0.001	<0.001*
SCR L	0.001 ± 0	0.001 ± 0	11.52†	1.4	<0.001	<0.001*
SCR R	0.001 ± 0	0.001 ± 0	14711‡	1.11	<0.001	<0.001*
SFO L	0.001 ± 0	0.001 ± 0	10.37†	1.27	<0.001	<0.001*
SFO R	0.001 ± 0	0.001 ± 0	12426‡	0.66	<0.001	<0.001*

SLF L	0.001 ± 0	0.001 ± 0	12.14†	1.47	<0.001	<0.001*
SLF R	0.001 ± 0	0.001 ± 0	7.34†	0.89	<0.001	<0.001*
SS L	0.001 ± 0	0.001 ± 0	13638‡	0.82	<0.001	<0.001*
SS R	0.001 ± 0	0.001 ± 0	6.06†	0.73	<0.001	<0.001*
UNC L	0.002 ± 0.001	0.002 ± 0	11951‡	0.57	<0.001	<0.001*
UNC R	0.002 ± 0.001	0.002 ± 0	11665‡	0.47	<0.001	<0.001*

Results are reported as mean ± standard deviation. For non-normally distributed variables, results are reported as median ± interquantile range. Cohen's d values are reported for each tract derived from the JHU atlas. Abbreviations: ACR, anterior corona radiata; ALIC, anterior limb of internal capsule; BCC, body of corpus callosum; CC, corpus callosum; CGC, cingulate gyrus; CGH, perihippocampal cingulum tract; CR, corona radiata; CST, cortico-spinal tract; EC, external capsule; FX, fornix; FXST, fornix - stria terminalis; GCC, genu of corpus callosum; IC, internal capsule; IFO, inferior fronto-occipital fasciculus; PCR, posterior corona radiata; PLIC, posterior limb of internal capsule; PTR, posterior thalamic radiation; RLIC, retrolenticular limb of the internal capsule; SCC, splenium of corpus callosum; SCR, superior corona radiata; SFO, superior fronto-occipital fasciculus; SS, sagittal stratum; UNC, uncinate fasciculus; R, right; L; left. †parametric two-sample t-test; ‡non-parametric Mann-Whitney U test; *FDR-corrected q<0.05.

Appendix 8. Differences in fractional anisotropy values for each tract between the FA-based clusters

Variable	Cluster 1 (N = 121)	Cluster 2 (N = 154)	t / U	d	p	q
ACR L	0.42 ± 0.03	0.38 ± 0.03	10.49†	1.27	<0.001	<0.001*
ACR R	0.43 ± 0.05	0.39 ± 0.04	14380‡	1.11	<0.001	<0.001*
ALIC L	0.57 ± 0.06	0.52 ± 0.04	15241‡	1.34	<0.001	<0.001*
ALIC R	0.57 ± 0.06	0.53 ± 0.05	14568‡	1.13	<0.001	<0.001*
BCC	0.65 ± 0.04	0.61 ± 0.04	14200‡	0.9	<0.001	<0.001*
CC	0.66 ± 0.03	0.62 ± 0.03	11.86†	1.43	<0.001	<0.001*
CGC L	0.61 ± 0.07	0.56 ± 0.07	13612‡	0.86	<0.001	<0.001*
CGC R	0.59 ± 0.05	0.53 ± 0.06	8.61†	1.04	<0.001	<0.001*
CGH L	0.51 ± 0.08	0.46 ± 0.09	12961‡	0.71	<0.001	<0.001*
CGH R	0.51 ± 0.09	0.48 ± 0.07	12311‡	0.62	<0.001	<0.001*
CR L	0.45 ± 0.02	0.41 ± 0.02	14.38†	1.75	<0.001	<0.001*
CR R	0.45 ± 0.03	0.41 ± 0.02	12.3†	1.51	<0.001	<0.001*
CST L	0.56 ± 0.06	0.53 ± 0.06	3.53†	0.43	<0.001	<0.001*
CST R	0.55 ± 0.05	0.53 ± 0.06	3.29†	0.4	0.001	0.001*
EC L	0.46 ± 0.03	0.42 ± 0.03	10.57†	1.29	<0.001	<0.001*
EC R	0.46 ± 0.03	0.43 ± 0.03	7.91†	0.96	<0.001	<0.001*
FX	0.48 ± 0.09	0.44 ± 0.09	3.62†	0.44	<0.001	<0.001*
FX ST L	0.54 ± 0.04	0.5 ± 0.04	7.05†	0.86	<0.001	<0.001*
FX ST R	0.54 ± 0.04	0.52 ± 0.04	5.66†	0.69	<0.001	<0.001*
GCC	0.62 ± 0.05	0.57 ± 0.05	8.82†	1.08	<0.001	<0.001*
IC L	0.62 ± 0.05	0.57 ± 0.04	16743‡	1.85	<0.001	<0.001*
IC R	0.61 ± 0.03	0.56 ± 0.03	12.76†	1.58	<0.001	<0.001*
IFO L	0.5 ± 0.05	0.47 ± 0.05	5.58†	0.68	<0.001	<0.001*
IFO R	0.52 ± 0.05	0.49 ± 0.05	3.42†	0.41	<0.001	<0.001*

PCR L	0.45 ± 0.03	0.42 ± 0.02	11.5†	1.41	<0.001	<0.001*
PCR R	0.46 ± 0.03	0.43 ± 0.03	11.11†	1.35	<0.001	<0.001*
PLIC L	0.69 ± 0.04	0.64 ± 0.04	9.89†	1.21	<0.001	<0.001*
PLIC R	0.68 ± 0.06	0.64 ± 0.04	14927‡	1.17	<0.001	<0.001*
PTR L	0.56 ± 0.04	0.52 ± 0.03	8.8†	1.08	<0.001	<0.001*
PTR R	0.56 ± 0.04	0.52 ± 0.03	8.99†	1.11	<0.001	<0.001*
RLIC L	0.58 ± 0.04	0.54 ± 0.03	10.85†	1.33	<0.001	<0.001*
RLIC R	0.57 ± 0.03	0.53 ± 0.03	10.82†	1.32	<0.001	<0.001*
SCC	0.72 ± 0.04	0.68 ± 0.05	15343‡	1.27	<0.001	<0.001*
SCR L	0.47 ± 0.04	0.43 ± 0.05	14747‡	1.18	<0.001	<0.001*
SCR R	0.46 ± 0.04	0.43 ± 0.04	14141‡	0.98	<0.001	<0.001*
SFO L	0.47 ± 0.1	0.43 ± 0.06	12462‡	0.63	<0.001	<0.001*
SFO R	0.46 ± 0.05	0.43 ± 0.05	4.65†	0.57	<0.001	<0.001*
SLF L	0.48 ± 0.03	0.44 ± 0.03	9.91†	1.19	<0.001	<0.001*
SLF R	0.47 ± 0.02	0.44 ± 0.03	8.52†	1.02	<0.001	<0.001*
SS L	0.55 ± 0.03	0.51 ± 0.03	10.81†	1.32	<0.001	<0.001*
SS R	0.55 ± 0.03	0.51 ± 0.03	11.72†	1.44	<0.001	<0.001*
UNC L	0.53 ± 0.06	0.47 ± 0.06	7.61†	0.91	<0.001	<0.001*
UNC R	0.55 ± 0.05	0.49 ± 0.05	9.57†	1.17	<0.001	<0.001*

Results are reported as mean ± standard deviation. For non-normally distributed variables, results are reported as median ± interquantile range. Cohen's d values are reported for each tract derived from the JHU atlas. Abbreviations: ACR, anterior corona radiata; ALIC, anterior limb of internal capsule; BCC, body of corpus callosum; CC, corpus callosum; CGC, cingulate gyrus; CGH, perihippocampal cingulum tract; CR, corona radiata; CST, cortico-spinal tract; EC, external capsule; FX, fornix; FXST, fornix - stria terminalis; GCC, genu of corpus callosum; IC, internal capsule; IFO, inferior fronto-occipital fasciculus; PCR, posterior corona radiata; PLIC, posterior limb of internal capsule; PTR, posterior thalamic radiation; RLIC, retrolenticular limb of the internal capsule; SCC, splenium of corpus callosum; SCR, superior corona radiata; SFO, superior fronto-occipital fasciculus; SS, sagittal stratum; UNC, uncinate fasciculus; R, right; L; left. †parametric two-sample t-test; ‡non-parametric Mann-Whitney U test; *FDR-corrected q<0.05.

Appendix 9. Differences in mean diffusivity values for each tract between the MD-based clusters

Variable	**Cluster 1 (N = 166)**	**Cluster 2 (N = 109)**	**t / U**	**d**	**p**	**q**
ACR L	0.001 ± 0	0.001 ± 0	-10.29†	1.29	<0.001	<0.001*
ACR R	0.001 ± 0	0.001 ± 0	3309‡	1.19	<0.001	<0.001*
ALIC L	0.001 ± 0	0.001 ± 0	3681‡	1.1	<0.001	<0.001*
ALIC R	0.001 ± 0	0.001 ± 0	4481‡	0.9	<0.001	<0.001*
BCC	0.001 ± 0	0.001 ± 0	4062‡	1.04	<0.001	<0.001*
CC	0.001 ± 0	0.001 ± 0	3426‡	1.17	<0.001	<0.001*
CGC L	0.001 ± 0	0.001 ± 0	3145‡	1.29	<0.001	<0.001*
CGC R	0.001 ± 0	0.001 ± 0	3811‡	1.17	<0.001	<0.001*
CGH L	0.001 ± 0	0.001 ± 0	6836‡	0.35	<0.001	<0.001*
CGH R	0.001 ± 0	0.001 ± 0	6210‡	0.45	<0.001	<0.001*
CR L	0.001 ± 0	0.001 ± 0	2484‡	1.56	<0.001	<0.001*

CR R	0.001 ± 0	0.001 ± 0	2318‡	1.62	<0.001	<0.001*
CST L	0.001 ± 0	0.001 ± 0	7490‡	0.28	0.016	0.017*
CST R	0.001 ± 0	0.001 ± 0	7473‡	0.36	0.015	0.016*
EC L	0.001 ± 0	0.001 ± 0	3815‡	1.04	<0.001	<0.001*
EC R	0.001 ± 0	0.001 ± 0	4635.5‡	0.88	<0.001	<0.001*
FX	0.002 ± 0	0.002 ± 0	7640‡	0.28	0.029	0.031*
FX ST L	0.001 ± 0	0.001 ± 0	5415‡	0.7	<0.001	<0.001*
FX ST R	0.001 ± 0	0.001 ± 0	4719‡	0.76	<0.001	<0.001*
GCC	0.001 ± 0	0.001 ± 0	4855‡	0.83	<0.001	<0.001*
IC L	0.001 ± 0	0.001 ± 0	2696.5‡	1.32	<0.001	<0.001*
IC R	0.001 ± 0	0.001 ± 0	2804‡	1.34	<0.001	<0.001*
IFO L	0.001 ± 0	0.001 ± 0	6319‡	0.53	<0.001	<0.001*
IFO R	0.001 ± 0	0.001 ± 0	6621‡	0.43	<0.001	<0.001*
PCR L	0.001 ± 0	0.001 ± 0	5993.5‡	0.66	<0.001	<0.001*
PCR R	0.001 ± 0	0.001 ± 0	5414‡	0.76	<0.001	<0.001*
PLIC L	0.001 ± 0	0.001 ± 0	-8.71†	1.07	<0.001	<0.001*
PLIC R	0.001 ± 0	0.001 ± 0	3512‡	1.13	<0.001	<0.001*
PTR L	0.001 ± 0	0.001 ± 0	7123‡	0.37	0.003	0.003*
PTR R	0.001 ± 0	0.001 ± 0	6382‡	0.44	<0.001	<0.001*
RLIC L	0.001 ± 0	0.001 ± 0	4450‡	0.77	<0.001	<0.001*
RLIC R	0.001 ± 0	0.001 ± 0	3519‡	1.03	<0.001	<0.001*
SCC	0.001 ± 0	0.001 ± 0	4586‡	0.71	<0.001	<0.001*
SCR L	0.001 ± 0	0.001 ± 0	-12.87†	1.59	<0.001	<0.001*
SCR R	0.001 ± 0	0.001 ± 0	2395‡	1.58	<0.001	<0.001*
SFO L	0.001 ± 0	0.001 ± 0	3346‡	1.25	<0.001	<0.001*
SFO R	0.001 ± 0	0.001 ± 0	3980‡	1.08	<0.001	<0.001*
SLF L	0.001 ± 0	0.001 ± 0	-11.16†	1.38	<0.001	<0.001*
SLF R	0.001 ± 0	0.001 ± 0	3498.5‡	1.21	<0.001	<0.001*
SS L	0.001 ± 0	0.001 ± 0	5969‡	0.57	<0.001	<0.001*
SS R	0.001 ± 0	0.001 ± 0	4984‡	0.79	<0.001	<0.001*
UNC L	0.001 ± 0	0.001 ± 0.001	7715‡	0.31	0.039	0.040*
UNC R	0.001 ± 0	0.001 ± 0.001	8333‡	0.17	0.269	0.269

Results are reported as mean ± standard deviation. For non-normally distributed variables, results are reported as median ± interquantile range. Cohen's d values are reported for each tract derived from the JHU atlas. Abbreviations: ACR, anterior corona radiata; ALIC, anterior limb of internal capsule; BCC, body of corpus callosum; CC, corpus callosum; CGC, cingulate gyrus; CGH, perihippocampal cingulum tract; CR, corona radiata; CST, cortico-spinal tract; EC, external capsule; FX, fornix; FXST, fornix - stria terminalis; GCC, genu of corpus callosum; IC, internal capsule; IFO, inferior fronto-occipital fasciculus; PCR, posterior corona radiata; PLIC, posterior limb of internal capsule; PTR, posterior thalamic radiation; RLIC, retrolenticular limb of the internal capsule; SCC, splenium of corpus callosum; SCR, superior corona radiata; SFO, superior fronto-occipital fasciculus; SS, sagittal stratum; UNC, uncinate fasciculus; R, right; L; left. †parametric two-sample t-test; ‡non-parametric Mann-Whitney U test; *FDR-corrected $q<0.05$.

Appendix 10. Differences in radial diffusivity values for each tract between the RD-based clusters

Variable	Cluster 1 (N = 137)	Cluster 2 (N = 138)	t / U	d	p	q
ACR L	0.001 ± 0	0.001 ± 0	-11.28†	1.36	<0.001	<0.001*
ACR R	0.001 ± 0	0.001 ± 0	3197.5‡	1.29	<0.001	<0.001*
ALIC L	0 ± 0	0.001 ± 0	4400‡	1.03	<0.001	<0.001*
ALIC R	0 ± 0	0.001 ± 0	4783.5‡	0.9	<0.001	<0.001*
BCC	0 ± 0	0.001 ± 0	3268‡	1.21	<0.001	<0.001*
CC	0 ± 0	0.001 ± 0	1953‡	1.65	<0.001	<0.001*
CGC L	0 ± 0	0.001 ± 0	2703‡	1.45	<0.001	<0.001*
CGC R	0.001 ± 0	0.001 ± 0	3559‡	1.27	<0.001	<0.001*
CGH L	0.001 ± 0	0.001 ± 0	7223‡	0.41	<0.001	<0.001*
CGH R	0.001 ± 0	0.001 ± 0	5549‡	0.68	<0.001	<0.001*
CR L	0.001 ± 0	0.001 ± 0	-12.67†	1.53	<0.001	<0.001*
CR R	0.001 ± 0	0.001 ± 0	1987‡	1.74	<0.001	<0.001*
CST L	0.001 ± 0	0.001 ± 0	7244‡	0.34	<0.001	<0.001*
CST R	0.001 ± 0	0.001 ± 0	7475‡	0.42	0.003	0.003*
EC L	0.001 ± 0	0.001 ± 0	3771‡	1.14	<0.001	<0.001*
EC R	0.001 ± 0	0.001 ± 0	4221‡	1.03	<0.001	<0.001*
FX	0.001 ± 0	0.001 ± 0	7618‡	0.38	0.005	0.006*
FX ST L	0.001 ± 0	0.001 ± 0	5202‡	0.83	<0.001	<0.001*
FX ST R	0.001 ± 0	0.001 ± 0	4754‡	0.88	<0.001	<0.001*
GCC	0 ± 0	0.001 ± 0	3347‡	1.23	<0.001	<0.001*
IC L	0 ± 0	0 ± 0	2752‡	1.36	<0.001	<0.001*
IC R	0 ± 0	0 ± 0	2654‡	1.42	<0.001	<0.001*
IFO L	0.001 ± 0	0.001 ± 0	-4.93†	0.59	<0.001	<0.001*
IFO R	0.001 ± 0	0.001 ± 0	-3.05†	0.37	0.002	0.003*
PCR L	0.001 ± 0	0.001 ± 0	6734‡	0.5	<0.001	<0.001*
PCR R	0.001 ± 0	0.001 ± 0	5377‡	0.79	<0.001	<0.001*
PLIC L	0 ± 0	0 ± 0	-8.09†	0.98	<0.001	<0.001*
PLIC R	0 ± 0	0 ± 0	4307‡	1.06	<0.001	<0.001*
PTR L	0.001 ± 0	0.001 ± 0	8315‡	0.2	0.085	0.087
PTR R	0.001 ± 0	0.001 ± 0	6750‡	0.42	<0.001	<0.001*
RLIC L	0.001 ± 0	0.001 ± 0	4937‡	0.76	<0.001	<0.001*
RLIC R	0.001 ± 0	0.001 ± 0	3709‡	1.04	<0.001	<0.001*
SCC	0 ± 0	0 ± 0	3338‡	1.01	<0.001	<0.001*
SCR L	0.001 ± 0	0.001 ± 0	-13.63†	1.64	<0.001	<0.001*
SCR R	0.001 ± 0	0.001 ± 0	2216‡	1.58	<0.001	<0.001*
SFO L	0.001 ± 0	0.001 ± 0	3736‡	1.16	<0.001	<0.001*
SFO R	0.001 ± 0	0.001 ± 0	3653‡	1.17	<0.001	<0.001*

SLF L	0.001 ± 0	0.001 ± 0	-11.6†	1.4	<0.001	<0.001*
SLF R	0.001 ± 0	0.001 ± 0	3616‡	1.2	<0.001	<0.001*
SS L	0.001 ± 0	0.001 ± 0	5855‡	0.67	<0.001	<0.001*
SS R	0.001 ± 0	0.001 ± 0	4243.5‡	0.97	<0.001	<0.001*
UNC L	0.001 ± 0	0.001 ± 0.001	8245‡	0.26	0.067	0.070
UNC R	0.001 ± 0	0.001 ± 0.001	9118‡	0.11	0.612	0.612

Results are reported as mean ± standard deviation. For non-normally distributed variables, results are reported as median ± interquantile range. Cohen's d values are reported for each tract derived from the JHU atlas. Abbreviations: ACR, anterior corona radiata; ALIC, anterior limb of internal capsule; BCC, body of corpus callosum; CC, corpus callosum; CGC, cingulate gyrus; CGH, perihippocampal cingulum tract; CR, corona radiata; CST, cortico-spinal tract; EC, external capsule; FX, fornix; FXST, fornix - stria terminalis; GCC, genu of corpus callosum; IC, internal capsule; IFO, inferior fronto-occipital fasciculus; PCR, posterior corona radiata; PLIC, posterior limb of internal capsule; PTR, posterior thalamic radiation; RLIC, retrolenticular limb of the internal capsule; SCC, splenium of corpus callosum; SCR, superior corona radiata; SFO, superior fronto-occipital fasciculus; SS, sagittal stratum; UNC, uncinate fasciculus; R, right; L; left. †parametric two-sample t-test; ‡non-parametric Mann-Whitney U test; *FDR-corrected q<0.05.

Appendix 11. Differences in neuroimaging features between the multimodal-based clusters

Variable	**Cluster 1 (N = 59)**	**Cluster 2 (N = 57)**	**t / U**	**d**	**p**	**q**
Spos A8m L	32.09 ± 21.17	35.05 ± 21.04	1413‡	-0.13	0.139	0.436
Spos A8m R	35.05 ± 13.17	43.75 ± 19.43	1377‡	-0.19	0.093	0.37
Spos A8dl L	27.71 ± 19.98	33.46 ± 19.13	1590‡	-0.02	0.615	0.826
Spos A8dl R	28 ± 16.21	30.38 ± 17.05	1516‡	-0.15	0.362	0.65
Spos A9l L	25.2 ± 14.07	31.86 ± 16.79	1268‡	-0.25	0.023	0.151
Spos A9l R	27.56 ± 16.42	31.17 ± 16.24	1415‡	-0.18	0.142	0.443
Spos A6dl L	30.47 ± 21.36	35.55 ± 18.84	1453‡	-0.08	0.208	0.523
Spos A6dl R	31.17 ± 19.29	34.48 ± 17.99	1498‡	-0.11	0.312	0.607
Spos A6m L	36.61 ± 21.32	44.52 ± 21.25	1309‡	-0.22	0.04	0.222
Spos A6m R	33.81 ± 21.06	48.2 ± 24.6	1248‡	-0.28	0.017	0.119
Spos A9m L	29.06 ± 18.49	36.24 ± 17.02	1385‡	-0.24	0.102	0.384
Spos A9m R	33.3 ± 18.39	37.85 ± 20.38	1500‡	-0.14	0.318	0.613
Spos A10m L	29.86 ± 13.6	34.39 ± 15.93	1554‡	-0.01	0.483	0.733
Spos A10m R	31.99 ± 17.48	35.75 ± 17.19	1518‡	-0.06	0.368	0.651
Spos A9 46d L	32.15 ± 19.8	35.98 ± 20.73	1525‡	-0.01	0.389	0.659
Spos A9 46d R	33.86 ± 16.05	35.48 ± 21.92	1626‡	-0.03	0.761	0.888
Spos IFJ L	29.26 ± 15.78	37.49 ± 14.61	1403‡	-0.15	0.125	0.42
Spos IFJ R	31.23 ± 18.29	33.59 ± 19.81	1490‡	-0.1	0.292	0.591
Spos A46 L	33.18 ± 19.13	36.57 ± 23.24	1536‡	-0.05	0.423	0.684
Spos A46 R	30.77 ± 16.9	32.92 ± 25.17	1570‡	-0.1	0.54	0.774
Spos A9 46v L	31.25 ± 19.99	36.04 ± 20.96	1439‡	-0.13	0.181	0.497
Spos A9 46v R	31.94 ± 17.32	34.63 ± 24.37	1575‡	-0.07	0.558	0.788
Spos A8vl L	31.58 ± 13.84	35.45 ± 17.34	1489‡	-0.11	0.289	0.59
Spos A8vl R	30.09 ± 18.08	36.71 ± 19.42	1536‡	-0.11	0.423	0.684

Spos A6vl L	31.02 ± 19.5	37.6 ± 17.22	1458‡	-0.1	0.218	0.532
Spos A6vl R	32.19 ± 21.03	35.13 ± 21.15	1669‡	-0.07	0.947	0.981
Spos A44d L	30.51 ± 17.18	30.72 ± 17.31	1617‡	-0.01	0.724	0.874
Spos A44d R	32.41 ± 17.52	33.9 ± 19.47	1572‡	-0.1	0.547	0.778
Spos IFS L	29.3 ± 19.92	32.65 ± 17.66	1520‡	-0.07	0.374	0.654
Spos IFS R	29.69 ± 15.08	35.32 ± 18.95	1412‡	-0.15	0.137	0.436
Spos A45c L	25.41 ± 8.02	28.93 ± 16.97	1383‡	-0.24	0.1	0.382
Spos A45c R	31.49 ± 13.74	36.11 ± 20.6	1353‡	-0.2	0.07	0.311
Spos A45r L	27.78 ± 16.96	29.6 ± 10.71	1439‡	-0.13	0.181	0.497
Spos A45r R	31.47 ± 16.05	29.38 ± 19.87	1722‡	0.1	0.825	0.923
Spos A44op L	28.87 ± 16.56	33.57 ± 17.22	1280‡	-0.31	0.027	0.168
Spos A44op R	32.07 ± 16.46	35.91 ± 19.74	1546‡	-0.11	0.456	0.712
Spos A44v L	31.21 ± 16.59	32.46 ± 21.43	1478‡	-0.21	0.262	0.558
Spos A44v R	30.2 ± 14.24	36.63 ± 17.8	1324‡	-0.27	0.049	0.252
Spos A12 47l L	30.65 ± 14.68	35.63 ± 15.84	1425‡	-0.14	0.157	0.468
Spos A12 47l R	31.99 ± 15.68	34.08 ± 18.06	1597‡	-0.05	0.643	0.836
Spos A4hf L	38.46 ± 18.39	45.41 ± 18.43	1404‡	-0.17	0.126	0.423
Spos A4hf R	35.35 ± 15.52	41.39 ± 17.68	1465‡	-0.15	0.233	0.543
Spos A6cdl L	34.98 ± 16.61	42.07 ± 24.91	1356‡	-0.27	0.073	0.316
Spos A6cdl R	35.53 ± 21.04	42.25 ± 23.77	1379‡	-0.21	0.095	0.371
Spos A4ul L	30.49 ± 18.33	40.41 ± 20.2	1282‡	-0.25	0.028	0.17
Spos A4ul R	35.09 ± 18.53	44.62 ± 21.41	1221‡	-0.31	0.011	0.087
Spos A4tl L	32.66 ± 20.5	35.09 ± 17.04	1518‡	-0.14	0.368	0.651
Spos A4tl R	34.12 ± 16.22	38 ± 19.41	1437‡	-0.24	0.178	0.491
Spos A6cvl L	33.86 ± 19.17	39.43 ± 20.13	1385‡	-0.16	0.102	0.384
Spos A6cvl R	35.86 ± 19.72	39.74 ± 24.48	1463‡	-0.15	0.229	0.543
Spos A1 2 3ll R	35.65 ± 15.39	41.78 ± 28.24	1371‡	-0.24	0.087	0.352
Spos A4ll L	33.46 ± 15.75	40.12 ± 24.97	1296‡	-0.31	0.033	0.198
Spos A4ll R	35.11 ± 18.78	42.83 ± 28.32	1352‡	-0.25	0.069	0.311
Spos A41 42 L	38.11 ± 15.44	41.69 ± 21.95	1545‡	-0.03	0.453	0.712
Spos A41 42 R	38.27 ± 20.72	38.13 ± 22.08	1688‡	0	0.974	0.993
Spos TE1.0 TE1.2 L	39.52 ± 18.4	41.2 ± 18.73	1472‡	-0.18	0.248	0.554
Spos TE1.0 TE1.2 R	37.9 ± 20.05	43.11 ± 23.32	1478‡	-0.16	0.262	0.558
Spos A22c L	28.68 ± 19.66	34.4 ± 19.99	1517‡	-0.09	0.365	0.65
Spos A22c R	35.47 ± 18.51	36.52 ± 23.33	1541‡	-0.1	0.439	0.7
Spos A38l L	27.4 ± 12.49	26.24 ± 16.65	1646‡	0.05	0.847	0.928
Spos A38l R	31.94 ± 11.26	32.03 ± 18.27	1623‡	-0.09	0.749	0.884
Spos A22r L	29.28 ± 18.18	34.76 ± 16.43	1446‡	-0.14	0.194	0.508
Spos A22r R	28.11 ± 13.11	26.34 ± 22.81	1749‡	0.02	0.711	0.864
Spos A37dl L	34.37 ± 18.35	36.17 ± 20	1421‡	-0.16	0.151	0.46
Spos A37dl R	33.64 ± 20.8	36.11 ± 21.27	1587‡	-0.07	0.604	0.816

Spos A37vl L	29.31 ± 20.94	38.22 ± 20.51	1390‡	-0.21	0.108	0.395
Spos A37mv L	39.99 ± 18.19	42.11 ± 24.44	1457‡	-0.18	0.216	0.53
Spos A37mv R	38.5 ± 20.33	40.8 ± 21.15	1396‡	-0.29	0.116	0.402
Spos TL L	24.84 ± 14.13	23.6 ± 14.81	1645‡	0.04	0.842	0.928
Spos TL R	27.18 ± 12.62	26.39 ± 12.05	1686‡	0.05	0.982	0.995
Spos TH L	24.01 ± 13.18	26.15 ± 14.68	1510‡	-0.2	0.345	0.635
Spos TH R	24.41 ± 13.3	25.23 ± 16.44	1519‡	-0.27	0.371	0.651
Spos rpSTS L	27.79 ± 13.46	29.29 ± 12.62	1614‡	-0.1	0.711	0.864
Spos rpSTS R	30.31 ± 18.1	30.33 ± 15.87	1663‡	-0.03	0.921	0.966
Spos cpSTS L	33.94 ± 19.52	33.83 ± 15.1	1651‡	0.06	0.868	0.933
Spos cpSTS R	33.72 ± 20.02	32.2 ± 20.5	1822‡	0.09	0.439	0.7
Spos A7r L	32.21 ± 21.63	40.29 ± 19.48	1496‡	-0.1	0.307	0.606
Spos A7r R	30.67 ± 19.99	42.83 ± 24.15	1343‡	-0.22	0.062	0.292
Spos A7c L	36.6 ± 24.02	37.11 ± 24.13	1559‡	-0.1	0.5	0.742
Spos A7c R	35.15 ± 19.37	36.53 ± 27.61	1519‡	-0.13	0.371	0.651
Spos A5l L	33.97 ± 22.14	39.35 ± 20.64	1444‡	-0.18	0.191	0.505
Spos A5l R	32.7 ± 17.67	40.24 ± 20.37	1342‡	-0.23	0.061	0.29
Spos A7ip L	33.37 ± 24.04	39.48 ± 22.41	1483‡	-0.15	0.274	0.573
Spos A7ip R	32.09 ± 22.95	42.75 ± 24.48	1394‡	-0.18	0.113	0.402
Spos A39c L	37.75 ± 19.08	37.46 ± 23.54	1636‡	0	0.804	0.91
Spos A39rd L	31.38 ± 16.01	33.73 ± 14.89	1466‡	-0.11	0.235	0.543
Spos A40rd L	36.14 ± 22.2	41.54 ± 19.93	1497‡	-0.1	0.31	0.606
Spos A40rd R	36.9 ± 20.99	42.12 ± 22.14	1422‡	-0.19	0.153	0.463
Spos A40c L	29.93 ± 22.97	38.4 ± 18.87	1391‡	-0.22	0.109	0.397
Spos A39rv L	35.2 ± 17.5	34.52 ± 19.63	1708‡	0.07	0.886	0.946
Spos A39rv R	34.73 ± 17.3	37.02 ± 20.22	1592‡	-0.08	0.623	0.829
Spos A40rv L	37.29 ± 23.64	40.2 ± 23.52	1454‡	-0.18	0.21	0.524
Spos A40rv R	38.2 ± 25.41	41.52 ± 20.77	1515‡	-0.12	0.359	0.65
Spos A7m L	36.95 ± 19.79	41.28 ± 24.65	1574‡	-0.02	0.555	0.787
Spos A7m R	37.03 ± 19.72	38.74 ± 23.42	1670‡	-0.05	0.952	0.984
Spos A5m L	40.11 ± 21.5	47.07 ± 24.27	1444‡	-0.13	0.191	0.505
Spos A5m R	40.56 ± 20.2	48.78 ± 31.04	1450‡	-0.17	0.202	0.517
Spos dmPOS L	39.41 ± 19.79	38.19 ± 19.62	1741‡	0.13	0.745	0.881
Spos dmPOS R	39.13 ± 16.76	40.9 ± 21.22	1721‡	-0.13	0.829	0.924
Spos A31 L	36.81 ± 17.99	37.14 ± 20.84	1714‡	-0.12	0.86	0.933
Spos A31 R	37.37 ± 15.98	38.81 ± 22.71	1717‡	-0.07	0.847	0.928
Spos A1 2 3ulhf L	38.7 ± 20.61	45.3 ± 19.5	1355‡	-0.22	0.072	0.314
Spos A1 2 3ulhf R	36.53 ± 20.76	43.72 ± 17.92	1385‡	-0.15	0.102	0.384
Spos A1 2 3tonIa L	37.91 ± 20.79	40.92 ± 20.49	1514‡	-0.12	0.356	0.649
Spos A1 2 3tonIa R	36.26 ± 17.99	38.48 ± 21.73	1551‡	-0.07	0.473	0.728
Spos A2 L	32 ± 19.84	36.41 ± 23.81	1495‡	-0.13	0.304	0.604

Spos A2 R	33.47 ± 25.48	38.77 ± 14.13	1376‡	-0.2	0.092	0.369
Spos G L	32.65 ± 20.22	35.1 ± 22.22	1523‡	-0.16	0.383	0.659
Spos G R	30.53 ± 13.87	31.64 ± 18.68	1580‡	-0.13	0.577	0.797
Spos vIa L	26.62 ± 11.59	24.94 ± 15.49	1709‡	0.01	0.881	0.943
Spos vIa R	23.34 ± 14.65	24.79 ± 18.26	1678‡	-0.04	0.987	0.995
Spos dIa L	30.36 ± 13.74	33.05 ± 16.75	1576‡	-0.07	0.562	0.789
Spos dIa R	32.89 ± 17.93	30.55 ± 17.84	1662‡	0.02	0.916	0.964
Spos vId vIg L	31.86 ± 18.07	29.19 ± 18.46	1766‡	0.08	0.643	0.836
Spos vId vIg R	33.82 ± 16.04	31.71 ± 24.55	1776‡	0.05	0.604	0.816
Spos dIg L	29.63 ± 16.95	33.54 ± 19.82	1420‡	-0.2	0.149	0.457
Spos dIg R	29.34 ± 13.1	30.39 ± 19.33	1539‡	-0.16	0.433	0.694
Spos dId L	32.59 ± 15.65	32.17 ± 18.73	1617‡	0.08	0.724	0.874
Spos dId R	35.08 ± 18.71	36.04 ± 17.15	1491‡	-0.16	0.294	0.593
Spos A23d L	34.95 ± 14.07	36.09 ± 22.12	1562‡	-0.07	0.511	0.75
Spos A23d R	34.19 ± 16.03	34.54 ± 20.67	1600‡	-0.07	0.655	0.836
Spos A24rv L	26.89 ± 20.81	27.23 ± 21.73	1597‡	-0.01	0.643	0.836
Spos A32p L	35.27 ± 12.77	35.92 ± 20.01	1529‡	-0.11	0.401	0.668
Spos A32p R	32.46 ± 15.6	34.28 ± 18.44	1487‡	-0.17	0.284	0.586
Spos A23v L	36.24 ± 18.73	36.7 ± 15.22	1545‡	-0.03	0.453	0.712
Spos A23v R	37.36 ± 15.77	38.03 ± 22.07	1580‡	-0.03	0.577	0.797
Spos A24cd L	33.35 ± 13.08	40.21 ± 22.79	1430‡	-0.23	0.166	0.474
Spos A24cd R	32.63 ± 16.7	40.41 ± 22.21	1418‡	-0.23	0.146	0.451
Spos A23c L	35.45 ± 21.09	42.36 ± 22.86	1434‡	-0.16	0.173	0.482
Spos A23c R	36.86 ± 23.51	42.56 ± 23.98	1435‡	-0.14	0.174	0.483
Spos A32sg R	29.29 ± 14.78	28.05 ± 16.79	1738‡	0.08	0.757	0.886
Spos cLinG L	39.09 ± 18.95	40.13 ± 22.77	1477‡	-0.17	0.26	0.558
Spos cLinG R	37.17 ± 22.73	40.51 ± 24	1465‡	-0.18	0.233	0.543
Spos rCunG L	41.43 ± 14.09	46 ± 22.28	1406‡	-0.18	0.129	0.424
Spos rCunG R	42.12 ± 15.5	47.13 ± 23.02	1411‡	-0.19	0.136	0.436
Spos cCunG R	33.78 ± 19.67	37.97 ± 22.45	1396‡	-0.22	0.116	0.402
Spos rLinG L	35.39 ± 17.84	36.29 ± 20.92	1480‡	-0.17	0.267	0.563
Spos rLinG R	35.1 ± 14.91	36.6 ± 21.38	1425‡	-0.22	0.157	0.468
Spos vmPOS L	42.85 ± 16.89	47.25 ± 20.21	1452‡	-0.11	0.206	0.521
Spos vmPOS R	41.97 ± 16.79	47.62 ± 20.49	1430‡	-0.13	0.166	0.474
Spos mOccG L	31.04 ± 14.34	36.58 ± 18.42	1468‡	-0.19	0.239	0.548
Spos mOccG R	31.72 ± 13.24	35.47 ± 21.31	1420‡	-0.22	0.149	0.457
Spos V5 MTpos L	38.16 ± 18.19	41.73 ± 27.14	1524‡	-0.13	0.386	0.659
Spos V5 MTpos R	35.48 ± 20.87	37.09 ± 20.87	1453‡	-0.18	0.208	0.523
Spos msOccG L	33.43 ± 14.42	38.71 ± 23.78	1394‡	-0.2	0.113	0.402
Spos msOccG R	35.72 ± 13.86	40.29 ± 22.88	1443‡	-0.14	0.189	0.505
Spos lsOccG L	38.77 ± 20.95	42.81 ± 26.27	1485‡	-0.14	0.279	0.579

Spos lsOccG R	40.84 ± 23.71	40.37 ± 19.28	1511‡	0.11	0.348	0.638
Spos lAmyg L	19.91 ± 11.38	23.11 ± 10.93	1370‡	-0.18	0.086	0.352
Spos lAmyg R	20.95 ± 12.22	23.23 ± 14.69	1468‡	-0.27	0.239	0.548
Spos rHipp L	26.87 ± 12.6	33.49 ± 14.35	1388‡	-0.31	0.106	0.392
Spos rHipp R	24.46 ± 9.33	26.7 ± 15.99	1547‡	-0.24	0.459	0.714
Spos cHipp L	30.16 ± 14.03	34.59 ± 15.58	1427‡	-0.3	0.161	0.47
Spos cHipp R	31.68 ± 16.65	34.63 ± 16.97	1522‡	-0.19	0.38	0.659
Spos vCa L	26.97 ± 14.59	29.91 ± 16.82	1506‡	-0.12	0.334	0.625
Spos vCa R	26.74 ± 12.37	29.59 ± 14.68	1528‡	-0.12	0.398	0.666
Spos GP L	24.5 ± 15.97	28.65 ± 15.94	1497‡	-0.13	0.31	0.606
Spos GP R	26.31 ± 16.49	28.54 ± 17.53	1557‡	-0.04	0.493	0.735
Spos NAC L	23.63 ± 14.68	24.7 ± 17	1510‡	-0.17	0.345	0.635
Spos vmPu L	27.96 ± 16.68	31.44 ± 16.31	1455‡	-0.17	0.212	0.526
Spos vmPu R	26.9 ± 17.58	28.5 ± 18.33	1647‡	-0.01	0.851	0.928
Spos dCa L	26.48 ± 20.59	31.64 ± 19.53	1431‡	-0.15	0.167	0.474
Spos dCa R	28.66 ± 19.18	33.13 ± 27.44	1534‡	-0.12	0.417	0.684
Spos dlPu L	30.1 ± 18.1	34.79 ± 22.13	1429‡	-0.22	0.164	0.474
Spos dlPu R	31.49 ± 18.21	35.1 ± 20.41	1536‡	-0.15	0.423	0.684
Spos mPFtha L	32.19 ± 22.68	35.6 ± 21.61	1509‡	-0.1	0.342	0.635
Spos mPFtha R	33.67 ± 18.06	34.17 ± 26.73	1533‡	-0.13	0.414	0.681
Spos mPMtha L	17.83 ± 12.13	19.72 ± 13.22	1295‡	-0.3	0.033	0.198
Spos mPMtha R	28.54 ± 20.53	27.34 ± 19.21	1628‡	0.01	0.77	0.888
Spos Stha L	22.33 ± 18.96	25.66 ± 14.57	1446‡	-0.23	0.194	0.508
Spos Stha R	23.8 ± 17.74	24.63 ± 15.48	1474‡	-0.15	0.253	0.554
Spos rTtha L	26.38 ± 18.52	30.36 ± 20.62	1296‡	-0.19	0.033	0.198
Spos rTtha R	24.8 ± 12.73	27.57 ± 12.49	1474‡	-0.1	0.253	0.554
Spos PPtha L	30.72 ± 19.43	32.9 ± 20.19	1451‡	-0.22	0.204	0.518
Spos PPtha R	32.14 ± 19.12	33.51 ± 25.64	1458‡	-0.27	0.218	0.532
Spos Otha L	23.92 ± 18.88	36.44 ± 18.04	1206‡	-0.44	0.009	0.077
Spos Otha R	25.72 ± 10.38	31.78 ± 18.01	1332‡	-0.41	0.054	0.264
Spos cTtha L	29.85 ± 16.67	31.63 ± 22.68	1483‡	-0.17	0.274	0.573
Spos cTtha R	24.8 ± 16.45	31.37 ± 19.29	1398‡	-0.33	0.118	0.405
Spos lPFtha L	31.22 ± 17.22	32.81 ± 15.95	1515‡	-0.12	0.359	0.65
Spos lPFtha R	32.4 ± 23.23	35.73 ± 19.8	1469‡	-0.15	0.242	0.549
Spos Buckner2011 17Networks 1	30.17 ± 19.19	27.53 ± 19.39	1768‡	0.16	0.635	0.836
Spos Buckner2011 17Networks 2	24.53 ± 18.63	28.15 ± 12.7	1592‡	-0.05	0.623	0.829
Spos Buckner2011 17Networks 4	39.45 ± 24.76	38.38 ± 21.3	1466‡	0.21	0.235	0.543
Spos Buckner2011 17Networks 5	21.23 ± 14.89	17.39 ± 12.09	1823‡	0.16	0.436	0.697
Spos Buckner2011 17Networks 9	28.83 ± 18.22	33.07 ± 22.6	1530‡	-0.1	0.404	0.67
Sneg A8m L	5.52 ± 7.23	2.74 ± 4.92	2052‡	0.25	0.041	0.225
Sneg A8m R	4.4 ± 6.17	2.99 ± 5.17	2032‡	0.2	0.053	0.262

Sneg A8dl L	7.05 ± 7.82	4.58 ± 7.11	1898‡	0.18	0.233	0.543
Sneg A8dl R	6.93 ± 6.29	4.17 ± 9.36	1908‡	0.04	0.212	0.526
Sneg A9l L	7.04 ± 6.52	5.63 ± 7.04	1998‡	0.27	0.081	0.342
Sneg A9l R	6.49 ± 6.96	4.47 ± 7.26	1936‡	0.25	0.161	0.47
Sneg A6dl L	4.33 ± 5.63	2.32 ± 4.03	2033.5‡	0.37	0.052	0.261
Sneg A6dl R	4.47 ± 7.36	2.31 ± 5.17	1952.5‡	0.12	0.135	0.436
Sneg A6m L	3.32 ± 5.17	2.44 ± 4.86	1971‡	0.21	0.11	0.398
Sneg A6m R	4.02 ± 5.99	2.12 ± 4.25	2025‡	0.2	0.058	0.277
Sneg A9m L	4.97 ± 6.36	3.25 ± 4.14	2094‡	0.38	0.023	0.151
Sneg A9m R	4.36 ± 6.22	3.3 ± 5	1786‡	0.02	0.566	0.791
Sneg A10m L	6.5 ± 8.49	4.09 ± 7.13	1868‡	0.15	0.304	0.604
Sneg A10m R	6.88 ± 7.66	4.19 ± 7.72	1880‡	0.11	0.274	0.573
Sneg A9 46d L	4.37 ± 5.85	2.65 ± 4.18	1844‡	0.1	0.371	0.651
Sneg A9 46d R	3.69 ± 5	3.12 ± 5.04	1763‡	0.06	0.655	0.836
Sneg IFJ L	4.95 ± 6.12	4.55 ± 5.32	1792‡	0.14	0.544	0.775
Sneg IFJ R	5.46 ± 7.4	3.72 ± 6.35	1779‡	0.12	0.592	0.808
Sneg A46 L	4.49 ± 7.68	3.65 ± 6.12	1838‡	0.14	0.389	0.659
Sneg A46 R	4.22 ± 6.68	3.64 ± 6.98	1704‡	0.13	0.903	0.957
Sneg A9 46v L	5.92 ± 7.14	3.55 ± 6.6	1894.5‡	0.25	0.241	0.548
Sneg A9 46v R	4.96 ± 6.06	5.13 ± 7.77	1659‡	-0.06	0.903	0.957
Sneg A8vl L	4.64 ± 6.95	4.13 ± 7.56	1754‡	0.02	0.691	0.857
Sneg A8vl R	6.42 ± 7.02	4.74 ± 7.35	1807‡	0.12	0.49	0.733
Sneg A6vl L	5.05 ± 5.28	4.08 ± 4.24	1950‡	0.2	0.139	0.436
Sneg A6vl R	4.27 ± 5.77	3.58 ± 7.38	1646‡	0.08	0.847	0.928
Sneg A44d L	4.76 ± 8.36	3.91 ± 6.45	1932‡	0.27	0.167	0.474
Sneg A44d R	4.12 ± 6.96	3.72 ± 4.52	1827‡	0.14	0.423	0.684
Sneg IFS L	4.7 ± 5.38	3.64 ± 5.59	1851‡	0.19	0.351	0.64
Sneg IFS R	3.4 ± 6.41	3.58 ± 4.56	1837.5‡	-0.17	0.39	0.66
Sneg A45c L	7.14 ± 7.67	3.95 ± 5.38	2066‡	0.42	0.034	0.199
Sneg A45c R	5.85 ± 7.68	3.96 ± 4.84	2112‡	0.39	0.018	0.123
Sneg A45r L	6.48 ± 5.9	3.93 ± 3.81	2173‡	0.43	0.007	0.063
Sneg A45r R	5.31 ± 8.17	4.54 ± 7.99	1853‡	0.18	0.345	0.635
Sneg A44op L	5.19 ± 5.47	3.39 ± 4.94	2150‡	0.44	0.01	0.082
Sneg A44op R	6.43 ± 6.81	5.03 ± 6.34	1839‡	0.17	0.386	0.659
Sneg A44v L	6.99 ± 8.58	4.53 ± 6.85	2088‡	0.49	0.025	0.161
Sneg A44v R	6.51 ± 7.53	5.05 ± 6.82	1950‡	0.24	0.139	0.436
Sneg A12 47l L	4.56 ± 4.32	2.72 ± 5.47	1946‡	0.16	0.145	0.449
Sneg A12 47l R	4.81 ± 5.53	3.76 ± 5.11	1907‡	0.15	0.214	0.528
Sneg A4hf L	2.55 ± 3.92	2.67 ± 3.33	1859.5‡	-0.16	0.327	0.619
Sneg A4hf R	3.8 ± 5.41	2.83 ± 5.28	1867.5‡	0.18	0.306	0.605
Sneg A6cdl L	3.41 ± 4.82	2.45 ± 5.4	1914‡	0.15	0.2	0.514

Sneg A6cdl R	3.26 ± 5.88	2.02 ± 4.8	1938‡	0.19	0.157	0.468
Sneg A4ul L	3.85 ± 5.41	2.52 ± 4.63	1961.5‡	0.26	0.123	0.415
Sneg A4ul R	3.92 ± 5.79	2.72 ± 4.14	2038‡	0.35	0.049	0.253
Sneg A4tl L	5.25 ± 6.48	4.57 ± 6.04	1783‡	0.13	0.577	0.797
Sneg A4tl R	4.99 ± 6.25	4.36 ± 6.71	1801‡	0.09	0.511	0.75
Sneg A6cvl L	4.93 ± 5.74	3.37 ± 5.77	1873.5‡	0.08	0.29	0.59
Sneg A6cvl R	4.73 ± 6.85	3.76 ± 4.48	1920.5‡	0.22	0.188	0.505
Sneg A1 2 3ll R	2.84 ± 3.07	2.31 ± 4.57	1778‡	0.01	0.596	0.812
Sneg A4ll L	3.6 ± 5.04	2.55 ± 4.38	1932‡	0.2	0.167	0.474
Sneg A4ll R	3.63 ± 4.96	2.51 ± 4.67	1958‡	0.23	0.127	0.423
Sneg A41 42 L	2.53 ± 5.07	2.36 ± 4.83	1688.5‡	0	0.971	0.993
Sneg A41 42 R	2.13 ± 4.13	2.47 ± 4.48	1647‡	-0.19	0.851	0.928
Sneg TE1.0 TE1.2 L	2.68 ± 5.25	2.35 ± 6.11	1844.5‡	0.14	0.37	0.651
Sneg TE1.0 TE1.2 R	2.96 ± 5.15	2.39 ± 5.14	1864‡	0.14	0.315	0.61
Sneg A22c L	3.24 ± 6.02	2.37 ± 4.64	1930‡	0.24	0.171	0.479
Sneg A22c R	2.63 ± 5.83	1.96 ± 4.23	1898‡	0.21	0.233	0.543
Sneg A38l L	4.3 ± 4.35	4.44 ± 6.38	1730‡	-0.02	0.791	0.903
Sneg A38l R	2.86 ± 3.88	2.95 ± 4.38	1717‡	-0.04	0.847	0.928
Sneg A22r L	3.17 ± 5.01	2.76 ± 3.83	1871‡	0.12	0.297	0.595
Sneg A22r R	4.02 ± 5.3	3.42 ± 5.83	1795‡	0.07	0.533	0.767
Sneg A37dl L	3.96 ± 5.48	2.64 ± 4.65	1900‡	0.25	0.229	0.543
Sneg A37dl R	4.26 ± 7.36	3.31 ± 6.2	1875‡	0.22	0.286	0.587
Sneg A37vl L	3.77 ± 5.97	2.94 ± 5.24	1842‡	0.15	0.377	0.657
Sneg A37mv L	3.1 ± 4.02	1.85 ± 4.47	1974‡	0.24	0.107	0.392
Sneg A37mv R	3.04 ± 6.52	2.46 ± 4.91	1955‡	0.23	0.132	0.431
Sneg TL L	4.9 ± 4.83	2.87 ± 5.55	1846‡	0.02	0.365	0.65
Sneg TL R	4.2 ± 4.31	4.33 ± 4.58	1775‡	-0.08	0.608	0.82
Sneg TH L	5.19 ± 6.32	3.13 ± 6.6	1923‡	0.12	0.183	0.5
Sneg TH R	6.17 ± 5.59	4.85 ± 6.77	1890‡	0.14	0.251	0.554
Sneg rpSTS L	4.7 ± 6.91	4.32 ± 5.46	1742‡	0.09	0.74	0.881
Sneg rpSTS R	4.83 ± 6.09	3.08 ± 4.45	1917‡	0.26	0.194	0.508
Sneg cpSTS L	4.1 ± 5.61	3.02 ± 4.8	1765‡	0.02	0.647	0.836
Sneg cpSTS R	4.06 ± 6.53	3.89 ± 4.83	1856‡	0.14	0.337	0.629
Sneg A7r L	4.28 ± 6.93	3.02 ± 6	1793.5‡	0.09	0.538	0.773
Sneg A7r R	5.4 ± 7.15	2.29 ± 7.01	2048‡	0.31	0.043	0.234
Sneg A7c L	3.82 ± 5	2.98 ± 5.59	1831.5‡	0.13	0.409	0.675
Sneg A7c R	4.01 ± 6.39	2.76 ± 6.87	1840.5‡	0.07	0.381	0.659
Sneg A5l L	3.25 ± 6.29	2.69 ± 6.54	1862‡	0.18	0.32	0.614
Sneg A5l R	3.39 ± 6.22	2.49 ± 5.58	1891.5‡	0.17	0.247	0.554
Sneg A7ip L	3.8 ± 7.29	2.86 ± 5.08	2005‡	0.3	0.074	0.321
Sneg A7ip R	4.8 ± 7.87	2.49 ± 5.55	2017‡	0.3	0.064	0.297

Sneg A39c L	4.21 ± 5.5	3.35 ± 7.3	1808‡	0.09	0.487	0.733
Sneg A39rd L	5.18 ± 4.83	4.17 ± 7.55	1739‡	0.03	0.753	0.886
Sneg A40rd L	5.33 ± 6.6	3.03 ± 5.54	1990‡	0.28	0.089	0.359
Sneg A40rd R	4.2 ± 8.06	2.73 ± 5.32	1937‡	0.22	0.159	0.469
Sneg A40c L	6.1 ± 7.3	3.26 ± 5.21	2143‡	0.51	0.011	0.087
Sneg A39rv L	4.54 ± 7.06	4.61 ± 6.79	1676‡	-0.02	0.978	0.993
Sneg A39rv R	4.77 ± 6.7	4.38 ± 6.42	1840‡	0.05	0.383	0.659
Sneg A40rv L	4.04 ± 5.72	2.66 ± 6.25	1800‡	0.07	0.515	0.754
Sneg A40rv R	4.23 ± 7.11	3.22 ± 6.46	1806‡	0.09	0.493	0.735
Sneg A7m L	5.25 ± 5.14	2.53 ± 5.3	1937‡	0.12	0.159	0.469
Sneg A7m R	4.49 ± 5.73	2.57 ± 7.11	1879.5‡	0.04	0.275	0.574
Sneg A5m L	2.55 ± 3.57	1.08 ± 3.08	2096‡	0.19	0.022	0.15
Sneg A5m R	2.94 ± 4	1.68 ± 4.04	1985‡	0.1	0.094	0.37
Sneg dmPOS L	5.48 ± 7.72	2.34 ± 6.48	1935‡	0.25	0.162	0.473
Sneg dmPOS R	5.38 ± 6.95	2.94 ± 5.71	2018‡	0.29	0.064	0.295
Sneg A31 L	6.69 ± 7.93	5.61 ± 9.32	1772‡	0.02	0.619	0.826
Sneg A31 R	6.03 ± 6.86	5.61 ± 8.87	1796‡	0.05	0.529	0.764
Sneg A1 2 3ulhf L	2.87 ± 4.89	1.82 ± 4.05	1954‡	0.25	0.133	0.432
Sneg A1 2 3ulhf R	3.89 ± 6	1.99 ± 3.46	2034‡	0.36	0.052	0.261
Sneg A1 2 3tonIa L	3.55 ± 4.63	3.98 ± 5.77	1682‡	-0.06	1	1
Sneg A1 2 3tonIa R	3.46 ± 6.01	3.68 ± 5.52	1740‡	-0.03	0.749	0.884
Sneg A2 L	3.13 ± 5.8	3.58 ± 5.19	1777.5‡	-0.23	0.598	0.813
Sneg A2 R	4.32 ± 8.47	2.88 ± 5.15	1965‡	0.35	0.118	0.405
Sneg G L	2.34 ± 3.97	3 ± 3.74	1625‡	-0.12	0.757	0.886
Sneg G R	3.45 ± 4.24	2.6 ± 5.14	1628‡	0.16	0.77	0.888
Sneg vIa L	3.15 ± 3.85	3.86 ± 4.29	1630‡	-0.01	0.778	0.893
Sneg vIa R	4.48 ± 4.63	3.52 ± 4.71	1788‡	0.19	0.558	0.788
Sneg dIa L	4.83 ± 5.51	4.69 ± 5.49	1787‡	0.13	0.562	0.789
Sneg dIa R	4.92 ± 4.8	4.32 ± 6.49	1742‡	0.13	0.74	0.881
Sneg vId vIg L	3.34 ± 4.98	2.57 ± 5.55	1753‡	0.04	0.695	0.859
Sneg vId vIg R	2.95 ± 4.92	2.94 ± 4.08	1725‡	0.05	0.812	0.914
Sneg dIg L	3.84 ± 4.76	3.62 ± 3.84	1702‡	0.05	0.912	0.962
Sneg dIg R	3.74 ± 5.29	3 ± 5.01	1782.5‡	0.01	0.579	0.797
Sneg dId L	4.04 ± 5.71	4.16 ± 5.9	1673‡	-0.07	0.965	0.992
Sneg dId R	4.03 ± 6.64	3.67 ± 5.81	1600‡	0.05	0.655	0.836
Sneg A23d L	4.65 ± 6.82	4.21 ± 6.93	1837‡	0.06	0.392	0.661
Sneg A23d R	5.13 ± 5.03	4.05 ± 7.52	1872‡	0.05	0.294	0.593
Sneg A24rv L	3.76 ± 4.26	3.29 ± 4.98	1765‡	0.07	0.647	0.836
Sneg A32p L	4.07 ± 5.27	3.03 ± 5.42	1841‡	0.07	0.38	0.659
Sneg A32p R	3.65 ± 6.92	2.63 ± 7.56	1717‡	0.05	0.847	0.928
Sneg A23v L	6.58 ± 8.49	3.27 ± 4.65	2058‡	0.38	0.038	0.214

Sneg A23v R	5.16 ± 7.01	3.08 ± 5.91	2060‡	0.34	0.037	0.211
Sneg A24cd L	3 ± 4.3	2.51 ± 5.51	1677‡	0.07	0.982	0.995
Sneg A24cd R	3.17 ± 4.46	2.83 ± 5.41	1685‡	0.09	0.987	0.995
Sneg A23c L	2.21 ± 3.32	1.41 ± 2.19	1860‡	0.11	0.326	0.618
Sneg A23c R	2.56 ± 3.67	1.45 ± 2.99	1866‡	0.09	0.31	0.606
Sneg A32sg R	4.96 ± 4.33	4.41 ± 6.72	1593‡	0.2	0.627	0.831
Sneg cLinG L	3.75 ± 5.14	1.99 ± 4.62	1920‡	0.13	0.189	0.505
Sneg cLinG R	4.22 ± 6.79	2.38 ± 5.62	1938‡	0.27	0.157	0.468
Sneg rCunG L	3.63 ± 5.87	2.07 ± 4.03	2083.5‡	0.43	0.027	0.168
Sneg rCunG R	3.85 ± 6.63	1.47 ± 4.61	2132‡	0.45	0.013	0.096
Sneg cCunG R	4.94 ± 5.61	3.01 ± 5.85	1992‡	0.24	0.087	0.352
Sneg rLinG L	3.65 ± 7.36	2.17 ± 5.25	1976‡	0.31	0.104	0.391
Sneg rLinG R	4.38 ± 7.54	3.04 ± 5.73	1958‡	0.31	0.127	0.423
Sneg vmPOS L	4.09 ± 6.38	1.81 ± 3.82	2153.5‡	0.46	0.009	0.08
Sneg vmPOS R	4.38 ± 7.38	1.84 ± 4.43	2134.5‡	0.45	0.012	0.095
Sneg mOccG L	5.44 ± 6.22	3.64 ± 5.42	2010‡	0.33	0.07	0.311
Sneg mOccG R	5.31 ± 7.87	4.43 ± 7.14	1946‡	0.31	0.145	0.449
Sneg V5 MTpos L	4.58 ± 6.31	3.53 ± 6.35	1871‡	0.19	0.297	0.595
Sneg V5 MTpos R	5.03 ± 7.48	3.59 ± 6.4	1879‡	0.16	0.277	0.575
Sneg msOccG L	5.22 ± 5.71	3.25 ± 6.24	2002‡	0.36	0.077	0.328
Sneg msOccG R	4.67 ± 6.03	3.03 ± 4.36	2083‡	0.48	0.027	0.168
Sneg lsOccG L	3.57 ± 4.6	2.88 ± 5.56	1931‡	0.24	0.169	0.476
Sneg lsOccG R	3.25 ± 7.25	2.53 ± 4.33	1971‡	0.29	0.11	0.398
Sneg lAmyg L	3.43 ± 3.87	3.35 ± 3.6	1721‡	0.02	0.829	0.924
Sneg lAmyg R	3.13 ± 5.38	3.31 ± 4.47	1726‡	-0.07	0.808	0.912
Sneg rHipp L	3.67 ± 4.41	2.78 ± 5.46	1932‡	0.25	0.167	0.474
Sneg rHipp R	5.69 ± 6.16	4.53 ± 5.89	1899‡	0.2	0.231	0.543
Sneg cHipp L	4.1 ± 4.5	2.78 ± 3.81	2025‡	0.3	0.058	0.277
Sneg cHipp R	3.93 ± 4.32	2.51 ± 4.74	1985‡	0.15	0.094	0.37
Sneg vCa L	3.5 ± 3.86	2.71 ± 4	1751‡	0	0.703	0.86
Sneg vCa R	2.7 ± 4.76	2.32 ± 4.28	1712‡	0.04	0.868	0.933
Sneg GP L	3.11 ± 4.69	3.05 ± 4.58	1760‡	0.09	0.667	0.841
Sneg GP R	2.73 ± 5.15	2.09 ± 4.2	1827‡	0.24	0.423	0.684
Sneg NAC L	3.22 ± 3.51	2.39 ± 4.49	1950‡	0.14	0.139	0.436
Sneg vmPu L	2.89 ± 4.2	1.55 ± 2.86	2013‡	0.3	0.068	0.31
Sneg vmPu R	2.98 ± 4.89	1.79 ± 3.8	1900‡	0.26	0.229	0.543
Sneg dCa L	3.2 ± 5.74	3.21 ± 5.24	1717‡	-0.04	0.847	0.928
Sneg dCa R	3.05 ± 4.61	2.75 ± 4.07	1833‡	0.01	0.404	0.67
Sneg dlPu L	3.25 ± 4.51	1.78 ± 4.66	1862‡	0.23	0.32	0.614
Sneg dlPu R	2.23 ± 2.52	1.63 ± 3.82	1783‡	0.05	0.577	0.797
Sneg mPFtha L	2.6 ± 4.69	1.9 ± 3.17	1912.5‡	0.17	0.203	0.517

Sneg mPFtha R	2.23 ± 4.61	1.5 ± 3.6	1954‡	0.19	0.133	0.432
Sneg mPMtha L	3.96 ± 6.09	3.4 ± 3.17	2072‡	0.47	0.031	0.191
Sneg mPMtha R	2.29 ± 4.08	2.17 ± 2.26	1772‡	0.16	0.619	0.826
Sneg Stha L	3.08 ± 4.55	2.39 ± 3.69	1938‡	0.29	0.157	0.468
Sneg Stha R	3.28 ± 4.48	2.79 ± 3.37	1888‡	0.24	0.255	0.554
Sneg rTtha L	4.06 ± 6.13	1.98 ± 3.08	2129‡	0.27	0.014	0.1
Sneg rTtha R	4.41 ± 5.91	2.97 ± 6.27	1975.5‡	0.22	0.105	0.391
Sneg PPtha L	2.45 ± 5.05	1.74 ± 3.6	1891.5‡	0.28	0.247	0.554
Sneg PPtha R	2.08 ± 4.27	1.92 ± 3.27	1855.5‡	0.23	0.338	0.63
Sneg Otha L	2.82 ± 5.52	1.56 ± 5.02	2052‡	0.34	0.041	0.225
Sneg Otha R	3.66 ± 7.17	2.8 ± 4.3	2010‡	0.34	0.07	0.311
Sneg cTtha L	3.72 ± 5.18	2.43 ± 4.45	1965‡	0.13	0.118	0.405
Sneg cTtha R	4.48 ± 5.61	3.49 ± 5.68	1885‡	0.07	0.262	0.558
Sneg lPFtha L	2.16 ± 5.55	1.89 ± 3.3	1902‡	0.27	0.224	0.543
Sneg lPFtha R	2.74 ± 5.38	1.47 ± 3.25	2008‡	0.33	0.072	0.314
Sneg Buckner2011 17Networks 1	3.44 ± 6.34	4.13 ± 5.89	1622‡	-0.06	0.745	0.881
Sneg Buckner2011 17Networks 2	2.72 ± 3.23	3.06 ± 4.57	1598‡	-0.04	0.647	0.836
Sneg Buckner2011 17Networks 4	1.46 ± 2.6	1.63 ± 2.74	1764‡	-0.04	0.651	0.836
Sneg Buckner2011 17Networks 5	3.44 ± 5.61	3.97 ± 4.21	1604‡	-0.08	0.671	0.841
Sneg Buckner2011 17Networks 9	1.92 ± 4.08	2.03 ± 4.63	1603‡	-0.28	0.667	0.841
AD ACR L	0 ± 0	0 ± 0	-3.79†	-0.7	<0.001	0.005*
AD ACR R	0 ± 0	0 ± 0	-3.2†	-0.59	0.002	0.024*
AD ALIC L	0 ± 0	0 ± 0	1464.5‡	-0.12	0.232	0.543
AD ALIC R	0 ± 0	0 ± 0	1479‡	-0.19	0.265	0.561
AD BCC	0 ± 0	0 ± 0	1463‡	-0.33	0.229	0.543
AD CC	0 ± 0	0 ± 0	1221‡	-0.56	0.011	0.087
AD CGC L	0 ± 0	0 ± 0	-1.97†	-0.37	0.051	0.259
AD CGC R	0 ± 0	0 ± 0	-2.3†	-0.43	0.023	0.151
AD CGH L	0 ± 0	0 ± 0	1360‡	-0.22	0.076	0.327
AD CGH R	0 ± 0	0 ± 0	1543‡	-0.08	0.446	0.706
AD CR L	0 ± 0	0 ± 0	-3.72†	-0.69	<0.001	0.006*
AD CR R	0 ± 0	0 ± 0	1171‡	-0.63	0.005	0.049*
AD CST L	0 ± 0	0 ± 0	2043‡	0.34	0.046	0.242
AD CST R	0 ± 0	0 ± 0	2122‡	0.51	0.015	0.109
AD EC L	0 ± 0	0 ± 0	-2.74†	-0.51	0.007	0.066
AD EC R	0 ± 0	0 ± 0	-2.05†	-0.38	0.043	0.234
AD FX	0 ± 0	0 ± 0	-1.63†	-0.3	0.106	0.392
AD FX ST L	0 ± 0	0 ± 0	-0.85†	-0.16	0.396	0.665
AD FX ST R	0 ± 0	0 ± 0	-2.24†	-0.42	0.027	0.169
AD GCC	0 ± 0	0 ± 0	-3†	-0.56	0.003	0.037*
AD IC L	0 ± 0	0 ± 0	1252‡	-0.44	0.018	0.123

AD IC R	0 ± 0	0 ± 0	1178‡	-0.51	0.005	0.054
AD IFO L	0 ± 0	0 ± 0	1650‡	-0.07	0.864	0.933
AD IFO R	0 ± 0	0 ± 0	1673‡	-0.07	0.965	0.992
AD PCR L	0 ± 0	0 ± 0	1495‡	-0.16	0.304	0.604
AD PCR R	0 ± 0	0 ± 0	1477‡	-0.19	0.26	0.558
AD PLIC L	0 ± 0	0 ± 0	-1.01†	-0.19	0.313	0.607
AD PLIC R	0 ± 0	0 ± 0	-1.19†	-0.22	0.237	0.544
AD PTR L	0 ± 0	0 ± 0	1516‡	-0.16	0.362	0.65
AD PTR R	0 ± 0	0 ± 0	1215‡	-0.35	0.01	0.083
AD RLIC L	0 ± 0	0 ± 0	-3.11†	-0.58	0.002	0.029*
AD RLIC R	0 ± 0	0 ± 0	-3.49†	-0.65	0.001	0.01*
AD SCC	0 ± 0	0 ± 0	1186‡	-0.53	0.006	0.06
AD SCR L	0 ± 0	0 ± 0	1107‡	-0.59	0.002	0.021*
AD SCR R	0 ± 0	0 ± 0	1119‡	-0.59	0.002	0.024*
AD SFO L	0 ± 0	0 ± 0	-2.62†	-0.49	0.01	0.083
AD SFO R	0 ± 0	0 ± 0	1495‡	-0.19	0.304	0.604
AD SLF L	0 ± 0	0 ± 0	-3.94†	-0.73	<0.001	0.004*
AD SLF R	0 ± 0	0 ± 0	-3.99†	-0.74	<0.001	0.003*
AD SS L	0 ± 0	0 ± 0	-1.95†	-0.36	0.053	0.262
AD SS R	0 ± 0	0 ± 0	-2.82†	-0.52	0.006	0.056
AD UNC L	0 ± 0	0 ± 0	1559‡	-0.12	0.5	0.742
AD UNC R	0 ± 0	0 ± 0	1742‡	0.07	0.74	0.881
FA ACR L	0.39 ± 0.03	0.38 ± 0.03	1.17†	0.22	0.246	0.554
FA ACR R	0.4 ± 0.03	0.39 ± 0.04	1.75†	0.33	0.083	0.346
FA ALIC L	0.54 ± 0.04	0.52 ± 0.04	2.72†	0.5	0.008	0.068
FA ALIC R	0.54 ± 0.04	0.52 ± 0.04	3.34†	0.62	0.001	0.016*
FA BCC	0.63 ± 0.05	0.62 ± 0.05	1967‡	0.28	0.116	0.402
FA CC	0.64 ± 0.03	0.62 ± 0.04	3.04†	0.56	0.003	0.035*
FA CGC L	0.57 ± 0.06	0.57 ± 0.08	1808‡	0.22	0.487	0.733
FA CGC R	0.53 ± 0.06	0.52 ± 0.1	1792‡	0.15	0.544	0.775
FA CGH L	0.5 ± 0.06	0.47 ± 0.06	2.11†	0.39	0.037	0.212
FA CGH R	0.5 ± 0.05	0.49 ± 0.06	1.59†	0.29	0.115	0.402
FA CR L	0.43 ± 0.03	0.41 ± 0.03	1.93†	0.36	0.057	0.274
FA CR R	0.43 ± 0.03	0.42 ± 0.03	2.02†	0.38	0.046	0.241
FA CST L	0.54 ± 0.06	0.55 ± 0.06	-1.26†	-0.23	0.21	0.524
FA CST R	0.53 ± 0.05	0.54 ± 0.05	-0.7†	-0.13	0.483	0.733
FA EC L	0.43 ± 0.04	0.42 ± 0.04	0.47†	0.09	0.639	0.836
FA EC R	0.44 ± 0.03	0.43 ± 0.03	1.68†	0.31	0.096	0.371
FA FX	0.46 ± 0.11	0.42 ± 0.15	2055‡	0.37	0.039	0.221
FA FX ST L	0.53 ± 0.05	0.5 ± 0.04	2.93†	0.54	0.004	0.044*
FA FX ST R	0.53 ± 0.04	0.51 ± 0.04	3†	0.56	0.003	0.037*

FA GCC	0.6 ± 0.06	0.57 ± 0.05	2.55†	0.47	0.012	0.092
FA IC L	0.6 ± 0.03	0.58 ± 0.04	2.56†	0.48	0.012	0.092
FA IC R	0.58 ± 0.03	0.57 ± 0.04	2.78†	0.52	0.006	0.061
FA IFO L	0.47 ± 0.09	0.47 ± 0.05	1781‡	0.11	0.585	0.799
FA IFO R	0.5 ± 0.05	0.49 ± 0.04	1.39†	0.26	0.168	0.476
FA PCR L	0.43 ± 0.03	0.42 ± 0.05	2133‡	0.51	0.013	0.096
FA PCR R	0.45 ± 0.03	0.44 ± 0.03	1.74†	0.32	0.085	0.352
FA PLIC L	0.67 ± 0.05	0.65 ± 0.05	2064‡	0.38	0.035	0.203
FA PLIC R	0.66 ± 0.04	0.64 ± 0.05	1.79†	0.33	0.077	0.328
FA PTR L	0.54 ± 0.04	0.53 ± 0.04	1.68†	0.31	0.096	0.371
FA PTR R	0.54 ± 0.04	0.53 ± 0.03	2.11†	0.39	0.037	0.211
FA RLIC L	0.56 ± 0.04	0.55 ± 0.06	2011‡	0.26	0.069	0.311
FA RLIC R	0.54 ± 0.05	0.52 ± 0.05	2128‡	0.42	0.014	0.1
FA SCC	0.7 ± 0.03	0.68 ± 0.04	3.55†	0.66	0.001	0.009*
FA SCR L	0.46 ± 0.04	0.45 ± 0.04	1.29†	0.24	0.198	0.514
FA SCR R	0.44 ± 0.03	0.44 ± 0.04	1.25†	0.23	0.214	0.528
FA SFO L	0.45 ± 0.05	0.41 ± 0.05	4.15†	0.77	<0.001	0.003*
FA SFO R	0.44 ± 0.05	0.42 ± 0.04	3.41†	0.63	0.001	0.013*
FA SLF L	0.47 ± 0.03	0.44 ± 0.03	4.16†	0.77	<0.001	0.003*
FA SLF R	0.45 ± 0.03	0.44 ± 0.03	3.05†	0.57	0.003	0.033*
FA SS L	0.54 ± 0.04	0.52 ± 0.04	2.94†	0.55	0.004	0.043*
FA SS R	0.53 ± 0.03	0.51 ± 0.03	3.68†	0.68	<0.001	0.006*
FA UNC L	0.5 ± 0.08	0.47 ± 0.08	2142‡	0.36	0.011	0.087
FA UNC R	0.53 ± 0.05	0.5 ± 0.06	2.92†	0.55	0.004	0.044*
MD ACR L	0 ± 0	0 ± 0	-4.56†	-0.84	<0.001	0.002*
MD ACR R	0 ± 0	0 ± 0	-4.47†	-0.83	<0.001	0.002*
MD ALIC L	0 ± 0	0 ± 0	962‡	-0.77	<0.001	0.003*
MD ALIC R	0 ± 0	0 ± 0	1021‡	-0.74	<0.001	0.005*
MD BCC	0 ± 0	0 ± 0	1172‡	-0.54	0.005	0.05
MD CC	0 ± 0	0 ± 0	1023‡	-0.73	<0.001	0.005*
MD CGC L	0 ± 0	0 ± 0	-3.83†	-0.71	<0.001	0.005*
MD CGC R	0 ± 0	0 ± 0	-3.91†	-0.73	<0.001	0.004*
MD CGH L	0 ± 0	0 ± 0	1475‡	-0.16	0.255	0.554
MD CGH R	0 ± 0	0 ± 0	1447‡	-0.04	0.196	0.511
MD CR L	0 ± 0	0 ± 0	-4.03†	-0.75	<0.001	0.003*
MD CR R	0 ± 0	0 ± 0	-4†	-0.74	<0.001	0.003*
MD CST L	0 ± 0	0 ± 0	2035‡	0.36	0.051	0.259
MD CST R	0 ± 0	0 ± 0	2102‡	0.45	0.02	0.14
MD EC L	0 ± 0	0 ± 0	1074‡	-0.62	0.001	0.012*
MD EC R	0 ± 0	0 ± 0	1145‡	-0.62	0.003	0.035*
MD FX	0 ± 0	0 ± 0	1380.5‡	-0.32	0.097	0.373

MD FX ST L	0 ± 0	0 ± 0	1229‡	-0.52	0.013	0.095
MD FX ST R	0 ± 0	0 ± 0	-3.78†	-0.7	<0.001	0.005*
MD GCC	0 ± 0	0 ± 0	1111‡	-0.56	0.002	0.022*
MD IC L	0 ± 0	0 ± 0	-4.08†	-0.76	<0.001	0.003*
MD IC R	0 ± 0	0 ± 0	918‡	-0.84	<0.001	0.002*
MD IFO L	0 ± 0	0 ± 0	1502‡	-0.25	0.323	0.614
MD IFO R	0 ± 0	0 ± 0	1473‡	-0.32	0.251	0.554
MD PCR L	0 ± 0	0 ± 0	1559.5‡	-0.07	0.502	0.743
MD PCR R	0 ± 0	0 ± 0	1510‡	-0.12	0.345	0.635
MD PLIC L	0 ± 0	0 ± 0	-2.32†	-0.43	0.022	0.149
MD PLIC R	0 ± 0	0 ± 0	-3.72†	-0.69	<0.001	0.006*
MD PTR L	0 ± 0	0 ± 0	1598‡	-0.09	0.647	0.836
MD PTR R	0 ± 0	0 ± 0	1247‡	-0.32	0.017	0.118
MD RLIC L	0 ± 0	0 ± 0	-2.65†	-0.49	0.009	0.08
MD RLIC R	0 ± 0	0 ± 0	1009‡	-0.61	<0.001	0.005*
MD SCC	0 ± 0	0 ± 0	967‡	-0.67	<0.001	0.003*
MD SCR L	0 ± 0	0 ± 0	-4.47†	-0.83	<0.001	0.002*
MD SCR R	0 ± 0	0 ± 0	913‡	-0.86	<0.001	0.002*
MD SFO L	0 ± 0	0 ± 0	944‡	-0.78	<0.001	0.003*
MD SFO R	0 ± 0	0 ± 0	1119‡	-0.55	0.002	0.024*
MD SLF L	0 ± 0	0 ± 0	-4.68†	-0.87	<0.001	0.002*
MD SLF R	0 ± 0	0 ± 0	-4.39†	-0.82	<0.001	0.002*
MD SS L	0 ± 0	0 ± 0	1333‡	-0.42	0.055	0.266
MD SS R	0 ± 0	0 ± 0	-3.26†	-0.6	0.001	0.02*
MD UNC L	0 ± 0	0 ± 0	1608‡	-0.08	0.687	0.854
MD UNC R	0 ± 0	0 ± 0	1733‡	-0.03	0.778	0.893
RD ACR L	0 ± 0	0 ± 0	-4.1†	-0.76	<0.001	0.003*
RD ACR R	0 ± 0	0 ± 0	984‡	-0.8	<0.001	0.003*
RD ALIC L	0 ± 0	0 ± 0	870‡	-0.89	<0.001	0.002*
RD ALIC R	0 ± 0	0 ± 0	945‡	-0.73	<0.001	0.003*
RD BCC	0 ± 0	0 ± 0	1198‡	-0.52	0.008	0.068
RD CC	0 ± 0	0 ± 0	1038‡	-0.72	<0.001	0.007*
RD CGC L	0 ± 0	0 ± 0	-3.51†	-0.65	0.001	0.01*
RD CGC R	0 ± 0	0 ± 0	-3.68†	-0.68	<0.001	0.006*
RD CGH L	0 ± 0	0 ± 0	1498‡	-0.13	0.312	0.607
RD CGH R	0 ± 0	0 ± 0	1472‡	-0.02	0.248	0.554
RD CR L	0 ± 0	0 ± 0	-3.63†	-0.68	<0.001	0.007*
RD CR R	0 ± 0	0 ± 0	-3.83†	-0.71	<0.001	0.005*
RD CST L	0 ± 0	0 ± 0	2019‡	0.35	0.063	0.293
RD CST R	0 ± 0	0 ± 0	2046‡	0.38	0.044	0.236
RD EC L	0 ± 0	0 ± 0	-2.65†	-0.49	0.009	0.08

RD EC R	0 ± 0	0 ± 0	1194‡	-0.59	0.007	0.066
RD FX	0 ± 0	0 ± 0	1399‡	-0.32	0.119	0.406
RD FX ST L	0 ± 0	0 ± 0	1087‡	-0.68	0.001	0.015*
RD FX ST R	0 ± 0	0 ± 0	955‡	-0.69	<0.001	0.003*
RD GCC	0 ± 0	0 ± 0	1148‡	-0.51	0.003	0.037*
RD IC L	0 ± 0	0 ± 0	-3.94†	-0.73	<0.001	0.004*
RD IC R	0 ± 0	0 ± 0	991‡	-0.77	<0.001	0.004*
RD IFO L	0 ± 0	0 ± 0	-1.29†	-0.24	0.2	0.514
RD IFO R	0 ± 0	0 ± 0	1371‡	-0.37	0.087	0.352
RD PCR L	0 ± 0	0 ± 0	1612‡	-0.02	0.703	0.86
RD PCR R	0 ± 0	0 ± 0	1554‡	-0.08	0.483	0.733
RD PLIC L	0 ± 0	0 ± 0	-2.16†	-0.4	0.033	0.198
RD PLIC R	0 ± 0	0 ± 0	1164‡	-0.58	0.004	0.044*
RD PTR L	0 ± 0	0 ± 0	1647‡	-0.05	0.851	0.928
RD PTR R	0 ± 0	0 ± 0	1317‡	-0.28	0.044	0.236
RD RLIC L	0 ± 0	0 ± 0	-1.7†	-0.32	0.093	0.37
RD RLIC R	0 ± 0	0 ± 0	1121‡	-0.47	0.002	0.025*
RD SCC	0 ± 0	0 ± 0	1021‡	-0.69	<0.001	0.005*
RD SCR L	0 ± 0	0 ± 0	-4†	-0.74	<0.001	0.003*
RD SCR R	0 ± 0	0 ± 0	954‡	-0.82	<0.001	0.003*
RD SFO L	0 ± 0	0 ± 0	955‡	-0.82	<0.001	0.003*
RD SFO R	0 ± 0	0 ± 0	1050‡	-0.68	<0.001	0.008*
RD SLF L	0 ± 0	0 ± 0	976‡	-0.83	<0.001	0.003*
RD SLF R	0 ± 0	0 ± 0	-3.85†	-0.72	<0.001	0.005*
RD SS L	0 ± 0	0 ± 0	1322‡	-0.42	0.047	0.247
RD SS R	0 ± 0	0 ± 0	-3.16†	-0.59	0.002	0.025*
RD UNC L	0 ± 0	0 ± 0	1610‡	-0.06	0.695	0.859
RD UNC R	0 ± 0	0 ± 0	1713‡	0.02	0.864	0.933
Accumbens Area R	0.34 ± 0.05	0.32 ± 0.06	1807‡	0.18	0.49	0.733
Accumbens Area L	0.37 ± 0.05	0.37 ± 0.06	1611‡	-0.07	0.699	0.86
Amygdala R	0.83 ± 0.13	0.83 ± 0.11	1660.5‡	-0.03	0.91	0.961
Amygdala L	0.84 ± 0.13	0.83 ± 0.1	1659‡	0	0.903	0.957
Caudate R	2.79 ± 0.37	2.7 ± 0.49	1750‡	0.01	0.707	0.862
Caudate L	2.72 ± 0.38	2.66 ± 0.44	1817‡	0.09	0.456	0.712
Cerebellum Exterior R	39.98 ± 4.69	41.47 ± 7.14	1442‡	-0.27	0.187	0.505
Cerebellum Exterior L	40.18 ± 3.98	41.7 ± 8	1543‡	-0.18	0.446	0.706
Hippocampus R	3.01 ± 0.39	2.97 ± 0.39	1746‡	0.01	0.724	0.874
Hippocampus L	2.87 ± 0.4	2.81 ± 0.37	1826‡	0.1	0.426	0.688
Pallidum R	0.15 ± 0.13	0.15 ± 0.11	1704.5‡	0	0.901	0.957
Pallidum L	0.19 ± 0.11	0.19 ± 0.08	1761‡	0.03	0.663	0.839
Putamen R	3.36 ± 0.63	3.24 ± 0.42	1698‡	0.02	0.93	0.971

Putamen L	3.47 ± 0.7	3.48 ± 0.68	1613‡	-0.1	0.707	0.862
Thalamus Proper R	4.8 ± 0.7	4.56 ± 0.76	1.75†	0.33	0.082	0.345
Thalamus Proper L	4.83 ± 0.62	4.75 ± 0.75	0.64†	0.12	0.522	0.76
VentralDC R	0.88 ± 0.16	0.88 ± 0.18	1707‡	0.08	0.89	0.95
VentralDC L	0.86 ± 0.14	0.87 ± 0.17	1666‡	-0.06	0.934	0.974
Optic Chiasm R	0.08 ± 0.03	0.08 ± 0.03	0.34†	0.06	0.735	0.881
Cerebellar Vermal Lobules I-V	3.39 ± 0.43	3.48 ± 0.7	1474.5‡	-0.27	0.254	0.554
Cerebellar Vermal Lobules VI-VII	1.59 ± 0.3	1.71 ± 0.28	1398.5‡	-0.26	0.119	0.405
Cerebellar Vermal Lobules VIII-X	2.05 ± 0.29	2.08 ± 0.42	1549‡	-0.19	0.466	0.72
Basal Forebrain R	0.36 ± 0.07	0.37 ± 0.07	1602‡	-0.06	0.663	0.839
Basal Forebrain L	0.36 ± 0.06	0.37 ± 0.08	1545.5‡	-0.07	0.454	0.712
Anterior cingulate gyrus R	2.95 ± 0.7	2.93 ± 0.59	1644‡	0.01	0.838	0.928
Anterior cingulate gyrus L	3.5 ± 0.72	3.5 ± 0.63	1723‡	0.09	0.821	0.92
Anterior insula R	3.36 ± 0.59	3.4 ± 0.74	1524‡	-0.15	0.386	0.659
Anterior insula L	3.36 ± 0.56	3.5 ± 0.54	1502‡	-0.15	0.323	0.614
Anterior orbital gyrus R	1.5 ± 0.19	1.47 ± 0.23	0.7†	0.13	0.484	0.733
Anterior orbital gyrus L	1.3 ± 0.2	1.34 ± 0.27	1528‡	-0.13	0.398	0.666
Angular gyrus R	7.91 ± 1.83	8.09 ± 1.41	1696.5‡	-0.11	0.936	0.975
Angular gyrus L	6.85 ± 1.28	6.82 ± 1.28	1665‡	0.08	0.93	0.971
Calcarine cortex R	2.39 ± 0.47	2.29 ± 0.37	1812‡	0.16	0.473	0.728
Calcarine cortex L	2.37 ± 0.57	2.32 ± 0.51	1797‡	0.09	0.525	0.762
Central operculum R	2.99 ± 0.8	3.03 ± 0.74	1690‡	-0.09	0.965	0.992
Central operculum L	2.93 ± 0.74	3.01 ± 0.75	1683‡	-0.09	0.996	1
Cuneus R	3.71 ± 0.69	3.77 ± 0.82	1785‡	-0.15	0.569	0.795
Cuneus L	3.4 ± 0.71	3.58 ± 0.77	1478‡	-0.2	0.262	0.558
Ententorhinal area R	1.87 ± 0.23	1.87 ± 0.3	1729‡	0.01	0.795	0.905
Ententorhinal area L	1.84 ± 0.21	1.83 ± 0.22	0.3†	0.06	0.764	0.888
Frontal operculum R	1.4 ± 0.34	1.42 ± 0.29	1742‡	-0.07	0.74	0.881
Frontal operculum L	1.41 ± 0.32	1.38 ± 0.3	1808.5‡	0.12	0.485	0.733
Frontal pole R	3.04 ± 0.47	3.07 ± 0.46	1562‡	-0.08	0.511	0.75
Frontal pole L	2.82 ± 0.49	2.9 ± 0.67	1506‡	-0.21	0.334	0.625
Fusiform gyrus R	6.27 ± 0.98	6.18 ± 0.91	1733‡	0.18	0.778	0.893
Fusiform gyrus L	5.9 ± 0.82	5.86 ± 0.97	1751‡	0.08	0.703	0.86
Gyrus rectus R	1.71 ± 0.39	1.75 ± 0.33	1627‡	-0.04	0.766	0.888
Gyrus rectus L	1.69 ± 0.34	1.76 ± 0.3	1411‡	-0.14	0.136	0.436
Inferior occipital gyrus R	4.88 ± 0.85	4.95 ± 0.9	1600‡	-0.05	0.655	0.836
Inferior occipital gyrus L	4.83 ± 0.86	4.76 ± 0.89	1682‡	0.01	1	1
Inferior temporal gyrus R	9.78 ± 1.24	9.8 ± 1.62	1662‡	-0.02	0.916	0.964
Inferior temporal gyrus L	9.71 ± 1.39	9.84 ± 1.92	1581‡	-0.03	0.581	0.797
Lingual gyrus R	6.83 ± 1.03	7.01 ± 1.14	1663‡	-0.05	0.921	0.966
Lingual gyrus L	6.32 ± 1.04	6.47 ± 1.37	1575‡	-0.06	0.558	0.788

Lateral orbital gyrus R	1.71 ± 0.24	1.73 ± 0.37	1694‡	-0.1	0.947	0.981
Lateral orbital gyrus L	1.78 ± 0.31	1.76 ± 0.28	1682‡	0.01	1	1
Middle cingulate gyrus R	3.34 ± 0.78	3.3 ± 0.57	1742‡	0.13	0.74	0.881
Middle cingulate gyrus L	3.26 ± 0.57	3.18 ± 0.48	1772‡	0.12	0.619	0.826
Medial frontal cortex R	1.34 ± 0.38	1.34 ± 0.34	1676‡	0.05	0.978	0.993
Medial frontal cortex L	1.36 ± 0.33	1.39 ± 0.33	1581‡	-0.03	0.581	0.797
Middle frontal gyrus R	14 ± 2.67	13.67 ± 2.5	1625‡	0.05	0.757	0.886
Middle frontal gyrus L	13.9 ± 2.56	14.15 ± 2.32	1604‡	-0.07	0.671	0.841
Middle occipital gyrus R	3.88 ± 0.61	3.91 ± 0.94	1609‡	-0.08	0.691	0.857
Middle occipital gyrus L	4.58 ± 0.62	4.6 ± 0.74	-0.17†	-0.03	0.866	0.933
Medial orbital gyrus R	3.32 ± 0.56	3.29 ± 0.48	1599.5‡	0.06	0.653	0.836
Medial orbital gyrus L	3.4 ± 0.5	3.59 ± 0.56	1444‡	-0.19	0.191	0.505
Postcentral gyrus medial segment R	0.78 ± 0.2	0.79 ± 0.19	1719‡	-0.03	0.838	0.928
Postcentral gyrus medial segment L	0.75 ± 0.11	0.74 ± 0.11	0.59†	0.11	0.559	0.788
Precentral gyrus medial segment R	2 ± 0.4	1.95 ± 0.54	1857‡	0.18	0.334	0.625
Precentral gyrus medial segment L	1.98 ± 0.29	1.98 ± 0.3	0.04†	0.01	0.965	0.992
Superior frontal gyrus medial segment R	5.84 ± 1.35	5.89 ± 1.3	1675‡	0	0.974	0.993
Superior frontal gyrus medial segment L	5 ± 0.97	5.13 ± 0.96	1604‡	-0.07	0.671	0.841
Middle temporal gyrus R	11.46 ± 1.8	11.68 ± 2.42	1607‡	-0.19	0.683	0.852
Middle temporal gyrus L	10.84 ± 1.65	11.16 ± 2.15	1473‡	-0.18	0.251	0.554
Occipital pole R	2.69 ± 0.52	2.64 ± 0.58	1851‡	0.17	0.351	0.64
Occipital pole L	2.81 ± 0.41	2.78 ± 0.46	1783‡	0.04	0.577	0.797
Occipital fusiform gyrus R	3.07 ± 0.58	3.13 ± 0.51	1600‡	-0.04	0.655	0.836
Occipital fusiform gyrus L	3.16 ± 0.57	3.27 ± 0.53	1444‡	-0.19	0.191	0.505
Opercular part of the inferior frontal gyrus R	2.46 ± 0.45	2.44 ± 0.69	1755‡	0.07	0.687	0.854
Opercular part of the inferior frontal gyrus L	2.28 ± 0.66	2.33 ± 0.43	1650‡	-0.06	0.864	0.933
Orbital part of the inferior frontal gyrus R	1.06 ± 0.27	1.06 ± 0.23	1828‡	0.19	0.42	0.684
Orbital part of the inferior frontal gyrus L	1.25 ± 0.34	1.19 ± 0.24	1725‡	0.02	0.812	0.914
Posterior cingulate gyrus R	3.01 ± 0.59	3.03 ± 0.57	1713‡	-0.09	0.864	0.933
Posterior cingulate gyrus L	3.41 ± 0.56	3.51 ± 0.65	1642‡	0	0.829	0.924
Precuneus R	8.62 ± 1.57	8.67 ± 1.97	1525‡	-0.13	0.389	0.659
Precuneus L	8.57 ± 1.72	8.64 ± 1.85	1464‡	-0.16	0.231	0.543
Pparahippocampal gyrus R	2.7 ± 0.29	2.74 ± 0.29	-0.74†	-0.14	0.459	0.714
Parahippocampal gyrus L	2.84 ± 0.3	2.9 ± 0.31	-0.91†	-0.17	0.363	0.65
Posterior insula R	1.78 ± 0.36	1.92 ± 0.37	1445‡	-0.13	0.192	0.508
Posterior insula L	1.67 ± 0.4	1.79 ± 0.34	1395‡	-0.16	0.114	0.402
Parietal operculum R	1.42 ± 0.43	1.47 ± 0.43	1699‡	-0.1	0.925	0.969
Parietal operculum L	1.8 ± 0.43	1.74 ± 0.45	1834‡	0.15	0.401	0.668
Postcentral gyrus R	7.63 ± 1.04	7.71 ± 0.93	-0.46†	-0.09	0.645	0.836
Postcentral gyrus L	8.06 ± 1.45	8.54 ± 1.29	1473‡	-0.09	0.251	0.554
Posterior orbital gyrus R	2.32 ± 0.51	2.24 ± 0.54	1765‡	0.14	0.647	0.836

Posterior orbital gyrus L	2.4 ± 0.46	2.39 ± 0.45	1681‡	0.02	1	1
Planum polare R	1.34 ± 0.28	1.34 ± 0.33	1681‡	-0.04	1	1
Planum polare L	1.54 ± 0.32	1.48 ± 0.33	1808‡	0.17	0.487	0.733
Precentral gyrus R	9.55 ± 1.4	9.42 ± 1.59	1735‡	0	0.77	0.888
Precentral gyrus L	9.39 ± 1.25	9.51 ± 1.57	1720‡	-0.02	0.834	0.927
Planum temporale R	1.47 ± 0.27	1.45 ± 0.31	1773‡	0.14	0.615	0.826
Planum temporale L	1.6 ± 0.47	1.51 ± 0.4	1889‡	0.19	0.253	0.554
Subcallosal area R	0.91 ± 0.22	0.94 ± 0.24	1619‡	0	0.732	0.881
Subcallosal area L	0.95 ± 0.24	0.96 ± 0.23	1688‡	-0.02	0.974	0.993
Superior frontal gyrus R	11.56 ± 2.01	11.33 ± 2.18	1564‡	0.13	0.518	0.758
Superior frontal gyrus L	11.34 ± 2.06	11.61 ± 2.02	1480‡	-0.19	0.267	0.563
Supplementary motor cortex R	4.04 ± 0.67	4.03 ± 0.73	1710‡	0.04	0.877	0.94
Supplementary motor cortex L	4.23 ± 0.88	4.24 ± 0.98	1620‡	-0.02	0.736	0.881
Supramarginal gyrus R	6.11 ± 1.45	6.19 ± 1.28	1703‡	-0.09	0.908	0.96
Supramarginal gyrus L	6.6 ± 1.31	6.76 ± 1.11	1565‡	-0.03	0.522	0.76
Superior occipital gyrus R	2.95 ± 0.55	3.13 ± 0.7	1501‡	-0.16	0.32	0.614
Superior occipital gyrus L	2.47 ± 0.31	2.61 ± 0.38	1270‡	-0.31	0.023	0.151
Superior parietal lobule R	7.56 ± 1.2	7.72 ± 1.54	1581‡	-0.07	0.581	0.797
Superior parietal lobule L	7.99 ± 1.65	8.2 ± 1.58	1556‡	-0.11	0.49	0.733
Superior temporal gyrus R	5.61 ± 1	5.7 ± 1.2	1631‡	-0.01	0.782	0.895
Superior temporal gyrus L	5.3 ± 1.01	5.32 ± 0.93	1762‡	-0.11	0.659	0.836
Temporal pole R	7.39 ± 0.91	7.66 ± 1.42	1567‡	-0.14	0.529	0.764
Temporal pole L	7.35 ± 0.91	7.63 ± 1.48	1517‡	-0.15	0.365	0.65
Triangular part of the inferior frontal gyrus R	2.72 ± 0.38	2.64 ± 0.54	1738.5‡	0.01	0.755	0.886
Triangular part of the inferior frontal gyrus L	2.64 ± 0.44	2.58 ± 0.66	1711‡	0.03	0.873	0.937
Transverse temporal gyrus R	0.97 ± 0.24	0.93 ± 0.24	1810‡	0.12	0.48	0.733
Transverse temporal gyrus L	1.09 ± 0.25	1.03 ± 0.3	1810‡	0.14	0.48	0.733
bankssts L	2.34 ± 0.14	2.36 ± 0.15	-0.58†	-0.11	0.563	0.789
bankssts R	2.4 ± 0.16	2.38 ± 0.23	1718‡	0.18	0.842	0.928
caudalanteriorcingulate L	2.45 ± 0.22	2.38 ± 0.22	1.83†	0.34	0.07	0.311
caudalanteriorcingulate R	2.35 ± 0.18	2.31 ± 0.19	1.06†	0.2	0.29	0.59
caudalmiddlefrontal L	2.38 ± 0.14	2.4 ± 0.15	-0.79†	-0.15	0.432	0.694
caudalmiddlefrontal R	2.4 ± 0.15	2.38 ± 0.16	0.75†	0.14	0.454	0.712
cuneus L	1.87 ± 0.16	1.9 ± 0.14	-0.81†	-0.15	0.418	0.684
cuneus R	1.89 ± 0.16	1.87 ± 0.14	0.46†	0.08	0.649	0.836
entorhinal L	3.41 ± 0.35	3.49 ± 0.35	1487‡	-0.24	0.284	0.586
entorhinal R	3.41 ± 0.41	3.51 ± 0.29	1506‡	-0.17	0.334	0.625
fusiform L	2.47 ± 0.13	2.48 ± 0.12	-0.45†	-0.08	0.656	0.836
fusiform R	2.49 ± 0.14	2.5 ± 0.12	-0.7†	-0.13	0.488	0.733
inferiorparietal L	2.32 ± 0.11	2.33 ± 0.13	-0.74†	-0.14	0.461	0.715
inferiorparietal R	2.33 ± 0.11	2.32 ± 0.14	0.25†	0.05	0.8	0.909

inferiortemporal L	2.58 ± 0.11	2.59 ± 0.14	-0.77†	-0.14	0.441	0.701
inferiortemporal R	2.66 ± 0.15	2.63 ± 0.16	1724.5‡	0.18	0.814	0.915
isthmuscingulate L	2.22 ± 0.17	2.25 ± 0.15	-1.14†	-0.21	0.259	0.558
isthmuscingulate R	2.26 ± 0.16	2.24 ± 0.16	0.44†	0.08	0.659	0.836
lateraloccipital L	2.11 ± 0.12	2.12 ± 0.13	-0.73†	-0.14	0.465	0.72
lateraloccipital R	2.13 ± 0.12	2.14 ± 0.13	-0.64†	-0.12	0.523	0.76
lateralorbitofrontal L	2.6 ± 0.12	2.6 ± 0.13	-0.18†	-0.03	0.861	0.933
lateralorbitofrontal R	2.49 ± 0.13	2.49 ± 0.12	0.13†	0.02	0.901	0.957
lingual L	2.01 ± 0.14	2 ± 0.12	0.26†	0.05	0.792	0.903
lingual R	2 ± 0.14	2 ± 0.12	-0.07†	-0.01	0.943	0.979
medialorbitofrontal L	2.32 ± 0.14	2.32 ± 0.11	0.29†	0.05	0.771	0.888
medialorbitofrontal R	2.36 ± 0.12	2.36 ± 0.12	-0.28†	-0.05	0.782	0.895
middletemporal L	2.61 ± 0.13	2.65 ± 0.14	-1.53†	-0.29	0.128	0.423
middletemporal R	2.62 ± 0.13	2.65 ± 0.16	-1.07†	-0.2	0.286	0.587
parahippocampal L	2.21 ± 0.33	2.17 ± 0.27	1770‡	0.06	0.627	0.831
parahippocampal R	2.32 ± 0.2	2.36 ± 0.21	-1.2†	-0.22	0.234	0.543
paracentral L	2.19 ± 0.14	2.21 ± 0.16	-0.92†	-0.17	0.361	0.65
paracentral R	2.2 ± 0.15	2.21 ± 0.17	-0.3†	-0.06	0.768	0.888
parsopercularis L	2.45 ± 0.14	2.44 ± 0.14	0.55†	0.1	0.583	0.798
parsopercularis R	2.43 ± 0.15	2.4 ± 0.14	1.23†	0.23	0.219	0.533
parsorbitalis L	2.44 ± 0.16	2.45 ± 0.15	-0.24†	-0.05	0.807	0.912
parsorbitalis R	2.45 ± 0.16	2.45 ± 0.18	0.04†	0.01	0.972	0.993
parstriangularis L	2.31 ± 0.15	2.32 ± 0.12	-0.38†	-0.07	0.703	0.86
parstriangularis R	2.32 ± 0.15	2.31 ± 0.15	0.23†	0.04	0.82	0.92
pericalcarine L	1.73 ± 0.16	1.72 ± 0.12	0.08†	0.01	0.939	0.976
pericalcarine R	1.74 ± 0.16	1.73 ± 0.14	0.61†	0.11	0.542	0.775
postcentral L	1.96 ± 0.13	1.98 ± 0.12	-0.83†	-0.15	0.408	0.675
postcentral R	1.99 ± 0.12	2 ± 0.13	-0.79†	-0.15	0.429	0.69
posteriorcingulate L	2.26 ± 0.12	2.25 ± 0.11	0.41†	0.08	0.683	0.852
posteriorcingulate R	2.21 ± 0.12	2.22 ± 0.13	-0.41†	-0.08	0.682	0.852
precentral L	2.25 ± 0.16	2.26 ± 0.17	-0.17†	-0.03	0.868	0.933
precentral R	2.28 ± 0.19	2.25 ± 0.23	1635.5‡	0.01	0.802	0.909
precuneus L	2.26 ± 0.1	2.28 ± 0.12	-0.89†	-0.17	0.374	0.654
precuneus R	2.27 ± 0.12	2.28 ± 0.12	-0.33†	-0.06	0.743	0.881
rostralanteriorcingulate L	2.54 ± 0.14	2.55 ± 0.15	-0.51†	-0.1	0.61	0.821
rostralanteriorcingulate R	2.61 ± 0.14	2.59 ± 0.13	0.87†	0.16	0.388	0.659
rostralmiddlefrontal L	2.23 ± 0.11	2.23 ± 0.13	-0.02†	0	0.985	0.995
rostralmiddlefrontal R	2.21 ± 0.12	2.22 ± 0.13	-0.29†	-0.05	0.77	0.888
superiorfrontal L	2.5 ± 0.15	2.53 ± 0.14	-0.86†	-0.16	0.393	0.662
superiorfrontal R	2.52 ± 0.14	2.53 ± 0.15	-0.37†	-0.07	0.716	0.868
superiorparietal L	2.1 ± 0.12	2.13 ± 0.13	-1.2†	-0.22	0.233	0.543

superiorparietal R	2.09 ± 0.11	2.12 ± 0.12	-1.29†	-0.24	0.2	0.514
superiortemporal L	2.56 ± 0.16	2.58 ± 0.17	-0.53†	-0.1	0.599	0.813
superiortemporal R	2.61 ± 0.17	2.62 ± 0.16	-0.48†	-0.09	0.631	0.834
supramarginal L	2.34 ± 0.12	2.35 ± 0.13	-0.35†	-0.06	0.729	0.878
supramarginal R	2.35 ± 0.13	2.35 ± 0.14	0.3†	0.06	0.762	0.888
frontalpole L	2.32 ± 0.23	2.34 ± 0.18	-0.63†	-0.12	0.532	0.767
frontalpole R	2.31 ± 0.19	2.3 ± 0.22	0.38†	0.07	0.702	0.86
temporalpole L	3.59 ± 0.27	3.62 ± 0.27	-0.67†	-0.12	0.505	0.746
temporalpole R	3.7 ± 0.39	3.71 ± 0.3	1687‡	-0.18	0.978	0.993
transversetemporal L	2.16 ± 0.2	2.16 ± 0.21	0.03†	0.01	0.976	0.993
transversetemporal R	2.2 ± 0.2	2.23 ± 0.17	-0.99†	-0.18	0.323	0.614
insula L	3.04 ± 0.17	3.08 ± 0.18	-1.37†	-0.25	0.174	0.483
insula R	3.06 ± 0.18	3.07 ± 0.2	-0.46†	-0.09	0.646	0.836

Results are reported as mean ± standard deviation. For non-normally distributed variables, results are reported as median ± interquantile range. Cohen's d values are reported for each region of tract according to the specific neuroimaging modality. Abbreviations: Spos, positive strength; Sneg, negative strength; AD, axial diffusivity; FA; fractional anisotropy; MD, mean diffusivity; RD, radial diffusivity; ACR, anterior corona radiata; ALIC, anterior limb of internal capsule; BCC, body of corpus callosum; CC, corpus callosum; CGC, cingulate gyrus; CGH, perihippocampal cingulum tract; CR, corona radiata; CST, cortico-spinal tract; EC, external capsule; FX, fornix; FXST, fornix - stria terminalis; GCC, genu of corpus callosum; IC, internal capsule; IFO, inferior fronto-occipital fasciculus; PCR, posterior corona radiata; PLIC, posterior limb of internal capsule; PTR, posterior thalamic radiation; RLIC, retrolenticular limb of the internal capsule; SCC, splenium of corpus callosum; SCR, superior corona radiata; SFO, superior fronto-occipital fasciculus; SS, sagittal stratum; UNC, uncinate fasciculus; R, right; L; left. †parametric two-sample t-test; ‡non-parametric Mann-Whitney U test; *FDR-corrected q<0.05.

Appendix 12. Differences in immune cells count between the FACS-based clusters

Variable	**Cluster 1 (N = 41)**	**Cluster 2 (N = 96)**	**t / U**	**d**	**p**	**q**
CD4+/CM/CD25+	3.57 ± 4.49	5.73 ± 4.41	1107.5‡	-0.71	<0.001	<0.001*
CD4+/CM/CD69+	23.1 ± 25.6	8.48 ± 14.27	2714‡	0.59	<0.001	0.001*
CD4+/EM/CD25+	2.43 ± 5.63	4.5 ± 4.21	1307‡	-0.26	0.002	0.004*
CD4+/EM/CD69+	21.8 ± 22.89	10.8 ± 19.11	2497.5‡	0.42	0.013	0.023*
CD4+/Naive/CD25+	1.46 ± 2.49	2.56 ± 1.49	1168.5‡	-0.75	<0.001	<0.001*
CD4+/Naive/CD69+	9.36 ± 9.47	3.82 ± 8.03	2718‡	0.44	<0.001	0.001*
CD8+/CM/CD25+	1.99 ± 3.63	2.03 ± 2.33	1749.5‡	-0.06	0.305	0.373
CD8+/CM/CD69+	31.7 ± 44.06	16.65 ± 24.96	2257.5‡	0.43	0.174	0.246
CD8+/EM/CD25+	1.86 ± 3.46	1.68 ± 3.04	1788.5‡	0.01	0.4	0.468
CD8+/EM/CD69+	20.9 ± 25.36	15.45 ± 16.11	2191.5‡	0.25	0.295	0.368
CD8+/Naive/CD25+	0.64 ± 1.2	0.35 ± 0.78	1947.5‡	0.10	0.925	0.942
CD8+/Naive/CD69+	15.2 ± 21.9	7.51 ± 15.28	2303‡	0.30	0.116	0.172
Mait Cells CD161+	59.9 ± 21.7	51.25 ± 32.15	2382‡	0.37	0.052	0.082
CD4+/GM-CSF	0.05 ± 0.33	0.05 ± 0.19	2207‡	-0.35	0.262	0.335
CD4+/IFN-γ	4.64 ± 5.33	3.15 ± 4.76	2397‡	0.37	0.044	0.071
CD4+/IL-2	0.1 ± 0.28	0.03 ± 0.14	2686‡	0.41	0.001	0.002*

CD4+/IL-4	1.03 ± 1.12	0.91 ± 1.13	2246‡	0.38	0.192	0.264
CD4+/IL-17	0.22 ± 0.45	0.07 ± 0.15	2769.5‡	0.51	<0.001	<0.001*
CD4+/TNF-α	1.76 ± 7.84	0.71 ± 1.6	2627‡	0.84	0.002	0.004*
CD8+/GM-CSF	0.11 ± 0.41	0.08 ± 0.22	2405.5‡	0.38	0.04	0.067
CD8+/IFN-γ	15.8 ± 12.68	11.8 ± 16.8	2274.5‡	0.22	0.15	0.218
CD8+/IL-2	0.23 ± 0.4	0.07 ± 0.3	2579.5‡	0.33	0.004	0.008*
CD8+/IL-4	1.24 ± 2.17	1.11 ± 1.55	2207.5‡	0.34	0.261	0.335
CD8+/IL-17	0.13 ± 1.38	0.06 ± 0.14	2572‡	0.66	0.005	0.009*
CD8+/TNF-α	2.92 ± 7.81	1.22 ± 3.35	2565‡	0.79	0.005	0.01*
NK cells/GM-CSF	1.82 ± 4.58	0.83 ± 2.41	2596.5‡	0.22	0.003	0.007*
NK cells/IFN-γ	24.6 ± 29.7	20.55 ± 28.27	2221.5‡	0.21	0.234	0.314
NK cells/IL-2	0.22 ± 0.85	0.18 ± 0.41	2130.5‡	0.38	0.445	0.51
NK cells/IL-4	1.9 ± 4.19	2.18 ± 4.17	1889.5‡	-0.10	0.714	0.785
NK cells/IL-17	0.63 ± 7.43	0.05 ± 0.38	2633.5‡	0.83	0.002	0.004*
NK cells/TNF-α	3.28 ± 12.12	1.98 ± 3.84	2525.5‡	0.71	0.009	0.016*
FoxP3- CD39+	3.46 ± 11.96	2.82 ± 6.83	2009‡	0.05	0.849	0.881
FoxP3+ CD39+	26.3 ± 39.26	23.75 ± 36.73	2024‡	0.10	0.794	0.84
Treg (CD49d+)	70.8 ± 37.5	68.8 ± 18.9	1976‡	0.10	0.972	0.972
Treg (CD49d-)	25.8 ± 31.3	28.7 ± 14.88	1909.5‡	-0.11	0.785	0.84
FoxP3+ CD39-	27.6 ± 27.4	34.45 ± 34.25	1853.5‡	0.00	0.592	0.665
FoxP3- CD39-	20.9 ± 43.13	22.2 ± 33.88	1785‡	-0.08	0.391	0.467
CD8+/CM/Perf- GrzB+	7.28 ± 10.36	3.85 ± 5.34	2412‡	0.60	0.037	0.064
CD8+/CM/Perf+ GrzB+	0.09 ± 0.31	6.53 ± 7.92	104‡	-1.56	<0.001	<0.001*
CD8+/CM/Perf+ GrzB-	0.02 ± 0.14	7.51 ± 12.49	84.5‡	-1.25	<0.001	<0.001*
CD8+/EM/CM/Perf- GrzB+	39.3 ± 22.9	19.85 ± 11.85	3188‡	1.35	<0.001	<0.001*
CD8+/EM/Perf+ GrzB+	3.17 ± 10.41	24.3 ± 29.9	327.5‡	-1.46	<0.001	<0.001*
CD8+/EM/Perf+ GrzB-	0 ± 0.09	4 ± 6.39	176‡	-1.12	<0.001	<0.001*
CD8+/Naive/Perf- GrzB+	2.29 ± 3.42	1.03 ± 1.99	2376‡	0.12	0.055	0.085
CD8+/Naive/Perf+ GrzB+	0.05 ± 0.43	2.18 ± 3.74	461.5‡	-0.78	<0.001	<0.001*
CD8+/Naive/Perf+ GrzB-	0.03 ± 0.09	2.08 ± 2.67	229‡	-0.77	<0.001	<0.001*
CD8+/TEMRA/CM/Perf- GrzB+	56.6 ± 30.3	12 ± 15.96	3358.5‡	1.96	<0.001	<0.001*
CD8+/TEMRA/Perf+ GrzB+	8.2 ± 19	57.95 ± 30.05	377‡	-1.93	<0.001	<0.001*
CD8+/TEMRA/Perf+ GrzB-	0 ± 0.11	2.4 ± 4.13	425‡	-0.86	<0.001	<0.001*
CD3+/Tγδ/Perf- GrzB+	20.7 ± 20.25	8.35 ± 8.81	2889‡	0.96	<0.001	<0.001*
CD3+/Tγδ/Perf+ GrzB+	2.23 ± 3.79	23.1 ± 21.98	345.5‡	-1.27	<0.001	<0.001*
CD3+/Tγδ/Perf+ GrzB-	0.08 ± 0.51	9.43 ± 12.91	185‡	-1.18	<0.001	<0.001*
NK cells/Perf- GrzB+	15.3 ± 23.8	4.17 ± 5.79	3415‡	1.56	<0.001	<0.001*
NK cells/Perf+ GrzB+	37.1 ± 62.1	78.85 ± 25.25	841‡	-1.37	<0.001	<0.001*
NK cells/Perf+ GrzB-	1.85 ± 2.86	6.76 ± 8.01	610.5‡	-0.81	<0.001	<0.001*

Results are reported as mean ± standard deviation. For non-normally distributed variables, results are reported as median ± interquantile range. Cohen's d values are reported for each immune cell population. Abbreviations: CM, central memory; EM, effective memory; GM-CSF; granulocyte macrophage colony stimulating factor; IL, interleukin; INF; interferon; TNF, tumor necrosis factor; Treg; regulatory T cells; Perf; perforin; GrzB; granzyme; TEMRA, T cells

re-expressing CD45RA; NK, natural killer. †parametric two-sample t-test; ‡non-parametric Mann-Whitney U test; *FDR-corrected q<0.05.

Appendix 13. Differences in immune-inflammatory Z-scores between the clusters derived from immune-inflammatory profiles.

Variable	Cluster 1 (N = 116)	Cluster 2 (N = 69)	t / U	d	p	q
M1 macrophage	-0.35 ± 0.57	0.51 ± 0.63	582‡	-1.94	<0.001	<0.001*
Th1	-0.43 ± 0.63	0.6 ± 0.87	593‡	-1.96	<0.001	<0.001*
Th2	-0.26 ± 0.53	0.43 ± 0.54	-8.47†	-1.29	<0.001	<0.001*
Th17	-0.39 ± 0.64	0.44 ± 0.86	707‡	-0.2	<0.001	<0.001*
CIRS	-0.37 ± 0.56	0.6 ± 0.83	881‡	-1.68	<0.001	<0.001*
IRS	-0.29 ± 0.5	0.45 ± 0.55	184‡	-0.15	<0.001	<0.001*
T cell growth	-0.36 ± 0.49	0.54 ± 0.57	394‡	-0.21	<0.001	<0.001*
Neurotoxicity	-0.33 ± 0.37	0.54 ± 0.42	-14.39†	-2.25	<0.001	<0.001*
Growth factors	-0.38 ± 0.6	0.62 ± 0.61	-10.82†	-1.65	<0.001	<0.001*

Results are reported as mean ± standard deviation. For non-normally distributed variables, results are reported as median ± interquantile range. Cohen's d values are reported for each immune-inflammatory profile. Abbreviations: Th, T helper cells; CIRS, compensatory immunoregulatory system; IRS, immune-inflammatory response system. †parametric two-sample t-test; ‡non-parametric Mann-Whitney U test; *FDR-corrected q<0.05.